UNIWERSYTET MIKOŁAJA KOPERNIKA W TORUNIU

Collegium Medicum
im. Ludwika Rydygiera w Bydgoszczy

Bydgoszcz, 2025

UNIWERSYTET
MIKOŁAJA KOPERNIKA
W TORUNIU
Wydział Farmaceutyczny
Collegium Medicum w Bydgoszczy

Paulina Szeliska

Ocena efektywności wybranego modelu farmakoterapii glejaków na podstawie profilowania metabolomicznego i lipidomicznego linii komórkowych tych nowotworów wyprowadzonych od pacjentów jako krok w stronę personalizacji terapii

Rozprawa na stopień doktora nauk medycznych i nauk o zdrowiu

Promotor:

Prof. dr hab Barbara Bojko

Bydgoszcz, 2025

Składam serdeczne podziękowania
Pani prof. dr hab. Barbarze Bojko za nieustanną motywację,
otworzenie drzwi na rozwój osobisty
oraz wsparcie w sytuacjach, w których najbardziej potrzebowałam pomocy.
Dziękuję za wiarę w moją wiedzę i możliwości
oraz wsparcie merytoryczne na każdym etapie realizowania niniejszej rozprawy.

Dziękuję Koleżankom i Kolegom
z Katedry Farmakodynamiki i Farmakologii Molekularnej
za to, iż w każdym momencie mogłam poprosić o pomoc i wsparcie, które zawsze zostało mi udzielone. Dziękuję za dzielenie wiedzy ale również trosk i radości.

Szczególne podziękowania składam dr hab. Karolowi Jarochowi, prof. UMK za wprowadzenie mnie w świat metabolomiki i cierpliwe odpowiadanie na wszystkie pytania.

Dziękuję członkom zespołu „Innovation in Personalized Medicine" z Katedry Urologii i Andriologi, byłego Zakładu Inżynierii Tkankowej za wsparcie merytoryczne i badawcze oraz za świetną atmosferę. Szczególne podziękowania składam dr Łukaszowi Kaźmierskiemu, na którego ogromną wiedzę i pomoc zawsze mogłam liczyć.

Szczególne podziękowania składam mojej wspaniałej rodzinie, Rodzicom i Siostrze,
za wiarę we mnie, wspieranie na każdym etapie mojej drogi naukowej. Wasza troska i zaangażowanie są dla mnie ogromnym źródłem siły i motywacji. Jestem niesamowicie wdzięczna, iż zawsze mogę na Was liczyć.

Specjalne podziękowania pragnę złożyć naukowcowi, którego wkładu w niniejszą rozprawę oraz moją naukową drogę nie da się zmierzyć. Mojemu mężowi, Kamilowi, dziękuję za wszystkie chwilę, którą poświęcił na wspieranie mnie na każdym etapie, nawet w najcięższych momentach. Dziękuję za służenie radą, słuchanie rozterek ale przede wszystkim wiarę w moje siły i nieustanną motywację do dalszego działania.

Spis treści

Wykaz skrótów

Skrót	Angielskie rozwinięcie	Polskie rozwinięcie
ADME	Absorption, Distribution, Metabolism, Excretion	wchłanianie, dystrybucja, metabolizm, wydalanie
BrdU	5-Bromo-2′-deoxyuridine	5-bromo-2′-deoksyurydyna
CBS	Coated Blade Spray	natrysk z powlekanego ostrza
EGFR	Epidermal Growth Factor Receptor	receptor naskórkowego czynnika wzrostu
FBS	Fetal Bovine Serum	surowica płodowa bydlęca
FDR	False Discovery Rate	odsetek fałszywych odkryć
GBM	Glioblastoma	glejak wielopostaciowy
GaM	Gallium Maltolate	maltolan galu
HIF	Hypoxia-Inducible Factor(s)	czynniki indukowane hipoksją
IC	Inhibitory Concentration	stężenie hamujące
IDH	Isocitrate Dehydrogenase	dehydrogenaza izocytrynianowa
LC-MS	Liquid Chromatography Mass Spectrometry	chromatografia cieczowa sprzężona z spektrometrią mas
OCR	Oxygen Consumption Rate	tempo zużycia tlenu
PCA	Principal Component Analysis	analiza głównych składowych
PLS-DA	Partial Least Squares Discriminant Analysis	analiza dyskryminacyjna PLS
QC	Quality Control	kontrola jakości
SPME	Solid-Phase Microextraction	mikroekstrakcja do fazy stałej
TCA	Tricarboxylic Acid Cycle (Krebs cycle)	cykl kwasów trikarboksylowych (cykl Krebsa)
TERT	Telomerase Reverse Transcriptase	odwrotna transkryptaza telomerazy
TFRC	Transferrin Receptor	receptor transferyny (gen TFRC)
TMZ	Temozolomide	temozolomid
TfR1	Transferrin Receptor 1	receptor transferyny 1
VEGF	Vascular Endothelial Growth Factor	naczyniowo-śródbłonkowy czynnik wzrostu
VIP	Variable Importance in Projection	znaczenie zmiennych w projekcji
WHO	World Health Organization	Światowa Organizacja Zdrowia

1. Wykaz publikacji stanowiących podstawę postępowania w sprawie o nadanie stopnia naukowego doktora

P.1. Jaroch, K.*; **Modrakowska, P.*;** Bojko, B. Glioblastoma metabolomics—in vitro studies. *Metabolites* **2021**, *11*, 315. DOI:10.3390/metabo11050315, punktacja MNiSW: 100, IF: 3,7

*Dwóch równorzędnych autorów

P.2. **Szeliska, P.**, Jaroch, Charemski, B., Kahremanoğlu, K., Çetin, E., Boyaci E., Bojko, B. Protocol for the upgraded high-throughput SPME system for biocompatible in vitro extraction from small volume for metabolomics and pharmaceutical assays. Green Analytical Chemistry 2025, 13, 100238. DOI: 10.1016/j.greeac.2025.100238, punktacja MniSW: -, IF: 6.2

P.3. **Szeliska, P.**, Jaroch, K., Wróblewska, W., Kaźmierski, Ł., Maj, M., Bojko, B. Culture dimensionality governs gallium maltolate response in glioblastoma: comparative analyses in 2D and 3D models. (nr submission BIORXIV/2025/676610) DOI: 10.1101/2025.09.17.676610.

2. Streszczenie w języku polskim

Celem rozprawy było zintegrowanie podejścia farmako-metabolomicznego do badania glejaka o wysokim stopniu złośliwości (GBM) z naciskiem na dobre praktyki projektowania eksperymentów *in vitro* i ich translację, rozwój biokompatybilnego, wysokoprzepustowego przygotowania próbek metodą mikroekstrakcji do fazy stałej (SPME) oraz charakterystykę odpowiedzi GBM na maltolan galu (GaM) w modelach 2D i 3D. W części przeglądowej zestawiono kluczowe czynniki kształtujące profil metaboliczny komórek GBM (format hodowli, hipoksja, skład pożywki) oraz omówiono techniki przygotowania próbek i platformy analityczne sprzyjające rzetelnej ekstrapolacji in vitro–in vivo. W części metodycznej zaprojektowano i zweryfikowano zmodernizowany system biokompatybilnego, wielokrotnego i w pełni inkubatorowego pobierania próbek z płytek 96-dołkowych, zgodny z zasadami zielonej chemii i skalowalny do badań farmakologicznych. W części badawczej oceniono działanie GaM w liniach klasycznych (A-172, U-87 MG) oraz wyprowadzonych od pacjentów (3005, 3019, 3034, 3048, 3073) hodowanych w 2D i 3D, łącząc modelowanie krzywych dawka–odpowiedź (IC10/IC50/IC90), oznaczenie receptora dla transferyny (ang. Transferrin Receptor, TFRC), pomiar zużycia tlenu (ang. Oxygen Consumption Rate, OCR) oraz metabolomikę z wykorzystaniem chromatografii cieczowej sprzężonej ze spektrometrią mas (LC-MS).

GaM obniżał żywotność we wszystkich modelach, przy czym w 3D obserwowano prawostronne przesunięcie krzywych (wyższe IC) oraz silniejsze tłumienie OCR, co wskazuje na większą tolerancję mikrootoczenia 3D i nasilony stres mitochondrialny. Zależność między wyjściowym poziomem TFRC a wrażliwością na GaM była widoczna w 2D (istotna korelacja z IC50), lecz zanikała w 3D, co potwierdza zależny od kontekstu charakter biomarkerów żelazowych. Analizy wielowymiarowe wykazały, że dominujące źródło wariancji różni się między liniami (efekt leczenia w 3005/3048, efekt formy hodowli w 3019/3034, efekt czasu w A-172/U-87 MG/3073). Obserwowane zmiany profili metabolomicznych obejmowały głównie tryptofan, metioninę, uracyl i allantoinę, co wskazuje na skoordynowane zakłócenia w szlakach aminokwasowych, jednowęglowych/nukleotydowych i redoks równolegle z dysfunkcją mitochondrialną. Łącznie wyniki dowodzą, że wymiar hodowli jest kluczową determinantą odpowiedzi na GaM, a zestawienie OCR z metabolomiką w modelach 3D i liniach wyprowadzonych od pacjentów dostarcza bardziej predykcyjną ocenę skuteczności i mechanizmu działania. Ponadto,

zaproponowana metoda SPME, która charakteryzuje się prostotą w zastosowaniu i jest bardziej ekologiczna, umożliwia łatwą integrację z hodowlami komórkowymi i tradycyjnymi testami, co ułatwia projektowanie badań łączących farmakologię z metabolomiką.

Słowa kluczowe: maltolan galu, glejak wielopostaciowy, hodowla 3D, mikroekstrakcja w fazie stałej, farmakometabolomika.

3. Streszczenie w języku angielskim

The aim of this dissertation was to integrate a pharmaco-metabolomic approach to glioblastoma (GBM) by outlining best practices for in-vitro metabolic studies and their translation, developing a biocompatible, high-throughput solid-phase microextraction (SPME) workflow, and characterizing GBM responses to gallium maltolate (GaM) in 2D and 3D culture models. The review component synthesizes key determinants of GBM metabolic readouts (culture dimensionality, hypoxia, media composition, stem-like state), discusses sample-preparation strategies and analytical platforms that support reliable in vitro–in vivo extrapolation, and provides practical guidance to avoid common pitfalls in supervised modelling. The methodological component introduces an upgraded system enabling repeated, in-incubator sampling from 96-well cultures with minimal perturbation and reduced solvent/plastic use, offering a scalable route for metabolomics in pharmaceutical testing. The research component evaluated GaM across established (A-172, U-87 MG) and patient-derived (3005, 3019, 3034, 3048, 3073) GBM lines grown in 2D and 3D, combining dose–response modelling (IC10/IC50/IC90), transferrin receptor (TFRC) quantification, oxygen consumption rate (OCR), and metabolomics with liquid chromatography combined with mass spectrometry (LC-MS).

GaM reduced viability in all models, with a consistent rightward shift of dose–response and stronger OCR suppression in 3D than in 2D, indicating greater microenvironment-driven tolerance and heightened mitochondrial stress. Baseline TFRC associated with GaM sensitivity in 2D (significant TFRC–IC50 correlation) but not in 3D, underscoring context-dependent biomarker performance. Multivariate analyses showed line-specific drivers of variance: treatment-dominant separation in 3005/3048, culture format dominance in 3019/3034, and time effects in A-172/U-87 MG/3073. The observed metabolomic alteration mainly involved tryptophan, methionine, uracil, and allantoin and pointed to coordinated perturbations in amino-acid, one-carbon/nucleotide, and redox pathways alongside mitochondrial dysfunction. Collectively, the findings identify culture dimensionality as a primary determinant of GaM response and support 3D, patient-derived systems with integrated OCR and metabolomics as more predictive platforms for efficacy assessment, mechanism elucidation, and biomarker development. Moreover, the proposed SPME method, which is simple to use and more ecological, allows for easy integration with cell cultures and

traditional assays, which facilitates the design of studies combining pharmacology with metabolomics.

Key words: gallium maltolate; glioblastoma; 3D culture; Solid Phase Micorextraction, Pharmacometabolomic

4. Wstęp

Glejaki o wysokim stopniu złośliwości (ang. Glioblastoma, GBM) należą do najbardziej agresywnych nowotworów ośrodkowego układu nerwowego. Standard diagnostyczny obejmuje badanie histopatologiczne oraz testy molekularne [1], jednak mimo postępu diagnostycznego i terapeutycznego GBM pozostaje najgroźniejszym, pierwotnym złośliwym guzem OUN. Maltolan galu (ang. Gallium Maltolate, GaM) jest obiecującym kandydatem terapeutycznym, ponieważ wpływa na zaburzoną u chorych gospodarkę żelaza [2]. W przebiegu GBM wykazano kluczową rolę żelaza; liczne zmiany nowotworowe charakteryzują się wysoką ekspresją receptora transferryny (TfR), co stwarza możliwość selektywnego oddziaływania na komórki GBM z wysoką ekspresją TfR i stanowi alternatywę dla klasycznej farmakoterapii [3–5].

4.1. Glejak o wysokim stopniu złośliwości i metabolizm żelaza

GBM należą do IV stopnia klasyfikacji Światowej Organizacji Zdrowia (ang. World Health Organization, WHO) i obejmują najbardziej agresywne nowotwory ośrodkowego układu nerwowego (OUN) [1]. W 2021 r. WHO wprowadziła zaktualizowany system klasyfikacji guzów OUN, oparty nie tylko na obrazie histopatologicznym, lecz także na markerach genetycznych, m.in. gen dehydrogenazy izocytrynianowej (ang. Isocitrate Dehydrogenase, IDH) typu dzikiego, amplifikacja receptor naskórkowego czynnika wzrostu (ang. Epidermal Growth Factor Receptor, EGFR_, mutacja promotora genu odwrotnej transkryptazy telomerazy (ang. Telomerase Reverse Transcriptase , TERT) czy trisomia chromosomu 7 I monosomia chromosomu 10 [1]. Mimo rozwoju tej spersonalizowanej diagnostyki, GBM pozostaje najbardziej śmiertelnym pierwotnym złośliwym guzem OUN [6]. Współcześnie markery molekularne stanowią ważne narzędzie w kwalifikacji i ocenie leczenia.

Niezależnie od profilu molekularnego guza, postępowaniem pierwszego wyboru jest jego chirurgiczne usunięcie, a następnie radioterapia i chemioterapia podtrzymująca temozolomidem (ang. Temozolomide TMZ). Inne opcje obejmują pochodne nitrozomocznika oraz nowszy lek anty-VEGF, bewacyzumab [7]. Skuteczność chemioterapii w GBM wysokiego stopnia jest jednak ograniczona i w dużej mierze zależy od statusu IDH i metylacji MGMT; u chorych z niezmetylowanym promotorem MGMT aktywność temozolomidu jest znikoma, co znacząco

zawęża możliwości terapeutyczne [8]. Stąd wciąż poszukuje się nowych schematów leczenia i strategii dla GBM wysokiego stopnia złośliwości.

Guzy GBM charakteryzują się złożoną architekturą i skomplikowanym mikrośrodowiskiem [9]. Wysoki indeks proliferacyjny, nasilona angiogeneza, martwica o układzie „pseudopalisadowym" oraz niedotlenienie wewnątrzguzowe sprzyjają agresywnemu przebiegowi choroby i oporności na leczenie — komórki nowotworowe skutecznie adaptują się do zmieniających się warunków. Wśród tych procesów kluczową rolę w oporności na chemioterapię i radioterapię odgrywa przeprogramowanie metabolizmu [10]. Jest to zjawisko dobrze opisane: środowisko niedotlenienia upośledza fosforylację oksydacyjną i aktywność cyklu kwasów trikarboksylowych (ang. TCA, a równocześnie nasilą glikolizę i produkcję mleczanu [11,12].

Hipoksja indukuje ponadto czynniki transkrypcyjne z rodziny czynników indukowanych hipoksją (ang. Hypoxia-Inducible Factors, HIF), które odgrywają kluczową rolę w progresji, agresywności i oporności GBM [13]. Enzymy hydroksylujące HIF są zależne od żelaza, dlatego regulacja metabolizmu żelaza wywiera istotny wpływ na biologię GBM [14]. Żelazo jest niezbędne dla funkcjonowania organizmu (m.in. transport tlenu, synteza DNA) [15]. Receptor transferyny 1 (ang. transferrin receptor 1, TfR1) jest głównym transporterem żelaza do komórki i w prawidłowych tkankach jego ekspresja jest ściśle kontrolowana w celu utrzymania homeostazy żelaza [16,17]. W komórkach nowotworowych nadekspresja TfR1 sprzyja nagromadzeniu żelaza, które napędza proliferację i wzrost guza. Gen receptora dla transferryny (TFRC) oraz inne geny związane z gospodarką żelaza są deregulowane w guzach mózgu, zaburzając homeostazę żelaza. W konsekwencji, modulacja homeostazy żelaza jest postrzegana jako obiecujący kierunek terapii GBM.

4.2. Maltolan galu

Coraz więcej badań koncentruje się na terapiach zaburzających metabolizm żelaza w komórkach nowotworowych i wtórnie prowadzi do hamowania reduktazy rybonukleotydów oraz upośledzenia funkcji mitochondriów. GaM, doustnie biodostępny kompleks galu(III), wyłania się jako obiecujący kandydat terapeutyczny i jest stosunkowo nowy w leczeniu GBM [18]. Wykazano jego aktywność przeciwnowotworową w wielu modelach, m.in. raka pęcherza i piersi, chłoniaka oraz raka wątrobowokomórkowego [3,19–21]. W glejaku wielopostaciowym Chitambar i wsp.

zademonstrowali w hodowlach 2D/3D oraz w modelu ksenograftu szczurzego, że GaM zaburza komórkową homeostazę żelaza, wywołując apoptozę komórek nowotworowych [2]. Ponieważ gal może przekraczać barierę krew–mózg po związaniu z endogenną transferyną, GaM zyskuje ułatwione dostarczanie do komórek GBM z ekspresją TfR. GaM upośledza funkcję mitochondriów i hamuje zależną od żelaza podjednostkę RRM2 reduktazy rybonukleotydów, ograniczając syntezę dNTP; wpływa także na cykl TCA i hamuje mitochondrialne zużycie tlenu w komórkach GBM, oszczędzając komórki prawidłowe. Obecnie badanie kliniczne fazy I (NCT04319276) prowadzone jest w celu oceny efektywności GaM u chorych z guzami nawrotowymi i/lub opornymi na leczenie [22].

4.3. Hodowle komórkowe w badaniach glejaka mózgu

Tkanki nowotworowe zawierają ogniska martwicy i hipoksji, które tworzą niejednorodne mikrośrodowisko o zmiennych właściwościach fizykochemicznych i biologicznych, takich jak gradienty pH i pO_2 oraz zróżnicowane wzorce ekspresji białek, co w konsekwencji indukuje zmiany metaboliczne. Ponadto, takie warunki wpływają na stabilność leków przeciwnowotworowych i mogą sprzyjać ich swoistym biotransformacjom [23]. Dlatego idealny model nowotworu do badania działania leku i jego interakcji z metabolomem powinien jak najwierniej odtwarzać te zjawiska.

Atrakcyjnym i nowoczesnym modelem przedklinicznym są wielokomórkowe sferoidy. Otrzymuje się je z proliferujących komórek nowotworowych poprzez hodowlę w warunkach ograniczających adhezję do podłoża, co wymusza adhezję międzykomórkową i w prosty sposób prowadzi do powstania trójwymiarowych (3D) struktur o cechach nieobecnych w konwencjonalnych, dwuwymiarowych (2D) monowarstwach. W centrum sferoidu rozwija się hipoksja, a ograniczona dyfuzja powoduje niedobór składników odżywczych, co lepiej odzwierciedla warunki *in vivo*. Hipoksji towarzyszą gradienty pH i potencjału redoks, które mogą modyfikować działanie leków; przede wszystkim jednak pojawia się gradient proliferacji: komórki powierzchowne dzielą się najszybciej, odsetek komórek spoczynkowych jest większy niż w 2D, a w większych sferoidach tworzy się martwiczy rdzeń. Systemy 3D lepiej oddają mikrośrodowisko guza, ponieważ uwzględniają kluczowe interakcje komórka–macierz i komórka–komórka, nieobecne w hodowlach monowarstwowych [24,25].

W ostatnich latach badania *in vitro* z wykorzystaniem zarówno utrwalonych linii GBM, jak i komórek pierwotnych zyskały na popularności dzięki szybkiemu rozwojowi technik hodowli 3D. Model 3D był szeroko stosowany w badaniach metabolomicznych i okazał się bardziej sprzyjać komórkom o fenotypie macierzystym [26], który wiąże się z zaburzeniami metabolizmu żelaza i nadekspresją TfR1 [27]. Należy jednak pamiętać, że ze względu na heterogeniczność GBM podejście „one-size-fits-all" nie zawsze się sprawdza. Hodowla 3D nie jest z definicji lepsza od 2D; przy projektowaniu eksperymentu trzeba uwzględnić także inne czynniki niż sam model wzrostu. Aby utrzymać oryginalny fenotyp komórek, kluczowe są dobór pożywki i czynników wzrostowych [28]. Doniesienia wskazują, że komórki hodowane w monowarstwie na pożywkach z dodatkiem surowicy płodowej bydlęcej (ang. Fetal bonive serum, FBS) mogą właściwie odzwierciedlać cechy guza, natomiast neurosfery w warunkach bezsurowiczych często lepiej oddają stan *in vivo*. Z tego względu warto stosować różne protokoły izolacji i hodowli, aby zachować heterogenną populację komórek w hodowli pierwotnej, a analizy prowadzić równolegle w układach 2D, 3D, a nawet w ko-kulturach 2D–3D w obrębie tej samej linii komórkowej [29].

4.4. Mikroekstrakcja do fazy stałej

Analiza metabolomu/lipidomu linii komórkowych GBM może obejmować zarówno metabolom zewnątrzkomórkowy, tj. metabolity uwalniane przez komórki do środowiska, jak i metabolom wewnątrzkomórkowy, tj. związki transportowane i akumulowane wewnątrz komórek. Badania zewnątrzkomórkowe wykonuje się zwykle z wykorzystaniem pożywki hodowlanej jako matrycy: pożywkę pobiera się z hodowli, a następnie dodaje rozpuszczalnik organiczny w celu ekstrakcji metabolitów/lipidów, ewentualnie z dodatkowymi etapami przygotowania próbki [28,30,31]. Przygotowanie próbek do analizy metabolizmu wewnątrzkomórkowego obejmuje zazwyczaj wygaszenie metabolizmu zimnym buforem fosfoanowym, odklejenie komórek z pomocą trypsyny lub zeskrobywanie komórek, wirowanie oraz odparowanie; następnie próbki odtwarza się w odpowiednim rozpuszczalniku.

Mikroekstrakcja do fazy stałej (ang. Solid-Phase Microextraction, SPME) nie należy do najczęściej stosowanych technik przygotowania próbek, stanowi jednak niezwykle obiecujące narzędzie w badaniach farmaceutycznych *in vitro* [32–35]. SPME to technika równowagowa, która łączy pobieranie, przygotowanie i ekstrakcję próbki w jednym etapie [36]. Procedura nie zużywa próbki,

pozwala uniknąć współekstrakcji białek i, w przypadku analizy metabolitów zewnątrzkomórkowych, nie jest toksyczna dla komórek. Dzięki temu na tej samej hodowli można wykonać kolejne testy komórkowe, np. oznaczenia cytotoksyczności czy barwienia fluorescencyjne [32]. Metoda jest również prosta i elastyczna, co ułatwia jej adaptację do nowych modeli hodowli, w tym trójwymiarowych (3D) [33].

Tkanka mózgowa jest szczególnie trudna do analizy ze względu na ograniczony dostęp kliniczny. W praktyce klinicznej dominują techniki obrazowania, które – mimo przydatności – pozostają ograniczone i nie dostarczają informacji o dokładnym składzie chemicznym tkanek [37]. SPME było wcześniej wykorzystywane do analizy guzów mózgu i mózgu *in vivo* (Ryc. 1). Wyniki wykazały, że SPME może dostarczać przestrzennie rozdzielczych informacji o składzie metabolicznym i lipidomicznym mózgu u pacjentów *in vivo* dzięki minimalnej inwazyjności stosowanych sond i wyeliminowaniu konieczności fizycznego poboru próbki. Ze względu na tę unikalną cechę, technika ta jest również znana jako „biopsja chemiczna". Ponadto, zastosowanie specjalnie zoptymalizowanej biokompatybilnej powłoki umożliwia ekstrakcję zarówno związków hydrofobowych (np. lipidów), jak i polarnych (np. aminokwasów). Tę samą metodę zastosowano następnie w badaniach guzów mózgu po ich resekcji: włókno SPME wprowadzano do tkanki guza w celu pobrania metabolomu/lipidomu. Uzyskane dane pokazały, że taka procedura pozwala uzyskać charakterystyczny fenotyp guza, dostarczając markerów lipidomicznych [38] i metabolomicznych [39]. W kolejnych badaniach przeprowadzono ukierunkowaną analizę lipidomiczną z użyciem Coated Blade Spray (CBS). Wykazano zróżnicowanie poziomów karnityny i acylokarnityn względem mutacji IDH i kodelecji 1p/19q, a ponadto, dzięki temu że CBS pomija rozdział poprzez chromatografię cieczową (ang. liquid chromatography, LC) i umożliwia szybką analizę instrumentalną bez pogorszenia oczyszczania próbki, podejście to wykazało potencjał do szybkiego, screeningu biomarkerów w warunkach „on-site" (na miejscu, np. śródoperacyjnie) [40–42].

4.5. Farmako-metabolomika w glejaku mózgu

Zmiany metaboliczne w komórkach nowotworowych od dawna bada się pod kątem ich przydatności w profilowaniu fenotypów różnych typów guzów. W przypadku GBM wykazano dobrą korelację między obecnymi mutacjami (np. PDGFRA, IDH1, EGFR, NF1) a

metabolomicznym „odciskiem palca" danego guza. Zaproponowano także potencjalne onkometabolity istotne dla stopnia złośliwości glejaków, m.in. stosunek całkowitej choliny do całkowitej kreatyny oraz fosfocholiny do glicerofosfocholiny [20,43–46]. Markery takie jak inozytol i mio-inozytol wiązano z mutacjami IDH, PDGFRA i EGFR w tkance guza [43,47]. Glutamina, glutaminian i kwas γ-aminomasłowy (GABA) odgrywają kluczową rolę w funkcjonowaniu mózgu; monitorowanie ich poziomów może dostarczać ważnych informacji o stopniu złośliwości guza i statusie mutacji [29,43,47–49]. Nadregulacja zredukowanego glutationu (GSH), pośród linii komórkowych różnych guzów mózgu była łączona z grupą linii komórkowych pochodzących z glejaków WHO stopnia IV, co sugeruje związek z transformacją do form bardziej złośliwych [50]. Wskazywano również inne metabolity i szlaki, których zaburzenia mogą mieć znaczenie dla diagnostyki, rokowania i testowania leków w GBM, np. N-acetyloasparaginian [45,51].

Dzięki szeroko zakrojonym pracom nad profilami metabolomicznymi GBM, metabolomika stała się obiecującym narzędziem do przedklinicznego screeningu leków oraz badania oporności guza na terapię. Opisywano zależności między poziomami metabolitów, takich jak cytrynian, kreatyna czy alanina, a opornością guza na TMZ [52]. Identyfikacja szlaków zaburzonych w GBM umożliwia także wskazanie nowych inhibitorów o potencjale terapeutycznym, np. inhibitorów GLS (w szlakach glutaminowych) czy inhibitorów Gli1 w guzach z nadekspresją tego czynnika [31,53]. Metabolomika *in vitro* była z powodzeniem stosowana do monitorowania wpływu różnych leków na syntezę lipidów (m.in. inhibitor FK866, inhibitory fosfolipazy D oraz kwas γ-linolenowy) [54–56].

Przeglądu szklaków metabolomicznych zmienionych w GMB *in vitro,* ich potencjalne znaczenie w diagnostyce, monitorowaniu choroby i opracowywaniu procesu leczenia dokonano w pracy poglądowej pt. „Glioblastoma metabolomics—in vitro studies" (Metabolites 2021, 11, 315), będącej częścią cyklu publikacji prezentowanych w tej pozprawie doktorskiej (publikacja P.1.).

metabolites

MDPI

Review

Glioblastoma Metabolomics—In Vitro Studies

Karol Jaroch †, Paulina Modrakowska † and Barbara Bojko *

Department of Pharmacodynamics and Molecular Pharmacology, Faculty of Pharmacy, Collegium Medicum in Bydgoszcz, Nicolaus Copernicus University in Toruń, dr A. Jurasza 2 Street, 85-089 Bydgoszcz, Poland; karol.jaroch@cm.umk.pl (K.J.); p.modrakowska@cm.umk.pl (P.M.)

* Correspondence: bbojko@cm.umk.pl

† Both authors contributed equally to this work.

Abstract: In 2016, the WHO introduced new guidelines for the diagnosis of brain gliomas based on new genomic markers. The addition of these new markers to the pre-existing diagnostic methods provided a new level of precision for the diagnosis of glioma and the prediction of treatment effectiveness. Yet, despite this new classification tool, glioblastoma (GBM), a grade IV glioma, continues to have one of the highest mortality rates among central nervous system tumors. Metabolomics is a particularly promising tool for the analysis of GBM tumors and potential methods of treating them, as it is the only "omics" approach that is capable of providing a metabolic signature of a tumor's phenotype. With careful experimental design, cell cultures can be a useful matrix in GBM metabolomics, as they ensure stable conditions and, under proper conditions, are capable of capturing different tumor phenotypes. This paper reviews in vitro metabolomic profiling studies of high-grade gliomas, with a particular focus on sample-preparation techniques, crucial metabolites identified, cell culture conditions, in vitro-in vivo extrapolation, and pharmacometabolomics. Ultimately, this review aims to elucidate potential future directions for in vitro GBM metabolomics.

Keywords: glioblastoma multiforme; in vitro metabolomics; phamacometabolomics

Citation: Jaroch, K.; Modrakowska, P.; Bojko, B. Glioblastoma Metabolomics—In Vitro Studies. *Metabolites* **2021**, *11*, 315. https://doi.org/10.3390/metabo11050315

Academic Editor: James McCullagh

Received: 15 March 2021
Accepted: 10 May 2021
Published: 13 May 2021

1. Introduction

Glioblastoma (GBM) is one of the most aggressive and difficult-to-treat central nervous system (CNS) brain tumors. Since 2007, the World Health Organization (WHO) has classified gliomas based on their cell type and aggressiveness, with Class I consisting of benign tumors, and Class IV comprising the most aggressive types of tumors. GBM is a Class IV brain tumor [1]. While this classification system allows clinicians to determine appropriate treatments and prognoses, years of studies have indicated that this approach should be supplemented with genetic testing, as it lacks adequate specificity on its own. xAs a result, in 2016 the WHO introduced a novel CNS grading system that provided a level of precision surpassing all known CNS diagnostic and classification methods. This novel grading system incorporated new genetic markers—for example, IDH1/IDH2, O^6-mtehylguanine DNA methyltransferase (MGMT), and epidermal growth factor receptors (EGFR)—thereby allowing clinicians to differentiate tumors not only by their cell type and aggressiveness, as was possible with pre-existing methods, but also by the genetic phenotype of the neoplastic cells, thus providing better correlation with the tumor prognosis [2]. Despite this new, improved diagnostic system, GBM continues to be the most lethal primary malignant CNS tumor. Indeed, in the USA, patients diagnosed with GBM have an average life-expectancy of eight months, with only 7.2% surviving beyond five years of diagnosis [3].

The treatment of GBM remains a challenge, as newly proposed drugs must meet specific requirements, such as being able to cross the blood-brain barrier (BBB) and efficiently infiltrating the tumor. GBM tumors are known for their complex structure, which is the result of a demanding growth environment. Other features of GBM tumors that make them so challenging to treat include high proliferation indices, angiogenesis, and

pseudopalisading necrosis [4]. Intratumoral hypoxia is caused by rapid cell proliferation and vascular collapse, and it induces the expression of hypoxia-inducible factor-1 (HIF-1), which is responsible for regulating many key processes involved in tumor progression and invasion. Among these processes, metabolic reprogramming appears to be critical in understanding the resistance of GBM tumors to chemotherapy and radiation therapy [5]. The most commonly used method of treating GBM is tumor resection followed by radiation therapy and/or chemotherapy with temozolomide (TMZ) [6], an alkylating agent that targets cells undergoing intense proliferation. TMZ works by inducing DNA methylation, which in turn arrests the cell cycle and, consequently, induces apoptosis, autophagy and senescence [7]. Since the methylation of the O^6 position of guanine caused by TMZ can only be repaired by the enzyme, MGMT [8], tumors expressing MGMT may exhibit a natural resistance to TMZ. However, resistance to TMZ can still develop over time, even in tumors that responded positively to treatment with it. Studies examining the role of hypoxia in TMZ resistance have found that, while hypoxia mediates some important processes that facilitate TMZ resistance in GBMs, the tumors can be resensitized via hyperoxia [9–11]. Similarly, anti-angiogenesis-based therapies such as targeted therapy using the vascular endothelial growth factor (VEGF) inhibitor, bevacizumab are also susceptible to the same problem of resistance due to hypoxia. As with TMZ, bevacizumab resistance has also been linked to hypoxia [12,13]. Moreover, GBM tumors are difficult to treat due to their heterogeneous nature. In particular, their concentration of glioma stem-like cells (GSCs) can pose a distinct challenge, as these cells possess properties that allow them to change their cellular phenotypes in response to existing microenvironment conditions. This plasticity has also been linked to hypoxia [14,15]. The key role played by hypoxia in regulating the microenvironments of many different types of tumors has led researchers to focus greater amounts of attention on the potential of therapies targeting hypoxic regions [16].

The metabolomic reprogramming of cancer cells is a well-known phenomenon. The stressful environment created by hypoxia generally impairs oxidative phosphorylation and TCA cycle activity in the intensely proliferating tumor cells and enhances glycolysis and lactic acid production. This phenomenon, also known as the Warburg effect, is indirectly strengthened by HIF-1 expression in hypoxic environments. However, it remains unclear how exactly hypoxia influences the metabolomic reprogramming of tumor cells. As such, the development of models that more accurately represent tumor microenvironment metabolomics is required [17–19].

Metabolomics, along with genomics, transcriptomics, and proteomics, comprise the group of sciences known as "Omics." Metabolomics focuses on the analysis of small molecules (<1.5 kDa) produced as a result of metabolism [20]. It is possible to obtain a relatively full picture of the state of a given cell or tissue by analyzing its endogenous and exogenous metabolites [21]. The great advantage of metabolomics is that the metabolome accurately mirrors the phenotype and influence of factors external to the analyzed cell, which cannot be captured as precisely with genomics or proteomics [22].

Recently, in vitro studies using both established GBM cell lines and primary GBM cells have been gaining in popularity due to rapid developments in 3D in vitro culture techniques. One reason for this surge in popularity is that 3D culture systems provide a more accurate microenvironment, as they capture important cell-matrix and cell-cell interactions that are absent from cells cultured as a two-dimensional monolayer (2D) [23,24]. However, there are many challenges that must be overcome in order to efficiently conduct metabolomic research using in vitro cell cultures, both 2D and 3D. For example, metabolomics requires careful experimental design with regards to cell culture normalization, cell disruption, metabolism quenching, and metabolome extraction [25]. 2D cell culture is a well-known model for in vitro studies that is easier to normalize, opposed to 3D cell cultures, where each cell spheroid can have different cell number, size, and shape. Standard monolayer culture is also easy to conduct, as protocols for culturing and testing 2D cell cultures were well established through the years. In turn, 3D cell culture reflects in vivo tumor complexity better, yet it is a relatively new culture method and standard culturing and testing protocols are yet to be established. Nevertheless, with appropriate experimental design, metabolomics of GBM cell

cultures can deliver information about alternate metabolic pathways, potential biomarkers, and with proper in vitro-in vivo extrapolation (IVIVE), drug development and repurposing.

This review provides an overview of the major sample-preparation methods for metabolomics analysis, and analyzes promising metabolomics studies with GBM cell lines within the context of the potential biomarkers, therapeutic targets, and IVIVE.

2. Sample Preparation for In Vitro Studies

Investigations of the metabolomes of various GBM cell lines consist of two parts: extracellular and intracellular. The extracellular investigation is performed using a cell-culture medium that is simply pulled after cell growth, followed by an optional centrifugation step and the addition of an organic solvent for LC-MS and GC analysis (e.g., methanol, acetonitrile) [26–28]. An additional derivatization step is required for GC analysis [27,29], while medium filtration with either deuterated water [30], deuterated water with sodium 3-trimethylsilyl [2,2,3,3-2H4] propionate (TMSP), sodium 3-(trimethylsilyl)propionate-2,2,3,3-d4 (TSP), or sodium (2,2-dimethyl-2-silapentane-5-sulfonate) (DSS) is required for nuclear magnetic resonance (NMR) analysis [31]. The extracts are subjected to ultracentrifugation prior to LC and GC analysis in order to remove proteins and debris (e.g., from serum used in medium or cell debris). In one case, extracellular amino acid profiling was performed via protein precipitation with sulfosalicylic acid, followed by labelling with aTRAQ^{TM} agent [32].

The first step in most documented intracellular analysis protocols entails washing the sample in cold PBS solution in order to quench the metabolism of cells, which prevents alterations to metabolomics patterns from further manipulation. After this initial metabolism-quenching step one of two major approaches can be employed: examining cell detachment, or directly applying cold organic solvent to the surface of the growing cells. Cell detachment is assessed via trypsinization or manual cell scraping, followed by the addition of a solvent. These two steps are sometimes combined by adding the organic solvent directly onto the cell culture plate/Petri dish, followed by cell scraping. Next, the sample is transferred into tubes and vortexed/shaken, followed by ultracentrifugation in order to remove any debris. After ultracentrifugation, the samples are evaporated and either (1) reconstituted with a solvent that is compatible with liquid chromatography, (2) derivatized and injected on gas chromatography, or (3) reconstituted with deuterated water spiked with TSP [33–35], TMSP [31,36,37], DSS [38], and propionic-2,2,3,3,-d4 acid [38] or TMS [39] for nuclear magnetic resonance analysis. Aside from the above-described simple liquid-liquid extraction approach, researchers have also employed a dual-phase extraction approach. Briefly, this protocol entails the sequential addition of methanol, chloroform, and water (adding order varied) to a final ratio of 1:1:1 v/v/v, followed by sample mixing and centrifugation to separate the upper phase, which contains water-soluble polar metabolites, from the lower chloroform phase, which contains non-polar/lipid compounds. After separation, one or both phases are transferred into separate vials, evaporated, and reconstituted. The methanol:water phase can be further cleaned using divalent ions from Chelex-100 resin [40]. Another unique approach was developed by Izquierdo-Garcia et al. [33], wherein U87 and Normal Human Astrocytes (NHA) cells were incubated in a medium containing 1-13C-glucose or L 3-13C-glutamine (Gln) in order to allow these isotopes to be incorporated into low-molecular-mass compounds, which were further determined via 13C-MRS. In addition, Izquierdo-Garcia et al. [32] also used 2-13C-pyruvic acid for their hyperpolarized 13C-MRS experiments. They performed their MRS experiments using a perfusion system, which enabled the medium to circulate from the cells immobilized on the bead and into a 10-mm MR tube [33,41]. Summarizing, sample preparation among described articles is not sophisticated as the extraction is driven by the partitioning of compounds from sample into an organic solvent. Next, a clean-up is performed, in most cases by centrifugation, followed by manipulation needed for particular instrumental platform, e.g., evaporation and resuspension in deuterated water for NMR or derivatization for GC, etc. Despite the simplicity, a high number of compounds were found and described by authors. An updated list of the sample preparation methods for an in vitro extra- and intracellular metabolome are described in Tables 1 and 2.

Table 1. Metabolites detected in in vitro GBM by metabolomics.

Project Goal	Sample Prep	Instrumental Analysis	Cell Culture Model	Cell Source	Compounds Found	IVIVE	Refrence
Cells differentiation	Intracellular metabolome: PBS wash, MeOH addition, snap freeze in liquid nitrogen, thaw, vortex, centrifugation, supernatant collection, resuspension of cell pellet with water, combining of supernatant and pellet, centrifugation, supernatant transfer and evaporation, reconstitution in 80% MeOH	LC-MS/MS Q-Exactive Orbitrap (Thermo Scientific, Waltham, MA, USA) ACQUITY UPLC CSH C18 column (2.1 mm × 100 mm, 1.7 mm, Waters); QTRAP 5500 (AB Sciex, Milford, MA, USA) Synergi Hydro-RP column (4.6 mm 250 mm, 4 mm, Phenomenex, Torrance, CA, USA)	2D	U87MG U87MG GSCs	Kynurenie; L-Formylkynurenine; Stearoylcarnitine; Propionylcarnitine; Gamma-Glu–Leu; Acetylcarnitine; Carnitine; Tetradecanoylcarnitine; NAD; LPC (18:0); Pantothenic acid; LPE (18:0); Glutathione; Hypoxanthine Xanthosine; XMP; LPC (15:0); Oxidized glutathione;trans-2-Hexadecenoyl-carnitine; Spermidine; ADP; N-Oleoylethanolamine; LPC (14:0); trans-Cinnamic acid; LPC (20:1); Proline; Valine; 2-Hydroxycinnamic; Leucine; IMP; D-Glucose 6-phosphate; LPC (22:6); Pentanoylcarnitine; Palmitoylcarnitine; Oleoylcarnitine; Guanosine; Methionine sulfoxide; Guanine; Pyrrolidonecarboxylic acid; Creatine; GMP; UMP; N-Acetyl-D-glucosamine; Choline; Tryptophan; Indoleacrylic acid; Glycerophosphocholine; 5′-Methylthioadenosine; Phenylalanine; UDP-N-acetyl-glucosamine; Pantothenic acid; LPE (18:1); UDP-glucose; Tyrosine; N1-Acetylspermine; N1-Acetylspermidine	ND	[42]
Biomarker discovery	Quenching: Ice-cold PBS wash, MeOH add, mechanical scraping chloroform and water add, vortex, orbital shake, centrifugation, transfer of polar phase (methanol:water) into separate vial, evaporation, reconstitution with deuterated water (with 1.5 M KH2PO4 and 0.1% TSP), vortex, centrifugation, supernatant analysis	^{1}H NMR Bruker Avance III600 MHz spectrometer, (Billerica, MA, USA)	2D	CHG5 SHG44 U87 U118 U251	Valine; Leucine; Isoleucine; Lysine; Glutamate; Glutamine; Glutathione; Threonine; Tyrosine; Phenylalanine; Taurine; Creatine; Lactate; Glycerophosphocholine; Myo-inositol; Formate; Acetate	ND	[34]

Table 1. *Cont.*

Project Goal	Sample Prep	Instrumental Analysis	Cell Culture Model	Cell Source	Compounds Found	IVIVE	Refrence
Drug treatment	Extracellular metabolome: cell culture medium collection, centrifugation, store (−80 °C), addition of Na2HPO4:deuterated water and TMSP, pH adjustment with HCL Intracellular metabolome: Cell pellet ice-cold PBS wash ×4, trypsinization, centrifugation, reconstitution with buffer, sonication, centrifugation, freeze, deuterated water with H2O containing 10 mM TMSP add	^{1}H NMR Bruker 900-MHz spectrometer, (Billerica, MA, USA)	2D	GL261	Acetate; Acetoacetate; N-acetylaspartate; Alanine; L-alanyl-l-glutamine; arginine; l-asparagine; l-aspartic acid; cadaverine; citrate; creatine; choline; dimethylamine; ethanol; fumarate; formate; d-glucose; glucose-6 phosphate; glutamate; l-glutamine; glycine; l-sistidine; l-isoleucine; lactate; l-leucine; l-lysine; malate; l-methionine; methyloxovalerate; myo-inositol; niacinamide; Puryvate; Succinate; l-phenylalanine; Phosphocreatine; l-threonine; l-tyrosine; l-tryptophan; l-valine;	ND	[31]
Biomarker discovery	Targeted intracellular metabolome: cold PBS wash, cold MeOH:water add, mechanical scraping, transfer into tube, chloroform add, sonication, centrifugation, lyophilization, dissolving with MeOH:water, derivatization with AccQTag kit (Waters, Milford, MA, USA)	Untargeted approach CE-MS Agilent 7100 coupled with 6224 TOF-LC/MS (Agilent Technologies, Santa Clara, CA, USA) Targeted approach Agilent 6460 Triple Quad LC/MS Agilent C18 Column (2.1 mm × 100 mm, 1.8 um (Agilent, Santa Clara, CA, USA)	2D	U251 U87	Cysteine; Hypotaurine; Taurine; Cystine; Cysteinesulfinic acid	Achieved—targeted compounds were found within glioma tissue derived from patients	[43]

Table 1. *Cont.*

Project Goal	Sample Prep	Instrumental Analysis	Cell Culture Model	Cell Source	Compounds Found	IVIVE	Refrence
Biomarker discovery—ASS negative vs. ASS positive GBM	Extracellular metabolome: Frozen supernatant (−80 °C) thaw, MeOH:water (9:1) add, shake, centrifugation, supernatant transfer evaporation, storage (−80 °C), methoxyamine solution in pyridine add, trimethylsilylation, heptane with methyl stearate add Intracellular metabolome: Frozen cell pellet (−80 °C) thaw, MeOH:water (9:11) add, beads homogenization, centrifugation, supernatant transfer, evaporation, storage (−80 °C), methoxyamine solution in pyridine add, trimethylsilylation, heptane with methyl stearate add	GC-TOFMS Agilent 6980 GC (Agilent, Santa Clara, CA, USA) Pegasus III TOFMS (Leco Corp, St Joseph, MI, USA) DB5-MS Column (10 m × 0.18 mm × 0.18 µm, J&W Scientific, Folsom, CA, USA) 2D GC-TOFMS Pegasus 4D (Leco Corp, St Joseph, MI, USA) coupled with Agilent 6890 GC (Agilent Technologies, Palo Alto, GA, USA) Column BPX-50 (30 m × 0.25 mm × 0.25 µm, SGE) Column VF-1MS (1.5 m × 0.15 mm × 0.15 µm; J&W Scientific Inc, Folsom, CA, USA)	2D	LN229 SNB19 GAMG U118 T98G U87 Normal Human Astrocytes (NHA)	Pyrophosphate; Erythrose-4-Phosphate; Glucaric Acid; 1,4 Lactone; Ribofuranose; Ribose; Ribose-5-Phosphate; Putrescine; Spermidine; Adenine; Hypoxanthine; Uracil; Uridine; Erythritol; Taurine; Tryptophan; Tyrosine; Arginine; Ammonia; Proline; Arginine; Asymetrical-N,N-Dimethylarginine; Citrulline; Ornthine; Citrulline; N-Acetylornithine; Ornithine; 2-Oxoisocaproic Acid; Isoleucine; Leucine; Valine; 1,2-Ethandimine; 1,3,5-Trioxepane; 1-Monostearoylglycerol; 2-Pyrrolidone-5-Carboxylic Acid; Aminomalonic Acid; Cadaverine; Cellotriose; Dihydroxyacetonephosphate; Elaidic Acid; Glucopyranos; N-Acetyl Glutamyl Phosphate; Nonanoic Acid; Phosphoric Acid; Pyrazine; Stearic Acid; Xylitol	ND	[29]
Subtype determination	Intracellular metabolome: Cell harvest by scraping, PBS wash x2, centrifugation, incubation on ice, suspension in ice-cold acetonitrile (50%), incubation on ice, centrifugation, evaporation, dissolve in deuterium oxide	^{1}H NMR Bruker Avance III 400 MHz spectrometer, (Billerica, MA, USA)	2D	LN229 VLN319	Taurine; Glutamine; UDP; Glutamate; Choline; Citric acid; Phosphocholine; Aspartate; Glycerophosphocholine; Asparagine; Glycine; Methionine; myo-Inositol	ND	[30]
				HS683 LN405	Valine; Glutamate; Leucine; Citric acid; Isoleucine; Aspartate; Alanine; Asparagine; Lactate; Methionine		
				A172 U343 LN18	GABA; Methionine; Proline; Citric acid; Glutamine; Aspartate; Glutamate; Asparagine;		
				U373 BS149	Succinic acid; Glycerol 3-phosphate; Serine; Glucose; Adenine; cis-Aconitic acid; Taurine; GABA; Lysine; Proline; Tyrosine		

Table 1. *Cont.*

Project Goal	Sample Prep	Instrumental Analysis	Cell Culture Model	Cell Source	Compounds Found	IVIVE	Refrence
Drug treatment	Intracellular metabolome: Ice-cold PBS wash, cell scraping, centrifugation, cold PBS wash, snap freeze in liquid N2, deuterated water add	^{1} H NMR Varian 600MHz (14.1 T) spectrometer, (Oxford, UK)	2D	BT4C (rat)	Acetate; Alanine; Aspartate; Choline; Creatine; Glutathione; Glutamate; Glutamine; Glycerophosphocholine; Glycine; Lactate; myo-Inositol; PC; Peth; Scyllo-Inositol; Succinate; Taurine; Hypotaurine; Guanosine		[44]
Culture conditions evaluation	Intracellular metabolome: PBS wash, cold MeOH add, cell scrapping, transfer into tube, chloroform add, vortex, water add, vortex, transfer of water:MeOH phase, Chelex-100 add, centrifugation, lyophilization, resolving in deuterated water based buffer with DSS and propionic-2,2,3,3,-d4 acid	1 H NMR Bruker Avance 500 spectrometer, (Billerica, MA, USA) Bruker Avance III HD 600 spectrometer, (Billerica, MA, USA)	2D and 3D	U87	Adenine; myo-inositol; Glycine; PC; Glycerophosphocholine; Free choline; Total choline; Total creatine; Glutathione; Glutamine; Glutamate; N-acetylaspartylglutamate; Alanine; Lactate; Threonine; Valine/isoleucine;	ND	[38]
Biomarker discovery—IDH1 wildtype	Live cells metabolomic: 1-13C-glucose and L-3-13C-glutamine or 2-13C-pyruvic acid add to cell culture medium intracellular metabolome: 1-13C-glucose or 3-13C-glutamine add to cell culture medium, cell trypsinization, centrifugation, cold MeOH addition, vortex, cold chloroform add, cold water add, transfer of MeOH:water phase, lyophilization, reconstitution with deuterated water with TSP	13C-MRS500 MHz INOVA spectrometer (Agilent Technologies, Santa Clara, CA, USA) 1H MRS 13C-MRS spectra 500 MHz Avance spectrometer (Bruker BioSpin, (Billerica, MA, USA))	2D and 3D	U87 NHA BT54 BT142	Glutamate; 2-Hydroxyglutarate	ND	[45]

Table 1. *Cont.*

Project Goal	Sample Prep	Instrumental Analysis	Cell Culture Model	Cell Source	Compounds Found	IVIVE	Refrence
Biomarker discovery	Intracellular metabolome: saline wash, cell scraping, transfer into tube, saline wash, centrifugation, cold MeOH:chloroform:water add, centrifugation, resuspension, sonication, centrifugation, supernatant transfer for derivatization and analysis	GC-TOF-MS Agilent 6890 (Waldbronn, Germany), LECO Pegasus 2 TOF (St Joseph, MI, USA)	2D	U87	Citric acid; Cis-aconitic acid; Succinate; Fumarate; Malate; Glucose-6-phosphate; Phosphoenolpyruvic acid; Pyruvate; Lactate; Isoleucine; Leucine; Lysine; Methionine; Phenylalanine; Threonine; Tryptophan; Valine; Cysteine; Tyrosine; Histidine; Alanine; Asparagine; Aspartate; Glutamate; Glutamine; Glycine; Proline; Serine; Ornithine; Hexadecanoic acid; Octadecanoic acid; Octodecenoic acid;Phosphatidyl-l-serine; Ethanolamine; Cholesterol; Glycerol; Glycerol-3-phosphate	ND	[46]
Drug treatment	Cell scraping, PBS wash, centrifugation, pellet PBS wash, centrifugation, resuspension with ACN:water (1:1), ultracentrifugation, supernatant evaporation, dissolving in deuterated water	1H NMR Bruker Avance III 400 MHz spectrometer, (Billerica, MA, USA)	2D	A172, LN18, LN71, LN229, LN319, LN405, U373, U373R*	Phosphorylcholine; Glycerol-3-phosphate; Serine; Choline; Histidine; Succinate; Taurine; Tryptophan; Glycine; Glutathione—reduced; Citric acid; Glutamine; Phosphorylcholine; Leucine; Choline; Lysine; Isoleucine; Alanine; Proline; Glycerol-3-phosphate; Phosphorylcholine; Aconitate; Taurine; Tryptophan; Alanine; Threonine; Valine; Acetone; Aconitate; Adenine; Adenosine; Alanine; Arginine; Asparagine; Choline; Citric; Creatine; Ethanol; Glucose; Glutamate; Glutamine; Glutathione—oxidized; Glutathione—reduced; Glycerol-3-phosphate; Glycerophosphocholine; Glycine; Histidine; Isocitrate; Isoleucine; Lactate; Leucine; Lysine; Methionine; myo-Inositol; Oxoglutarate; Phenylalanine; Phosphorylcholine; Proline; Serine; Succinic Acid; Taurine; Threonine; Tryptophan; Valine	Most compounds were found in primary GBM tissue	[47]
Drug treatment	Scrapping with cold PBS in deutered water, 2x wash, filling 50 µL inserts with cells, snap-freezing	HR-MAS Bruker 500 MHz spectrometer, (Billerica, MA, USA)	2D	U87	myo-Inositol; Glycerophosphocholine; Lipids; CH = CH; CH = CHCH2CH = CH	ND	[48]

Table 1. *Cont.*

Project Goal	Sample Prep	Instrumental Analysis	Cell Culture Model	Cell Source	Compounds Found	IVIVE	Refrence
Drug treatment	Intracellular metabolome: PBS wash, cold MeOH:water (4:1), ultracentrifugation, transfer into vial	LC-MS Agilent 1290, Agilent 6520 TOF (Santa Clara, CA, USA) column: Waters Acquity UPLC BEH (bridged ethyl hybrid) Amide 1.7 µm 2.1 × 100 mm HILIC, (Milford, MA, USA)	2D	Res259 Res186 BT66 JHH-NF1-PA1	Glutamine; Glutamate; Glutathione	Achieved—similar pathways were found in vivo in patient derived xenograft in mice	[49]
Drug treatment	Intracellular phosphometabolome: Cold saline wash, trypsinization, centrifugation, perchloric acid add, sonication, neutralization with KOH, ultracentrifugation, Chelex-100 add, filtration, pH adjustment, lyophilization, dissolving in deuterated water Intracellular phospholipidome: Cold saline wash, cell scrapping, transfer to tube prefilled with cold MeOH, chloroform add, shake, separation funnel filter, KCL wash, overnight separation, chloroform phase collection, evaporation, dissolving in chloroform, MeOH:EDTA add	31P MRS Varian Inova500, (Oxford, UK)	2D, 3D and cocultures	C6	Phosphatidic acid; Cardiolipin; Plasmenyl phosphatidylethanolamine; phosphatidylethanolamine; Phosphatidylserine; Sphingomyelin; Phosphotidylinosine; Plasmenyl phosphatidylcholine; Phosphatidylcholine	ND	[50]
Drug treatment	cell centrifugation, pellet resuspension in water, MeOH:chloroform with BHT add, periodical vortex, chloroform and KCL add, vortex, centrifugation, chloroform phase collection, evaporation, reconstitution in MeOH:chloroform (1:1)	LTQ-Orbitrap Elite instrument 538 (Thermo Fisher Scientific, Waltham, MA, USA) equipped with a robotic 539 nanoflow ion source TriVersa NanoMate (Advion BioSciences, Ithaca, NY, USA quantification with GC-MS GCMS-QP2010, Shimadzu, (Japan), column: 10 m × 0.1 mm ID, 0.2 µm film thickness	2D	U87	Cholesteryl ester; Cardiolipin; Glucosylceramide; Lysophosphatidylcholine; Lysophosphatidylethanolamine; Phosphatidic acid; Phosphatidylcholine (diacyl); Phosphatidylcholine (alkyl–acyl); Phosphatidylethanolamine (diacyl); Phosphatidylethanolamine plasmalogen (alkenyl–acyl); Phosphatidylglycerol; Phosphatidylinositol; Phosphatidylserine; Sphingomyelin; Triacylglycerol	ND	[51]

Table 1. *Cont.*

Project Goal	Sample Prep	Instrumental Analysis	Cell Culture Model	Cell Source	Compounds Found	IVIVE	Refrence
Biomarker discovery	Intracellular metabolome: Cell dissociation, PBS wash, centrifugation, freeze, upon analysis deuterated water add	NMR Bruker Avance III spectrometer (Bruker BioSpin, Billerica, MA, USA)	2D, 3D and mixed 2D/3D	Primary glioblastoma	Acetate; Alanine; Choline; Creatine; GABA; beta-Glucose; Glutamate; Glutamine; Glycerophosphocholine; Glycine; lactate; myo-Inositol; N-Acetylaspartate; PC; Serine; Taurine; Valine	Achieved—some pathways altered in 3D and 2D/3D matched pathways in patient tumor relapse	[52]
Drug treatment	Intracellular metabolome: PBS wash, cold MeOH add, cell scraping, transfer into tube, chloroform add, vortex, water add, vortex, separation of water:MeOH phase, Chelex-100 add, centrifugation, lyophilization, resolving in deuterated water with TSP	1H NMR Bruker Avance 500 spectrometer, (Billerica, MA, USA)	3D	Self-derived cell lines: GBM1 040922 GBM1016 GBM1417 commercial cell lines: LN229, U87	Valine/Isoleucine; Threonine; Lactate; Alanine N-acetylaspartylglutamate; Glutamate; Glutamine; Glutathione; Total Creatine; Free Choline; PC; Glycerophosphocholine; Glycine; myo-Inositol	ND	[35]
Drug treatment	Targeted intracellular metabolome: ice-cold PBS add, cell scraping centrifugation, pellet resuspension with MeOH:water (7:3), agitation, incubation in −20 °C, IS load, agitation, ultracentrifugation, supernatant collection, solvent evaporation, reconstitution with 2 mM ammonium acetate and 3 mM hexylamine solution.	LC-MS/MS MDS SCIEX 4000QTRAP hybrid triple quadrupole/ linear ion trap mass spectrometer (Applied Biosystems, Waltham, MA, USA) Waters Acquity BEH C18 column (2.1 × 50 mm, 1.7 µ) (Milford, MA, USA)	2D	U87MG	dATP; dCTP; TTP	ND	[53]
		Acquity HSS T3 column (2.1 Å~ 100 mm, 1.8 µm).			Carbamoyl aspartate; Orotic acid		
Biomarker discovery	PBS wash, centrifugation, pellet resuspension with deuterated water and TMSP, centrifugation	1H NMR Advance spectrometer (Bruker, AG, Darmstadt, Germany)		T98G primary glioma cells and neural stem/progenitor cells	myo-Inositol; UDP-hex; N-Acetylaspartate; O-2A; Glycine; Aspartate; O-2A; Total Creatine; Glycine; Lip; Glutamine; GSH; Glutamate; GABA; GalNAc;	ND	[37]

Table 1. *Cont.*

Project Goal	Sample Prep	Instrumental Analysis	Cell Culture Model	Cell Source	Compounds Found	IVIVE	Refrence
Therapeutic targets/drug treatement	Intracellular metabolome: Cell harvest, PBS wash, ice-cold NaCL (0.9 mM) wash x2, suspension in ice-cold H2O, of ice-cold MeOH add, vortex, incubation, ice-cold chloroform add, vortex, incubation, ice-cold H2O add, vortex, incubation, centrifugation, water-methanol phase collection, Chelex-100 add, filtration, evaporation, freezing (−80 °C) lyophilization	1H NMR Bruker AVANCE III HD 700 spectrometer 700 MHz (Billerica, MA, USA))	2D and 3D Tissue samples	JHH520 GBM1 23, 233, 268, 349 407 SF188 NCH644	Alanine; Aspartate; Glutamine; Glutamate; Glycine; Glutathione; Lactate; Myo-inositol; PC; Succinate; Tricarboxylic acid; Total choline; Total creatin	ND	[54]
Therapeutic targets assesement	Intracellular metabolome GC-MS HOG, NHA: ice-cold saline wash, culture plate snap freeze with liquid N2, cold MeOH:water (7:3) add, chloroform add, vortex, centrifugation, MeOH:water phase separation, evaporation GSC lines: cold saline addition, neurosphere transfer into tube, centrifugation, freeze of pellet with liquid N2, cold MeOH:water (7:3) add, chloroform add, vortex, centrifugation, MeOH:water phase separation, evaporation Derivatization with methoxyamine and N-(tert-butyldimethylsilyl) -N-methyl-trifluoroacetamide/1% tert-butyldimethylchlorosilane LC-MS/MS performed as for GC-MS with exception that MeOH:water (4:1) was used and dried extract were resuspended with water Extracellular metabolome medium collection, MeOH, Water (7:3) add, rest as above for GC-MS and LC-MS/MS	GC-MS using an Agilent 7890A (Santa Clara, CA, USA) 5500 QTRAP hybrid triple quadrupole mass spectrometer (AB/SCIEX, Framingham, MA, USA), Amide HILIC chromatography (Waters, Milford, MA, USA)		NHA HT1080 HOG IDH1 R132H mutant IDH2 R172K mutant HCT116 NCI-H82 HEK293T GSC lines: TS603, TS516, TS676, MGG152 BT054 BT260	Glutamate; 2-Hydroxyglutarate; alpha-Ketoisocaproate; Valine; Leucine; Isoleucine; alpha-Keto-beta-methylvalerate	Achieved—increased BCAT activity in vitro and in vivo in xenograft mice	[27]

Table 1. *Cont.*

Project Goal	Sample Prep	Instrumental Analysis	Cell Culture Model	Cell Source	Compounds Found	IVIVE	Refrence
Drug treatment	Intracellular metabolomie: 3× freeze/thaw cycles of water based cell suspension, cold MeOH add, agitation, chloroform add, agitation, ultracentrifugation, collection of chloroform phase, evaporation, reconstitution with TMS:deuterated MeOH Intracellular lipidomice: Cold PBS wash, cell scraping on dry ice, freeze, sonication, centrifugation, pellets resuspend in water, centrifugation, pellet snap freeze on dry ice, storage (−80 °C), extraction: resuspension in water, probe sonication, bath sonication, MeOH:water spiked with IS add, vortex, ice bath incubation, cold chloroform add, incubation 1 h, ultracentrifugation, separation of MeOH;water and chloroform phases, ACN:W (1:1) add, centrifugation, evaporation, snap freezing with dry ice, −80° C storage, combining of both phases in MeOH:ACN:water buffer live cell culture imaging	1H NMR Bruker Avance III 600 MHz spectrometer (Structural Biophysics Laboratory, NCI, Frederick, MD, USA) LC-TOF Q-TOF SYNAPT G2 Si (Waters Corporation, (Milford, MA, USA) Acquity UPLC CSH 1.7 m, 2.1 × 100 mm column (Waters Corp., Milford, MA, USA Raman spectroscopy DXR2xi Raman microscope (ThermoFisher Scientific, Madison, WI, USA)	2D	HT1080	Lipidomics: 1-O-eicosanoyl-Cer d18-1,16-0; 1-O-tricosanoyl-Cer d18-1,18-0; 5-methyldeoxycytidine; Acetylcysteine; Cholesteryl Ester—CE 31-0; Cer d45-1; Cer d50-2; Cer d51-1; PhytoCer t48-1; PhytoCer t53-1; Diacylglycerol: 46-5, 56-9, 57-0, 60-0, 61-1, 64-0, 64-1, 66-1, 67-0, P-36-3, P-39-0, P-43-0, P-44-4, P-48-0, P-48-4, P-49-0, P-50-0, 60-0, P-51-0 Dopamine; Dopamine quinone; pinephrine sulfate; GluCer d39-0; Glutaminyl-arginine; Glutaminylcysteine; Glyceraldehyde; Isovaleric acid amine; Isovalerylglutamic acid; LacPhytoCer t50-0; L-histidine; Methyldeoxycytidine; N2,N2-dimethylguanosine; N-acetyldopamine; N-succinyl-2-amino-6-ketopimelate;O-tricosanoyl-N-hexadecanoyl PA: 43-2, 49-4, 52-4, O-41-0; PC: 22-4, 21-0, 39-6, 40-3; PE: 40-2, 49-4; Phosphoglycolic acid; PI P-36-4; PS 43-2; Pyroglutamic acid; Pyrrolidonecarboxylic acid; Sn-glycero-3-phosphoethanolamine; S-Succinyldihydrolipoamide; Succinyl acetoacetate; TG 15-0,18-1,14-1	Achieved—decrease in lipids observed via Raman imaging microscopy both in vitro and in vivo after dug treatement	[39]

Table 1. *Cont.*

Project Goal	Sample Prep	Instrumental Analysis	Cell Culture Model	Cell Source	Compounds Found	IVIVE	Refrence
Biomarker discovery	Intracellular metabolome: Cell harvest, PBS wash, centrifugation, incubation on-ice, cold acetonitrile:water (1:1) resuspension, centrifugation, freeze drying, D_2O add Extracellular metabolome: Medium supernatant filtration, storage (−80 °C), mixing with D_2O Exosomal metabolome: ultracentrifugation, PBS wash, centrifugation, incubation on-ice, cold acetonitrile:water (1:1) resuspension, centrifugation, freeze drying, D_2O add	1H NMR Bruker 600 MHz spectrometer, (Billerica, MA, USA)	2D	U118 LN-18 A172 NHA	Formate; Asparagine; Taurocholic acid; Glycerol; Malate; Niacinamide; Lactate; Acetone; 5-oxoproline; Citrate; Proline; Succinate; Ethanol; GSH; GABA; G6P; Isoleucine; Glucose; Taurocholate; Homoserine; Glycine; Carnitine; GSSG	ND	[55]
Drug treatment	culture plates place on ice, cold PBS wash, cell scraping into PBS, transfer into tube, cold MeOH add, sonication, centrifugation, supernatant transfer evaporation, reconstitution in deuterated water with TMSP	1H–NMR AVANCE III 600M NMR Bruker (Germany)	2D	U87	Leucine; Alanine; Creatine; Glutamate; Glycine; Lactate; myo-Inositol; Glycerophosphocholine; Isoleucine; Taurine; Glutathione; Lysine; NAD+; UDP–NAG	ND	[36]
Biomarker discovery/Culture conditions evaluation	intracellular metabolome: cold MeOH add, water add, grinder homogenization, sonication, ultracentrifugation, lyophilization, resuspension with deuterated water	1H-NMR Bruker Avance III HDX 600-MHz FT-NMR Spectrometer, Billerica, MA, USA)		primary	Alpha-ketoglutarate; Succinic acid; Glutathione; Fumarate; Dodecanoic acid; Caproic acid; N-Acetylserotonin; Stachyose; Glyceraldehyde; Serine; Fructose; Lysine; Arginine; Glucose-6-phosphate, Selenomethionine; Glycine; Choline; Guanidoacetic acid; Guaiacol; Oxoglutaric acid; Gamma-Aminobutyric acid	Achieved—similar spatial differences of the metabolic environment	[56]
drug treatment	extracellular amino acid profiling: medium transfer, sulfosalicylic acid add, buffer add, labeling with aTRAQ™(Sciex, Milford, MA, USA), incubation, evaporation, resuspension	C-MS/MS C18 Column Reverse Phase (5 µm, 4.6 mm × 150 mm)	2D	primary U87-MG	Serine; Methionine; Glycine; Tyrosine; Aspartic acid; Isoleucine; Alanine; Leucine; Threonine; Norleucine; Glutamate; Phenylalanine; Histidine; Proline; Arginine; Methionine sulfoxide; Cystine; Lysine; Valine; Norvaline	ND	[32]

Table 1. *Cont.*

Project Goal	Sample Prep	Instrumental Analysis	Cell Culture Model	Cell Source	Compounds Found	IVIVE	Refrence
Biomarker discovery/Culture conditions evaluation	extracellular metabolome: medium collection, ACN add, −80 °C store untill analysis, dilution intracellular metabolome: cold PBS wash, cold ACN add, −80 °C short incubation (3 min), cell scrapping, transfer into tube, cold water add, freeze/thaw lysis with vortex (3× times), ultracentrifugation, supernatant store at −80 °C	LC-QTOF 6520 Accurate Mass Q-TOF LC/MS (Agilent Technologies, Santa Clara, CA, USA) biomarker validation 6430 Triple Quad LC/MS (Agilent Technologies, Santa Clara, CA, USA), doczytac czy do metabo byl tez ten MS reverse-phase C18 stable bond column (2.1 mm × 50 mm × 1.8 µ) (Agilent Technologies, Santa Clara, CA, USA).		primary U118 U87 LN18 LN229 NHA	Kynurenine; Tryptophan; Methionine; 5′-methylthioadenosine; S-adenosylmethionine; S-adenosylhomocysteine	Achieved—methionine was found in ex vivo in fresh glioblastoma biopsy tissue	[28]
Therapeutic targets assessment	Intracellular metabolome: Ice-cold PBS wash, cell lysis with dry ice/methanol − 80 °C, (80% methanol), scrapping, centrifugation, supernatant collection	UHPLC/MS Waters Acquity UHPLC (Waters Corporation, Milford, MA, USA) LTQ mass spectrometer (Thermo Fisher Scientific Inc. Madison, WI, USA) GC/MS Thermo-Finnigan Trace DSQ MS (Thermo Fisher Scientific, Inc. Madison, WI, USA)	2D in hypoxia	U87	Aldolase; Enolase 2; Glucose-6-phosphate isomerase; Hexokinase; Lactate dehydrogenase A; Pyruvate dehydrogenase kinase 3; Phosphofructokinase; Phosphofructo-2-kinase/fructose-2,6-biphosphatase; Phosphoglycerate mutase; Phosphoglycerate kinase 1; Pyruvate kinase isoenzyme type-M2	ND	[57]
Gln deprivation influence	Intracellular metabolome: Ice-cold PBS wash ×3, H2O:MeOH:acetonitrile (2:5:3) add, centrifugation, supernatant collection Extracellular metabolome: Culture media dilution with H2O:MeOH:acetonitrile (2:5:3), centrifugation, supernatant collection	HPLC-MS ZIC-HILIC (SeQuant) with a guard column (Hichrom) Exactive Orbitrap mass spectrometer (Thermo Scientific, Madison, WI, USA)	2D	MOG-G-VW LN-18 LN-229 SF-188 U-251 MG U-87 MG Primary rat astrocytes Primary human GBM: E2 R10 R24	Glutamine; Leucine; Isoleucine; Serine; Valine; Alanine; Lysine; Cysteine S-S; Threonine; Arginine; Proline; Methionine; Asparagine; Ornithine; Taurine; Phenylalanine; Tyrosine; Citrulline; Histidine; Tryptophan; Aspartate; Glycine; Glutamate; Pyruvate; Lacate	ND	[26]

Table 1. *Cont.*

Project Goal	Sample Prep	Instrumental Analysis	Cell Culture Model	Cell Source	Compounds Found	IVIVE	Refrence
Nanoparticles toxicity	intracellular metabolome: ACN:MeOH (1:1) with α-cyano-4-hydroxycinnamic add onto cells	MALDI-MS/MS MALDI LTQ-XL instrument (Thermo Scientific, Madison, WI, USA)	2D	NG97	2-hydroxy-eicosanoic acid; Docosapentaenoic acid/octadecanoic acid (stearic acid); N-oleyl-alanine; N-stearoyl-alanine;	ND	[58]
Stem-like cells metabolome evaluation	Intracellular metabolome 2D culture: Cold ammonium acetate wash, snap-freezing in liquid nitrogen, ice-cold MeOH:H2O (4:1) add, scrapping, mix, centrifugation, supernatant collection Intracellular metabolome 3D culture: Neurospheres collection, cold ammonium acetate wash, snap-freezing in liquid nitrogen, ice-cold MeOH:H2O (4:1) add, mix, centrifugation, supernatant collection	LC-MS DIONEXUltimate 3000 UPLC HILIC column (AcclaimMixed-Mode HILIC-1, 3 µm, 2.1 × 150 mm) Q Exactive mass spectrometer (QE-LC-MS(Thermo Scientific, Madison, WI, USA)	2D and 3D	U87 NCH644—patient derived stem-like cells	Carbomyloaspartate; Citruline; Proline; Arginine; Aspartate; Ornithine	ND	[59]
IDH1-mutant glioma metabolic reprogramming	intracellular metabolome: cell trypsinization, centrifugation, cold MeOH add, vortex, cold chloroform add, cold water add, separation of MeOH:water phase, lyophilization, reconstitution with deuterated water with TSP	1H–MRS 600 MHz Bruker Avance spectrometer (Bruker Biospin, Rheinstetten, Germany)	2D	U87 NHA with or without IDH1 mutation	Aspartate; Glutamate; Glutamine; Glutathione; Lactate; myo-Inositol; PC; Glycerophosphocholine; 2-Hydroxyglutarate; alfa-Butyrate; Creatine; Hydroxybutyrate; Valine	ND	[33]

Table 2. Sample preparation techniques used for in vitro GBM cell lines.

Sample Prep Technique	Instrumentation	Simplicity (Number of Steps)	Derivatization Step Included	Advantages	Disadvantages	Reference
dual-phase extraction	1H NMR	complicated (10–19)	-	broad metabolome coverage: polar metabolites and lipids	time consuming, phase separation required, lyophilisation: additional lab equipment needed	[32–34,37,38,44,53]
	1H MRS					
	LC-MS					[26,38,50]
	GC-MS		+			[26]
liqiud-liquid extraction	1H NMR	easy (1–11)	-	no sample prep required	low sensitivity	[29,30,35,36,43,46,47,51,54,55]
	LC-MS		+	quantification included	Can be consider, dirty' for instrumentation: frequent maintenance needed	[31,42]
			-	High sensitivity, broad metabolome coverage		[25,27,41,48,52,56,58]
	MALDI-MS		-	fast	low metabolite coverage	[57]
	GC-MS		+	High sensitivity, broad metabolome coverage	bead homogenization requires additional lab equipment [28]	[28,45]
	31P MRS	complicated (12)	-	broader metabolome coverage: phosphometabolites and phospholipids	lyophilisation: additional lab equipment needed	[49]
none (live imaging)	13C-MRS	easy (1)	-	live imaging, possibility of time-course cell culture monitoring	targeted approach, low metabolite coverage	[44]
	Raman spectroscopy	easy (0)	-	possible application to tissue analysis suitable for imaging	direct annotation of individual compounds not possible	[38]
liquid-liquid extraction	31P MRS	complicated (12)	-	broader metabolome coverage: phosphometabolites and phospholipids	lyophilisation: additional lab equipment needed	[49]

3. Metabolomics of GBM In Vitro

Many recent studies on the development of tumor malignancy and resistance to treatment have focused on the metabolic reprogramming of cancer cells. Investigations into the metabolomic phenotype of various tumors, including brain tumors, have revealed interesting correlations between a tumor's mutations, metabolic footprint, and microenvironment [60,61]. Given these correlations, metabolomics and lipidomics may be effective tools in drug development and brain tumor diagnostics, grading, and prognosis [61,62]. Prior studies have successfully detected numerous metabolic alterations, particularly in relation to the metabolism of fatty acids and amino acids, such as Gln, choline (Cho), and cysteine (Cys) [63–66]. However, these findings represent only a small fraction of the work that has been done in GBM metabolomics and lipidomics—a body of work that is constantly growing, as researchers continue to work to identify important metabolites in GBM development. Generally, studies examining the metabolic reprogramming of cancer have utilized matrices such as blood and serum, urine, tissue samples, and established cell lines and primary cells [60,61]. While all of these matrices have been successfully employed, in vitro studies using both established cell lines and primary cells ensure replicable and strictly controlled conditions between each replicate sample. Furthermore, the analysis of culture media and disintegrated cells, along with careful sample preparation, can provide useful information about both the endo- and exo-metabolome. However, cells growing in vitro as a monolayer do not adequately recreate the tumor microenvironment. As such, researchers have increasingly been exploring the use of three-dimensional (3D) in vitro culture models, as they reflect the actual tumor phenotype more adequately than standard 2D cell cultures [67]. For these reasons, in vitro cell cultures remain of great interest in explorations of metabolic reprogramming in GBM tumors. For the sake of clarity, from now on when discussing metabolic studies on in vitro cell cultures it will refer to the 2D culture model, as it is still considered the standard in in vitro studies, unless specified otherwise.

Metabolic alterations in cancer cells have long been explored for their usefulness in profiling of the phenotypes of many different types of tumors [68]. Prior to the development of the WHO glioma tumor classification method, researchers obtained information about different patterns in the metabolic pathways between normal and malignant cells through simple in vitro studies using established GBM cell lines (U87) and human mesenchymal stem cell lines (hMSC) [46]. In their work on intracellular metabolomes, Juerchott et al. observed alterations in the TCA cycle, with amplified concentrations of fumarate and succinate, and lower concentrations of citrate [46]. In addition, Juerchott et al. also observed that some glycolysis metabolites, such as glucose-6-phosphate (G6P), were upregulated. Many of the metabolites detected in their study would appear in later studies, not only for grading GBMs and determining prognosis, but also for determining drug treatment efficiency.

Findings have also revealed good correlation between mutations found in GBM, e.g., PDGFRA, IDH1, EGFR, and NF1—and the tumor's metabolic fingerprint. Cuperlovic-Culf et al. conducted metabolic profiling on nine established GBM cell lines and categorized them into four subtypes based on the alterations to their metabolites [30]. Their findings proved that it is necessary to monitor alterations in metabolic pathways instead of focusing on DNA mutations alone. For instance, alterations to Cho—which is known to be present in cancer cells at different concentrations than in normal cells—and its derivatives (phosphocholine (PC) and glycerophosphocholine (GPC)) were only observed in the first group of cell lines [30]. The cells in this group had a genetic profile of PDGFRA+ and EGFR-, as well as significantly higher concentrations of Cho, PC, and GPC. Izquierdo-Garcia et al.'s examination of IDH1-mutated U87 GBM cells found decreased concentrations of PC and increased concentrations of GPC [33]. Since IDH1 mutations are generally more common in low-grade gliomas, the general ratio of PC to GPC could serve as a prediction factor, such that elevated levels of PC and decreased levels of GPC would indicate high-level gliomas, such as GBM [69,70]. Moreover, a low lipids-to-GPC ratio was found to connect patient-derived cell lines and neural progenitor cells; as such, this ratio can be used to

characterize the neural phenotype of the tumor, and thus discern a better prognosis [37]. Another study revealed a correlation between the upregulation of GPCs and Cho and the differentiated state of the cells. This finding implies that impaired glycophospholipids metabolism is correlated with the tumor self-renewal and, thus, a worse prognosis [42]. Furthermore, a comparison of PC and GPC levels in pediatric GBM tumors and tumor-derived cells showed a decrease in the levels of both metabolites in both late passage cell lines and the tumor at relapse, indicating that both the tumor and derived cells had transitioned from stem-like cells into differentiated cells [52]. Nonetheless, it remains an open question whether a low PC-to-GPC ratio is a clear indicator of low malignancy grade in gliomas, with research still ongoing to determine the efficacy of these two metabolic markers. However, the ratio of total Cho to total creatine is indeed an indicator of the worse prognosis [38,71].

Inositol and myo-inositol are two additional metabolites that could potentially be useful in GBM diagnostics and prognostics, as they are known to play roles in osmoregulation and phosphatidylinositol lipids synthesis [72]. In a study conducted by Cuperlovic-Culf et al. a correlation was observed between the upregulation of myo-inositol and the PDGFRA+ and EGFR- genotypes in one of these subtypes [30]. Conversely, findings have shown that IDH mutant cells have decreased myo-inositol levels compared to an IDH wild-type cell line [33]. Kahlert et al. reported a high myo-inositol-to-glycine ratio for a U87 cell line grown in neutrospheres, which could be a marker for GBM [38]. Moreover, since myo-inositol plays a role in the metabolism of glycerophospholipids, its high concentration could be explained by the self-renewing properties of GBM tumors [42,73]. On the basis of the research discussed, it can be concluded that elevated levels of myo-inositol could be markers indicating high grade glioma.

Gln, glutamate (Glu), and γ-amniobutyric acid (GABA) each play an extremely important role in brain development. Changes in the metabolism of Gln can cause disturbances in Glu, GABA, and aspartate (Asp), as it is the precursor of these neurotransmitters [74]. Furthermore, Gln can be converted into α-ketoglutarate (α-KG), which subsequently takes part in the TCA cycle [75]. Tardito et al. highlighted GBM's dependency on Gln. Their findings indicated that synthesized Gln can be used to synthesize AMP [26]. In their study, Cuperlovic-Culf et al. determined that differences in the upregulation of Gln, Glu, Asp, and citrate were dependent on the subtype of the studied cell lines [30]. They found that the levels of these metabolites in each subtype correlated with the expression of genes for some transporters such as SLC38A1, SLC7A8, and SLC1A. Specifically, they found that the overexpression of certain cellular or mitochondrial transporters influenced the levels of these metabolites. In turn, decreases in Gln were associated with IDH1mut status [33], and enforced glutaminolysis was connected to the ASS negative cell lines [29] and the accelerated growth rate of Gln-dependent GBM cells [32]. Glutaminolysis tends to be also overexpressed in relapse tumors and cells grown in nerurospheres [52]. A study on IDH wild-type primary GBM cell cultures yielded similar results, with two clear subtypes emerging: one with increased Gln uptake, and another with low Gln uptake. The findings showed that this high Gln dependency was correlated with a mesenchymal-type tumor and the worst prognosis [32]. In another study, Guidoni et al. compared patient-derived cells to GBM cell line T98G and neural stem/progenitor cells. They observed that the levels of GABA in one of the patient-derived cell lines increased while Glu simultaneously decreased, which could be used to determine the neuronal phenotype, as GABA synthesis mainly takes place in the neurons [37,74]. Moreover, the presence of neuronal metabolic markers is correlated with better prognoses [37].

Glutathione (GSH) is a tripeptide that is composed of Glu, Cys, and glycine (Gly). GSH can take on two forms, namely reduced GSH and oxidized GSSG, which allows it to play an important role in redox regulation and protecting cells from ROS [76]. The up-regulation of GSH has been associated with groups of cell lines from WHO grade IV gliomas, which connects it to the malignant transformation of the tumor [34]. A comparison of stem-like U87MG cells to U87 malignant glioma cells and stem-like cells after induced

differentiation revealed a drop in GSSG levels and a high GSH-to-GSSG ratio. Therefore, low levels of ROS metabolites could be associated with worse prognoses, while increased levels of these metabolites could induce the differentiation of stem-like cells in tumors [42]. Similarly, decrease in GSH has been associated with the IDH1mut genotype of the U87 cell line [33]. Low GSH levels have also been observed in cells grown in neurospheres, which show more astrocyte/glioma-like metabolism. This finding indicates that decreased GSH is connected to hypoxia, and thus a worse prognosis, as was confirmed by the study's patient results [37]. However, one needs to remember that GSH easily undergoes auto-oxidation during the sample preparation step, what makes it easy to get false results [77]. To the best of our knowledge, there is no GBM study which highlights this problem, the solutions proposed based on other cell cultures, i.e., adding N-ethylmaleimid and acetonitrile directly after removing the culture medium form the culture flask, can be considered in the in vitro GBM studies [78].

Studies performed on glioma cell models have successfully connected the widely known glioma marker, 2-hydroxyglutarate (2-HG) with the IDH1 mutation, as IDH-mutated cells gained a new, unique ability to convert α-KG into 2-HG, that IDH-wildtype glioma cells do not possess [30]. Live cell monitoring with 13C-MRS revealed elevated concentrations of 2-HG in the IDH1mut cells, along with a simultaneous drop in Glu concentrations [33]. This correlation was further explored in another study, where it was confirmed that 2-HG requires glucose in addition to Glu [45]. 2-HG is a good oncotarget for use in differentiating low-grade gliomas from GBMs, with Gln and glucose deprivation serving as useful therapeutic targets for such analyses.

Finally, a few other metabolites and altered pathways, such as N-acetyl aspartate (NAA), have been suggested as important for GBM metabolomic diagnostics, prognosis, and drug testing [37,52]. The full scope of important in vitro GBM metabolites analysed is presented in Table 1. Moreover, key metabolites that have been discussed in this paragraph, i.e., α-KG, 2-HG, Gln, Glu, GABA, GSH, and Asp, were analysed with the MetaboAnalyst 5.0 online. The most prevalent metabolic pathways are shown in the Figure 1, where Glu and Gln appear most often, suggesting them as metabolites important for the disease in question, while arginine metabolism and biosynthesis, Asp, D-Gln, and D-Glu metabolism are the most dominant pathways. To summarize metabolites such as Co, PC, GPC, myo-inositol, Gln, Glu, GABA, Asp, α-KG, GSH and 2-HG could be all used for GBM grading. Elevated myo-inositol, high Gln and Glu dependency and decrease in GSH could all indicate high grade glioma, while high 2-HG concentration could be associated with IDH1 mutation and therefore better prognosis. However, the most optimal solution would be to create a panel of key metabolites and analyze not only changes in levels of those, but also ratios between them.

Figure 1. Network of GBM related oncometabolites. Network generated with the MetaboAnalyst 5.0 online [79], pathways names and codes from Kyoto Encyclopedia of Genes and Genomes database [80].

4. Importance of GBM Microenvironment Reconstruction for In Vitro Metabolomics

GBM is a tumor that is known to have a highly complicated microenvironment, largely due to its heterogeneous nature, intratumor hypoxia, and angiogenesis [14,15]. Therefore, to carry out metabolomic in vitro studies that will translate to an in vivo environment, it is extremely important to consider culture conditions and cell source in metabolomic testing. For patient-derived GBM cells, special culture conditions, such as the use of an FBS-free culture medium supplemented with growth factors, as well as the use of 3D culturing in neurospheres, are recommended in order to acquire cells that actually feature all tumor characteristics [24,81,82]. 3D culture was more favorable for stem-like cells (CD133+). Furthermore, the cells in the 3D culture were also characterized by higher tCho-to-tCre, Gly-to-myo (myo-inositol), and Gly-to-tCho ratios, which are all indicators of high-grade gliomas [38]. In a similar, more recent study, Pexito et al. extended this investigation. They observed significant alterations in arginine metabolism in the cell lines that were cultured in the neurospheres [59]. Moreover, a comparison of patient-derived cells cultured in neutrospheres actually reflected the metabolic fingerprint of relapsed tumors [52]. Notably, neurospheres were used to culture glioma stem-like cells in many of the studies discussed in the current review (Table 1) [27,32,35,37,45,52,54].

Hypoxia is a common phenomenon in cancers, but it remains difficult to replicate hypoxic environments in vitro. Spheroid formation is one method that can be used to create low-oxygen conditions in cultures, as the core of the spheres is naturally hypoxic. However, this approach does not ensure the replicable conditions that are required in certain types of studies. These conditions can be achieved by lowering the O_2 content in the culture environment using equipment such as a CO_2 incubator. The profiling of U87MG cells grown in both hypoxic and normoxic environments revealed that hypoxia induces the non-glycolytic metabolism of glucose, which suggests that glycoproteins and glycolipids can be used as markers for hypoxia in GBM tumors. Moreover, the authors of the study further observed alterations to the TCA cycle, 2-HG accumulation, the altered metabolism of lipids, and increased catabolism of amino acids in hypoxic GBM cells [57]. A separate analysis of primary cell culture in hypoxic conditions revealed that oxygen deprivation induces changes in the α-KG-to-succinate ratio, as well as the Gly content [56]. Finally,

Blandin et al. showed that cells cultured in hypoxic conditions more closely resembled the actual metabolomic profile of a tumor [52]. Therefore, in order to pursue a truly accurate metabolomic analysis of GBM in vitro, it should be taken into account that standard culture conditions established over the years, e.g., 2D cell culture, culture medium supplemented with FBS, and normoxic conditions, do not accurately reflect the complexity of the tumor. When planning the experiment, it is advisable to conduct simultaneous experiment with the use of 3D cell culture, FBS-free medium and under hypoxic conditions.

5. In Vitro-In Vivo Extrapolation of Oncometabolites

To date, several low-molecular-weight compounds have been identified as possible biomarkers of GBM. In particular, the dysregulation of the oncometabolites, 2-HG [83–85], NAA [86], Glu [64], and α-KG) [64] has been shown to be connected to the altered enzymatic pathways that occur within cancerous cells. Thus, these low-molecular-mass compounds are potential targets for in vitro-in vivo extrapolation. All of the above-mentioned compounds were identified through a literature search. As mentioned above, 2-HG and Glu were found via live cell monitoring using 13C-MRS, wherein cell culture medium was supplemented with 3-13C-glutamine. This enabled the determination of 13C-Glu and 13C-2-HG in U87IDHmut, and the determination of 13C-Glu only in U87IDHwt cells [45]. Consequently, in terms of IVIVE, Glu and 2-HG can serve not only as GBM biomarkers, but also as markers of *IDH1* mutation, which plays key role in chemotherapy treatment optimization. In another study, researchers determined 2-HG through the extraction of intracellular components, followed by NMR analysis [33]. NAA and Glu were successfully found via NMR as the effect of intracellular metabolome investigation within cell cultures established from tissue of pediatric origin derived by NMR cell culture model [52], primary glioblastoma stem-like cells (GSC) [37] and GL261 cell line. Guidoni et al., observed that NAA was not present in the GBM T98G cell line, which suggests that primary GSC is closer to the in vivo state [37]. Glu was also identified in pediatric low-grade glioma using an LC-MS approach, wherein everolimus treatment resulted in glutaminase inhibition, which in turn led to reduced Glu levels [49], as well as result of extracellular metabolome study of U87-MG cell line [32]. Researchers have also utilized LC-MS/MS to analyse and compare Glu secretion and consumption in a medium-based extracellular metabolome and a cell-lysate-based intracellular metabolome [26]. The dual-phase extraction of intracellular components of U87 followed by GC-MS also revealed presence of Glu, which was observed at higher levels compared to normal hMSCs within the U87 cell line [46]. TMZ treatment caused difference in Glu levels between drug resistant and drug sensitive primary GBM cells with increased Glu levels in TMZ-sensitive cells [47]. Glu was also detected in both 2D and 3D cell cultures of established U87 and LN 229 cell lines [38], as well as various self-derived GBM models [35]. Furthermore, researchers have successfully identified Glu in GSC following treatment with a glutaminase inhibitor; as expected glutaminase levels were lower after the administration of the agent [54]. Moreover, an NMR approach has been successfully employed to detect Glu among the intrametabolome of U87 following treatment with TMZ or *Cibotium barometz* polysaccharides [36], and it has also been detected using astrocytoma cell lines derived from glioma tissue [34] and established cell lines [30,55]. The analysis of rat glioma BT4C cells revealed the presence of Glu and lactic acid within the intracellular metabolome, which suggests that these compounds can be used as a target for relatively easy (compared to human trials) investigations with in vivo rat models [44]. Except for α-KG, all of the well-established oncometabolites related with GBM were found within in vitro cell based studies (Table 3) proving the applicability of such approaches for diagnosis purposes, as well as a convenient and easy way for searching for further biomarkers.

Table 3. In vivo-in vitro extrapolation of oncometabolites in the reviewed literature.

Compound	In Vitro Model	In Vivo/Ex Vivo Investigation
NAA	Primary glioblastoma [52] T98G and primary [37]	[87–90]
2HG	U87, NHA [45] U87, NHA, BT54, BT142 [45]	[88–92]
Glu	U87 [46] A172, LN18, LN71, LN229, LN319, LN405, U373, U373R [47] Res 259, Res186, BT66, JHH-NF1-PA1 [49] Primary glioblastoma [52] U 87 [38] Self-derived cell lines: GBM1, 040922, GBM1016, GBM1417; commercial cell lines: LN229, U87 [35] T98G and primary [37] JHH520 GBM1, 23, 233, 268, 349, 407, SF188, NCH644 [54] U87 [36] Primary, U87-MG [32] MOG-G-VW, LN-18, LN-229, SF-188, U-251 MG, U-87 MG, Primary rat astrocytes, Primary human GBM: E2, R10, R24 [26] U87, NHA [33] U87, NHA, BT54, BT142 [45] CHG5, SHG44, U87, U118, U251 [34] LN229, VLN319m [30] BT4C (rat) [44]	[87,92–94]
α-KG	Not found	[93,94]
PC	BT4C (rat) [44] Primary glioblastoma [52] U87 [38] Self-derived cell lines: GBM1, 040922, GBM1016, GBM1417; commercial cell lines: LN229, U87 [35] HT1080 [39]	[87,95–98]
Lactic acid	LN229, VLN319 [30] U118 LN-18 A172 NHA [55] U87 [46] A172, LN18, LN71, LN229, LN319, LN405, U373, U373R [47] Self-derived cell lines: GBM1, 040922, GBM1016, GBM1417; commercial cell lines: LN229, U87 [35] U87 [36] CHG5, SHG44, U87, U118, U251 [34] BT4C (rat) [44]	[88]
Palmitic acid	U87 [46]	[88,99,100]
Stearic acid	NG97 [58] LN229, SNB19, GAMG, U118, T98G, U87, NHA [58]	[88,100]

6. Pharmaco-Metabolomics as a Tool for Glioma Drug Testing In Vitro

Thanks to the extensive work that was conducted to identify potential metabolites for glioma diagnostics and prognostics, cell cultures have emerged as a truly promising model for drug testing and the exploration of tumor resistance to therapy. Knowledge regarding significant pathways and alterations to their metabolism could be used to predict the effectiveness of different therapeutics depending on the phenotype of the cells. For instance, St-Coeur et al. compared TMZ-sensitive and TMZ-resistant U373 cell lines after combined treatment with either TMZ and lomeguatrib (MGMT inhibitor) or TMZ alone and discovered a panel of distinct metabolites that differed among the cell lines. Specifically, they found increased levels of glucose, citrate, and isocitrate in the TMZ-resistant line, and overconcentrations of creatine, PC, Cho and alanine in the TMZ-sensitive GBM cells [47].

Since Gln and glutaminolysis targeting have been previously suggested, Koch et al. examined the influence of glutaminase (GLS) inhibitors on GSC [32,54]. Their pharmaco-metabolomic approach to in vitro studies of the aforementioned inhibitors—in this case, evaluating their effectiveness—allowed for exceptional target specificity. Interestingly, even though both tested inhibitors were found to have a toxic influence on cultured cells,

only one of them resulted in actual glutaminolysis suppression [54]. The use of a GLS inhibitor, which can inhibit Glu synthesis in in vitro studies, has also been shown to sensitize gliomas with the IDH1 mutation to oxidative stress by McBrayer et al. [27]. Metabolomics analysis was also successfully used in the study conducted by Shi et al.to evaluate the ability of *Cibotium barometz* polysaccharides (CBPs) to resensitize TMZ-resistant cells. The findings showed changes in the metabolites involved in GSH metabolism (e.g., Glu, Gly, or taurine) and significant accumulation of ROS, thus proving the effectiveness of used compounds [36]. A similar pharmaco-metabolomic approach was used by D'Alessandro et al., to analyze how the Gli1 inhibitor affected murine glioma cells that overexpressed Gli1. This method was able to provide good target specify for the studied drug and its anti-tumor influence, both in vitro and in vivo [31]. This knowledge regarding alterations to the metabolism of Glu, Cho, and Gly in different types of GBM enabled further study of the Notch inhibitor mode of action and the determination of the Notch blockade as a promising target for GBM therapy [35]. In vitro metabolomics have also been successfully used to monitor the potential effect of various drugs on lipid synthesis for compounds such as FK866 inhibitor, phospholipase D (PLD) inhibitor, or gamma-linoleic acid [39,51,53]. It should be noted that some of the studies reviewed earlier also fit within the pharmacometabolomics approach. The full scope of analyzed literature is reported in Table 1. Moreover, metabolomics can also be used to assess cytotoxicity in in vitro applications, for example, particles for gene transfection [58]. The knowledge gained from the basic research discussed in metabolomic paragraph has been successfully used to select markers to determine the efficiency and target specificity of targeted drugs, making metabolomics in vitro an interesting tool for novel targeted therapies development. Gln, Glu, and GSH metabolism being especially useful in determining the effectiveness of analyzed drugs.

7. Conclusions

The studies reviewed in this paper highlight the importance of careful test planning for the accurate metabolomic profiling of GBM cells. Factors such as culture model, medium composition, established or patient-derived cell lines, and oxygen levels should all be chosen based on desired aspects of a tumor's particular microenvironment. Moreover, sample preparation should use only the most effective metabolism quenching or extraction methods. In vitro studies face a problem at the level of in vitro-in vivo extrapolation, as metabolic reactions in a living organism are much more complex than in vitro environments are able to capture. However, with careful design, e.g., the use of 3D culture models, hypoxic conditions when conducting a study, or usage of more efficient sample preparation methods, in vitro studies on GBM metabolomics can be extremely useful for the diagnosis and prognosis of brain tumors, as well as for studying new drugs or mechanisms of drug resistance.

Author Contributions: Writing—original draft preparation, P.M. and K.J.; supervision, review, B.B. All authors have read and agreed to the published version of the manuscript.

Funding: The linguistic correction was financed by funds provided by the Doctoral School of Medical Sciences and Health Sciences.

Institutional Review Board Statement: Not applicable.

Informed Consent Statement: Not applicable.

Data Availability Statement: Not applicable.

Acknowledgments: The authors are members of the Toruń Center of Excellence named "Towards Personalized Medicine" operating under the Excellence Initiative—Research University.

Conflicts of Interest: The authors declare no conflict of interest.

References

1. Louis, D.N.; Ohgaki, H.; Wiestler, O.D.; Cavenee, W.K.; Burger, P.C.; Jouvet, A.; Scheithauer, B.W.; Kleihues, P. The 2007 WHO classification of tumours of the central nervous system. *Acta Neuropathol.* **2007**, *114*, 547, Erratum in **2007**, *114*, 97–109. [CrossRef]
2. Louis, D.N.; Perry, A.; Reifenberger, G.; von Deimling, A.; Figarella-Branger, D.; Cavenee, W.K.; Ohgaki, H.; Wiestler, O.D.; Kleihues, P.; Ellison, D.W. The 2016 World Health Organization Classification of Tumors of the Central Nervous System: A summary. *Acta Neuropathol.* **2016**, *131*, 803–820. [CrossRef] [PubMed]
3. Ostrom, Q.T.; Patil, N.; Cioffi, G.; Waite, K.; Kruchko, C.; Barnholtz-Sloan, J.S. CBTRUS Statistical Report: Primary Brain and Other Central Nervous System Tumors Diagnosed in the United States in 2013–2017. *Neuro-Oncology* **2020**, *22*, iv1–iv96. [CrossRef] [PubMed]
4. Cavazos, D.A.; Brenner, A.J. Hypoxia in astrocytic tumors and implications for therapy. *Neurobiol. Dis.* **2016**, *85*, 227–233. [CrossRef] [PubMed]
5. Papale, M.; Buccarelli, M.; Mollinari, C.; Russo, M.A.; Pallini, R.; Ricci-Vitiani, L.; Tafani, M. Hypoxia, Inflammation and Necrosis as Determinants of Glioblastoma Cancer Stem Cells Progression. *Int. J. Mol. Sci.* **2020**, *21*, 2660. [CrossRef] [PubMed]
6. Fernandes, C.; Costa, A.; Osorio, L.; Lago, R.C.; Linhares, P.; Carvalho, B.; Caeiro, C. Current Standards of Care in Glioblastoma Therapy. *Glioblastoma, Codon Publications, Brisbane, Australia* **2017**, chapter 11. 197–241. [CrossRef]
7. Kaina, B. Temozolomide in Glioblastoma Therapy: Role of Apoptosis, Senescence and Autophagy. Comment on Strobel et al., Temozolomide and Other Alkylating Agents in Glioblastoma Therapy. *Biomedicines* **2019**, *7*, 69, Erratum in **2019**, *7*, 90. [CrossRef] [PubMed]
8. Wick, W.; Platten, M.; Weller, M. New (alternative) temozolomide regimens for the treatment of glioma. *Neuro-Oncology* **2009**, *11*, 69–79. [CrossRef] [PubMed]
9. Ge, X.; Pan, M.H.; Wang, L.; Li, W.; Jiang, C.F.; He, J.; Abouzid, K.; Liu, L.Z.; Shi, Z.M.; Jiang, B.H. Hypoxia-mediated mitochondria apoptosis inhibition induces temozolomide treatment resistance through miR-26a/Bad/Bax axis. *Cell Death Dis.* **2018**, *9*, 1128. [CrossRef] [PubMed]
10. Yin, J.X.; Ge, X.; Shi, Z.M.; Yu, C.; Lu, C.F.; Wei, Y.T.; Zeng, A.L.; Wang, X.F.; Yan, W.; Zhang, J.X.; et al. Extracellular vesicles derived from hypoxic glioma stem-like cells confer temozolomide resistance on glioblastoma by delivering miR-30b-3p. *Theranostics* **2021**, *11*, 1763–1779. [CrossRef] [PubMed]
11. Sun, S.; Lee, D.; Lee, N.P.; Pu, J.K.S.; Wong, S.T.S.; Lui, W.M.; Fung, C.F.; Leung, G.K.K. Hyperoxia resensitizes chemoresistant human glioblastoma cells to temozolomide. *J. Neuro-Oncol.* **2012**, *109*, 467–475. [CrossRef]
12. Keunen, O.; Johansson, M.; Oudin, A.; Sanzey, M.; Rahim, S.A.A.; Fack, F.; Thorsen, F.; Taxt, T.; Bartos, M.; Jirik, R.; et al. Anti-VEGF treatment reduces blood supply and increases tumor cell invasion in glioblastoma. *Proc. Natl. Acad. Sci. USA* **2011**, *108*, 3749–3754. [CrossRef]
13. Sathornsumetee, S.; Cao, Y.; Marcello, J.E.; Ii, J.E.H.; McLendon, R.E.; Desjardins, A.; Friedman, H.S.; Dewhirst, M.W.; Vredenburgh, J.J.; Rich, J.N. Tumor angiogenic and hypoxic profiles predict radiographic response and survival in malignant astrocytoma patients treated with bevacizumab and irinotecan. *J. Clin. Oncol.* **2008**, *26*, 271–278. [CrossRef]
14. Liau, B.B.; Sievers, C.; Donohue, L.K.; Gillespie, S.M.; Flavahan, W.A.; Miller, T.E.; Venteicher, A.S.; Hebert, C.H.; Carey, C.D.; Rodig, S.J.; et al. Adaptive Chromatin Remodeling Drives Glioblastoma Stem Cell Plasticity and Drug Tolerance. *Cell Stem Cell* **2017**, *20*, 233–246. [CrossRef]
15. Colwell, N.; Larion, M.; Giles, A.J.; Seldomridge, A.N.; Sizdahkhani, S.; Gilbert, M.R.; Park, D.M. Hypoxia in the glioblastoma microenvironment: Shaping the phenotype of cancer stem-like cells. *Neuro-Oncology* **2017**, *19*, 887–896. [CrossRef]
16. Jing, X.; Yang, F.; Shao, C.; Wei, K.; Xie, M.; Shen, H.; Shu, Y. Role of hypoxia in cancer therapy by regulating the tumor microenvironment. *Mol. Cancer* **2019**, *18*, 157. [CrossRef]
17. Ullmann, P.; Nurmik, M.; Begaj, R.; Haan, S.; Letellier, E. Hypoxia- and MicroRNA-Induced Metabolic Reprogramming of Tumor-Initiating Cells. *Cells* **2019**, *8*, 528. [CrossRef]
18. Eales, K.L.; Hollinshead, K.E.R.; Tennant, D.A. Hypoxia and metabolic adaptation of cancer cells. *Oncogenesis* **2016**, *5*, e190. [CrossRef]
19. Liberti, M.V.; Locasale, J.W. The Warburg Effect: How Does it Benefit Cancer Cells? *Trends Biochem. Sci.* **2016**, *41*, 211–218. [CrossRef]
20. Wishart, D.S.; Tzur, D.; Knox, C.; Eisner, R.; Guo, A.C.; Young, N.; Cheng, D.; Jewell, K.; Arndt, D.; Sawhney, S.; et al. HMDB: The human metabolome database. *Nucleic Acids Res.* **2007**, *35*, D521–D526. [CrossRef]
21. Johnson, C.H.; Ivanisevic, J.; Siuzdak, G. Metabolomics: Beyond biomarkers and towards mechanisms. *Nat. Rev. Mol. Cell Biol.* **2016**, *17*, 451–459. [CrossRef]
22. Schmidt, C.W. Metabolomics: What's happening downstream of DNA. *Environ. Health Perspect.* **2004**, *112*, A410–A415. [CrossRef]
23. Hickman, J.A.; Graeser, R.; de Hoogt, R.; Vidic, S.; Brito, C.; Gutekunst, M.; van der Kuip, H.; Consortium, I.P. Three-dimensional models of cancer for pharmacology and cancer cell biology: Capturing tumor complexity in vitro/ex vivo. *Biotechnol. J.* **2014**, *9*, 1115–1128. [CrossRef]
24. Musah-Eroje, A.; Watson, S. A novel 3D in vitro model of glioblastoma reveals resistance to temozolomide which was potentiated by hypoxia. *J. Neuro-Oncol.* **2019**, *142*, 231–240. [CrossRef]
25. Cuperlovic-Culf, M.; Barnett, D.A.; Culf, A.S.; Chute, I. Cell culture metabolomics: Applications and future directions. *Drug Discov. Today* **2010**, *15*, 610–621. [CrossRef]

26. Tardito, S.; Oudin, A.; Ahmed, S.U.; Fack, F.; Keunen, O.; Zhene, L.; Miletic, H.; Sakariassent, P.O.; Weinstock, A.; Wagner, A.; et al. Glutamine synthetase activity fuels nucleotide biosynthesis and supports growth of glutamine-restricted glioblastoma. *Nat. Cell Biol.* **2015**, *17*, 1556–1568. [CrossRef]
27. McBrayer, S.K.; Mayers, J.R.; DiNatale, G.J.; Shi, D.D.; Khanal, J.; Chakraborty, A.A.; Sarosiek, K.A.; Briggs, K.J.; Robbins, A.K.; Sewastianik, T.; et al. Transaminase Inhibition by 2-Hydroxyglutarate Impairs Glutamate Biosynthesis and Redox Homeostasis in Glioma. *Cell* **2018**, *175*, 101–116. [CrossRef]
28. Palanichamy, K.; Thirumoorthy, K.; Kanji, S.; Gordon, N.; Singh, R.; Jacob, J.R.; Sebastian, N.; Litzenberg, K.T.; Patel, D.; Bassett, E.; et al. Methionine and Kynurenine Activate Oncogenic Kinases in Glioblastoma, and Methionine Deprivation Compromises Proliferation. *Clin. Cancer Res.* **2016**, *22*, 3513–3523. [CrossRef] [PubMed]
29. Moren, L.; Perryman, R.; Crook, T.; Langer, J.K.; Oneill, K.; Syed, N.; Antti, H. Metabolomic profiling identifies distinct phenotypes for ASS1 positive and negative GBM. *BMC Cancer* **2018**, *18*, 268, Erratum in **2018**, *18*, 167. [CrossRef]
30. Cuperlovic-Culf, M.; Ferguson, D.; Culf, A.; Morin, P., Jr.; Touaibia, M. H-1 NMR Metabolomics Analysis of Glioblastoma Subtypes CORRELATION BETWEEN METABOLOMICS AND GENE EXPRESSION CHARACTERISTICS. *J. Biol. Chem.* **2012**, *287*, 20164–20175. [CrossRef] [PubMed]
31. D'Alessandro, G.; Quaglio, D.; Monaco, L.; Lauro, C.; Ghirga, F.; Ingallina, C.; De Martino, M.; Fucile, S.; Porzia, A.; Di Castro, M.A.; et al. H-1-NMR metabolomics reveals the Glabrescione B exacerbation of glycolytic metabolism beside the cell growth inhibitory effect in glioma. *Cell Commun. Signal.* **2019**, *17*, 108. [CrossRef]
32. Oizel, K.; Chauvin, C.; Oliver, L.; Gratas, C.; Geraldo, F.; Jarry, U.; Scotet, E.; Rabe, M.; Alves-Guerra, M.C.; Teusan, R.; et al. Efficient Mitochondrial Glutamine Targeting Prevails Over Glioblastoma Metabolic Plasticity. *Clin. Cancer Res.* **2017**, *23*, 6292–6304. [CrossRef]
33. Izquierdo-Garcia, J.L.; Viswanath, P.; Eriksson, P.; Chaumeil, M.M.; Pieper, R.O.; Phillips, J.J.; Ronen, S.M. Metabolic Reprogramming in Mutant IDH1 Glioma Cells. *PLoS ONE* **2015**, *10*, e0118781. [CrossRef]
34. Shao, W.; Gu, J.; Huang, C.; Liu, D.; Huang, H.; Huang, Z.; Lin, Z.; Yang, W.; Liu, K.; Lin, D.; et al. Malignancy-associated metabolic profiling of human glioma cell lines using H-1 NMR spectroscopy. *Mol. Cancer* **2014**, *13*, 197. [CrossRef]
35. Kahlert, U.D.; Cheng, M.L.; Koch, K.; Marchionni, L.; Fan, X.; Raabe, E.H.; Maciaczyk, J.; Glunde, K.; Eberhart, C.G. Alterations in cellular metabolome after pharmacological inhibition of Notch in glioblastoma cells. *Int. J. Cancer* **2016**, *138*, 1246–1255. [CrossRef]
36. Shi, Y.; Wang, X.; Wang, N.; Li, F.F.; You, Y.L.; Wang, S.Q. The effect of polysaccharides from Cibotium barometz on enhancing temozolomide-induced glutathione exhausted in human glioblastoma U87 cells, as revealed by H-1 NMR metabolomics analysis. *Int. J. Biol. Macromol.* **2020**, *156*, 471–484. [CrossRef]
37. Guidoni, L.; Ricci-Vitiani, L.; Rosi, A.; Palma, A.; Grande, S.; Luciani, A.M.; Pelacchi, F.; di Martino, S.; Colosimo, C.; Biffoni, M.; et al. H-1 NMR detects different metabolic profiles in glioblastoma stem-like cells. *NMR Biomed.* **2014**, *27*, 129–145. [CrossRef]
38. Kahlert, U.D.; Koch, K.; Suwala, A.K.; Hartmann, R.; Cheng, M.; Maciaczyk, D.; Willbold, D.; Eberhart, C.G.; Glunde, K.; Maciaczyk, J. The effect of neurosphere culture conditions on the cellular metabolism of glioma cells. *Folia Neuropathol.* **2015**, *53*, 219–225. [CrossRef]
39. Larion, M.; Dowdy, T.; Ruiz-Rodado, V.; Meyer, M.W.; Song, H.; Zhang, W.; Davis, D.; Gilbert, M.R.; Lita, A. Detection of Metabolic Changes Induced via Drug Treatments in Live Cancer Cells and Tissue Using Raman Imaging Microscopy. *Biosensors* **2018**, *9*, 5. [CrossRef]
40. Tyagi, R.K.; Azrad, A.; Degani, H.; Salomon, Y. Simultaneous extraction of cellular lipids and water-soluble metabolites: Evaluation by NMR spectroscopy. *Magn. Reson. Med.* **1996**, *35*, 194–200. [CrossRef]
41. Ward, C.S.; Venkatesh, H.S.; Chaumeil, M.M.; Brandes, A.H.; VanCriekinge, M.; Dafni, H.; Sukumar, S.; Nelson, S.J.; Vigneron, D.B.; Kurhanewicz, J.; et al. Noninvasive Detection of Target Modulation following Phosphatidylinositol 3-Kinase Inhibition Using Hyperpolarized C-13 Magnetic Resonance Spectroscopy. *Cancer Res.* **2010**, *70*, 1296–1305. [CrossRef] [PubMed]
42. Zhang, R.; Hu, P.; Zang, Q.; Yue, X.; Zhou, Z.; Xu, X.; Xu, J.; Li, S.; Chen, Y.; Qiang, B.; et al. LC-MS-based metabolomics reveals metabolic signatures related to glioma stem-like cell self-renewal and differentiation. *RSC Adv.* **2017**, *7*, 24221–24232. [CrossRef]
43. Gao, W.Q.; Wu, Z.R.; Bohl, C.E.; Yang, J.; Miller, D.D.; Dalton, J.T. Characterization of the in vitro metabolism of selective androgen receptor modulator using human, rat, and dog liver enzyme preparations. *Drug Metab. Dispos.* **2006**, *34*, 243–253. [CrossRef] [PubMed]
44. Mirbahai, L.; Wilson, M.; Shaw, C.S.; McConville, C.; Malcomson, R.D.G.; Griffin, J.L.; Kauppinen, R.A.; Peet, A.C. H-1 magnetic resonance spectroscopy metabolites as biomarkers for cell cycle arrest and cell death in rat glioma cells. *Int. J. Biochem. Cell Biol.* **2011**, *43*, 990–1001. [CrossRef]
45. Izquierdo-Garcia, J.L.; Viswanath, P.; Eriksson, P.; Cai, L.; Radoul, M.; Chaumeil, M.M.; Blough, M.; Luchman, H.A.; Weiss, S.; Cairncross, J.G.; et al. IDH1 Mutation Induces Reprogramming of Pyruvate Metabolism. *Cancer Res.* **2015**, *75*, 2999–3009. [CrossRef]
46. Juerchott, K.; Guo, K.-T.; Catchpole, G.; Feher, K.; Willmitzer, L.; Schichor, C.; Selbig, J. Comparison of metabolite profiles in U87 glioma cells and mesenchymal stem cells. *Biosystems* **2011**, *105*, 130–139. [CrossRef]
47. St-Coeur, P.D.; Poitras, J.J.; Cuperlovic-Culf, M.; Touaibia, M.; Morin, P. Investigating a signature of temozolomide resistance in GBM cell lines using metabolomics. *J. Neuro-Oncol.* **2015**, *125*, 91–102. [CrossRef]
48. Mesti, T.; Savarin, P.; Triba, M.N.; Le Moyec, L.; Ocvirk, J.; Banissi, C.; Carpentier, A.F. Metabolic Impact of Anti-Angiogenic Agents on U87 Glioma Cells. *PLoS ONE* **2014**, *9*, e0099198. [CrossRef]

49. Poore, B.; Yuan, M.; Arnold, A.; Price, A.; Alt, J.; Rubens, J.A.; Slusher, B.S.; Eberhart, C.G.; Raabe, E.H. Inhibition of mTORC1 in pediatric low-grade glioma depletes glutathione and therapeutically synergizes with carboplatin. *Neuro-Oncology* **2019**, *21*, 252–263. [CrossRef]
50. Sterin, M.; Ringel, I.; Lecht, S.; Lelkes, P.I.; Lazarovici, P. 31P Magnetic Resonance Spectroscopy of Endothelial Cells Grown in Three-Dimensional Matrigel Construct as an Enabling Platform Technology: I. The Effect of Glial Cells and Valproic Acid on Phosphometabolite Levels. *Endothel. J. Endothel. Cell Res.* **2008**, *15*, 288–298. [CrossRef]
51. Antal, O.; Peter, M.; Hackler, L.; Man, I.; Szebeni, G.; Ayaydin, F.; Hideghety, K.; Vigh, L.; Kitajka, K.; Balogh, G.; et al. Lipidomic analysis reveals a radiosensitizing role of gamma-linolenic acid in glioma cells. *Biochim. Biophys. Acta Mol. Cell Biol. Lipids* **2015**, *1851*, 1271–1282. [CrossRef]
52. Blandin, A.-F.; Durand, A.; Litzler, M.; Tripp, A.; Guerin, E.; Ruhland, E.; Obrecht, A.; Keime, C.; Fuchs, Q.; Reita, D.; et al. Hypoxic Environment and Paired Hierarchical 3D and 2D Models of Pediatric H3.3-Mutated Gliomas Recreate the Patient Tumor Complexity. *Cancers* **2019**, *11*, 1875. [CrossRef]
53. Mathews, T.P.; Hill, S.; Rose, K.L.; Ivanova, P.T.; Lindsley, C.W.; Brown, H.A. Human Phospholipase D Activity Transiently Regulates Pyrimidine Biosynthesis in Malignant Gliomas. *ACS Chem. Biol.* **2015**, *10*, 1258–1268. [CrossRef]
54. Koch, K.; Hartmann, R.; Tsiampali, J.; Uhlmann, C.; Nickel, A.C.; He, X.L.; Kamp, M.A.; Sabel, M.; Barker, R.A.; Steiger, H.J.; et al. A comparative pharmaco-metabolomic study of glutaminase inhibitors in glioma stem-like cells confirms biological effectiveness but reveals differences in target-specificity. *Cell Death Discov.* **2020**, *6*, 20. [CrossRef]
55. Cuperlovic-Culf, M.; Khieu, N.H.; Surendra, A.; Hewitt, M.; Charlebois, C.; Sandhu, J.K. Analysis and Simulation of Glioblastoma Cell Lines-Derived Extracellular Vesicles Metabolome. *Metabolites* **2020**, *10*, 88. [CrossRef]
56. Heiland, D.H.; Gaebelein, A.; Boerries, M.; Woerner, J.; Pompe, N.; Franco, P.; Heynckes, S.; Bartholomae, M.; Hailin, D.O.; Carro, M.S.; et al. Microenvironment-Derived Regulation of HIF Signaling Drives Transcriptional Heterogeneity in Glioblastoma Multiforme. *Mol. Cancer Res.* **2018**, *16*, 655–668. [CrossRef]
57. Kucharzewska, P.; Christianson, H.C.; Belting, M. Global Profiling of Metabolic Adaptation to Hypoxic Stress in Human Glioblastoma Cells. *PLoS ONE* **2015**, *10*, e0116740. [CrossRef]
58. Zanin, H.; Hollanda, L.M.; Ceragioli, H.J.; Ferreira, M.S.; Machado, D.; Lancellotti, M.; Catharino, R.R.; Baranauskas, V.; Lobo, A.O. Carbon nanoparticles for gene transfection in eukaryotic cell lines. *Mater. Sci. Eng. C-Mater. Biol. Appl.* **2014**, *39*, 359–370. [CrossRef]
59. Peixoto, J.; Janaki-Raman, S.; Schlicker, L.; Schmitz, W.; Walz, S.; Herold-Mende, C.; Soares, P.; Schulze, A.; Lima, J. Integrated Metabolomics and Transcriptomics Analysis of Monolayer and Neurospheres from Glioblastoma Cells. *Cancers* **2021**, *13*, 1327. [CrossRef]
60. Park, J.H.; Pyun, W.Y.; Park, H.W. Cancer Metabolism: Phenotype, Signaling and Therapeutic Targets. *Cells* **2020**, *9*, 2308. [CrossRef]
61. Pandey, R.; Caflisch, L.; Lodi, A.; Brenner, A.J.; Tiziani, S. Metabolomic signature of brain cancer. *Mol. Carcinog.* **2017**, *56*, 2355–2371. [CrossRef]
62. Yu, D.; Xuan, Q.H.; Zhang, C.Q.; Hu, C.X.; Li, Y.L.; Zhao, X.J.; Liu, S.S.; Ren, F.F.; Zhang, Y.; Zhou, L.N.; et al. Metabolic Alterations Related to Glioma Grading Based on Metabolomics and Lipidomics Analyses. *Metabolites* **2020**, *10*, 478. [CrossRef]
63. Heiden, M.G.V.; Cantley, L.C.; Thompson, C.B. Understanding the Warburg Effect: The Metabolic Requirements of Cell Proliferation. *Science* **2009**, *324*, 1029–1033. [CrossRef]
64. Maus, A.; Peters, G.J. Glutamate and alpha-ketoglutarate: Key players in glioma metabolism. *Amino Acids* **2017**, *49*, 1143, Erratum in **2017**, 49, 21. [CrossRef]
65. Chung, W.J.; Lyons, S.A.; Nelson, G.M.; Hamza, H.; Gladson, C.L.; Gillespie, G.Y.; Sontheimer, H. Inhibition of cystine uptake disrupts the growth of primary brain tumors. *J. Neurosci.* **2005**, *25*, 7101–7110. [CrossRef]
66. Lee, J.E.; Jeun, S.S.; Kim, S.H.; Yoo, C.Y.; Baek, H.-M.; Yang, S.H. Metabolic profiling of human gliomas assessed with NMR. *J. Clin. Neurosci.* **2019**, *68*, 275–280. [CrossRef]
67. Imamura, Y.; Mukohara, T.; Shimono, Y.; Funakoshi, Y.; Chayahara, N.; Toyoda, M.; Kiyota, N.; Takao, S.; Kono, S.; Nakatsura, T.; et al. Comparison of 2D-and 3D-culture models as drug-testing platforms in breast cancer. *Oncol. Rep.* **2015**, *33*, 1837–1843. [CrossRef]
68. Denkert, C.; Budczies, J.; Kind, T.; Weichert, W.; Tablack, P.; Sehouli, J.; Niesporek, S.; Koensgen, D.; Dietel, M.; Fiehn, O. Mass spectrometry-based metabolic profiling reveals different metabolite patterns in invasive ovarian carcinomas and ovarian borderline tumors. *Cancer Res.* **2006**, *66*, 10795–10804. [CrossRef]
69. Righi, V.; Roda, J.M.; Paz, J.; Mucci, A.; Tugnoli, V.; Rodriguez-Tarduchy, G.; Barrios, L.; Schenetti, L.; Cerdan, S.; Garcia-Martin, M.L. H-1 HR-MAS and genomic analysis of human tumor biopsies discriminate between high and low grade astrocytomas. *NMR Biomed.* **2009**, *22*, 629–637. [CrossRef]
70. Qi, S.; Yu, L.; Gui, S.; Ding, Y.; Han, H.; Zhang, X.; Wu, L.; Yao, F. IDH mutations predict longer survival and response to temozolomide in secondary glioblastoma. *Cancer Sci.* **2012**, *103*, 269–273. [CrossRef]
71. McKnight, T.R.; Smith, K.J.; Chu, P.W.; Chiu, K.S.; Cloyd, C.P.; Chang, S.M.; Phillips, J.J.; Berger, M.S. Choline Metabolism, Proliferation, and Angiogenesis in Nonenhancing Grades 2 and 3 Astrocytoma. *J. Magn. Reson. Imaging* **2011**, *33*, 808–816. [CrossRef] [PubMed]

72. Kallenberg, K.; Bock, H.C.; Helms, G.; Jung, K.; Wrede, A.; Buhk, J.-H.; Giese, A.; Frahm, J.; Strik, H.; Dechent, P.; et al. Untreated Glioblastoma Multiforme: Increased Myo-inositol and Glutamine Levels in the Contralateral Cerebral Hemisphere at Proton MR Spectroscopy. *Radiology* **2009**, *253*, 805–812. [CrossRef] [PubMed]
73. Benjamin, D.I.; Louie, S.M.; Mulvihill, M.M.; Kohnz, R.A.; Li, D.S.; Chan, L.G.; Sorrentino, A.; Bandyopadhyay, S.; Cozzo, A.; Ohiri, A.; et al. Inositol Phosphate Recycling Regulates Glycolytic and Lipid Metabolism That Drives Cancer Aggressiveness. *ACS Chem. Biol.* **2014**, *9*, 1340–1350. [CrossRef] [PubMed]
74. Albrecht, J.; Sidoryk-Wegrzynowicz, M.; Zielinska, M.; Aschner, M. Roles of glutamine in neurotransmission. *Neuron Glia Biol.* **2010**, *6*, 263–276. [CrossRef]
75. Seyfried, T.N.; Kiebish, M.A.; Marsh, J.; Shelton, L.M.; Huysentruyt, L.C.; Mukherjee, P. Metabolic management of brain cancer. *Biochim. Biophys. Acta-Bioenerg.* **2011**, *1807*, 577–594. [CrossRef]
76. Aquilano, K.; Baldelli, S.; Ciriolo, M.R. Glutathione: New roles in redox signaling for an old antioxidant. *Front. Pharmacol.* **2014**, 5. [CrossRef]
77. Giustarini, D.; Galvagni, F.; Tesei, A.; Farolfi, A.; Zanoni, M.; Pignatta, S.; Milzani, A.; Marone, I.M.; Dalle-Donne, I.; Nassini, R.; et al. Glutathione, glutathione disulfide, and S-glutathionylated proteins in cell cultures. *Free Radic. Biol. Med.* **2015**, *89*, 972–981. [CrossRef]
78. Herzog, K.; Ijlst, L.; van Cruchten, A.G.; van Roermund, C.W.T.; Kulik, W.; Wanders, R.J.A.; Waterham, H.R. An UPLC-MS/MS Assay to Measure Glutathione as Marker for Oxidative Stress in Cultured Cells. *Metabolites* **2019**, *9*, 45. [CrossRef]
79. MetaboAnalyst 5.0. Available online: https://www.metaboanalyst.ca (accessed on 18 April 2021).
80. Kanehisa, M.; Furumichi, M.; Sato, Y.; Ishiguro-Watanabe, M.; Tanabe, M. KEGG: Integrating viruses and cellular organisms. *Nucleic Acids Res.* **2021**, *49*, D545–D551. [CrossRef]
81. Lee, J.; Kotliarova, S.; Kotliarov, Y.; Li, A.G.; Su, Q.; Donin, N.M.; Pastorino, S.; Purow, B.W.; Christopher, N.; Zhang, W.; et al. Tumor stem cells derived from glioblastomas cultured in bFGF and EGF more closely mirror the phenotype and genotype of primary tumors than do serum-cultured cell lines. *Cancer Cell* **2006**, *9*, 391–403. [CrossRef]
82. Hasselbach, L.A.; Irtenkauf, S.M.; Lemke, N.W.; Nelson, K.K.; Berezovsky, A.D.; Carlton, E.T.; Transou, A.D.; Mikkelsen, T.; de Carvalho, A.C. Optimization of High Grade Glioma Cell Culture from Surgical Specimens for Use in Clinically Relevant Animal Models and 3D Immunochemistry. *JoVE-J. Vis. Exp.* **2014**, *83*, e51088. [CrossRef]
83. An, Z.X.; Ganji, S.K.; Tiwari, V.; Pinho, M.C.; Patel, T.; Barnett, S.; Pan, E.; Mickey, B.E.; Maher, E.A.; Choi, C.H. Detection of 2-hydroxyglutarate in brain tumors by triple-refocusing MR spectroscopy at 3T in vivo. *Magn. Reson. Med.* **2017**, *78*, 40–48. [CrossRef]
84. Sciacovelli, M.; Frezza, C. Oncometabolites: Unconventional triggers of oncogenic signalling cascades. *Free Radic. Biol. Med.* **2016**, *100*, 175–181. [CrossRef]
85. Yang, M.; Soga, T.; Pollard, P.J. Oncometabolites: Linking altered metabolism with cancer. *J. Clin. Investig.* **2013**, *123*, 3652–3658. [CrossRef]
86. Zand, B.; Previs, R.A.; Zacharias, N.M.; Rupaimoole, R.; Mitamura, T.; Nagaraja, A.S.; Guindani, M.; Dalton, H.J.; Yang, L.F.; Baddour, J.; et al. Role of Increased n-acetylaspartate Levels in Cancer. *JNCI-J. Natl. Cancer Inst.* **2016**, *108*, djv426. [CrossRef]
87. Alfaro, C.M.; Pirro, V.; Keating, M.F.; Hattab, E.M.; Cooks, R.G.; Cohen-Gadol, A.A. Intraoperative assessment of isocitrate dehydrogenase mutation status in human gliomas using desorption electrospray ionization-mass spectrometry. *J. Neurosurg.* **2020**, *132*, 180–187. [CrossRef]
88. Jarmusch, A.K.; Pirro, V.; Baird, Z.; Hattab, E.M.; Cohen-Gadol, A.A.; Cooks, R.G. Lipid and metabolite profiles of human brain tumors by desorption electrospray ionization-MS. *Proc. Natl. Acad. Sci. USA* **2016**, *113*, 1486–1491. [CrossRef]
89. Brown, H.M.; Pu, F.; Dey, M.; Miller, J.; Shah, M.V.; Shapiro, S.A.; Ouyang, Z.; Cohen-Gadol, A.A.; Cooks, R.G. Intraoperative detection of isocitrate dehydrogenase mutations in human gliomas using a miniature mass spectrometer. *Anal. Bioanal. Chem.* **2019**, *411*, 7929–7933. [CrossRef]
90. Pirro, V.; Llor, R.S.; Jarmusch, A.K.; Alfaro, C.M.; Cohen-Gadol, A.A.; Hattabd, E.M.; Cooks, R.G. Analysis of human gliomas by swab touch spray-mass spectrometry: Applications to intraoperative assessment of surgical margins and presence of oncometabolites. *Analyst* **2017**, *142*, 4058–4066. [CrossRef]
91. Santagata, S.; Eberlin, L.S.; Norton, I.; Calligaris, D.; Feldman, D.R.; Ide, J.L.; Liu, X.H.; Wiley, J.S.; Vestal, M.L.; Ramkissoon, S.H.; et al. Intraoperative mass spectrometry mapping of an onco-metabolite to guide brain tumor surgery. *Proc. Natl. Acad. Sci. USA* **2014**, *111*, 11121–11126. [CrossRef]
92. Pu, F.; Alfaro, C.M.; Pirro, V.; Xie, Z.E.; Ouyang, Z.; Cooks, R.G. Rapid determination of isocitrate dehydrogenase mutation status of human gliomas by extraction nanoelectrospray using a miniature mass spectrometer. *Anal. Bioanal. Chem.* **2019**, *411*, 1503–1508. [CrossRef]
93. Navis, A.C.; Niclou, S.P.; Fack, F.; Stieber, D.; van Lith, S.; Verrijp, K.; Wright, A.; Stauber, J.; Tops, B.; Otte-Holler, I.; et al. Increased mitochondrial activity in a novel IDH1-R132H mutant human oligodendroglioma xenograft model: In situ detection of 2-HG and alpha-KG. *Acta Neuropathol. Commun.* **2013**, *1*, 18. [CrossRef]
94. Yannell, K.E.; Smith, K.; Alfaro, C.M.; Jarmusch, A.K.; Pirro, V.; Cooks, R.G. N-Acetylaspartate and 2-Hydroxyglutarate Assessed in Human Brain Tissue by Mass Spectrometry as Neuronal Markers of Oncogenesis. *Clin. Chem.* **2017**, *63*, 1766–1767. [CrossRef]

95. Kononikhin, A.; Zhvansky, E.; Shurkhay, V.; Popov, I.; Bormotov, D.; Kostyukevich, Y.; Karchugina, S.; Indeykina, M.; Bugrova, A.; Starodubtseva, N.; et al. A novel direct spray-from-tissue ionization method for mass spectrometric analysis of human brain tumors. *Anal. Bioanal. Chem.* **2015**, *407*, 7797–7805. [CrossRef]
96. Jarmusch, A.K.; Alfaro, C.M.; Pirro, V.; Hattab, E.M.; Cohen-Gadol, A.A.; Cooks, R.G. Differential Lipid Profiles of Normal Human Brain Matter and Gliomas by Positive and Negative Mode Desorption Electrospray Ionization—Mass Spectrometry Imaging. *PLoS ONE* **2016**, *11*, e016318. [CrossRef]
97. Ferey, J.; Marguet, F.; Laquerriere, A.; Marret, S.; Schmitz-Afonso, I.; Bekri, S.; Afonso, C.; Tebani, A. A new optimization strategy for MALDI FTICR MS tissue analysis for untargeted metabolomics using experimental design and data modeling. *Anal. Bioanal. Chem.* **2019**, *411*, 3891–3903. [CrossRef]
98. Eberlin, L.S.; Dill, A.L.; Golby, A.J.; Ligon, K.L.; Wiseman, J.M.; Cooks, R.G.; Agar, N.Y.R. Discrimination of Human Astrocytoma Subtypes by Lipid Analysis Using Desorption Electrospray Ionization Imaging Mass Spectrometry. *Angew. Chem. -Int. Ed.* **2010**, *49*, 5953–5956. [CrossRef]
99. Eberlin, L.S.; Norton, I.; Dill, A.L.; Golby, A.J.; Ligon, K.L.; Santagata, S.; Cooks, R.G.; Agar, N.Y.R. Classifying Human Brain Tumors by Lipid Imaging with Mass Spectrometry. *Cancer Res.* **2012**, *72*, 645–654. [CrossRef]
100. Eberlin, L.S.; Norton, I.; Orringer, D.; Dunn, I.F.; Liu, X.H.; Ide, J.L.; Jarmusch, A.K.; Ligon, K.L.; Jolesz, F.A.; Golby, A.J.; et al. Ambient mass spectrometry for the intraoperative molecular diagnosis of human brain tumors. *Proc. Natl. Acad. Sci. USA* **2013**, *110*, 1611–1616. [CrossRef]

5. Cel rozprawy doktorskiej

Celem pracy było opracowanie platformy analitycznej pozwalającej na integrację różnych formatów hodowli komórkowych i tradycyjnych testów komórkowych z analizą metabolomiczną oraz jej zastosowanie w badaniach nad wrażliwością komórek glejaka wielopostaciowego na maltonian galu. Dostarczenie informacji o zależnościach między fenotypem metabolicznym komórek GBM w dwu- i trójwymiarowej hodowli *in vitro* a ich wrażliwością na leczenie GaM ma służyć wskazaniu optymalnego modelu do prowadzenia badań w układzie GaM-GBM. Identyfikacja kluczowych metabolitów określających potencjalny sposób działania leku może przyczynić się w przyszłości do określenia podatności tej zmiany nowotworowej na lek lub pomóc w dalszych poszukiwaniach nowych celi terapeutycznych.

W pierwszym etapie badań dopasowano narzędzie SPME, które zostały już z sukcesem użyte w identyfikacji potencjalnych onko-metabolitów glejaków *in vivo,* do warunków umożliwiających testowanie *in vitro* w systemie wysokoprzepustowym. Stworzono protokół umożliwiający próbkowanie egzometabolomu w czasie bez potrzeby przerywania hodowli, dostosowany do potrzeb komórek i niezaburzający warunki ich wzrostu.

Ostatecznym celem badań było scharakteryzowanie profilu metabolomicznego komórek GBM wyprowadzonych od pacjentów oraz linii ustalonych z zastosowaniem mikroekstrakcji do fazy stałej jako narzędzia preparatyki próbek oraz platformy LC-MS/MS do analizy instrumentalnej, a następnie skorelowanie wyników z rezultatami rutynowych testów. W analizach uwzględniono tradycyjny sposób hodowli w monowarstwie (2D) oraz w postaci trójwymiarowych neurosfer (3D) bliżej odzwierciedlających mikrośrodowisko guza. Eksperymenty *in vitro* na hodowlach pierwotnych GBM miały na celu zgłębienie efektu działania GaM na te komórki. Dzięki użyciu komórek wyprowadzonych od pacjentów możliwe było oddanie heterogeniczności guzów mózgu przekładającej się na konieczność personalizacji pacjentów. Zasadniczym zadaniem było porównanie efektów GaM w panelu modeli GBM obejmującym linie utrwalone (A-172, U-87 MG) oraz linie wyprowadzone od pacjentów (3005, 3019, 3034, 3048, 3073), przy jednoczesnej integracji odpowiedzi (przeżywalność, oddychanie mitochondrialne) z danymi metabolomicznymi oraz poziomem receptora transferryny TFRC.

6. Wyniki badań

6.1. Mikroekstrakcja do fazy stałej w badaniach metabolomicznych *in vitro*. Przygotowanie systemu integrującego 96-dołkowy system hodowli komórkowej z preparatyką próbki w kierunku analizy metabolomu zewnątrzkomórkowego połączonego z klasycznymi testami komórkowymi. – P.2.

Opis dotyczy pracy: **Szeliska, P.**, Jaroch, Charemski, B., Kahremanoğlu, K., Çetin, E., Boyaci E., Bojko, B. Protocol for the upgraded high-throughput SPME system for biocompatible in vitro extraction from small volume for metabolomics and pharmaceutical assays. Green Analytical Chemistry 2025, 13, 100238.

Hodowle komórkowe stanowią podstawową platformę do wstępnej oceny nowych leków i biomateriałów oraz do badania mechanizmów chorób, w tym nowotworów. We wczesnej fazie rozwoju terapii prowadzi się zwykle szerokie badania przesiewowe, w których linie komórkowe idealnie nadają się do oceny pierwszych efektów działania związków i do szybkiego odrzucania tych, które okazują się zbyt toksyczne lub nieskuteczne. Udoskonalenie analiz *in vitro* może realnie ograniczyć wykorzystanie zwierząt w badaniach przedklinicznych oraz zmniejszyć liczbę niepowodzeń na etapie klinicznym. Metabolomika wnosi do rozwoju leków kluczowe informacje: od parametrów wchłaniania, dystrybucji, metabolizmu i wydalania (ang. Absorption, Distribution, Metabolism, Excretion, ADME), przez wpływ związku na metabolom komórkowy, po identyfikację biomarkerów. Dotychczasowy postęp dotyczy głównie technik separacji i detekcji, podczas gdy przygotowanie próbki pozostaje w dużej mierze niestandaryzowane, co ogranicza porównywalność i powtarzalność wyników.

W pracy zaprezentowano zmodyfikowany, wysokoprzepustowy system przygotowania próbek oparty na włóknach SPME, przeznaczony do biokompatybilnego pobierania związków z małych objętości hodowli komórkowych *in vitro*. System, nazwany „SPME-lid", integruje włókna SPME z pokrywką płytki 96-dołkowej i umożliwia prowadzenie ekstrakcji bezpośrednio w inkubatorze CO_2. Dzięki temu zachowane są optymalne warunki wzrostu, ograniczane są zaburzenia fizjologii komórek, a z tego samego dołka można wykonywać powtarzane ekstrakcje w układzie czasowym, co jest szczególnie cenne w metabolomice farmaceutycznej i toksykologicznej oraz badaniach kinetyki leków i biomarkerów. Zestawienie różnic względem wcześniejszego systemu wskazuje właśnie te przewagi (pH, temperatura, brak parowania, elastyczniejszy czas ekstrakcji).

Autorzy przeprowadzili analizę zmian metabolomu w czasie (time-course analysis) na liniach B16F10 i LL2, wykonując 15-minutowe ekstrakcje co 24 godziny przez 4 dni i następnie oceniając wpływ procedury na żywotność (barwienia aneksyna V / jodek propidyny), proliferację poprzez oznaczenie z 5-bromo-2′-deoksyurydyną (ang. 5-Bromo-2′-deoxyuridine, BrdU) i żywotność metaboliczną (test MTT). Nie odnotowano istotnego wpływu ekstrakcji z wykorzystaniem SPME-lid na te parametry, co potwierdza neutralność nowego systemu. Ponadto, w badaniach testowano biokompatybilność i efektywność nowych sond SPME opartych o pokrycie teflonowe (HLB/PTFE) i porównano je z włóknami referencyjnymi (HLB/PAN). Przedstawiono też przykładowe ilości związków (aminokwasów) odzyskiwanych w kolejnych punktach czasowych uzyskane poprzez analizę z zastosowaniem wysokosprawnej chromatografii cieczowej sprzężonej ze spektrometrią mas.

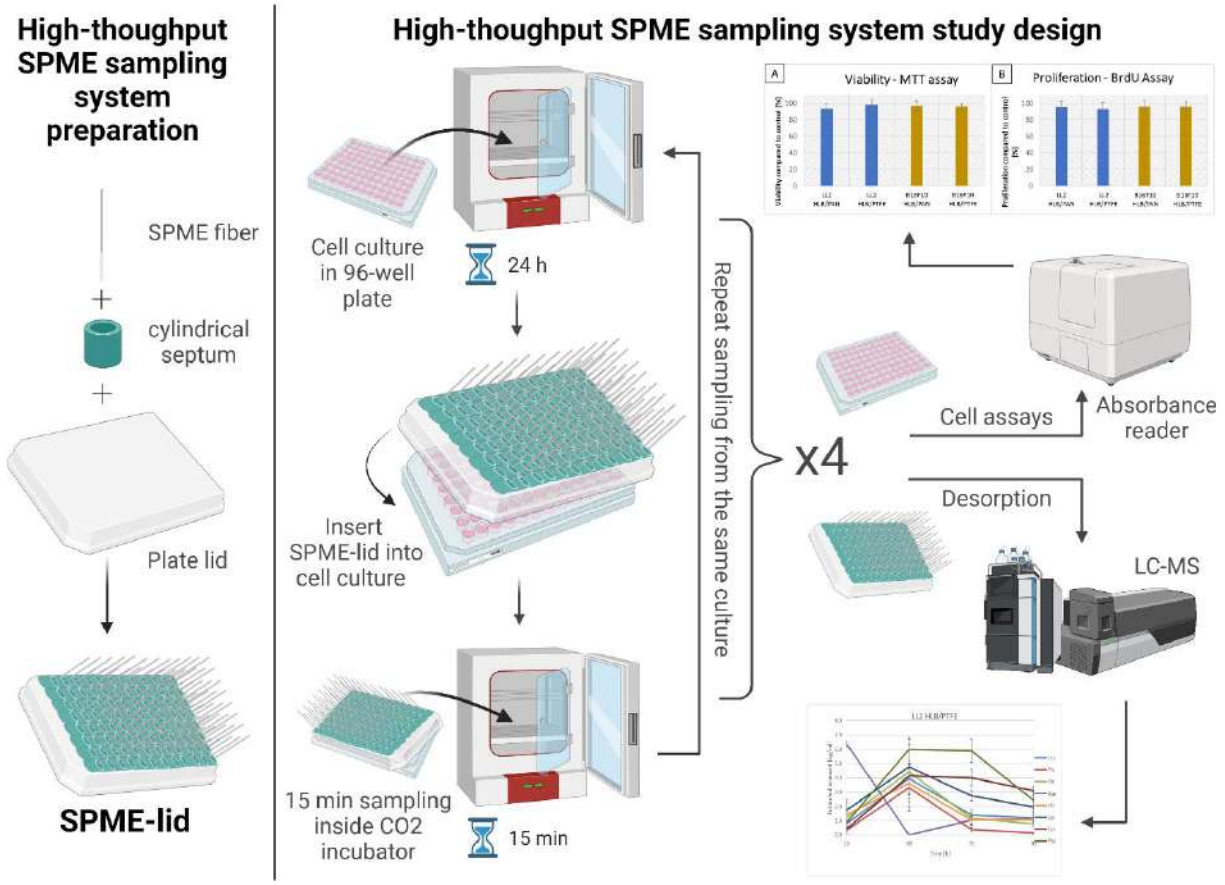

Rycina 1. *Schemat przygotowania próbki analizy metabolomicznej z użyciem SPME-lid w formacie 96-dołkowym w hodowli in vitro połączonym ze standardowymi testami wykonywanymi w hodowlach komórkowych.*

Zaproponowaną metodę oceniono pod kątem „zieloności” z wykorzystaniem narzędzia AGREEprep w 10 kategoriach obejmujących m.in. umiejscowienie przygotowania próbki, materiały niebezpieczne, odpady, ekonomię skali próbki, przepustowość, integrację/automatyzację, zużycie energii czy konfigurację post-prep dla analizy. Uzyskano wynik 0,75/1,0 – szczególnie wysokie noty przy przygotowaniu próbki „in-line” (inkubator), minimalnej objętości (100 µl) i wysokiej przepustowości (96 próbek jednocześnie). Niższe oceny dotyczyły m.in. integracji/automatyzacji (ręczne przenoszenie pokrywki między płytkami) i odpadów (wieloetapowe preconditioning/wash/cleaning), jednakże w tych kwestiach wskazano potencjał poprawy.

Praca dostarcza kompletnej instrukcji budowy i użycia systemu SPME dla płytek 96-dołkowych oraz pokazuje, że ekstrakcja wewnątrz inkubatora jest biokompatybilna i powtarzalna, a jednocześnie zgodna z trendami zielonej chemii (AGREEprep 0,75). Jest to istotny krok w kierunku standaryzacji i upowszechnienia wysokoprzepustowej, czasowo-rozdzielczej metabolomiki hodowli komórkowych na potrzeby badań farmaceutycznych i toksykologicznych. Wskazany został również kierunek dalszej optymalizacji, m.in. przez automatyzację i dobór bardziej ekologicznych materiałów.

Green Analytical Chemistry 13 (2025) 100238

Contents lists available at ScienceDirect

Green Analytical Chemistry

journal homepage: www.elsevier.com/locate/greeac

Protocol for the upgraded high-throughput SPME system for biocompatible *in vitro* extraction from small volume for metabolomics and pharmaceutical assays

Paulina Szeliska [a], Karol Jaroch [a], Bartłomiej Charemski [a], Kübra Kahremanoğlu [b], Enes Çetin [a,b], Ezel Boyaci [b], Barbara Bojko [a,*]

[a] Department of Pharmacodynamics and Molecular Pharmacology, Faculty of Pharmacy, Collegium Medicum in Bydgoszcz, Nicolaus Copernicus University in Toruń, Bydgoszcz, Poland
[b] Department of Chemistry, Middle East Technical University, Ankara, Türkiye

ARTICLE INFO

Keywords:
Solid phase microextraction
LC-MS
Cell cultures *in vitro*
High-throughput sample preparation
Metabolomics

ABSTRACT

This study presents an updated application of Solid Phase Microextraction (SPME) technology for high-throughput, time-course metabolomic analysis in *in vitro* cell culture models. SPME, a versatile and minimally invasive sample preparation technique, was integrated with 96-well plate systems to enhance metabolomic profiling while maintaining cell viability. The proposed SPME-lid system was used to evaluate employed SPME fibers with miniaturized polytetrafluoroethylene (PTFE)-based coatings.

The innovative SPME-lid system enables in-incubator sampling, preserving optimal cell growth conditions and permitting repeated extractions from the same culture over time. Experiments demonstrated the biocompatibility of the SPME coatings and their negligible influence on key cellular parameters. This approach's time-course analysis revealed shifts in metabolite levels, showcasing its potential for biochemical and drug development studies. Furthermore, the method aligns with green chemistry principles, reducing solvent and plastic consumption, and was evaluated with a 0.75 AGREEprep score for sustainability.

This protocol represents a significant advancement in metabolomic methodologies, providing a scalable, eco-friendly solution for comprehensive metabolomic profiling in pharmaceutical and toxicological research.

1. Introduction

Before a newly developed therapeutic compound can be distributed commercially, it must undergo a careful evaluation process consisting of discovery, preclinical analysis, and clinical trial. Before clinical trials on humans can start, compounds undergo rigorous analysis on *in vitro* and *in vivo* animal models [1]. Cell culture serves as a matrix of choice for the first-step evaluation of newly developed drugs or biomaterials as well as for studying the nature of diseases such as cancers. The first stage of development of potential therapeutic agents is usually based on wide-range screening. For that, cell lines are perfect candidates to assess the compounds' initial effect on studied diseases and eliminate those deemed too toxic or ineffective. Traditional cell culture models offer many advantages for the initial study of the influence of xenobiotics on living systems. They are usually on an established cell type; each cell has equal access to nutrients, and available assays are cheap, easy to conduct, and highly standardized. Those controlled conditions allow for high-level repeatability of results, which makes the results more transparent, and easier to interpret. Nowadays, scientists' interests have shifted towards improving cell culture models and assays for better extrapolation of results from *in vitro* to *in vivo* models (IVIVE)[2]. Improving the accuracy of *in vitro* analysis can benefit the researchers, having the influence on minimalization of animal use in *in vivo* pre-clinical experiments, as well as reducing failures in clinical testing, which can be very expensive [3,4]. Metabolomics are one of "omic" that focuses on the analysis of small molecules (<1500 Da). It can bring significant new information in the drug development process, such as measuring ADME (absorption, distribution, metabolism, and excretion), influence of the drug on cellular metabolome or identification of potential biomarkers. However, most of the described advances are in separation and detection techniques while sample preparation step is mostly unstandardized [5–7].

* Corresponding author.
E-mail address: b.bojko@cm.umk.pl (B. Bojko).

https://doi.org/10.1016/j.greeac.2025.100238
Received 30 December 2024; Received in revised form 22 February 2025; Accepted 24 February 2025
Available online 25 February 2025

1.1. SPME device

SPME device usually consists of solid support coated with the extraction phase of choice. SPME is highly flexible and can be adapted to the desired matrix and targeted compounds. To date, many different supporting materials and their geometries have been used to prepare SPME extraction devices, such as nitinol wire, stainless steel, or stiff fabric. SPME device can take the form of a flat metal plate in a blade-like shape for the higher surface area, providing higher extraction amounts without sacrificing the time needed for extraction [8], a small wire in the size of an acupuncture needle for negligible extraction or a tube form for reproducibility and speed of sampling and gas chromatography (GC) analysis [9,10]. The SPME device can be used to extract volatile organic compounds (VOCs) for GC applications or non-volatile compounds for liquid chromatography (LC) applications. The most common extraction phases of SPME devices differ between GC and LC applications. A wide choice of thermally stable SPME devices can be coupled directly to GC for analysis of VOCs, most of them available commercially. The most widely used are DVB/PDMS (divinylbenzene/polydimethylsiloxane), Car/PDMS (carboxen/polydimethylsiloxane), and HLB/PDMS (hydrophilic-lipophilic balanced/polydimethylsiloxane) [11,12]. SPME-LC-MS (using materials suitable for desorption in common LC solvents) can be similarly flexible regarding extraction particles; however, there has been one commercially available SPME coating for analysis of non-volatile compounds – C18. In the literature, more have been described – e.g. HLB (hydrophilic-lipophilic-balances particles), PFP (pentafluorophenylpropyl) [13]. The HLB coating is commercially available in Coated Blade Spray (CBS) SPME geometry – SPME in blade form offers higher extraction surface and analytes can be desorbed by introduction of solvent droplet on the coating surface and application of voltage. The blade then acts as a spray ionization source directing the analytes into the MS, meaningfully decreasing analysis time. However, it is not compatible with 96-well plate application for cell culture. Moreover, there are very limited number of coatings reported to date that can be used for the analysis of both volatile and non-volatile compounds, and the first reported one was for the home-made HLB coated SPME fibers introduced by Gionfriddo et al., which were based on the immobilization of extractive particles in polytetrafluoroethylene amorphous fluoroplastics (PTFE AF) [14]. However, the potential of PTFE based coatings for metabolomic analysis was not yet investigated. Recently, Kahremanoğlu et al. described the miniaturization of PTFE AF supported HLB coating with the possibility to analyze both volatile and non-volatile compounds [15] in small sample volumes and potential to perform analysis on living systems. Moreover, since PTFE based materials have proven biocompatibility in tissue in *in vivo* animal and human models [16–18], it should enhance the biocompatibility of SPME, making it particularly good candidate for analysis both *in vitro* and *in vivo*. The qualities of PTFE AF based coatings, especially in miniaturized form, make it particularly good candidate for studies of small compounds such as metabolites or drugs in preclinical trials. Miniaturized SPME with this coating would be also notably useful for analyzing small sample volumes or comparing volatile and non-volatile compounds, since it can withstand both solvent desorption and temperature desorption. The potential of the SPME coatings based on PTFE AF, especially in combination with HLB particles, is further explored in Kahremanoğlu et al. [15]. In this protocol, both HLB/PAN and novel miniaturized HLB/PTFE (polytetrafluoroethylene) fibers were prepared in-house.

1.2. Applications of SPME in cell culture analysis

The use of SPME in the analysis of Volatile Organic Compounds (VOCs) from various cell culture matrixes is well described. The most commonly used methods apply to head-space extraction (HS-SPME), but there are also protocols involving direct-immersion (DI-SPME) mode. HS-SPME is most commonly used to extract VOCs from cell culture medium as it offers excellent reproducibility, is affordable, and is commercially available [19]. The usual extraction protocol consists of conducting traditional cell culture, pooling cell culture media, and centrifuging to purify the sample from proteins. Media can then be stored or analyzed immediately. The extraction device for HS-SPME is placed above the studied liquid, and for DI-SPME it is immersed into the collected cell culture media. However, collecting medium from cell culture means either subtracting a particular volume from the sample and replacing the withdrawn volume with a new medium, thus resetting the in-culture metabolome, or a cell culture termination. The extraction of VOCs was performed from living cell culture in sterile, tightly sealed glass bottles. It was possible for cells to be cultured in suspension [20], and from adherent living cells, although it was not specified if the culture flasks were thigh-glass sealed [8]. Since specific SPME coatings were reported to be biocompatible, it is possible to extract non-volatile compounds by applying SPME probe directly into the cell culture media (DI-SPME) while cells continue to proliferate in the culture plate [21]. This analysis is less common, but it has the potential to capture a broader profile of compounds. Thin-film SPME (TFME) was first proposed to perform *in vitro* drug metabolism studies with the use of liver microsomes, where matrix composition was similar to the cell culture medium. Moreover extraction parameters such as temperature and pH were the same as extraction from the cell culture incubator [22]. Similar drug metabolism with liver microsomes analysis was performed by Jaroch et al., however, a time-course analysis of drug metabolism was performed by multiple extractions from the same samples [23]. Different study focused on non-depletive analysis performed from small sample volumes (100 µl) using miniaturized SPME probes [13]. The approach aimed to enable quantitative time course analysis from the same samples in *in vitro* high throughput conditions [13]. A similar protocol for time-course analysis was used for non-small cell lung carcinoma metabolome monitoring after drug administration [24]. It was the first time that SPME in fiber geometry was successfully used in a high-throughput format for metabolomic analysis of living cell culture. Moreover, it was proven that it can be useful for *in vitro-in vivo* extrapolation of results [25].

1.3. The proposed high-throughput model for time-course analysis

The proposed SPME system for high-throughput extraction with fibers is based on 96-well plate lid (Fig. 1). The system is an update on previously proposed by Boyaci et al. and Jaroch et al. [13,23,25]. First system used on a live cell culture was based on a Nitrogen Evaporator body. It allowed to secure the SPME fiber in the hypodermic needle in a way that allowed for the submersion of extraction phase in the liquid. However, due to the relatively big size of the evaporator, it could be problematic to insert the whole system into the CO_2 incubator. Moreover, this system was not equipped with any kind of plate cover. This forced extraction to be performed on the open plate, thus under the laminar flow hood to protect the cell culture from contamination. This, in turn, caused the cells to remain in the non-optimal temperature for growth, which consequently, could cause liquid evaporation. This lowered the precision and repeatability of the analysis. The system was developed to address the problem of maintaining the optimal conditions for cell culture during extraction, which would allow to elongate the extraction times, directly influencing the efficiency of extraction. Moreover, the proposed system was developed with the idea of compatibility with standard cell culture testing.

1.4. Experimental design - limitations of extraction in vitro living systems for DI-SPME method development

Cell culture is a matrix that requires very particular conditions that need to be maintained to not influence the results of a conducted experiment. Many of those, such as temperature or pH, have to be selected based on cell culture conditions rather than extraction efficiency.

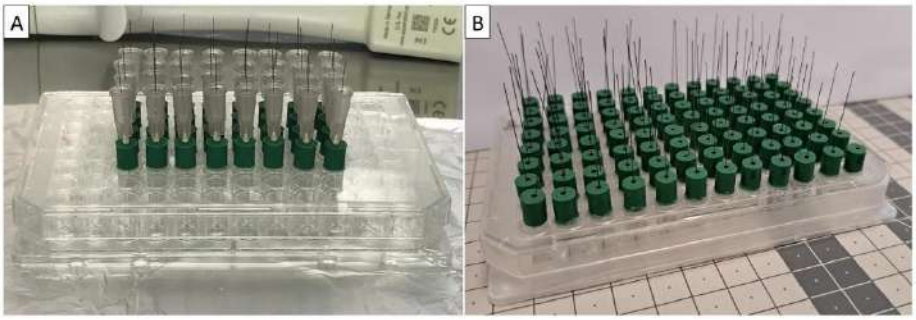

Fig. 1. The proposed high-throughput SPME-lid system with SPME fibers supported by hypodermic needle (A) or without the needle support (B). System is based on 96-well plate typically used for cell culture and cell based assays. Septum typically used in analysis of volatile compounds is used to ensure air-tightness of the lid.

1.4.1. Agitation during extraction

Agitation is an important parameter to consider during SPME extraction. It influences the extraction efficiency and therefore shortens the extraction time which in the case of living cells should be possibly short. However, all previously described agitation methods, such as rapid movement of fiber or vial, stirring, sample flow [26] cannot be applied for cell culture. Most of the established cell lines grow attached to the growth surface and are only detached when performing passaging, either by enzymatic digestion or mechanical dissociation [27]. Therefore, introducing rapid movement of/inside the cell culture might cause detachment of the cells or even cellular membrane disruption. Mechanical stress would then influence the results of the study. Extraction must be performed in static conditions for time-course analysis of cell culture. However, this limitation can be countered by the prolongation of incubation time with the SPME-fiber. Previously described systems for high-throughput were limited not only in the agitation parameter, but also extraction time. The proposed SPME-lid system compensates for static extraction with the possibility to prolong the time of SPME fiber submersion in the analyzed cell culture media. This ability is further discussed in the 1.4.5 Extraction Time section.

1.4.2. Sample pH

Most of the commercially available SPME coatings show a higher affinity for the neutral form of the analytes. Therefore, the analyte coverage might be enhanced by buffering the sample to keep the species with acidic or basic species in neutral form [19]. This strategy for improved recoveries does not apply to cell studies, as for acidic compounds, a neutral form will be achieved in acidic conditions, and analogously, basic compounds will reach a neutral form in basic conditions. Those extreme pH values would not allow for the cell culture to survive. In cell culture, cells constantly propagate which requires supplementation of nutrients such as glucose that can be used for energy acquisition. This, however, results in by-products secretion from the cells, such as lactic acid. Consequently, this causes acidification of the cell culture medium, which is usually neutralized by another component of the cell culture medium – $NaHCO_3$ (sodium bicarbonate). Cells are usually supplied with CO_2 by appropriate incubators, enabling them to keep the pH balanced by $NaHCO_3$ and CO_2 reaction at a physiological level, which is best for cells – 7.2 – 7.4 pH [27]. However, if cultured for too long, the pH of the cell culture might vary, which can be indicated by the color of the medium. Another cell culture medium component – phenol red – is added to monitor the medium pH visually. For pH below 6.8, the cell culture medium will have a yellow color; in turn, above 8.2 pH, it will be a fuchsia color [28]. Therefore, it is important to monitor if the cell culture medium is red during the experiments because it will ensure maintaining the same pH range and, consequently, observing the actual changes of metabolome occurring in the studied system and not the influence of the pH on the biological and extraction processes. Because the optimal pH of the medium in culture is supported by CO_2 supplementation in the incubator environment, conducting the extractions outside of the incubator can cause pH changes in the cell culture medium towards more basic, especially during prolonged operations such as metabolome extraction. The SPME-lid system proposed in this protocol allows for the extraction inside the incubator, protecting the maintenance of the neutral pH.

1.4.3. Ionic strength

The presence of salts in the sample strengthens the ionic strength of the sample, which can be heightened by the addition of more salts. Salts are permanent additives to various cell culture media types. It includes compounds such as $CaCl_2$, $Fe(NO_3)_3 \times 9\ H_2O$, $MgSO_4$, KCl, $NaHCO_3$, NaCl or NaH_2PO_4 [28]. This makes the cell culture medium a matrix of high ionic strength and might influence the profile of extracted compounds. For HS analysis, it might be of particular interest since it positively influences the passage of molecules to head-space [19]. For DI extraction, the efficiency is highly compound-dependent; however, it was shown that the addition of salts in biological samples reduces sample-sample variability and gives more reproducible results [29]. Therefore, DI-SPME extraction from cell culture would benefit from the nature of the matrix, but it might be challenging to perform analysis for low-abundant compounds, particularly at the late time points during time-course extraction.

1.4.4. Extraction temperature

Another parameter that can influence the efficiency of SPME extraction is temperature. Increased temperature not only favors compounds to enter head-space but also increases the mass transfer into the SPME coating. For both HS- and DI-SPME, the increased temperature of the sample allows for shortening the time needed to reach equilibrium, which is important in cases where obtaining the highest sensitivity for the given compound without sacrificing the analysis time is necessary [30,31]. For most mammalian cell lines, the optimal culturing temperature is 36–37 °C, and when it is increased to 40 °C and above, cells will start to die out after about an hour [27,28]. Therefore, the sampling must be performed quickly at room temperature (RT) under the laminar flow hood for on-plate high throughput extractions. Ideal conditions would allow for extraction directly inside the incubator, where a temperature of 37 °C can be maintained for the entire extraction, which is possible with the upgraded extraction system described in this protocol. Moreover, for the first time, it allows for simultaneous extraction from 96-wells at the optimal temperature. Systems used previously either allowed for the extraction of VOCs at the 37 °C with one fiber at a time, or in high-throughput format for non-volatile compounds, but outside of the incubator (Table 1).

Table 1
Sample preparation examples for analysis of living cell culture.

	Sample	Sample prep model	Extraction conditions		Reference
VOCs	Living cell culture in T25 flask	Head-space SPME (100 μm PDMS)	Time: Temp: No. of samples at a time	60 min 37 °C 1x T25 flask	1 Wang et al. 2012,[8]
	Living cell culture in sterile glass head-space vials	Head-space SPME DVB/CAR/PDMS	Time: Temp: No. of samples at a time	24h 37 °C 1x vial	Aksenov et al. [20]
Non-volatile compounds	Living cell culture, 96-well plate	Direct immersion SPME, 5 μm HLB particles 2 mm coating	Time: Temp: No. of samples at a time	30 min RT 32 wells	Jaroch et al. [24]
	2D and 3D living cell culture, 96-well plate	Direct immersion SPME,	Time: Temp: No. of samples at a time	30 min RT 32 wells Time-course extraction	Jaroch et al. [25]

1.4.5. Standardization and calibration method

When performing any form of sample prep there is a need to use standard compounds for proper monitoring of either extraction efficiency or the instrument condition during analysis. However, extraction from living systems introduces unique challenges when establishing proper controls. The most straightforward approach in sample preparation with SPME is the injection of standard solutions into the sample. The most desired compounds for this standardization would be derivatized or isotopically labeled substitutes of the analyzed compounds. However, it needs to be understood that standards added to the living cells can be absorbed and used by the cells as easily as the studied compound. Therefore, the actual concentration of the standard can differ from the spiked one and negatively affect the data. Moreover, it can influence cellular metabolome by competing with endogenous compounds or studied drugs, thus sabotaging the experiment.

There are a few alternative approaches for calibration when liquid standard injection into the sample is impossible. Because SPME is an equilibrium-based extraction, this can be used to calculate the sample concentration. The most common is calibration for equilibrium extraction [26]. However, in multi-residue analysis like metabolomics, it is practically impossible to optimize the method where all the compounds reach equilibrium. Moreover, sample complexity might influence studied compounds in such a way that previously established equilibrium will be changed.

The best-suited method for extraction standardization from living systems for selected compounds would be external matrix-match calibration. However, to prepare a reliable calibration curve for the studied compounds, one must consider the complexity of the matrix. Calibration curve of standards dissolved in water or organic solvent would not properly reflect the matrix effect occurring in the sample. The composition of complete cell culture media prepared for culturing consists not only of amino acids, vitamins and carbohydrates but also many enzymes and other proteins found in Fetal Bovine Serum (FBS). These proteins and enzymes can influence the concentration of free fraction of the compounds in the sample and, consequently, the binding of compounds to the coating. Therefore, the proper matrix should be based on cell culture media with FBS. When preparing a surrogate matrix for standardization of future analysis of a live culture in a time-course manner, it would be best also to add the lysed cell pellet into the mixture to properly reflect the possible matrix influence of cellular proteins. It would reflect the cells in culture during the actual extraction. The number of cells before lysis can be determined by counting with trypan blue. Counting with the use of trypan blue is the most accessible way for determining the number of cells in suspension since it requires only the trypan blue dye, hemocytometer for counting and brightfield microscope [27], which are usually standard reagents and equipment in cell culture laboratory. Performing a BCA assay for total protein concentration could be also useful, since the quantity of lysed cells to be added to surrogate matrix could be standardized based on the proteins acquired from these cells. The way of lysing the cells should be detergent free, therefore best methods would be freeze and thaw or sonication.

When surrogate matrix is used (i.e. a mix of cell culture media, FBS, necessary growth supplements, lysed (but no live!) cells) the dissolved standards might be added to prepare calibration curve. It is recommended that the calibration curve should consist of at least six calibration concentrations plus a zero standard point [32]. Solution like that, since it contains many possible contaminants for LC-MS, should not be injected directly into the instrument. Instead, it should be subjected to the same protocol for sample preparation as the intended samples. The preparation of calibration curve for metabolomic analysis is even more complicated, since, as mentioned above, metabolites such as amino acids are a component of most commercially available cell culture media. Moreover, many metabolites also occur in the FBS. Two approaches can be used to prepare appropriate matrix for calibration curve. First, less reflective of the complexity of media, however much more affordable is using of a substitute cell culture medium. For that, a base of mixture of salts can be used. Standard Phosphate Buffer Saline (PBS) is not recommended, similar to Hanks' Balanced Salt Solution (HBSS), since those buffers do not contain sodium bicarbonate and will not behave like a culture medium in terms of balancing pH. The most suited for this purpose would be EBSS, which is a mixture of salts containing sodium bicarbonate among others. Then, supplements can be added to recreate the medium composition, such as vitamin solution or Bovine Pituitary Extract (BPE), the latter reflecting proteins usually included in the FBS. The second method requires the purchase of standards that are isotopically labeled, so they are separated in the LC the same way as a studied compounds, but they can be easily differentiated from them by the mass detected by MS. The use of those standards allows for the use of the complete cell culture medium for the calibration curve, without the need for a surrogate matrix.

After preparing a calibration curve in the desorption solution of choice corresponding to the actual experiment (instrumental calibration) and the calibration curve using the matrix of choice, extract the standards from the matrix with SPME to determine extraction efficiency. Next use the instrumental calibration curve before running the batch of samples on LC-MS. If the batch is long, in addition of running the calibration curve before and after the batch, run it also between the samples (*e.g.* every 20 samples) to monitor the stability of compounds.

1.5. Extraction time

The time of extraction is a crucial step in SPME analysis. It is important to establish optimal extraction time to reach proper recoveries. It is generally recommended that extraction time be assessed based on the purpose needed. High throughput, sensitivity, or reproducibility are all influenced by the extraction time. The best sensitivity

and reproducibility can be achieved by extraction until equilibrium [19, 26]. However, this is not possible because different metabolites reach equilibrium at different times; for some, the process is too long, considering cell cultures are living systems, and sampling should be reasonably short (particularly when repeated analysis is the goal). Previously described protocols [24] proposed high-throughput SPME extraction under the laminar flow conditions for 30 min (Fig. 2.A). Comparative analysis performed by our team (Fig. 2.B) revealed significant differences between cell cultures that underwent extraction inside the incubator and those left for 30 min under the laminar flow hood (underwent extraction and serving as non-extracted control). The former system exposed cells to too low temperature and led to evaporation of cell culture media due to the removal of the cover plate during extraction. Creating the system for intra-incubator extraction allowed for prolonged SPME extraction without influencing the viability of the cells (Fig. 3). This made the high-throughput extraction method possible to be used for multiple extractions (Fig. 4) from the same plate with no significant influence on cell growth and viability compared to a cell culture with no extraction performed (Fig. 5).

1.6. Desorption method

The desorption method is one of the few steps in our high-throughput SPME optimization process that is not determined by the analyzed matrix. Therefore, it consists of all the parameters that need to be chosen in routine SPME protocol. The composition of the desorption solvent should be determined by the properties of the studied compounds and should be chosen individually for every planned experiment of new compounds. For metabolomics, ACN:H_2O in various proportions was proven to be efficient [24,25]. Agitation is recommended during this step to speed up the process. Various 96-well formats might be used, such as deep-well plates, non-treated plates or PCR plates. The latter is most recommended for the application described in this work since it is desirable for the desorption volume to be as small as possible for higher sensitivity [26].

In the case of VOCs, the SPME fiber following the extraction should be injected in the shortest possible time. The most advisable would be sampling at the GC site so the fiber can be transferred directly to the GC injector port to ensure that no analytes are lost. In the case of live cell experiments, where extraction would take place in a laboratory room meant for cell culture, fiber should be transferred in dry ice. Before sampling, desorption time and temperature optimization should be conducted to ensure that all analytes are desorbed from the fiber.

1.7. Anticipated results

1.7.1. Targeted metabolomic of cell lines in high-throughput, time-course analysis

The high-throughput 96-well SPME model for time-course cell culture analysis proposed in this manuscript was used to compare newly developed coatings based on polytetrafluoroethylene amorphous fluoroplastics (PTFE). The SPME fibers used in the 96-well high-throughput mode were produced as described elsewhere [14]. The SPME sampling was assessed on the cellular model in *in vitro* conditions. The cells seeded in a 96-well plate were subjected to 15 min extraction every 24 h, as shown in Fig. 3. The sampling process was completed in the 5th day of culturing, and the same cell culture was subjected to standard assays such as MTT (Sigma-Aldrich, cat. no. M5655), BrdU (Sigma-Aldrich, cat. no. QIA58) and Iodium Propidine and Annexin V-FITC staining (Kayman cat. no. 600300). The lack of influence of sampling with the new SPME probes on cell parameters such as viability (Fig. 6.A), proliferation (Fig. 6.B), and apoptosis induction (Figs. 7 and 8) confirmed the biocompatibility of the devices. Moreover, the data was compared with well-described PAN-based coatings, showing the same outcome.

The time-course metabolomic analysis was performed at four time points, as shown in Fig. 4. The SPME fibers underwent desorption as described in [15] with minor changes. Next, samples were analyzed via an LC-MS/MS system composed of Nexera UHPLC (Shimadzu, Kyoto, Japan) and LC-MS 8060 triple quadrupole mass spectrometer (Shimadzu, Kyoto, Japan). The chromatographic condition was modified based on the method described by Vuckovic et al. [33]. The MRM transitions are presented in Table 2. The pentafluorophenyl (PFP) Discovery HS F5 column (100 mm x 2.1 mm, 3 µm, Supelco, Bellefonte, PA, USA) was used for separation. The mobile phases comprised water + 0.1 % formic acid (mobile phase A) and acetonitrile + 0.1 % formic acid (mobile phase B). The chromatography gradient was as follows: 0–2 min 0 % B, 2–10 min linear gradient to 90 % B, 10–12 min, hold on 90 % B, 12–15 min 0 % B. Additional parameters were as follows: LC oven temperature was 40 °C, autosampler temperature was 4 °C, the flow rate was to 0.4 ml/min and the injection volume was 10 µl.

The total amounts extracted were back-calculated based on a six-point calibration curve that was run at the beginning and end of the batch. Each sample was collected in tetraplicate and the batch was randomized to eliminate possible errors of the analysis. The results showed that the method successfully captured metabolites in each time point even with just 15 min of static extraction (Fig. 9). The levels of detected metabolites were similar between HLB/PAN and HLB/PTFE, which indicates that the latter coating can be successfully used for metabolomic analysis in *in vitro culture* and does not influence the viability or proliferation of cells in any significant way, similar to well established HLB/PAN. However, the use of HLB/PTFE in this particular format might be challenging for inexperienced users due to its slightly

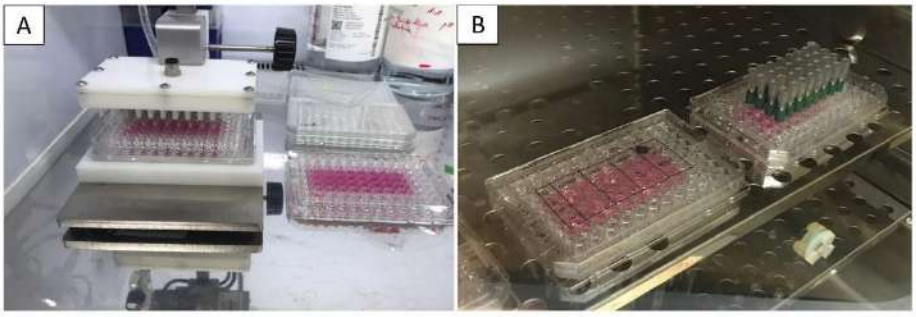

Fig. 2. High-throughput SPME system for (A) outer- and (B) intra-incubator extraction from cell culture. System used for (A) outer-incubator extraction is supported by the Nitrogen Evaporator body and not equipped with a lid. New system (B) supported by septum glued to the plate lid allows for easy intra-incubator extraction.

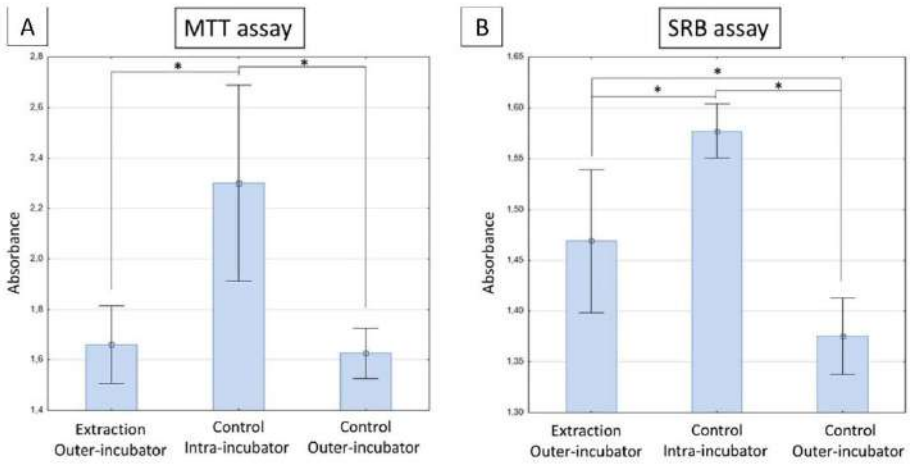

Fig. 3. The absorbance indicating viability (A) and cell mass (B) of B16F10 cell line after SPME extra-incubator system extraction every 24 h for 4 days compared to intra-incubator and outer-incubator control.

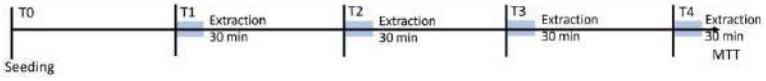

Fig. 4. The graphical abstract of time-course sampling from cell culture 96-well plate.

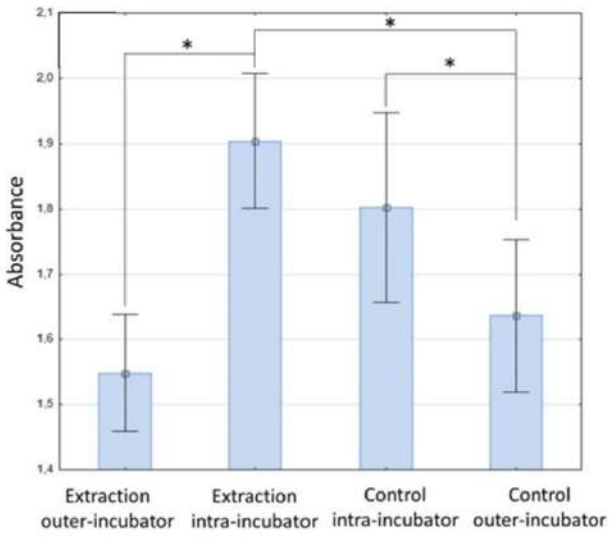

Fig. 5. The mean absorbance of B16F10 cell line after extraction with outer- and intra-incubator systems every 24 h for 4 days compared to controls.

higher susceptibility to mechanical damage compared to HLB/PAN and the risk of accidental scratching.

Time-course analysis revealed a shift of metabolite patterns over time. Fig. 9 demonstrates the levels at which metabolites mentioned in Table 2 were detected at a specific time. Not all metabolites behaved the same way in culture; aspargine seemed to be consumed by the cells in the first 24 h of culture, while compounds such as histidine or threonine were secreted into the cell culture medium by the cells. However, most of the metabolite levels stabilize between the 72nd and 96th hour of culture, which corresponds with the plateau phase in cell culture growth. Metabolic profiles also depended on the type of cells studied, which indicates different needs and ways of working between cell types.

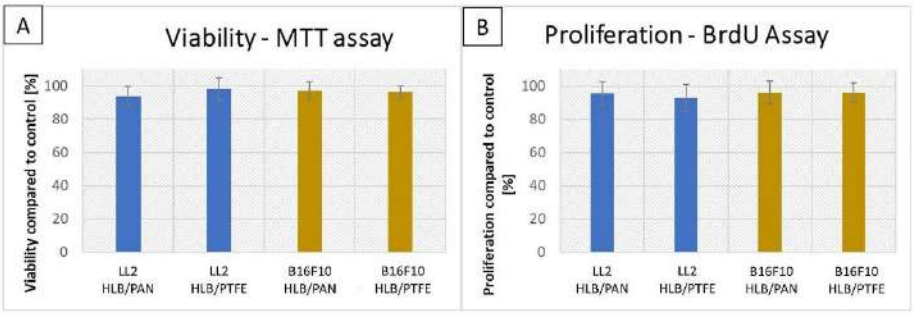

Fig. 6. Viability (A) and proliferation (B) of LL2 and B16F10 cell lines after 15 min extraction every 24 h for 4 days with new HLB-PTFE and commercial HLB-PAN fibers compared to control.

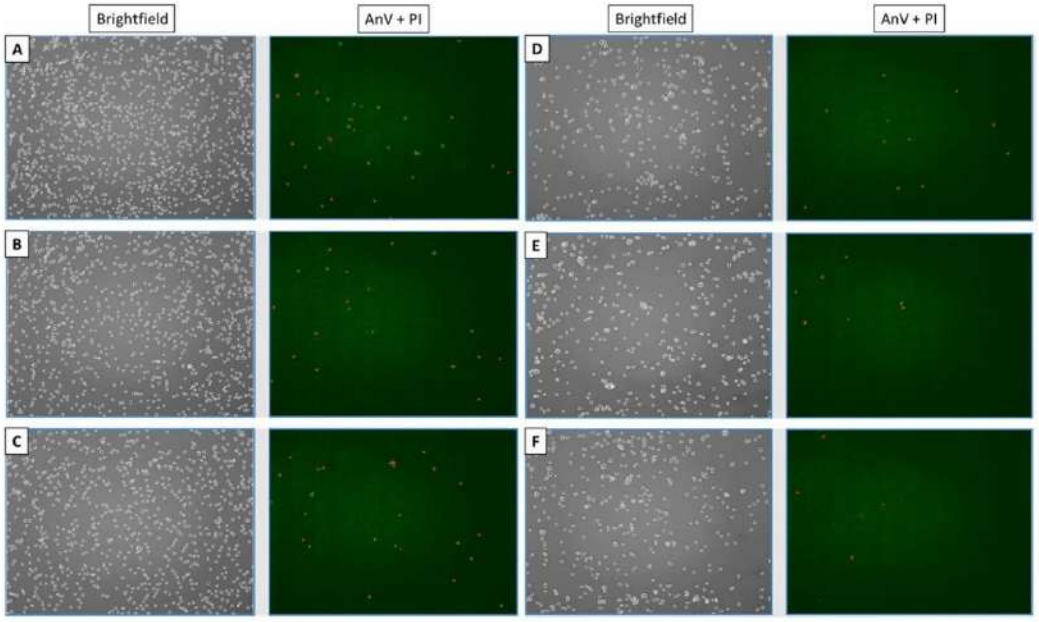

Fig. 7. Images of B16F10 cell line (A) after 4x, 15 min extractions with HLB/PAN fibers (B) and HLB/PTFE fibers (C) and LL2 cell line (D) after 4 extractions with HLB/PAN fibers (E) and HLB/PTFE fibers (F).

Even this basic information can showcase the condition of cells in culture, which can be of use in testing new drug formulations. Moreover, since SPME can also be used to analyze the level of drugs, it can be used to monitor the drug behavior over time with simultaneous metabolomic analysis and the use of standard cell culture assays. It favours biological precision of the results by reducing the variance and enables a more clear-cut comparison of results from different assays. This 96-well plate extraction allowed for the minimalization of the use of plastic (Tables 3 and 4) required to be used for analogical study prepared with standard extraction methods e.g., liquid-liquid extraction (LLE).

2. Materials and human resources

2.1. Materials

- Sterile 96-well plate (Nunc™ MicroWell™, cat no. 167008 or other 96-well plate)
- Cell culture medium chosen based upon manufacturer's recommendation (e.g. RPMI 1640, Corning, cat. no. 10-040-CV)
- Fetal Bonive Serum (Corning, cat. no. 35-079-CV or equivalent)
- Antibiotic Antymicotic Solution (Merck, cat. no. A5955-20 ml or equivalent)
- Cell line of choice (There is a wide choice of cell lines at the American Type Culture Collection, ATCC, with appropriate handling information and recommended media and supplements)
- 96-well PCR plate (Bionovo, cat. no. A-710880)

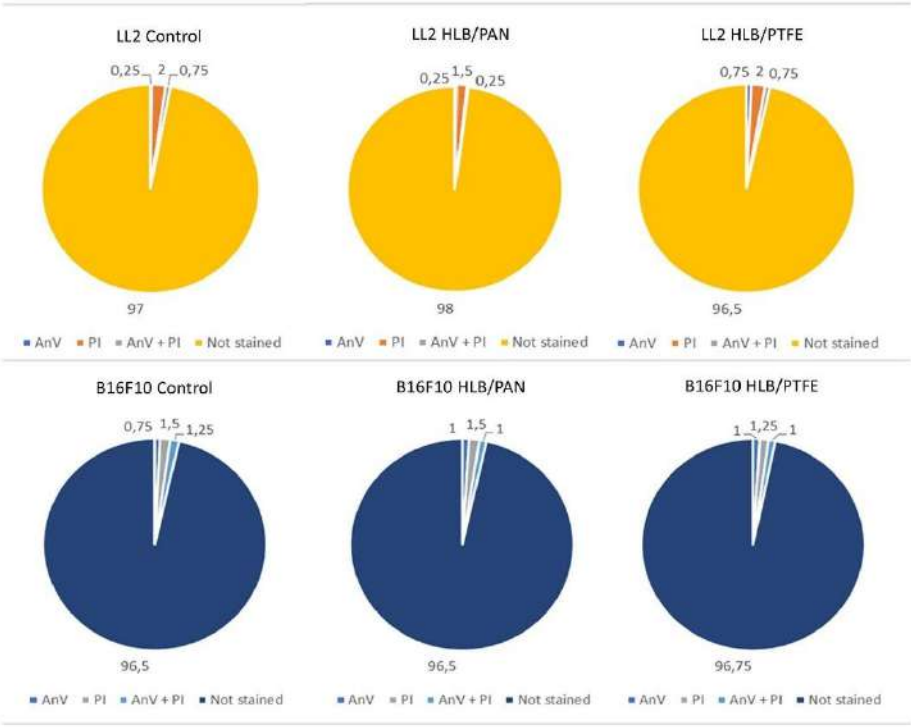

Fig. 8. Percentage of early apoptotic (AnV), late apoptotic (AnV + PI), dead (PI) and live (Not stained) of LL2 and B16F10 cell lines after 15 min extraction every 24 h for 4 days with new HLB/PTFE and commercial HLB/PAN SPME fibers compared to control.

Table 2
The list of analyzed compounds.

No	Compound	Precursor m/z	Product m/z (quant ion)
1	Leucine	132.10	86.15
2	Proline	116.1	70.0
3	Threonine	120.10	74.00
4	Asparagine	133.10	87.2
5	Arginine	175.10	70.10
6	Histidine	156.10	110.10
7	Lysine	147.2	84.2
8	Tyrosine	182.10	136.00

- Ultra-high purity water, sterilized (Merck, cat. no.1047351000)
- Methanol LC-MS grade (Honeywell, cat. no. 34966)
- Acetonitrile, LC-MS grade (Supelco, cat. no. 1.00029.2500)
- 2-propanol, LC-MS grade (Honeywell, cat. no. 34965)
- Internal standards *e.g.* Phenylalanine-D8 (TCR, cat. no. TCR-P319419))
- SPME fibers;
  - a solid support of nickel-titanium metal alloy (nitinol, *e.g.*, Nextmetal Corporation, cat. no. F2063, 0.2 mm diameter) of 4 cm length per fiber
  - 2 mm length of coating, 1 layer (can be created in-house based on the description provided by Gómez-Ríos [34] and Gionfriddo [14])
- Hypodermic needle (*e.g.*, 0.4 × 13 mm, Microlance, cat. no. 300635)
- Pipette tips – 20–200 µl (*e.g.* eppendorf, cat. no. 0030073825)
- Glass flasks and bottles to prepare solvent mixtures

2.2. Instruments

- Shaker (Ingeniereurobüro CAT, SH10 shaker, or equivalent)
- CO2 incubator for cell culture (Binder, CB 056, or equivalent)
- Laminar flow hood (Alpina, BIO130, or equivalent)
- A rotary tool with a milling bit (Parkside, X 12 V Team, or equivalent)

2.3. Equipment

- Lid for a microplate without cut corners (*e.g.*, WVR, Universal Lid, cat no. 250002)
- Sterile 96-well plate (Nunc™ MicroWell™, cat no. 167008 or other 96-well plate)
- Septum, cylindrical type (Merck, Thermogreen LB-1 Septa, cylindrical, cat. no. 20668)
- Glue (*e.g.* Infinitybond, biocompatible Cyanoacrylate Super Glue or equivalent)

2.4. Human resources

- 3 h working hours of personnel after short instructions on operating the rotary tool; preparation of SPME-lid system for intra-incubator extractions
- 1 working hour to train new personnel on working in sterile conditions under the laminar flow hood, 30 working minutes to train new personnel to working with the SPME-lid system
- 2–5 working hours of trained personnel for performing complete sampling of 96-wells with the SPME-lid

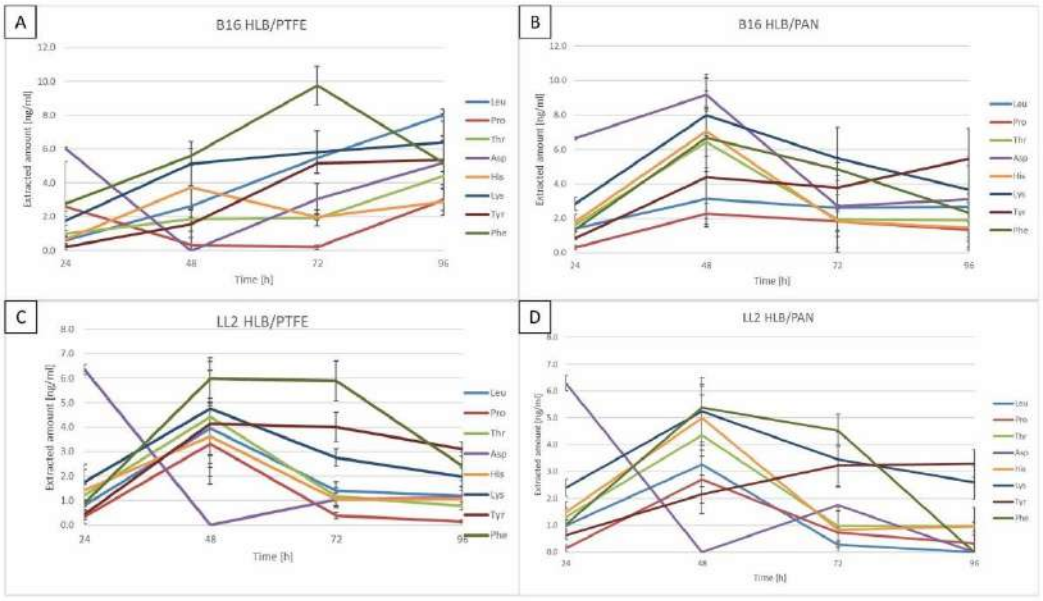

Fig. 9. The amount of extracted amino acids by 15 min extraction every 24 h with the SPME-lid system and HLB/PTFE (a and c) and HLB/PAN (b and d) coatings on B16F20 cell line (a and b) and LL2 cell line (c and d). Extracted amount was backcalculated using calibration curve and presented in ng/ml.

Table 3
Total analysis time and amount of waste generated for 1 sampling of 96 samples with high-throughput SPME.

Step	Duration	Volume of waste generated	Plastic utensils used
Pretreatment	24h (1440 min)	10–20 ml total; 100–200 µl/ sample	1 × 96-well plate; reusable
Wash	5s 5s	After preconditioning 10–20 ml total; 100–200 µl/ sample After extraction 10–20 ml total; 100–200 µl/ sample	After preconditioning 1 × 96-well plate; reusable After extraction 1 × 96-well plate; non reusable
Extraction	5–60 min	0 ml	0 additional plastic
Desorption	5–120 min	10 ml total; 100 µl/ sample	1 × 96-well PCR plate; non reusable
*Cleaning	60 min	10–20 ml total; 100–200 µl/ sample	1 × 96-well plate; reusable
Total	1510–1680 min	50–90 ml total; 500–900 µl/ sample	5 × 96-well plates; 3 reusable plates 3g of plastic/sample; can be minimized to 1.83 g with reusable plates

* Cleaning step is possible for targeted analysis only.

Table 4
Cost estimation of high-throughput, time course analysis with SPME for 96-well plate for single sampling.

Component	Real consumption	Approximated percentage of the total cost**
Plastic plates	5* 96-well plates	15 %
Extraction phase	1–5 mg/ fiber	15 %
Standards	0.01–5 µg/ sample	61 %
Solvents	500–900 µl/ sample	7 %
Energy	2.2 kWh	2 %

* It includes a plate for the cleaning procedure.
** Relative values, based on the time, location, and specific application, are provided to identify the costliest components of the described procedure.

3. Procedure

3.1. Equipment setup: 3 h for plate, 2 min per well

Step. 1.1 Separate the lid from a 96-well culture plate or open package with a single microplate lid.

Step 1.2 Use a rotary tool to drill small, 2 mm holes in the lid, one hole per well.

ATTENTION! Use safety glasses while drilling. Drill gently, and do not put too much force to avoid breaking the lid.

NOTE: The hole should not be smaller than 1 mm in diameter, so the supporting hypodermic needle should not be bigger than 2.5 mm so the glue that will hold the cylinder to the plate will have the binding surface.

Step 1.3 Carefully put a few glue droplets around the drilled hole.

Step 1.4 Put the cylindrical septum with the flat part touching the glue on the lid (half-hole facing upwards) so the septum completely covers the drilled hole. One cylinder per well.

TRICKY! Put the glue around the holes in the lid. Pay attention not to cover the drilled holes with the glue. Putting the fiber through a glue-covered surface after it hardens would be challenging and may contaminate the coating (Fig. 10).

PAUSE! Wait for the glue to set and cure (1–2 h, depending on the type of glue used).

Step 1.5 Insert SPME fibers through holes in the lid and septum so the wire goes through the septum, but the coating remains underneath it. If the fiber support is not sharp enough to pierce through the septum, use the hypodermic needle first. When the needle passes through the septum and the hole in the lid, insert the end of the fiber into the needle tip and push it further in (Fig. 11). Then, you can remove the needle to pierce through the rest of the septa (Fig. 1.B) or leave it inside (Fig. 1.A).

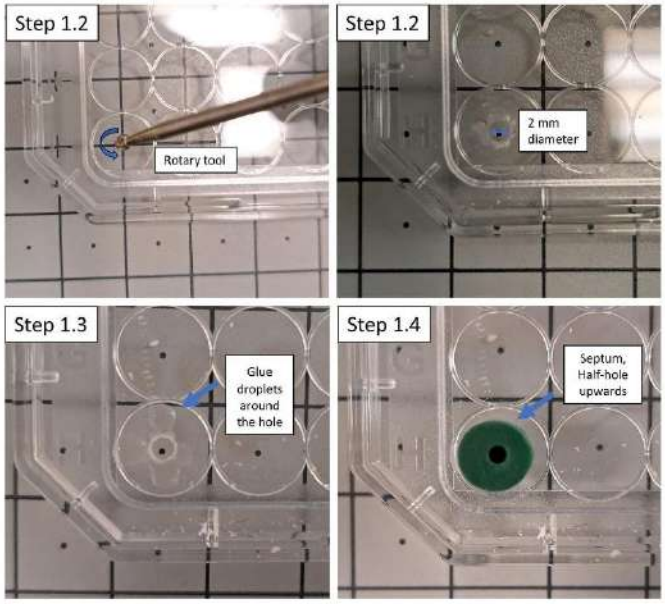

Fig. 10. Step-by-step visual instruction corresponding to challenging steps in SPME-lid assembly. Photographs corresponding to the step 1.2 show how to place the rotary tool tip on the lid and how big schould be the drilled hole. For step 1.3 the photograph shows reccomendeed placement of the glue droplets to prevent covering the hole with the glue. Step 1.4 presents the proper placement of the septum on the drilled hole.

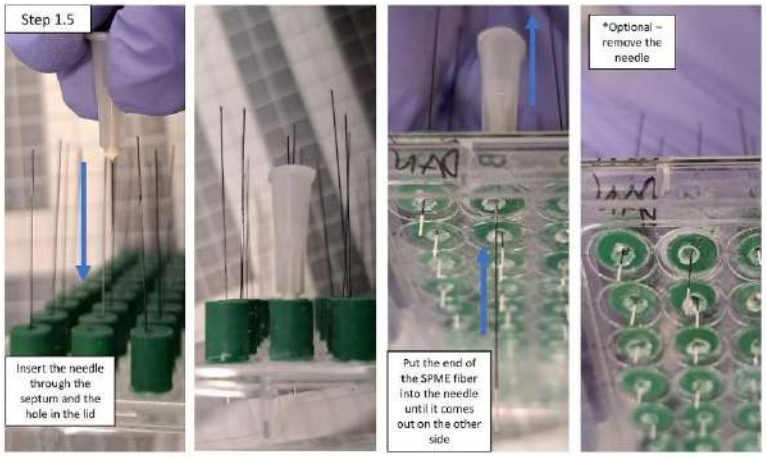

Fig. 11. The step-by-step visual presentation of the step 1.5 in the protocol. The photographs present the way the personnel schould insert the hypodermic needle into the septum and a hole in the lid, and then insert the SPME fiber into the needle so the coating does not go through the needle. Last pothograph presents the SPME fiber in the SPME-lid system after removing the hypodermic needle.

TRICKY! Ensure the fibers are placed perpendicular to the lid, not at an angle. Leaving the hypodermic needle inside the septum can support the proper position of the fiber but requires more needles.

NOTE: SPME fiber coating should be chosen based on application. SPME fiber preparation is described by Gionfriddo et al. [14].

3.2. Sampling procedure

STEP 2. Preconditioning of the fibers, 1.5h per plate

Step 2.1 Prepare the preconditioning solution by mixing methanol with ultrapure water, 1:1v/v.

Step 2.2 Transfer the SPME-lid and bottom of the 96-well plate under the laminar flow hood.

Step 2.3 Prop the SPME-lid on support (e.g., Tip boxes or vial racks)

so it is upside down, facing the UV bulb (Fig. 12).

Step 2.4 Close the laminar flow hood and turn on the UV light.

PAUSE! 15 min of UV light sterilization

Step 2.5 Inject 200 µl of preconditioning solution into the bottom part of the 96-well plate, 1 portion of preconditioning solution per well.

Step 2.6 Cover the 96-well plate with the SPME-lid.

Step 2.7 Carefully push each SPME fiber to entirely immerse in the solution.

Step 2.8 Seal the side walls of the plate with parafilm to prevent evaporation of preconditioning solution through the sides.

PAUSE! Leave the fibers in a preconditioning solution for 1 h, static.

NOTE: The fibers can remain in the preconditioning solution overnight.

STEP 3. Wash, 1.5 min

Step 3.1 Open a new, sterile 96-well plate under the laminar flow hood.

Step 3.2 Inject 200 µl of ultrapure water into the bottom part of the 96-well plate, 1 portion of water per well.

Step 3.2 Transfer the SPME-lid from the plate with preconditioning to the plate with water. Carefully lower the SPME-lid so the fibers do not scratch the walls of the wells.

SHORT PAUSE! Leave SPME fibers in water for 5 s.

STEP 4. Sample extraction, Time- 5–60 min per plate

Step 4.1 Transfer cells cultured in a 96-well plate from the CO_2 incubator under the laminar flow hood.

Step 4.2 Switch the cover lid to SPME-lid and carefully lower the SPME-lid so each fiber is submerged.

Step 4.3 Transfer the cells back into the CO_2 incubator with SPME fibers immersed in a cell culture medium.

PAUSE! Wait until the end of the extraction.

Step 4.4 Repeat the whole 3rd step in a new portion of water to perform a second wash.

NOTE: Fibers can be stored at −30 °C. The safe storage time will depend on the targeted compounds and type of the coating and should be assessed based on application.

STEP 5. Sample desorption, Time - 5–120 min per plate

Step 5.1 Prepare 10 ml of the desorption solution by mixing acetonitrile with ultrapure water, 1:1 v/v

NOTE: The composition and volume of the desorption solution should be determined for the given application.

Step 5.2 Spike desorption solvent with deuterated/isotopically labeled internal standards. Final concentration of 100 ng/ml.

NOTE: Concentration should be evaluated based on the available standards and recoveries of the analyte.

ATTENTION! Check the solubility data of the standards of choice before the experiment.

Step 5.3 Pipette 100 µl of spiked desorption solution into each well.

Step 5.4 Transfer the SPME-lid onto the PCR plate.

PAUSE! Wait for the end of the desorption time.

ATTENTION! 120 min is recommended for ensuring full desorption of compounds into the desorption solution. Use shaking to enhance the desorption efficiency (800–1500 RPM). Both the length and the agitation speed should be determined for the given application.

Step 5.5 Cover the plate with PCR plate sealer or transfer samples into gals inserts for storage or analyze immediately.

ATTENTION! When using new coatings for the application for the first time, repeat desorption from the same fibers into a fresh portion of desorption solution and perform instrumental analysis for carry-over.

STEP 5. Cleaning, Time – 1h

Step 5.1 Prepare 10 ml of a solvent mixture of methanol, acetonitrile, and isopropanol, 50:25:25 v/v/v, respectively.

Step 5.2 Prepare a new 96-well plate. Pipette 200 µl solution into each well.

Step 5.3 Immerse the fibers in the cleaning solution by carefully lowering the SPME-lid.

PAUSE! Wait for at least 1 h to ensure all remaining compounds are released from the SPME fiber. **NOTE:** You can use agitation to make the process more efficient.

NOTE: Perform the instrumental analysis the cleaning solution after the cleaning process to check for carry-over when performing the optimized protocol for the first time.

ATTENTION! You can reuse clean fibers for analysis if you perform targeted metabolomics or metabolism analysis. For untargeted metabolomics, exchanging fibers for each sampling is recommended.

NOTE: If fibers are to be reused, right after cleaning, put the fibers into a preconditioning solution as per step 2. The fibers will be activated appropriately for the next day sampling.

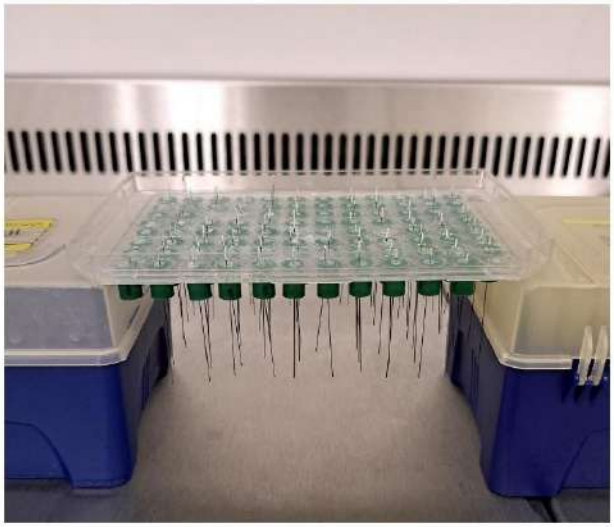

Fig. 12. The SPME-lid propped upside down on pipette tip boxes so it can face the UV bulb.

4. Problem-solving

A researcher can encounter a few problems while performing sample preparation with SPME coupled with LC-MS. Possible issues, with causes and potential solutions, are included in Table 5.

5. Protocol evaluation

SPME, as a whole, is a technique that is highly adaptable to different sample types, from liquid samples to tissue sampling. SPME in fiber geometry was successfully used to analyze both volatile and non-volatile compounds from cell cultures. Because it is very flexible, coating length can be miniaturized even to 2 mm coating – that makes it very compatible with the format most popular in cell culture testing, a 96-well plate. However, when performing assays on cell cultures, it is very important to design experiments to exclude any potential disruptive factors that can falsify results. Therefore, SPME sampling in this model is highly restricted in many parameters at the level of experimental design. However, the upgraded SPME-lid 96-well sampling model has been proven to have negligible influence on the growing cells, as presented in Fig. 5, enabling extraction of the cells inside the incubator *i.e.*, in the optimum growing conditions. The possibility to perform extractions inside an incubator provides many benefits compared to the previously introduced SPME high-throughput system for *in vitro* sampling, which are enlisted in Table 6. Overall, it ensures better control of the conditions, increasing the reliability of results as well as the repeatability of measurements while not increasing the sampling costs compared to the previously presented high-throughput SPME sampling method. Moreover, the expected results section presented that this model offers the unique possibility of multiple samplings from the same well in a time-course manner, of untargeted and targeted metabolomics, or drug analysis. Moreover, the SPME fibers can be cleaned and reused, making the protocol more cost-effective and environmentally friendly. The model itself can be created using universal microwell lids with no-cut corners, which makes it compatible with many plates from different vendors. The proposed SPME-lid system utilizes a septum typically used for volatile compounds analysis. It makes exchanging old fibers for new ones possible while isolating the cells from the potentially contaminated air. Because SPME does not consume cell culture media, this model is highly compatible with routine cell culture assays such as MTT assay, BrdU assay, and so on (Fig. 6). This method also allows the minimalization of the solvent used to no or less than 200 µl per sample and reduces the use of plastics in cell culture testing.

The possible limitations of the system arise mainly at the level of SPME-lid assembly. The materials for the creation of the system are widely available, but the personnel should be precise during steps 1.2, 1.4 and 1.5, that is, drilling holes in the lid, gluing the septum and inserting the SPME fiber. Tilted SPME fibres in the SPME-lid systems would be harder to insert into the wells of the plate and, therefore, be more exposed to mechanical damage. The SPME fibre coatings should be all at the same height so the whole coating is inserted into the liquid and the precision of sampling is achieved. However, after the SPME-lid system is set up properly, it can be used repeatedly in various experiments and is not limited to just one series of samplings. This system is specifically tailored to fit the 96-well format; however, in its current format, it cannot support the 384-well plate that is also commonly used in the initial screening of newly formulated drugs, which can also be considered as a limitation.

Table 6
Comparison of key improvements the SPME-lid system introduces upon previously presented high-throughput SPME system and in this protocol.

	Previous SPME high-throughput	SPME-lid
pH control	No pH stabilization due to the lack of CO_2 supplementation	pH stabilized by CO_2 supplementation inside incubator
Extraction tempererature	Room temperature	37 °C
Sample evaporation	Sample evaporation due to the lack of plate coverage	No sample evaporation – plate covered by SPME-lid
Extraction time	Short (up to 15 min)	Long (up to 60 min)

As a whole, the presented protocol aimed to ensure clarity of high throughput system setup and make the whole procedure easily repeatable by providing precise directions on which materials, solvents and instruments were used, as well as presenting written and graphic instructions in a step-by-step way (Fig. 13). The protocol contained additional warnings for particularly tricky parts and helpful tips that can aid in adapting the protocol towards extraction of different compouds. The introduction system highlighted the importance of study design and proper way in which to standarize the analysis when using SPME as sample preparation method, especially in *in vitro* analysis of living culture. Performing the protocol should therefore provide repeatable results, and if faced with problem the scientist can seek aid in the "Problem solving" section.

5.1. Greenness evaluation

A metric tool focusing on sample preparation, AGREEprep, was utilized to evaluate the greenness of the proposed high-throughput SPME method. The evaluation was based on 10 impact categories, each recalculated to 0–1 scale sub-scores, which were combined to determine

Table 5
Step-specific problems that might be encountered during the protocol with possible solutions.

Step	Problem	Possible reason	Solution
Step 1	The SPME-lid does not fit smoothly into the 96-well plate	SPME fibers are not perpendicular to the lid, at an angle	Leave the hypodermic needles inside the septum so they hold the SPME fibers perpendicular to the lid.
Step 2	Poor repeatability	Fibers were not preconditioned equally	Adjust the height of the SPME fibers to be the same level. Make sure that all the extraction phase is submerged in preconditioning solution
Step 4	Poor repeatability	Not all fibers were immersed into the cell culture medium	Adjust the height of the SPME fibers to be the same level. Make sure that all the extraction phase is submerged in preconditioning solution
Step 2–5	Poor repeatability	Damaged coating during inserting/removing SPME-lid	Make sure to lower and rise the SPME-lid carefully. Inspect coating condition after extraction.
Step 4	Poor repeatability and extraction efficiency	Adsorption of target analytes onto the well walls;	Perform extraction of standard in matrix in 96-well plate, remove the samples and wash the wells with organic solvent (e.g. MeOH, ACN, mix of both or other). Analyze performance of different 96-well plates. Choose the one that is the least absorptive to minimize the loss of analytes.
Step 4	Poor repeatability and extraction efficiency	Suboptimal desorption solution	Perform the optimalization of the desorption solution with different organic solvent-to-water ratio and addition of acids such as formic acid (e.g. 0,1 % FA, ANC:H_2O, 1:1)
Step 4	Poor repeatability and extraction efficiency	Suboptimal desorption time	Perform the desorption time optimization in various time points
Step 4	Poor repeatability and extraction efficiency	Unstable analyte present in the sample	Desorb the analytes in low temperatures, preferably on ice, shorten the desorption time. Perform the analysis as fast as possible after the desorption.

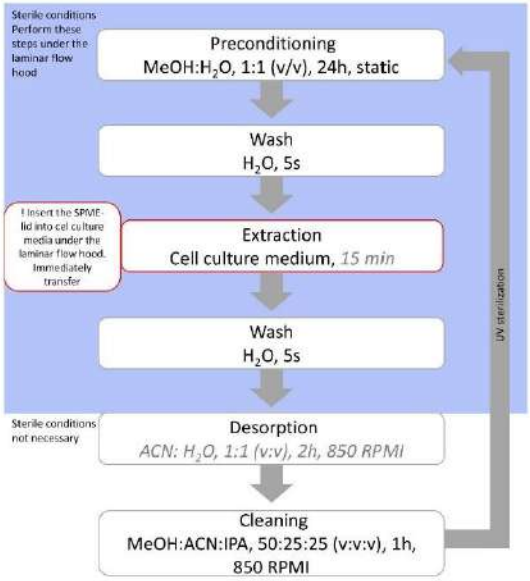

Fig. 13. Graphical abstract of the procedure. Steps presended on the blue background schould be performed in sterile conditions, under the laminar flow hood, while steps presented on the wite background do not require sterile conditions. Step in a red square takes place inside the 96-well plate containing cells in culture and should take place inside the CO_2 incubator. Parameters in gray-italic schould be determined by a given application.

the final assessment score. Additionally, the assessment allowed for differentiation between the importance of criteria by assigning weighted values. The criteria were as follows: 1 – sample preparation placement; 2 – hazardous materials; 3 – sustainability, renewability, and reusability of materials; 4 – waste; 5 – size economy of the sample; 6 – sample throughput; 7 – integration and automation; 8 – energy consumption; 9 – post-sample preparation configuration for analysis; 10 – operators safety. The use of SPME-lid high-throughput system for time-course targeted metabolomic analysis received 0.75 score on 0–1 scale (Fig. 14) with particularly good scores in category 1 with in-line sample preparation placement, category 5 with size of the sample being only 100 µl, and category 6 with sample throughput, where 96 samples can be extracted and then desorbed at once. However, some of the parameters could not be beneficially evaluated in terms of greenness. The steps specifically required in SPME sample preparation caused the parameters such as 7th - integration and automation, or 4th – waste, to have low scores. Multiple separate steps, such as preconditioning, washing and cleaning, that are necessary for the classical SPME, lower the score. Those steps generate manual labor, where SPME lid has to be transferred by-hand from plate to plate. Each of those steps also creates waste in form of solvents and plastic waste. Some of the plastic plates for steps such as preconditioning or first wash can be reused, which lowers the amount of waste created. Moreover, the SPME fibers themselves, after appropriate cleaning, can be reused for targeted approaches. The innovations in SPME fiber coating themselves, which minimize steps such as preconditioning, could further decrease the generated waste. The introduction of glass 96-well plates for all the steps, except for extraction, could also reduce the plastic waste generated because, after appropriate cleaning, the plates from the second wash and desorption could also be reused. The 9th parameter – post-sample preparation configuration for analysis also received a lower score. Generally, for metabolomic analysis, especially from small samples, it is required to

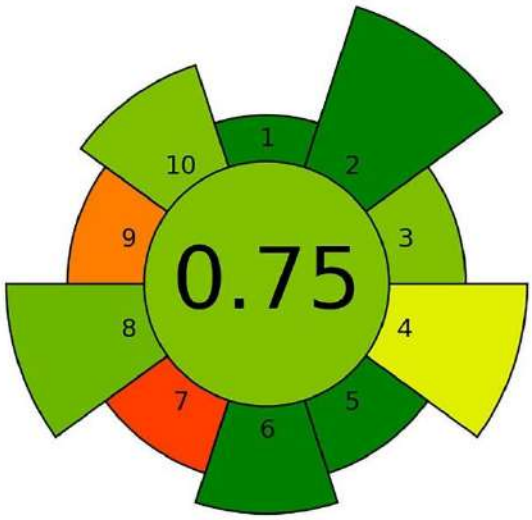

Fig. 14. Results of the AGREEprep analysis of high-throughput, time-course targeted metabolomic analysis of cell culture in 96-well plate format. 1 – sample preparation placement; 2 – hazardous materials; 3 – sustainability, renewability, and reusability of materials; 4 – waste; 5 – size economy of the sample; 6 – sample throughput; 7 – integration and automation; 8 – energy consumption; 9 – post-sample preparation configuration for analysis; 10 – operators safety.

use detectors of high sensitivity and resolution, therefore it is necessary to have an LC-MS platform [35]. This detector requires advanced knowledge, it is not readably available and consumes high amounts of energy. However, it is determined by the type of analysis performed in this protocol – the SPME-lid system can be also applied for targeted analysis of drugs or contaminants, where simpler detection devices can be used.

The SPME-lid system could benefit in terms of greenness with further work on automatization. While manual labor in form of transferring each fiber separately in-between steps, they could be transferred all at once by an automatized arm. An automation of SPME in high-throughput format has already been proposed [36]. A similar device could be proposed for the SPME-lid. However, adjustments should be made for the device so it can be light and miniaturized to fit under the laminar flow hood.

6. Summary and conclusions

This protocol presented the development and application of an upgraded high-throughput Solid Phase Microextraction (SPME) system designed for biocompatible *in vitro* extractions from small volumes for toxicological and pharmaceutical assays. The upgraded SPME system offers an eco-friendly, cost-effective, and scalable solution for high-throughput *in vitro* metabolomics, supporting pharmaceutical and toxicological research advancements.

CRediT authorship contribution statement

Paulina Szeliska: Writing – original draft, Visualization, Methodology, Investigation, Formal analysis, Data curation, Conceptualization. **Karol Jaroch:** Visualization, Methodology, Investigation, Formal analysis, Data curation, Conceptualization. **Bartłomiej Charemski:** Investigation. **Kübra Kahremanoğlu:** Investigation. **Enes Çetin:** Investigation. **Ezel Boyaci:** Writing – review & editing, Supervision,

Resources, Funding acquisition. **Barbara Bojko:** Writing – review & editing, Supervision, Resources, Project administration, Conceptualization.

Declaration of competing interest

The authors declare that they have no known competing financial interests or personal relationships that could have appeared to influence the work reported in this paper.

Acknowledgements

This study was supported by the National Centre for Research and Development (NCBR) under the Grant Number POLTUR4/MicroIVIVE/5/2021 and the Scientific and Technological Research Council of Turkey (TUBITAK) under the Grant Number 120N352.

Data availability

Data will be made available on request.

References

[1] K. Steinmetz, E. Spack, The basics of preclinical drug development for neurodegenerative disease indications, BMC Neurol. 9 (2009), https://doi.org/10.1186/1471-2377-9-S1-S2.
[2] J. Guitton, F. Gavotto, E. Cros-Perrial, L. Jordheim, C. Machon, A proposed methodology to deal with the impact of In vitro cellular matrix on the analytical performances of a targeted metabolomic LC-HRMS method, Int. J. Mol. Sci. 24 (2023), https://doi.org/10.3390/ijms24043770.
[3] K. Fitzgerald, M. Malhotra, C. Curtin, F. Brien, C. O'Driscoll, Life in 3D is never flat: 3D models to optimise drug delivery, J. Control. Release 215 (2015) 39–54, https://doi.org/10.1016/j.jconrel.2015.07.020.
[4] K. Jaroch, A. Jaroch, B. Bojko, Cell cultures in drug discovery and development: the need of reliable in vitro-in vivo extrapolation for pharmacodynamics and pharmacokinetics assessment, J. Pharm. Biomed. Anal. 147 (2018) 297–312, https://doi.org/10.1016/j.jpba.2017.07.023.
[5] D. Wishart, Applications of metabolomics in drug discovery and development, Drugs R. D. 9 (2008) 307–322.
[6] C. Russell, A. Rahman, A. Mohammed, Application of genomics, proteomics and metabolomics in drug discovery, development and clinic, Ther. Deliv. 4 (2013) 395–413, https://doi.org/10.4155/TDE.13.4.
[7] M. Beccaria, D. Cabooter, Current developments in LC-MS for pharmaceutical analysis, Analyst 145 (2020) 1129–1157, https://doi.org/10.1039/c9an02145k.
[8] Y. Wang, Y. Hu, D. Wang, K. Yu, L. Wang, Y. Zou, C. Zhao, X. Zhang, P. Wang, K. Ying, The analysis of volatile organic compounds biomarkers for lung cancer in exhaled breath, tissues and cell lines, Cancer Biomark. 11 (2012) 129–137, https://doi.org/10.3233/CBM-2012-00270.
[9] H. Kataoka, Automated sample preparation using in-tube solid-phase microextraction and its application - a review, Anal. Bioanal. Chem. 373 (2002) 31–45, https://doi.org/10.1007/s00216-002-1269-z.
[10] M. Queiroz, L. Melo, Selective capillary coating materials for in-tube solid-phase microextraction coupled to liquid chromatography to determine drugs and biomarkers in biological samples: a review, Anal. Chim. Acta 826 (2014) 1–11, https://doi.org/10.1016/j.aca.2014.03.024.
[11] X. Ji, Applications of headspace solid-phase microextraction in human biological matrix analysis, Rev. Anal. Chem. 41 (2022) 180–188, https://doi.org/10.1515/revac-2022-0042.
[12] K. Murtada, J. Pawliszyn, Protocol for the development of TFME-GC methods for analyzing multiclass organic constituents in water samples, Green Anal. Chem. 2 (2022), https://doi.org/10.1016/j.greeac.2022.100016.
[13] E. Boyaci, B. Bojko, N. Reyes-Garces, J.J. Poole, G.A. Gomez-Rios, A. Teixeira, B. Nicol, J. Pawliszyn, High-throughput analysis using non-depletive SPME: challenges and applications to the determination of free and total concentrations in small sample volumes, Sci. Rep. 8 (2018), https://doi.org/10.1038/s41598-018-19313-1.
[14] E. Gionfriddo, E. Boyaci, J. Pawliszyn, New generation of solid-phase microextraction coatings for complementary separation approaches: a step toward comprehensive metabolomics and multiresidue analyses in complex matrices, Anal. Chem. 89 (2017) 4046–4054, https://doi.org/10.1021/acs.analchem.6b04690.
[15] Kahremanoğlu, K.; Jaroch, K.; Szeliska, P.; Filipiak, W.; Charemski, B.; Żuchowska, K.; Çetin, E.; Eroğlu, A., E.; Bojko, B.; Boyaci, E. Assessment of thermal and solvent stable SPME fibers for metabolomics studies performed in living systems. 2025, doi:10.1016/j.talanta.2025.127646.
[16] J. Jacob, O. LaCour, C. Burgoyne, P. LaFleur, E. Duzman, Expanded polytetrafluoroethylene reinforcement material in glaucoma drain surgery, J. Glaucoma 10 (2001) 115–120.
[17] A. Langmann, S. Lindner, W. Wackernagel, M. Koch, R. Hörantner, Polytetrafluoroethylene (Goretex®) for muscle elongation in the surgical treatment of strabismus with restricted motility, Acta Ophthalmol. Scand. 84 (2006) 250–253, https://doi.org/10.1111/j.1600-0420.2005.00578.x.
[18] K. Nishida, H. Sakaguchi, P. Xie, Y. Terasawa, M. Ozawa, M. Kamei, K. Nishida, Biocompatibility and durability of Teflon-coated platinum-iridium wires implanted in the vitreous cavity, J. Artif. Organs 14 (2011) 357–363, https://doi.org/10.1007/s10047-011-0591-7.
[19] Handbook of Solid Phase Microextraction, Handbook of Solid Phase Microextraction, 2012, pp. 1–478.
[20] A. Aksenov, A. Gojova, W. Zhao, J. Morgan, S. Sankaran, C. Sandrock, C. Davis, Characterization of volatile organic compounds in Human leukocyte antigen heterologous expression systems: a cell's "chemical odor fingerprint", Chembiochem 13 (2012) 1053–1059, https://doi.org/10.1002/cbic.201200011.
[21] M. Musteata, F. Musteata, J. Pawliszyn, Biocompatible solid-phase microextraction coatings based on polyacrylonitrile and solid-phase extraction phases, Anal. Chem. 79 (2007) 6903–6911, https://doi.org/10.1021/ac070296s.
[22] R. Simoes, P. Bonato, F. Mirnaghi, B. Bojko, J. Pawliszyn, Bioanalytical method for *in vitro*metabolism study of repaglinide using 96-blade thin-film solid-phase microextraction and LC-MS/MS, Bioanalysis 7 (2015) 65–77, https://doi.org/10.4155/bio.14.203.
[23] K. Jaroch, P.Z. Gorynska, K. Gorynski, T. Stefanski, B. Bojko, Untargeted screening of phase I metabolism of combretastatin A4 by multi-tool analysis, Talanta 182 (2018) 22–31, https://doi.org/10.1016/j.talanta.2018.01.051.
[24] K. Jaroch, E. Boyaci, J. Pawliszyn, B. Bojko, The use of solid phase microextraction for metabolomic analysis of non-small cell lung carcinoma cell line (A549) after administration of combretastatin A4, Sci. Rep. 9 (2019), https://doi.org/10.1038/s41598-018-36481-2.
[25] K. Jaroch, P. Taczynska, M. Czechowska, J. Bogusiewicz, K. Luczykowski, K. Burlikowska, B. Bojko, One extraction tool for in vitro-in vivo extrapolation? SPME-based metabolomics of *in vitro* 2D, 3D, and *in vivo* mouse melanoma models, J. Pharm. Anal. 11 (2021) 667–674, https://doi.org/10.1016/j.jpha.2021.03.005.
[26] S. Risticevic, H. Lord, T. Górecki, C. Arthur, J. Pawliszyn, Protocol for solid-phase microextraction method development, Nat. Protoc. 5 (2010) 122–139, https://doi.org/10.1038/nprot.2009.179.
[27] L.V. Charis-P. Segeritz, Chapter 9 - cell culture: growing cells as model systems in vitro, in: F.Y.L.S. Morteza Jalali, Jalali Mehdi (Eds.), Basic Science Methods For Clinical Researchers, Academic Press, 2017, pp. 151–172.
[28] S. Weiskirchen, S. Schröder, E. Buhl, R. Weiskirchen, A beginner's guide to cell culture: practical advice for preventing needless problems, Cells 12 (2023), https://doi.org/10.3390/cells12050682.
[29] H. Lord, J. Pawliszyn, Method optimization for the analysis of amphetamines in urine by solid-phase microextraction, Anal. Chem. 69 (1997) 3899–3906.
[30] H. Lord, J. Pawliszyn, Evolution of solid-phase microextraction technology, J. Chromatogr. A 885 (2000) 153–193.
[31] U. Kotowska, K. Bienczyk, Use of direct immersion solid-phase microextraction on polyacrylate and polydimethylsiloxane stationary phases for simultaneous determination of the neutral and basic pharmaceuticals in wastewater, Cent. Eur. J. Chem. 11 (2013) 1634–1643, https://doi.org/10.2478/s11532-013-0296-2.
[32] W. Cheng, C. Markus, C. Lim, R. Tan, S. Sethi, T. Loh, LW.G.M. Evaluation, Calibration practices in clinical mass spectrometry: review and recommendations, Ann. Lab. Med. 43 (2023) 5–18, https://doi.org/10.3343/alm.2023.43.1.5.
[33] D. Vuckovic, J. Pawliszyn, Systematic evaluation of solid-phase microextraction coatings for untargeted metabolomic profiling of biological fluids by liquid chromatography-mass spectrometry, Anal. Chem. 83 (2011) 1944–1954, https://doi.org/10.1021/ac102614v.
[34] G.A. Gomez-Rios, M. Tascon, N. Reyes-Garces, E. Boyaci, J. Poole, J. Pawliszyn, Quantitative analysis of biofluid spots by coated blade spray mass spectrometry, a new approach to rapid screening, Sci. Rep. 7 (2017), https://doi.org/10.1038/s41598-017-16494-z.
[35] J. Wang, J. Byun, S. Pennathur, Analytical approaches to metabolomics and applications to systems biology, Semin. Nephrol. 30 (2010) 500–511, https://doi.org/10.1016/j.semnephrol.2010.07.007.
[36] D. Vuckovic, E. Cudjoe, D. Hein, J. Pawliszyn, Automation of solid-phase microextraction in high-throughput format and applications to drug analysis, Anal. Chem. 80 (2008) 6870–6880, https://doi.org/10.1021/ac800936r.

6.2. Zastosowanie opracowanego systemu próbkowania SPME-lid w analizie zmian metabolomu zewnątrzkomórkowego linii ustalonych glejaka mózgu A-172 oraz U-87 MG w czasie po potraktowaniu maltolanem galu.

Metabolomika stanowi kluczowe uzupełnienie klasycznych badań farmakologicznych *in vitro*, ponieważ pozwala równocześnie ocenić wpływ związku na sieci metaboliczne komórki oraz wychwycić wczesne, mechanistyczne sygnały działania i toksyczności. Profilowanie małocząsteczkowych metabolitów umożliwia powiązanie odpowiedzi fenotypowej z konkretnymi szlakami, identyfikację biomarkerów farmakodynamicznych oraz wgląd w zdarzenia ADME na poziomie komórkowym. Zewnętrznokomórkowa metabolomika, polega na profilowaniu zmian stężeń metabolitów w pożywce hodowlanej, co odzwierciedla bilans poboru i wydzielania przez komórki i pozwala nieinwazyjnie śledzić ich odpowiedź na leki w czasie. Zastosowania w modelach ssaczych obejmują standardowe protokoły poboru kondycjonowanego medium komórkowego i wykazują przydatność metabolomiki zewnątrzkomórkowej do porównywania odpowiedzi na leczenie oraz do odkrywania biomarkerów skuteczności [57,58].

Komórki linii ustalonych glejaka mózgu A-172 (CLS, Eppelheim, Niemcy) hodowano w medium komórkowym RPMI 1640 (Corning, NY, USA) oraz U-87 MG (ATCC, Manassas, USA) w medium MEM (Corning, NY, USA), oba suplementowane 10% FBS (Corning, NY, USA) oraz 1% rozworu antybityków i antymikotyku (Merck Group, Darmstadt, Niemcy). Komórki posiano w gęstości 2500 kom/dołek. W skrócie, po 24h inkubacji komórki poddano działaniu GaM (THE BioTech, Los Angeles, CA, USA) w różnych stężeniach: 100, 90, 80, 70, 60, 50, 40, 30, 20, 10 µM dla linii A-172 oraz 240, 210, 180, 150, 120, 90, 75, 50, 35, 20 µM dla linii U-87 MG. Po 72h inkubacji wykonano test MTT (Merck Group, Darmstadt, Niemcy), którego wyniki pozwoliły na wyłonienie stężenia hamującego (ang. Inhibitory Concentration, IC) IC90, IC50 i IC10 dla każdej z linii (Ryc. 2).

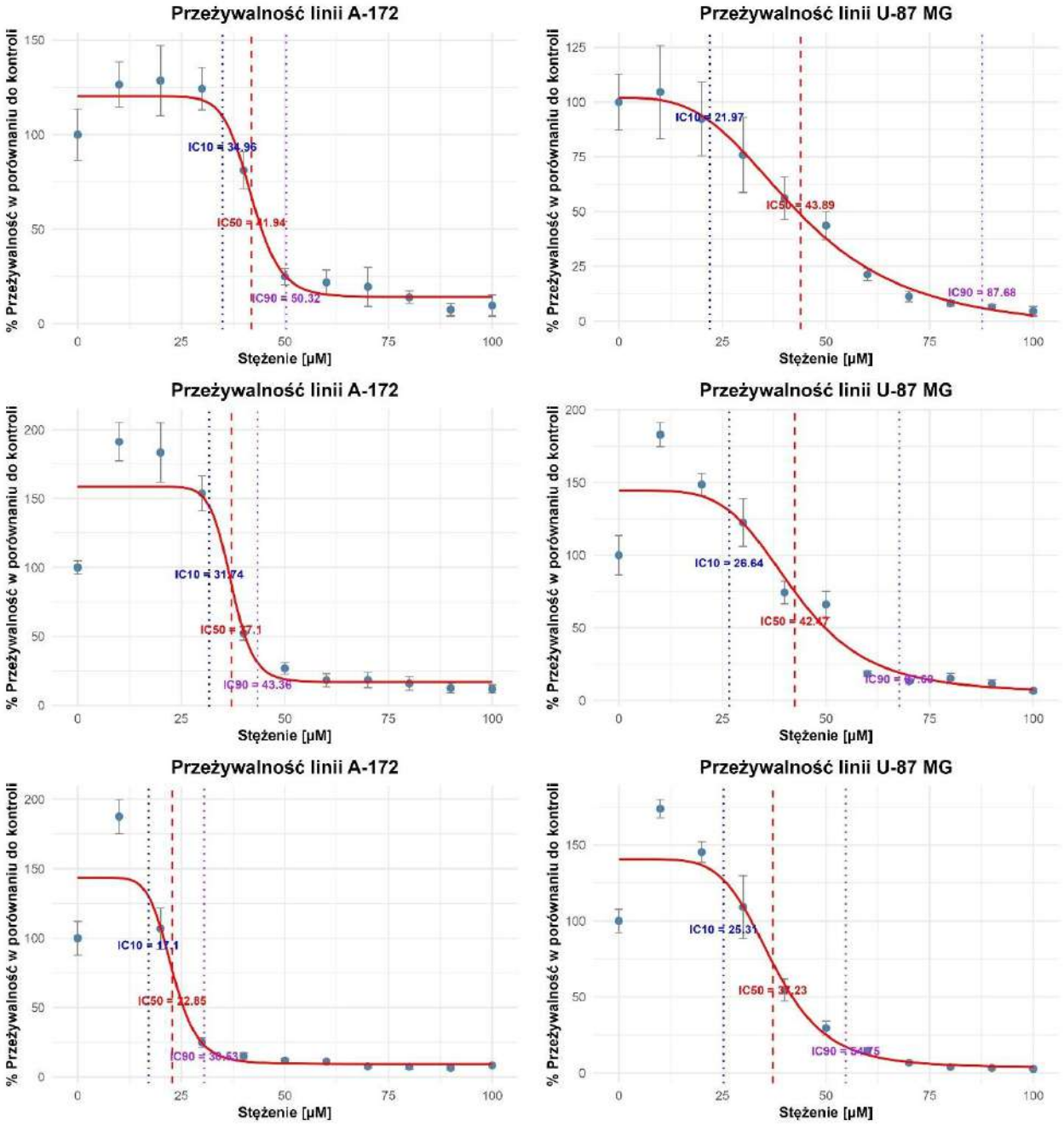

Rycina 2. *Przeżywalność linii komórkowych A-172 (po lewej) i U-87 MG (po prawej) oraz stężenia IC90, IC50 i IC10 określone na podstawie wykonanego testu MTT przedstawiona jako zależność przeżywalności (procent w porównaniu do kontroli) od stężenia po 72h inkubacji z GaM.*

Obliczone na podstawie wyników testu MTT średnie stężenie IC50 (A-172 - 34 ± 9.9 µM, U-87 MG - 41 ± 3.5 µM) zostało następnie zastosowane w dalszych testach.

Komórki ponownie posiano na płytkę 96-dołkową i po 24h do dołków dodano 100 µl świeżego medium lub zawierającego GaM, końcowe stężenie GaM w dołku wynosiło 34 µM dla linii A-172 i 41 µM dla linii U-87 MG. Kolejny etap eksperymentu przeprowadzono analogicznie do protokołu opisanego w publikacji P.2. Pobieranie próbek z pomocą SPME-lid (włókna PAN-HLB, 3 mm pokrycia) trwało 20 minut i obywało się 1h po dodaniu GaM a następnie co 24h aż do 72h inkubacji. Po ostatniej ekstrakcji dla części dołków zakończono eksperyment testem MTT (n = 4) (Ryc.3), natomiast resztę poddano testowi na pomiar konsumpcji tlenu (ang. Oxygen Consumption Rate, OCR) (n = 2) (Ryc. 4). Dane z MTT zostały przeliczone na procent przeżywalności w stosunku do kontroli, wykonano test Wilcoxona z korektą Homla w celu wyłonienia istotnych statystycznie zmian (Ryc. 3).

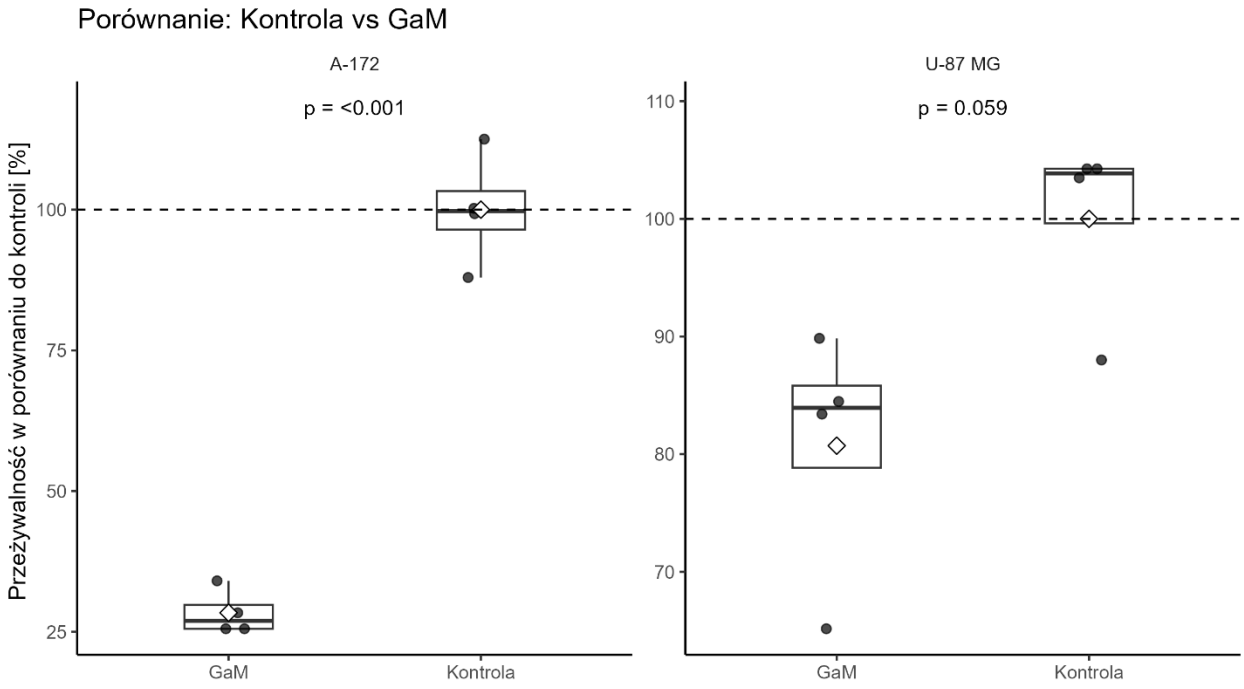

Rycina 3. *MTT —Przeżywalność dla U-87 MG i A-172 po 72h inkubacji z GaM lub czystym medium (kontrola) i 4-krotnej ekstrakcji z pomocą SPME-lid.*

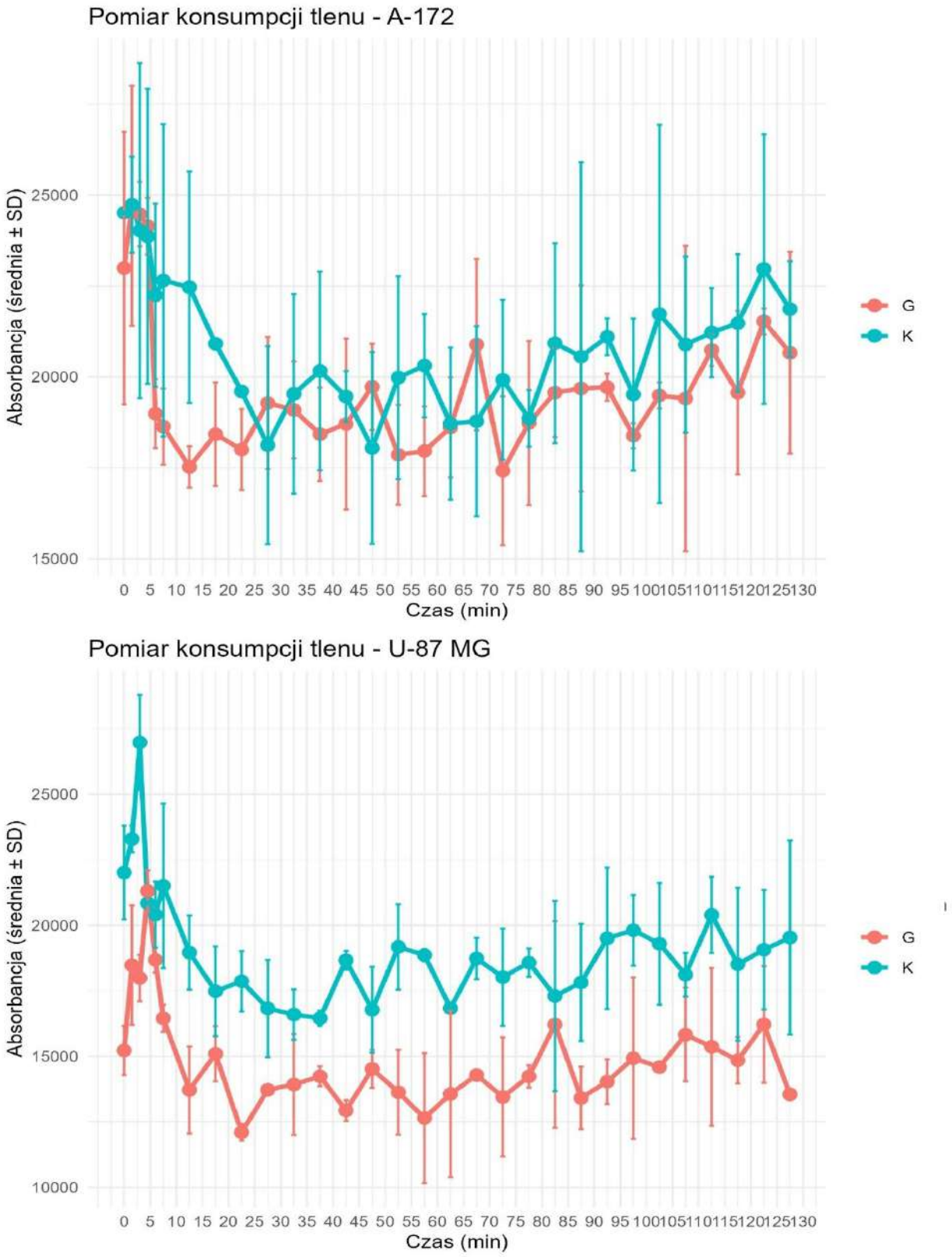

Rycina 4. *Pomiar konsumpcji tlenu linii komórkowych A-172 oraz U-87 MG po 72h inkubacji z GaM (G) lub czystym medium komórkowym (K).*

Włókna SPME poddano desorpcji i przeanalizowano z użyciem LC sprzężonym ze spektrometrią mas (ang. mass spectometry, MS), jak opisano w P.2. Uzyskane wyniki znormalizowano w programie Metaboanalyst (normalizacja medianowa, log-transformacja, autoskalowanie), następnie analizowano zmiany poziomu metabolitów w czasie z użyciem modelu liniowego mieszanego. Dla efektów stałych przeprowadzono testy F z korekcją Kenwarda–Rogera dla stopni swobody. Następnie obliczono porównania post-hoc. Na wielokrotność testowania nałożono kontrolę odseteka fałszywych odkryć (ang. False Discovery Rate, FDR). Za istotne uznawano FDR < 0,05. Wizualizacje trajektorii przedstawiały średnią ± odchylenie standardowe w funkcji czasu dla obu grup. Następnie wyłoniono 6 najistotniej zmienionych metabolitów dla linii A-172 (Ryc. 5) oraz linii U-87 MG (Ryc. 6).

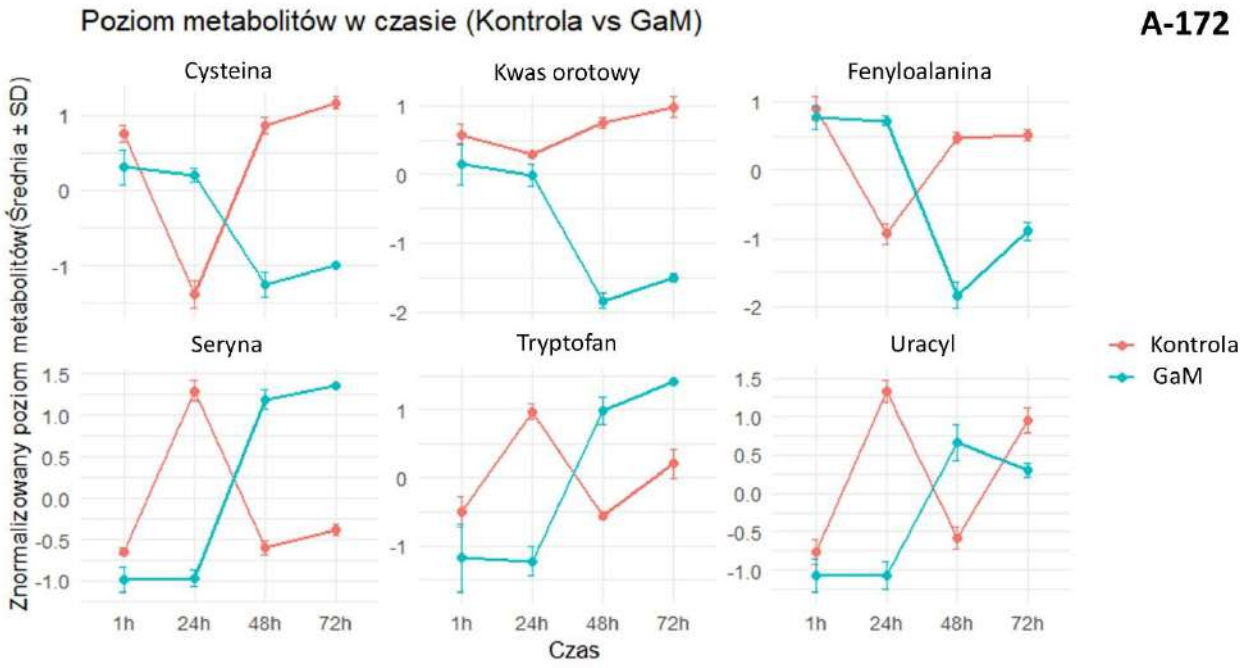

Rycina 5. *Znormalizowany poziom metabolitów w czasie (1-72h) dla 6 metabolitów najbardziej zmienionych dla komórek traktowanych i kontrolnych linii A-172.*

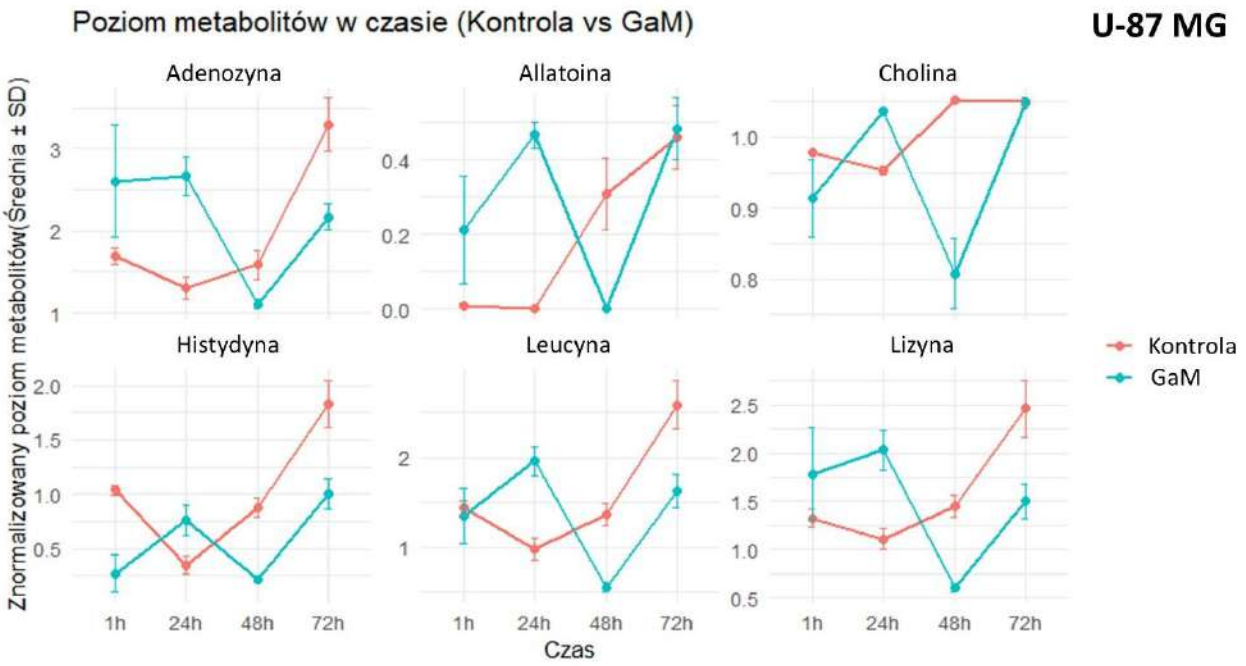

Rycina 6. *Znormalizowany poziom metabolitów w czasie (1-72h) dla 6 metabolitów najbardziej zmienionych dla komórek traktowanych i kontrolnych linii U-87 MG.*

W obu liniach komórkowych dodatek GaM obniżał aktywność metaboliczną i przeżywalność w porównaniu do kontroli. W pomiarze OCR, po początkowym piku krzywe stabilizują się, a sygnał w kontroli pozostaje wyraźnie wyższy niż w komórkach traktowanych GaM przez większość czasu, szczególnie w U-87 MG; zmienność maleje po 20–30 min (Ryc. 4). W teście MTT A-172 wykazuje silny spadek przeżywalności po potraktowaniu GaM (ok. 25–35% wartości kontrolnej) z istotnością statystyczną $p < 0{,}001$, natomiast w U-87 MG obserwujemy umiarkowane obniżenie (mediana ~80–85% vs ~100% w kontroli) z trendem do istotności ($p = 0{,}059$) (Ryc. 3). Krzywe przeżywalności mają przebieg sigmoidalny; dla A-172 są przesunięte w lewo względem U-87 MG, co oznacza niższe wartości IC (Ryc. 2). Przy niskich stężeniach pojawia się miejscami niewielka stymulacja (>100%), bardziej widoczna w U-87 MG, natomiast przy wysokich stężeniach osiągane jest plateau niskiej przeżywalności. Zestawiając te wyniki, GaM wyraźnie osłabia funkcje metaboliczne i żywotność komórek, przy czym efekt jest silniejszy w A-172 niż w U-87 MG, co potwierdzają niższe wartości IC10/IC50/IC90 w A-172.

Na wykresach zmiany metabolitów w czasie dla A-172 widać silną zależność efektu od czasu (Ryc. 5). Dla cysteiny, kwasu orotowego i fenyloalaniny około 48h w GaM występuje wyraźny spadek,

podczas gdy w kontroli poziomy pozostają dodatnie lub rosną. Odmienny wzorzec mają seryna, tryptofan i uracyl - po wczesnym obniżeniu dla komórek traktowanych następuje wzrost i w przedziale 48–72h wartości w GaM przewyższają kontrolę. Największe różnice między grupami skupiają się wokół 48h. Dla U-87 MG trajektorie są bardziej zmienne i często się przecinają, a rozbieżności również kulminują około 48 h (Ryc. 6). Adenozyna jest wyższa w dla komórek traktowanych GaM na początku (1–24h), po czym spada i przy 72h dominuje kontrola. Allantoina rośnie do 24 h, ma minimum przy 48h i wyrównuje do 72h. W cholinie kontrola systematycznie rośnie, a dla komórek inkubowanych z substancją badaną obserwowany jest spadek w 48h i zbliża się do kontroli w 72h. Dla histydyny, leucyny i lizyny obserwujemy, iż poziomy metabolitów zmieniają się w sposób odwrotny między kontrolą a komórkami traktowanymi. Maksimum poziomu dla komórek traktowanych plasuje się około 24h i minimum 48h, podczas gdy w kontroli odwrotnie; przy 72h kontrola jest wyższa, szczególnie dla lizyny. Całościowo wskazuje to na wyraźny, zależny od czasu wpływ GaM, najsilniejszy w okolicy 48h.

Krzywe przeżywalności wykazały większą wrażliwość farmakodynamiczną linii A-172 niż U-87 MG, natomiast pomiary OCR potwierdziły trwałe obniżenie konsumpcji tlenu w obecności GaM względem kontroli w obu liniach, bardziej konsekwentne w U-87 MG po ustąpieniu wczesnego piku. Analiza trajektorii metabolitów ujawniła wyraźną zależność efektu od czasu z maksymalnymi różnicami około 48h. Dla linii A-172 po potraktowaniu GaM obserwowano spadek poziomów m.in. cysteiny, kwasu orotowego i fenyloalaniny, przy jednoczesnym późnym wzroście seryny, tryptofanu i uracylu; w U-87 MG dominował spadek poziomu metabolitów w 48h inkubacji oraz przewagą kontroli do 72h. Zestawienie wyników wskazuje, że GaM hamuje oddychanie mitochondrialne i moduluję metabolizm aminokwasów/prekursorów nukleotydów w sposób zależny od linii i czasu; przy niższych wartościach IC w A-172 i bardziej konsekwentnej supresji OCR w U-87 MG.

6.3. Wpływ maltolanu galu na hodowle komórkowe glejaków mózgu w hodowli jednowarstwowej (2D) oraz trójwymiarowej (3D) *in vitro*. Analiza metabolomu wewnątrzkomórkowego linii komórkowych ustalonych oraz komórek wyprowadzonych od pacjentów połączona z oceną poziomu receptora dla transferyny i pomiarem oddychania mitochondrialnego. – P.3.

Opis dotyczy pracy: **Szeliska, P.**, Jaroch, K., Wróblewska, W., Kaźmierski, Ł., Maj, M., Bojko, B. Culture Dimensionality Governs Gallium Maltolate Response in Glioblastoma: Comparative Analyses in 2D and 3D Models.

GBM pozostaje nowotworem o bardzo złym rokowaniu, a skuteczność dostępnych terapii jest ograniczona. W pracy oceniono, w jakim stopniu wymiar hodowli komórkowej (2D vs 3D) kształtuje odpowiedź GBM na GaM – związek ukierunkowany na procesy zależne od żelaza, w tym funkcję mitochondriów oraz rybonukleotydoreduktazę, postrzegany jako obiecujący kandydat terapeutyczny. Zasadniczym celem było porównanie efektów GaM w panelu modeli GBM obejmującym linie utrwalone (A-172, U-87 MG) oraz linie wyprowadzone od pacjentów (3005, 3019, 3034, 3048, 3073), przy jednoczesnej integracji odpowiedzi fenotypowej (przeżywalność, oddychanie mitochondrialne) z danymi metabolomicznymi oraz poziomem receptora transferyny TFRC.

Projekt badania łączył klasyczne testy cytotoksyczności z analizą metabolomiczną. W warunkach 2D wykorzystano test MTT, natomiast w 3D (sferoidy) – CellTiter-Glo 3D, co pozwoliło wyznaczyć parametry IC10/IC50/IC90 i porównać wrażliwość między modelami i formatami hodowli. Równolegle oznaczono poziom TFRC (ELISA, normalizacja do białka całkowitego) oraz oceniono OCR jako wskaźnik funkcji mitochondrialnej. Do profilowania metabolitów zastosowano ukierunkowaną metodę LC–MS/MS sprzężoną z przygotowaniem próbek wykorzystując SPME/CBS; dane wstępnie przetwarzano (kontrola jakości QC, batch correction, log-transformacja, autoskalowanie), a następnie analizowano z użyciem analizy głównych składowych (ang. Principal Component Analysis, PCA) i analizy dyskryminacyjnej (ang. Partial Least Squares Discriminant AnalysisPLS, PLS-DA), przyjmując próg znaczenia zmiennych w projekcji (ang. Variable Importance in Projection, VIP) > 1 oraz kontrolę FDR dla selekcji cech

różnicujących. Dla porównań wielogrupowych zastosowano test Kruskala–Wallisa z post-hoc Dunna, a dla dwugrupowych – test Wilcoxona; do oceny związku TFRC z wrażliwością na GaM wykorzystano korelację Pearsona.

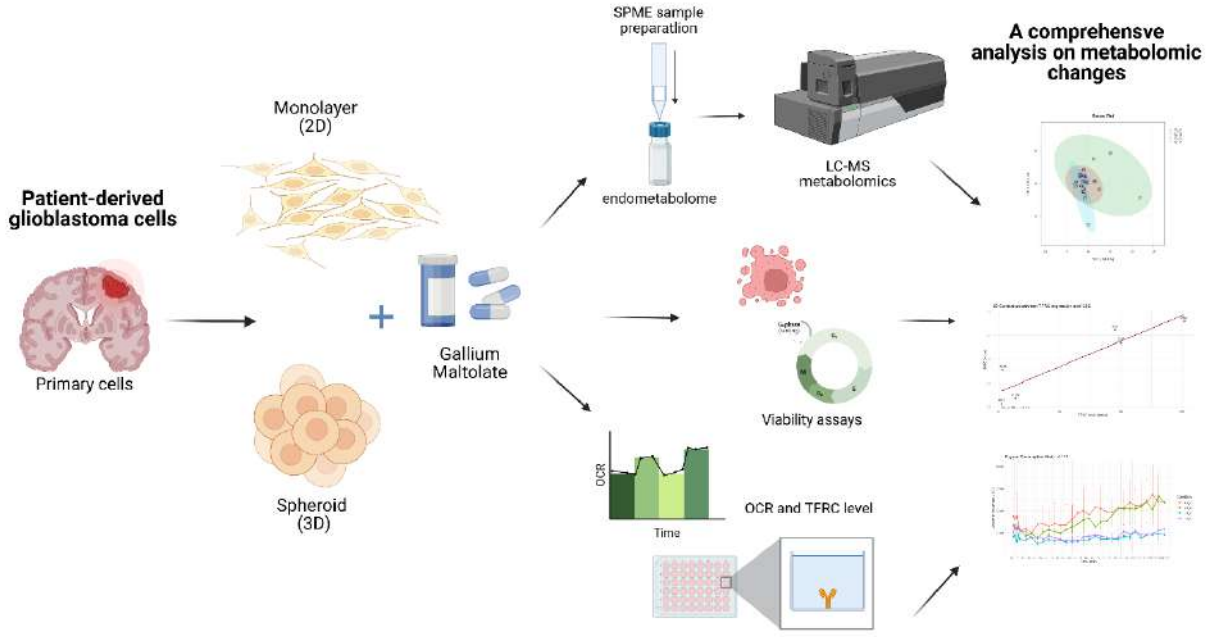

Rycina 7. *Schemat eksperymentu na liniach komórkowych ustalonych GBM oraz komórkach wyprowadzonych od pacjentów GBM w modelu hodowli 2D oraz 3D po potraktowaniu GaM.*

Najważniejszym wynikiem pomiaru przeżywalności komórek w zależności od stężenia GaM jest obserwowana w większości modeli zmiana w kierunku większej pozornej wrażliwości w 3D. Efekt ten sugeruje, iż sferoidy 3D są bardziej złożonymi mikrośrodowiskami, których odpowiedź trudniej przewidzieć. Jednocześnie między liniami obserwowano zróżnicowanie siły i kształtu odpowiedzi: w części z nich krzywe były wyraźnie bardziej strome w 3D, w innych różnice między 2D i 3D były mniejsze.

Analiza zależności TFRC wykazała, że w 2D poziom TFRC istotnie korelował z IC50, co wskazuje, że ekspresja receptora transferyny może odzwierciedlać zapotrzebowanie komórek na żelazo i współkształtować odpowiedź na GaM. W 3D zależność ta zanikała lub była słabsza, co sugeruje, że mikrośrodowisko sferoidu (np. architektura, gradienty, bariery dyfuzji) staje się czynnikiem nadrzędnym wobec pojedynczego biomarkera. Zwrócono również uwagę na

zachowanie linii U-87 MG w 3D, która odbiegała od pozostałych modeli; po wyłączeniu jej z analizy korelacja między TFRC a IC50/IC10 ulegała istotnemu wzmocnieniu, co podkreśla znaczenie heterogeniczności modeli przy interpretacji biomarkerów.

Pomiary OCR potwierdziły oddziaływanie GaM na funkcję mitochondriów: w liniach A-172, U-87 MG, 3048 i 3073 obserwowano wyraźne obniżenie zużycia tlenu, szczególnie w 3D. Niektóre modele hodowli pierwotnej (np. 3005, 3019) wykazywały względną „odporność" oddychania na leczenie, co może wskazywać na alternatywne strategie metaboliczne i/lub ograniczone dotarcie związku do stref aktywnej proliferacji w sferoidzie. Obserwowane również rozbieżności między OCR a TFRC (np. stabilny OCR przy spadku TFRC), co sugeruje przebudowę szlaków wspierających bioenergetykę przy zmieniającej się gospodarce żelazem.

Wyniki metabolomiczne zinterpretowano na trzech poziomach: (i) separacja grup w przestrzeni wielowymiarowej (PCA/PLS-DA), (ii) identyfikacja zmiennych o wysokim znaczeniu projekcyjnym (VIP > 1) przy kontroli FDR, (iii) analiza szlakowa. Stopień i kierunek separacji różnił się między liniami i zależał zarówno od formatu, jak i czasu inkubacji: w A-172 i U-87 MG dominowały efekty czasowe, w 3005 i 3048 separacja była obserwowana głównie przy porównaniu komórek traktowanych z kontrolą, w 3019 i 3034 kluczowy okazywał się format hodowli, a w 3073 widoczny był efekt łączny czasu i formatu. Jako wspólny mianownik przedstawiono zestaw metabolitów, który najtrafniej streszcza oddziaływanie GaM: tryptofan, metionina, uracyl i allantoina. Tryptofan ulegał systematycznemu obniżeniu (wpływ na szlak kynureninowy/oś immunometaboliczną), poziom metioniny spadał (presja na cykl folianowy i potencjał metylacyjny), uracyl zmieniał się w sposób świadczący o zaburzeniach puli pirymidyn i obrocie kwasów nukleinowych, a allantoina – wskaźnik stresu oksydacyjnego i przemian puryn – wzrastał, zgodnie z hipotezą redoksowego obciążenia pod wpływem GaM. Analiza ścieżek potwierdziła udział szlaków aminokwasów (tryptofan, metionina), nukleotydów (pirymidyny/puryny) oraz redoks.

Wyniki te wzmacniają argument za stosowaniem modeli 3D i linii pierwotnych wyprowadzonych od pacjentów w ocenie GaM, gdyż lepiej odzwierciedlają one warunki *in vivo* i ujawniają ograniczenia wnioskowania na podstawie monowarstw. Jednocześnie pokazują one, że odpowiedź na GaM jest kształtowana jednocześnie przez dostępność żelaza, sprawność mitochondriów oraz szlaki metaboliczne (aminokwasy, nukleotydy, redoks), a więc ma charakter wielotorowy.

Wskazane zostały potencjalne kierunki rozwoju: rozszerzenie panelu modeli pierwotnych, bezpośrednie pomiary akumulacji galu i penetracji GaM wewnątrz sferoidu, a także ocena strategii łączonych ukierunkowanych na mitochondria.

Podsumowując, sposób hodowli istotnie modyfikuje odpowiedź GBM na GaM. W ujęciu ilościowym GaM obniża przeżywalność i aktywność mitochondrialną, a efekt jest na ogół silniejszy i bardziej widoczny w 3D niż w 2D; jednocześnie relacja między TFRC a wrażliwością na GaM powinna być ostrożnie interpretowana, ponieważ nie zawsze pozostaje bezpośrednia i nie musi przenosić się z monowarstwy na sferoid. Zidentyfikowany panel czterech metabolitów – w powiązaniu z OCR – może stać się potencjalnym kandydatem do dalszej weryfikacji pod względem stanowienia wskaźnika odpowiedzi. Praca dostarcza spójnych przesłanek, że modele 3D i linie pierwotne stanowią środowisko bliższe *in vivo* dla GaM i innych związków ingerujących w gospodarkę żelaza oraz bioenergetykę GBM.

Title: Culture Dimensionality Governs Gallium Maltolate Response in Glioblastoma: Comparative Analyses in 2D and 3D Models

Author names: Paulina Szeliska[1], Karol Jaroch[1], Weronika Wróblewska[1], Łukasz Kaźmierski[2], Małgorzata Maj[2], Barbara Bojko[1,]*

Affiliation:

1. Department of Pharmacodynamics and Molecular Pharmacology, Faculty of Pharmacy, Collegium Medicum, Nicolaus Copernicus University, Jurasza 2, 85-089 Bydgoszcz, Poland

2. Urology and Andrology, Department of Tissue Engineering, Collegium Medicum, Nicolaus Copernicus University, M. Curie Skłodowskiej 9, 85-094 Bydgoszcz, Poland

*Corresponding author: bbojko@cm.umk.pl

Abstract: Gallium maltolate (GaM) targets iron-dependent processes in glioblastoma (GBM), but responses vary with model context. We evaluated GaM across established (A-172, U-87 MG) and patient-derived (3005, 3019, 3034, 3048, 3073) GBM lines in 2D and 3D using viability modelling (IC10/IC50/IC90), TFRC quantification, oxygen consumption rate (OCR), and PCA/PLS-DA–guided metabolomics with FDR and VIP-based selection. GaM reduced viability in all models, with a right-shift of dose–response in 3D. TFRC correlated with IC50 in 2D but not 3D, unless excluding U-87 MG from the analysis. OCR was markedly suppressed in A-172, U-87 MG, 3048, and 3073, particularly in 3D, while 3005 and 3019 were more respiration-resilient. Multivariate analyses showed treatment-dominant separation in 3005/3048, format dominance in 3019/3034, and time effects in A-172/U-87 MG/3073. A concise metabolic signature (tryptophan, methionine, uracil, allantoin) indicated coordinated perturbations in amino acid, nucleotide, and redox pathways. These findings support 3D, patient-derived systems for more predictive GaM evaluation.

Key words: gallium maltolate; glioblastoma; 3D culture; Solid Phase Micorextraction, Pharmacometabolomic

1. Introduction

Glioblastoma (GBM) is a very heterogeneous tumor associated with a poor survival rate. According to WHO's classification for 2021, histological analysis of tissue is no longer sufficient to classify a central nervous system tumor[1]. GBM diagnosis includes investigation of mutation in isocitrate dehydrogenase (IDH-wildtype) and three genetic characteristics: TERT promoter mutation, EGFR amplification, and +7/-10 chromosome copy number. This new grading system allowed classifying histologically II or III grade diffuse gliomas into IV grade. Standard GBM treatment is composed of tumor resection followed by radiotherapy and temozolomide chemotherapy. However, research on molecular subtypes of glioblastoma suggested further differentiating them based on molecular changes. It would allow for personalized treatment. Novel GBM therapy focuses on a targeted approach. Immunotherapy, molecular-targeted, and angiogenesis-targeted approaches are most intensely researched[2]. However, bevacizumab is the only targeted drug for recurring GBM treatment approved so far. There is still a need for new therapeutic approaches to improve the survival rate of patients[3].

Gallium was first introduced in the medical field in the late 1960s as a radioisotope[4]. However, some Ga(III) complexes showed potential in oncological therapy. Ga(III) shares some properties with iron and can be introduced into metabolic pathways as an iron substitute. Ga(III) can bind to iron-binding proteins and cause iron deficiency in rapidly proliferating cells such as cancer cells[5]. Transferrin (Tf) is a protein with two iron-binding sites and is responsible for delivering iron to cells; therefore, it is a potential way to provide Ga-based compounds as well. Approximately one-third of the circulating Tf is an iron-loaded Tf, also known as holo-Tf. This loaded Tf enters the

cell by binding to the Tf receptor (TfR1 and TfR2), and the non-loaded Tf (apo-Tf) remains circulating in the organism. It leaves about 2/3 of Tf available to deliver Ga(III)-complexes into cells [6,7]. Nowadays, researchers focus on three Ga-complexes with the highest potential in clinical applications, and they are currently undergoing clinical trials: gallium nitrate (GaN), tris(8- 8-quinolinolato)gallium(III) (KP46), and gallium maltoalte (GaM) [8]. GaM is a complex of a gallium ion and three deprotonated gallium groups. It was proven to have a few times higher bioavailability than gallium salts[9]. It is an orally administered compound due to its high bioavailability; moreover, most of it is Tf-bound in the blood[10]. It has been proven to inhibit cell proliferation in lymphoma resistant to GaN [11]. Lately, Chitambar et al. analyzed the mechanism of action of GaM in 2D and 3D glioblastoma cell culture, as well as in tumor rat xenograft, and showed the potential of GaM to induce tumor cell apoptosis via disrupting the iron homeostasis. The ability of gallium to cross the blood-brain barrier (BBB) by binding to endogenous Tf has enhanced delivery and targets TfR-bearing GBM. GaM has been shown to influence mitochondrial function of tumor cells as well as RRM2 activity, leading to blocking DNA synthesis in GMB cells without affecting normal cells. GaM has an impact on the TCA cycle and inhibits mitochondrial oxygen consumption[12]. A phase 1 clinical trial is being conducted to determine the response of patients with relapsed and/or treatment-refractory tumors [13].

Metabolic alterations in cancer cells have long been explored for their usefulness in profiling the phenotypes of many tumors. Research revealed a good correlation between mutations found in GBM, e.g., PDGFRA, IDH1, EGFR, and NF1 and the tumor's metabolic fingerprint. Thanks to extensive work on determining possible GMB metabolomic profiles, it became a promising tool for preclinical drug screening and tumor resistance to therapy exploration. However, the correlations between tumor metabolomic profile, TFRC, and the GaM treatment response have not yet been made. The comparison of the metabolomic profile with the results of standard cell culture

assays will help to evaluate potential onco-metabolic targets for assessing the efficiency of the GaM therapy.

SPME is not a commonly used sample preparation method, yet it is an extremely promising tool for in vitro pharmaceutical research, as proven in previous studies conducted in our laboratory [14,15] and other studies[16,17]. Moreover, SPME was previously used for the analysis of brain and brain tumors in vivo[18–23]. Results revealed that SPME can provide spatially resolved metabolic and lipidomic profiles of patients' brains in vivo by utilizing minimally invasive sampling, which omits physical sample consumption. Due to this unique feature, the technique is also known as "chemical biopsy". In addition, the use of specially optimized biocompatible coating enables covering both hydrophobic (e.g., lipids) and polar compounds (e.g., amino acids)[18]. The same method was proposed for the studies of brain tumors. SPME in fiber form was used to penetrate tumor tissue for metabolome/lipidome sampling. The results showed that this sample preparation method was capable of providing a characteristic phenotypic snapshot of the brain tumor, providing lipidomic[22] and metabolomic[23] markers of disease. Following these investigations, targeted lipidomic analysis with the use of Coated Blade Spray was carried out. The results showed different levels of carnitine and acylcarnitines correlating with IDH-mutation and 1p/19q co-deletion status. Moreover, utilizing CBS, which omits LC separation and allows for fast instrumental analysis without compromising sample cleanup, demonstrated the potential of the approach for rapid on-site screening of potential biomarkers.[19–21]

Combining pharmaco-metabolomics with cell phenotype and genetic analyses in 3D culture models may advance understanding of glioblastoma, particularly within the iron-imbalanced microenvironment. Linking these profiles with therapeutic response could provide novel insight into gallium maltolate as a potential treatment. Applying SPME for the studies, which has proven

its usefulness in glioma metabo-lipidomic profiling, *in vitro* and *in vivo* temporal studies, would help bridge the presented *in vitro* data with subsequent *in vivo* animal research.

2. Materials and Methods

Unless stated otherwise, all chemicals were purchased from Merck Group (Darmstadt, Germany).

2.1. Gallium malotlate (GaM) preparation

Gallium maltolate was purchased from THE BioTech (Los Angeles, CA, USA) and kept at 4°C. Stock solution of 1 mM was prepared by suspending in sterile, ultra-pure water, vortexing and 5 min sonication, followed by another thorough vortexing.

2.2. 2D Cell culture

Cell line U-87MG was purchased from American Type Culture Collection (ATCC, Manassas, USA), A-172 cell line was purchased from Cell Line Service (CLS, Eppelheim, Germany). Both cell lines were cultivated in DMEM (Corning, NY, USA) supplemented with 10% Fetal Bovine Serum (Corning, NY, USA) and Antibiotic Antimycotic Solution. Cells were cultured at 37°C, 5% CO2, and constant humidity. Patient-derived glioblastoma cells were acquired from the Human Glioblastoma Cell Culture resource (www.hgcc.se) at the Department of Immunology, Genetics and Pathology, Uppsala University, Uppsala, Sweden [24]. The 3005, 3019, 3034, 3048, and 3073 cells (basic characetristics in Tab. S1) were cultured according to the HGCC guidelines; DMEM: F12 (high glucose):Neurobasal, 1:1 (Thermo Fisher Scientific Inc., Waltham, MA, USA) supplemented with N1 supplement (0.5x) and N2 supplement (0.5x), B27 supplement (1x), Epidermal Growth Factor (EGF, 10 ng/ml) and basic Fibroblast Growth Factor (bFGF, 10 ng/ml) and Antibiotic Antimycotic Solution. HGCC cells were cultured on culture dishes coated with

polyornithine (10 µg/ml) and laminin (10 µg/ml). Cells were passaged at 70-80% confluence. U-87MG and A-172 cell lines were detached with trypsin, while accutase was used for HGCC cells. Cell counting was performed by mixing with trypan blue and counted by an automated cell counter (Countess® II FL, Invitrogen by Thermo Fisher Scientific Inc., Waltham, MA, USA).

2.3. 3D cell culture

3D cell cultures were established from the 2D cell cultures described above. The protocol described by Wanigasekara et al. was followed with minor changes[25]. Briefly, cells were counted with an automatic cell counter, and a cell suspension of 10000 cells/ 200µl was prepared, and 200 µl of cell suspension was added to a 96-well ultra-low attachment culture plate (Nunc™, Thermo Fisher Scientific Inc., Waltham, MA, USA). The plate was then spun (230 xg, 5 min) and cell clusters incubated for 24h, and then 100 µl of media was removed and an equal volume of fresh medium was added. 100 µl of cell culture media was changed every 2nd-3rd day. Spheroids were cultured for 10 days before GaM was added.

2.4. Viability assay

Cell viability was assessed using the MTT assay (2D cultures) or the CellTiter-Glo® 3D assay (spheroid cultures). Cells of U-87MG, A-172, 3073, 3048, 3034, 3019, 3005 were seeded at a density of 2500, 2500, 7500, 10000, 10000, 7500, and 12000 cells/well, respectively, in a 2D culture and 10000 cells/well for spheroids (12000 for 3005 cell line). Cells were then incubated (24h for 2D and 10 days for 3D spheroids). After incubation, 100 µl of fresh cell culture media was added with GaM in a 15 to 165 µM concentration range. For 2D cells, the MTT assay was performed after 24h and 72h. Celltiter Glo was performed after 72h and 7-day incubation for spheroids.

For 2D cell culture, after incubation, the medium was changed for 100 µL of MTT solution (1 mg/ml in DMEM with no phenol red, 10% FBS) and incubated for 3h. Formed formazan crystals were dissolved in isopropanol (100 µl), and absorbance (570nm/690nm) was measured using a microplate reader (Synergy H1, BioTek, Winoosky, VT, USA). Cell viability was expressed as a percentage relative to the untreated control.

Cell viability in 3D spheroid cultures was determined using CellTiter-Glo® 3D Cell Viability Assay (Promega). Following treatment with GaM, spheroids were gently transferred with a cut pipette tip to a white 96-well plate. An equal volume of CellTiter-Glo® 3D reagent was added directly to each well. Plates were incubated for 30 min at room temperature on an orbital shaker to allow complete cell lysis and ATP stabilization. Luminescence, proportional to the amount of metabolically active cells, was measured using a microplate reader. Cell viability was expressed as a percentage relative to the untreated control.

2.5. Oxygen consumption assay

Extracellular oxygen consumption was measured using the Extracellular Oxygen Consumption Assay (OCR) Kit (Abcam, ab197243, Cambridge, UK) following the manufacturer's protocol. Briefly, cells were seeded in black, clear-bottom 96-well plates at a density of 1×10^5 cells per well and cultured overnight. After adding GaM, 10 µL of Extracellular Oxygen Consumption Reagent was added to each well. Plates were immediately sealed with the supplied mineral oil overlay to prevent oxygen diffusion and incubated at 37 °C. Fluorescence (Ex/Em = 380/650 nm) was measured kinetically using a microplate reader, and oxygen consumption rates were calculated from the change in signal over time.

2.6. Protein Extraction and Quantification

Cells were collected and transferred to 15 mL conical tubes. After centrifugation at 300 × g for 7 min at room temperature, cell pellets were resuspended in ice-cold PBS and centrifuged again at 300 × g for 7 min at 4 °C. Pellets were lysed in Complete Cell Extraction Buffer supplemented with protease inhibitors (1 mL per 1 × 10^8 cells). Lysates were vortexed briefly, incubated on ice for 30 min with intermittent mixing, and clarified by centrifugation at 13,000 × g for 10 min at 4 °C. Supernatants were transferred to fresh tubes and stored at –80 °C. Total protein concentration was determined using the BCA Protein Assay Kit (Thermo Fisher Scientific) according to the manufacturer's protocol.

2.7. Human Transferrin Receptor (TfR/CD71) ELISA

Following the manufacturer's protocol, TfR/CD71 levels were quantified using the Human Transferrin Receptor ELISA Kit (Thermo Fisher Scientific Inc., Waltham, MA, USA). Based on BCA quantification, equal amounts of protein were diluted in assay buffer and loaded in duplicate into antibody-coated 96-well plates along with standards. After incubation at room temperature for 2.5h, wells were washed and incubated sequentially with biotinylated detection antibody and HRP-conjugated streptavidin. Signal was developed with TMB substrate, and reactions were stopped with 2 NH_2SO_4. Absorbance was measured at 450 nm using a microplate reader. TfR concentrations were calculated from the standard curve and normalized to total protein.

2.8. Cell lysis for endometabolome analysis

2D cells were collected during a standard passage procedure and counted by an automatic cell counter as described in 2.2. Cells were resuspended in PBS (1 x 10^6 cells/ml). 3D spheroids were transferred into Eppendorf tubes and centrifuged, then resuspended in PBS (1 spheroid/100µl). Both 2D and 3D cells were submerged in liquid nitrogen for metabolome quenching and kept at -80 °C until further analysis. Defrosted samples were sonicated (1 cycle, 5 min, 70%) and then

cooled on ice (5 min). Extracts were centrifuged at 10,000 x g for 10 min, and the supernatant was transferred into fresh collection tubes. Extracts were then spiked with an internal standard L-Tryptophan-d8 (TRC, Vaughan, Canada) to monitor extraction in the final concentration of 100 ppb.

2.9. SPME-LC-MS/MS

Solid-phase microextraction (SPME) coated blade spray (CBS) devices (CB-HLB, 10 mm coating, Restek Cat No. 23248) were purchased from Anchem (Warsaw, Poland). Before use, the blades were preconditioned overnight in methanol: water (1:1, v/v) under static conditions. Immediately before extraction, CBS blades were rinsed for 5 s with ultrapure water. For extraction, 120 µL of spiked sample was agitated for 2 h at 850 rpm using a BenchMixer™ XLQ QuEChERs Shaker/Vortexer (Merck Group). After extraction, blades were briefly rinsed again in ultrapure water (5 s) before desorption. Analyte desorption was performed in acetonitrile: water (1:1, v/v) for 2h under agitation at 850 rpm. Desorbed samples were analyzed using a Nexera UHPLC system (Shimadzu, Kyoto, Japan) coupled to an LC–MS 8060 triple quadrupole mass spectrometer (Shimadzu, Kyoto, Japan). The LC–MS/MS method was based on the Primary Metabolites Version 3 method package (Shimadzu, Kyoto, Japan). Chromatographic separation was performed on a reversed-phase Discovery HS F5 column (100 mm × 2.1 mm, 3 µm; Supelco, Bellefonte, PA, USA). Quality control (QC) was ensured by including pooled QC samples and probe blanks throughout the study

2.10. Data Processing and Statistical Analysis

Dose–response curves for GaM were generated from MTT and CellTiter-Glo viability assays using R (tidyverse, drc, and stringr packages). Inhibitory concentrations (IC10, IC50, IC90) were estimated using the drc package ED function.

Transferrin receptor (TFRC) expression levels were quantified, and statistical significance of group differences was assessed in R using tidyverse, ggplot2, ggpubr, dplyr, and FSA packages. Comparisons between groups were performed with a two-tailed Student's *t*-test, with $p < 0.05$ considered statistically significant.

The association between baseline TFRC levels in untreated control cells and GaM sensitivity (IC10 and IC50 values) was evaluated using Pearson's correlation test, implemented in R with tidyverse and ggpubr packages.

LC-MS/MS raw data were processed with Skyline software with MRM transitions provided in the Primary Metabolites Version 3 method package (Shimadzu, Kyoto, Japan).

Pooled QC and blank samples were used for data pre-processing. Pre-processed data sets were implemented into Metaboanalyst 6.0, a free online software[26]. Metaboanalyst's batch correction module was used in automated mode. Batch corrected data were further normalized based on internal standard and analyzed in Metaboanalyst, Statistical Analysis [one factor] with the following parameters for normalization node: sample normalization was set to none, data were log10 transformed, and auto scaling data scaling was implemented. Principal component analysis (PCA) and partial least squares discriminant analysis (PLS-DA) were performed to evaluate the separation among sample groups. Variables with variable importance in projection (VIP) scores exceeding 1 were designated as significant, reflecting their contribution to the model's discriminative power and predictive reliability.

Further statistical analyses were performed in R (version 4.5.0) using the dplyr, ggplot2, ggpubr, ggsignif, tibble, tidyverse, FSA, and purrr packages. The Kruskal–Wallis test followed by Dunn's post hoc test with false discovery rate (FDR) correction was applied for four-group comparisons. For two-group comparisons, the Wilcoxon rank-sum test with FDR correction was used.

Metabolites were considered significant if they passed the statistical threshold and exhibited a variable importance in projection (VIP) score greater than 1.

3. Results

3.1. TFRC Expression and Its Association with GaM Sensitivity in 2D and 3D Culture Systems

Dose–response analyses revealed apparent differences in GaM cytotoxicity between 2D and 3D culture formats across the tested glioblastoma cell lines (Fig. 1). In 2D cultures, IC50 values ranged widely among cell lines. In contrast, in 3D cultures, a general shift toward higher drug tolerance was observed, with some lines showing pronounced resistance at clinically relevant concentrations. Specific lines (e.g., A-172, 3019, 3048) displayed a steeper dose–response curve in 3D compared with 2D conditions, indicating enhanced protection conferred by the 3D environment.

Basal TFRC expression levels differed substantially between 2D and 3D cultures (Fig. 2). Several cell lines (3005, 3019, 3034, 3073, U-87 MG) exhibited significantly higher TFRC protein abundance in 3D compared with 2D conditions, suggesting that culture dimensionality impacts iron metabolism–related pathways. Conversely, A-172 cells showed minimal differences between formats.

Correlation analysis further revealed that TFRC expression was positively associated with GaM sensitivity in 2D cultures, with a strong correlation observed between TFRC levels and IC50 values ($R = 0.82$, $p = 0.024$; Fig. 3). A similar but weaker, non-significant trend was seen for IC10 values ($R = 0.39$, $p = 0.42$). By contrast, no meaningful associations were detected in 3D cultures, where TFRC levels did not correlate with IC50 ($R = 0.11$, $p = 0.82$) or IC10 ($R = –0.07$, $p = 0.87$). However, the U-87 MG cell line behaved differently under 3D conditions. Excluding it as an outlier strengthened the Pearson correlation, yielding IC10 ($R = 0.38$, $p = 4.45$) and IC50 ($R = 0.92$, $p = 0.01$).

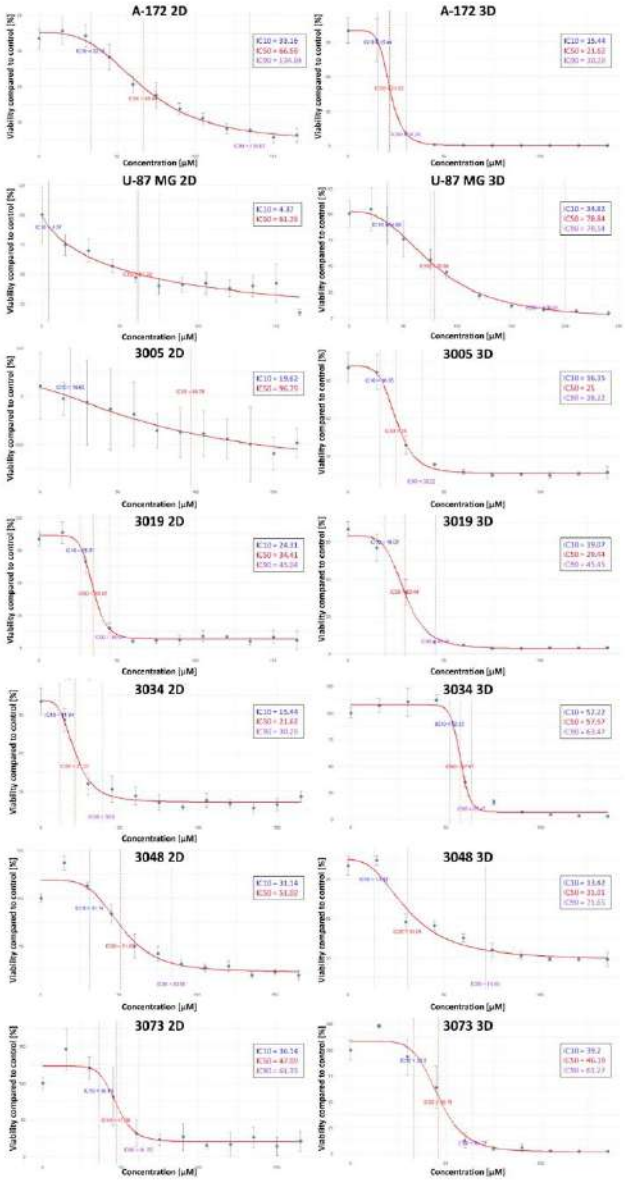

Figure 1. Percentage of cell viability compared to control after 72h incubation with GaM (15-165 µM – 2D, left; 15-135 µM -3D, right).

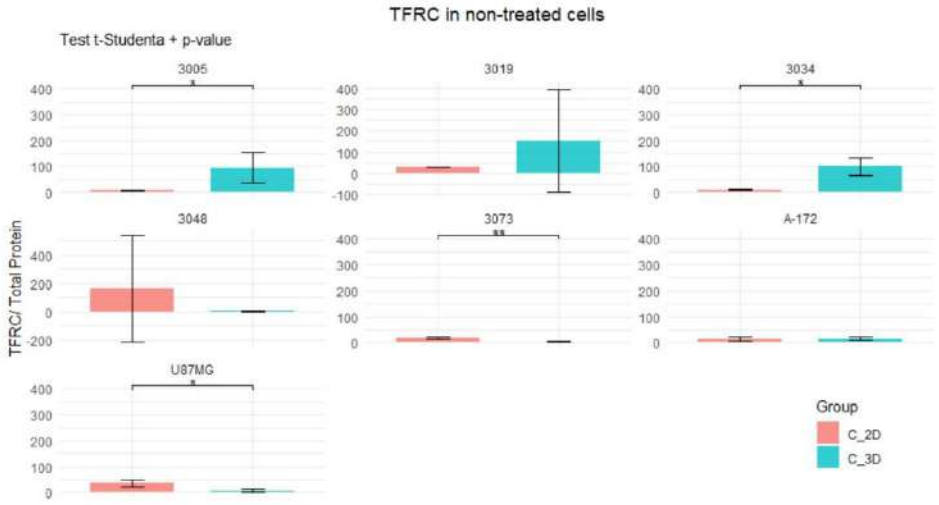

Figure 2. TFRC normalized for total protein content in non-treated control cells cultured in 2D and 3D format.

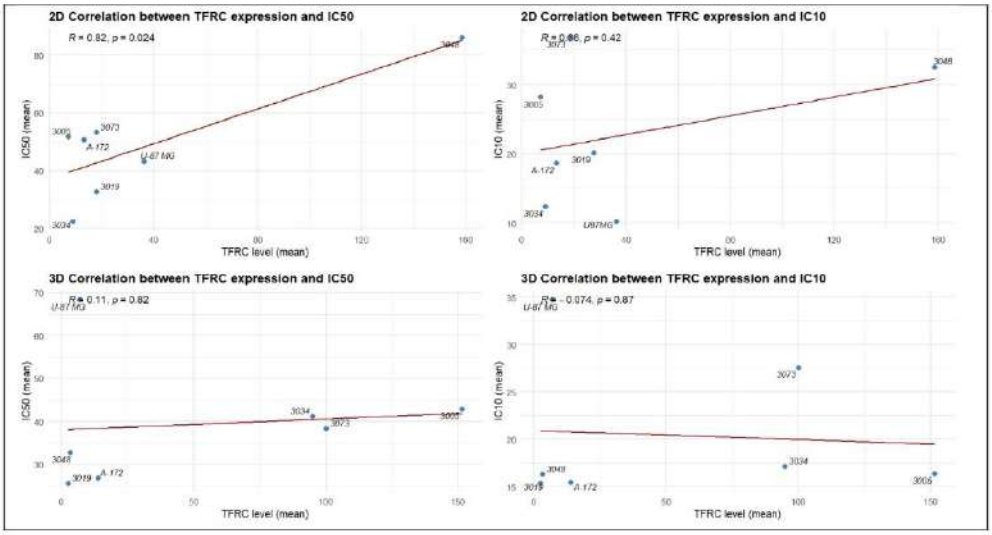

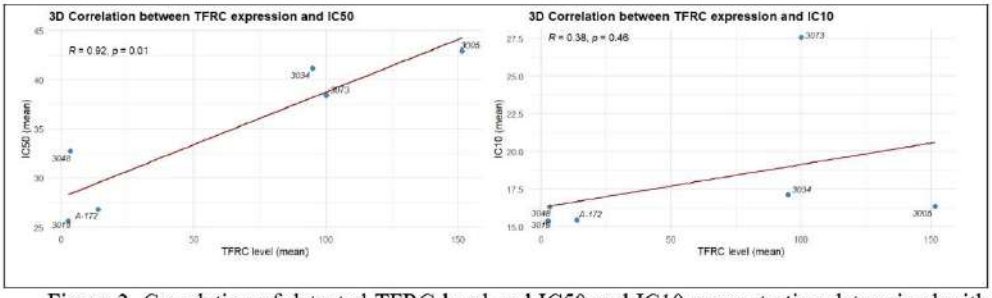

Figure 3. Correlation of detected TFRC level and IC50 and IC10 concentration determined with MTT (2D - top) and CellTiter Glo (3D - middle) assay and 3D correlation withoul U87MG (bottom).

3.2. Effects of GaM on TFRC Expression and Mitochondrial Respiration in 2D and 3D Culture Models

GaM treatment induced marked and cell line–dependent alterations in TFRC expression, with distinct responses observed between 2D and 3D culture formats (Fig. 1). In 2D conditions, a significant drop of TFRC level was observed in several lines (e.g., 3019, 3073, A-172) following 24h or 72h of exposure. In contrast, other lines (e.g., 3005, 3048) displayed variable or non-significant changes. By contrast, in 3D cultures, TFRC modulation was more heterogeneous: U-87 MG and 3034 exhibited a pronounced decrease after treatment, while 3073 demonstrated a transient upregulation at 72h, and 3019 showed no significant reduction even at 168h. These findings highlight both format-specific and temporal differences in the regulation of iron uptake pathways upon GaM exposure. Consistent with the TFRC data, OCR measurements revealed that GaM also differentially influenced mitochondrial respiration across culture formats (Fig. 2). In A-172, U-87 MG, 3073, and 3048 cells, GaM treatment led to a pronounced suppression of oxygen consumption, most evident under 3D conditions, suggesting impaired mitochondrial activity. In contrast, 3019 and 3005 cells maintained relatively stable OCR profiles irrespective of treatment, reflecting a

higher metabolic resilience. Interestingly, 3034 cells displayed sustained OCR in 3D despite TFRC downregulation, indicating a possible shift to alternative metabolic pathways to support respiration.

Taken together, these results demonstrate that GaM exerts a dual effect on glioblastoma cells by modulating TFRC expression and impairing mitochondrial respiration, with both responses being strongly dependent on cell line identity and the dimensionality of the culture system.

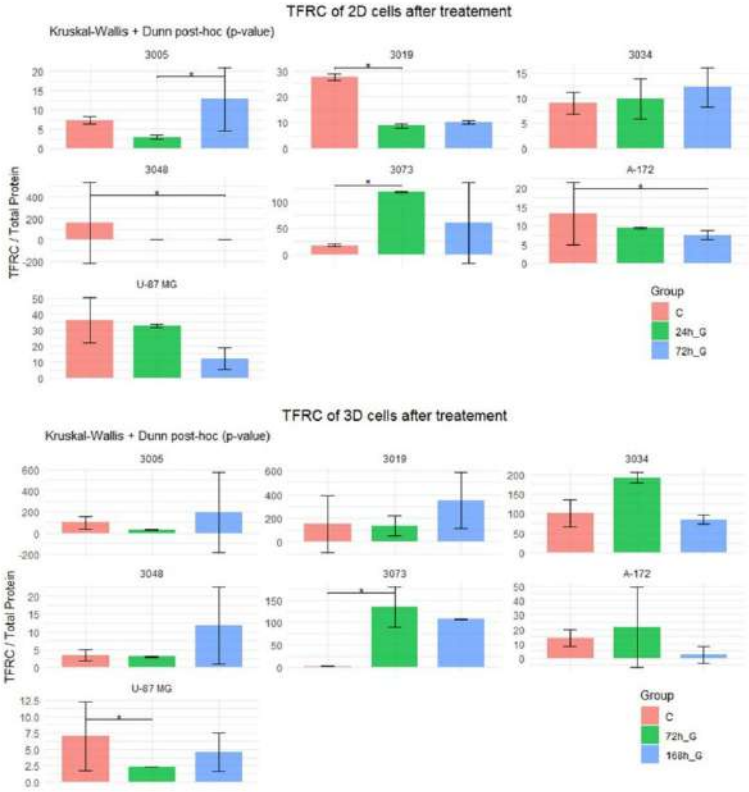

Figure 4. FTCR TFRC normalized total protein content in 2D cells (top) treated with IC50 concentration of GaM for 24h and 72h, and untreated control; 3D (bottom) treated with 2D IC50 concentration for 72h and 168h, and untreated control.

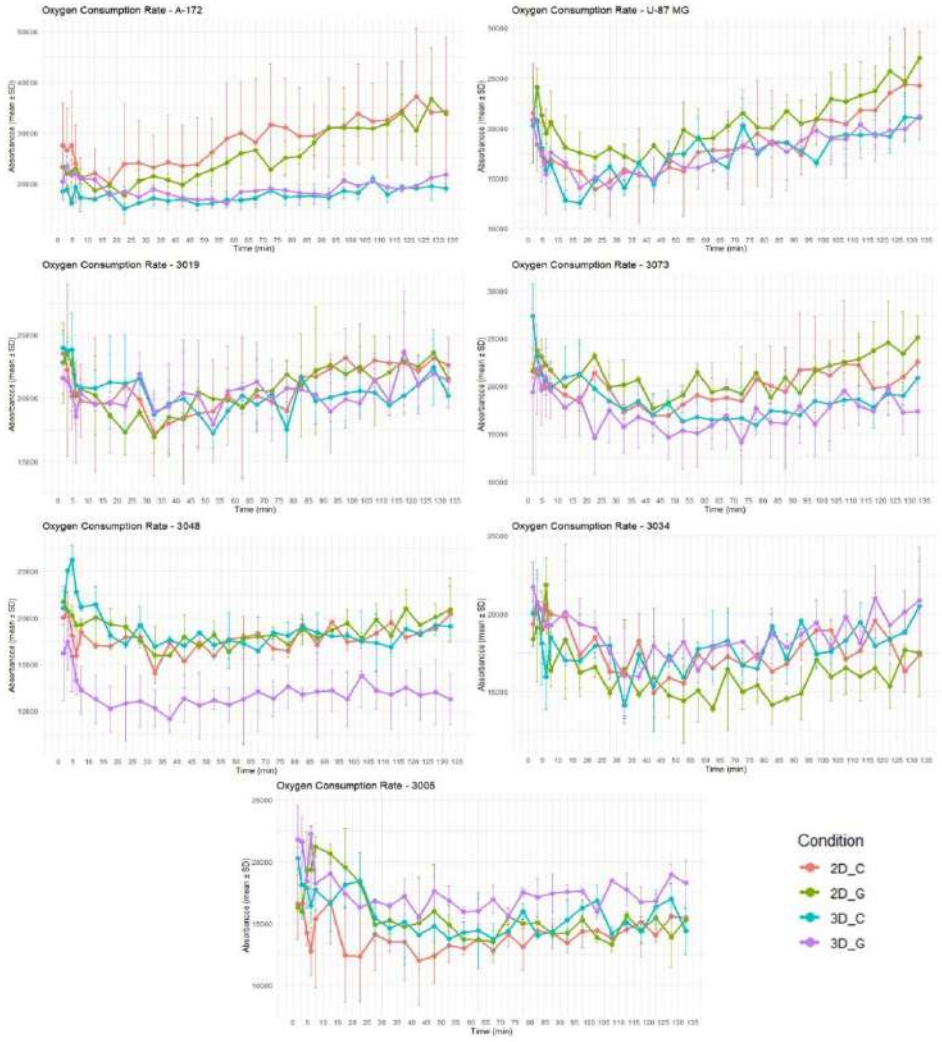

Figure 5. OCR level in 2D and 3D culture immediately after 2DIC50 concentration and untreated control.

3.3. Multivariate Analysis of Metabolic Profiles in 2D and 3D Cultures

To investigate global metabolic alterations induced by GaM treatment, principal component analysis (PCA) (Fig. S2, Tab. S2) and partial least squares discriminant analysis (PLS-DA) were performed for each cell line under different experimental conditions (Fig. 6). Clear separation between sample groups was observed, with the degree of clustering varying according to cell line, treatment duration, and culture format.

In A-172 and U-87 MG cells, temporal effects were the predominant drivers of variance, with early (24 h) and late (72–168 h) treatment groups forming distinct clusters. Treatment-dependent separation was also evident, particularly at later time points, although overlap between control and GaM-exposed samples persisted in some comparisons. Among the patient-derived glioblastoma models, 3005 and 3048 exhibited a stronger treatment-dependent response, as GaM exposure led to pronounced segregation of metabolic profiles from untreated controls, especially under 3D conditions. In contrast, 3019 and 3034 cells demonstrated striking format-specific clustering, with 2D and 3D cultures forming distinct groups regardless of treatment, underscoring the dominant effect of dimensionality in shaping metabolic programs. Finally, 3073 cells displayed combined influences of both time and culture format, with 3D groups clearly separated from their 2D counterparts and temporal clustering evident within each format.

These analyses indicate that GaM induces robust and cell line–specific metabolic reprogramming. In some lines (e.g., 3005, 3048), treatment was the dominant factor, whereas in others (e.g., 3019, 3034) the culture format exerted the most decisive influence. In contrast, for A-172, U-87 MG, and 3073, metabolic variation was driven primarily by treatment duration.

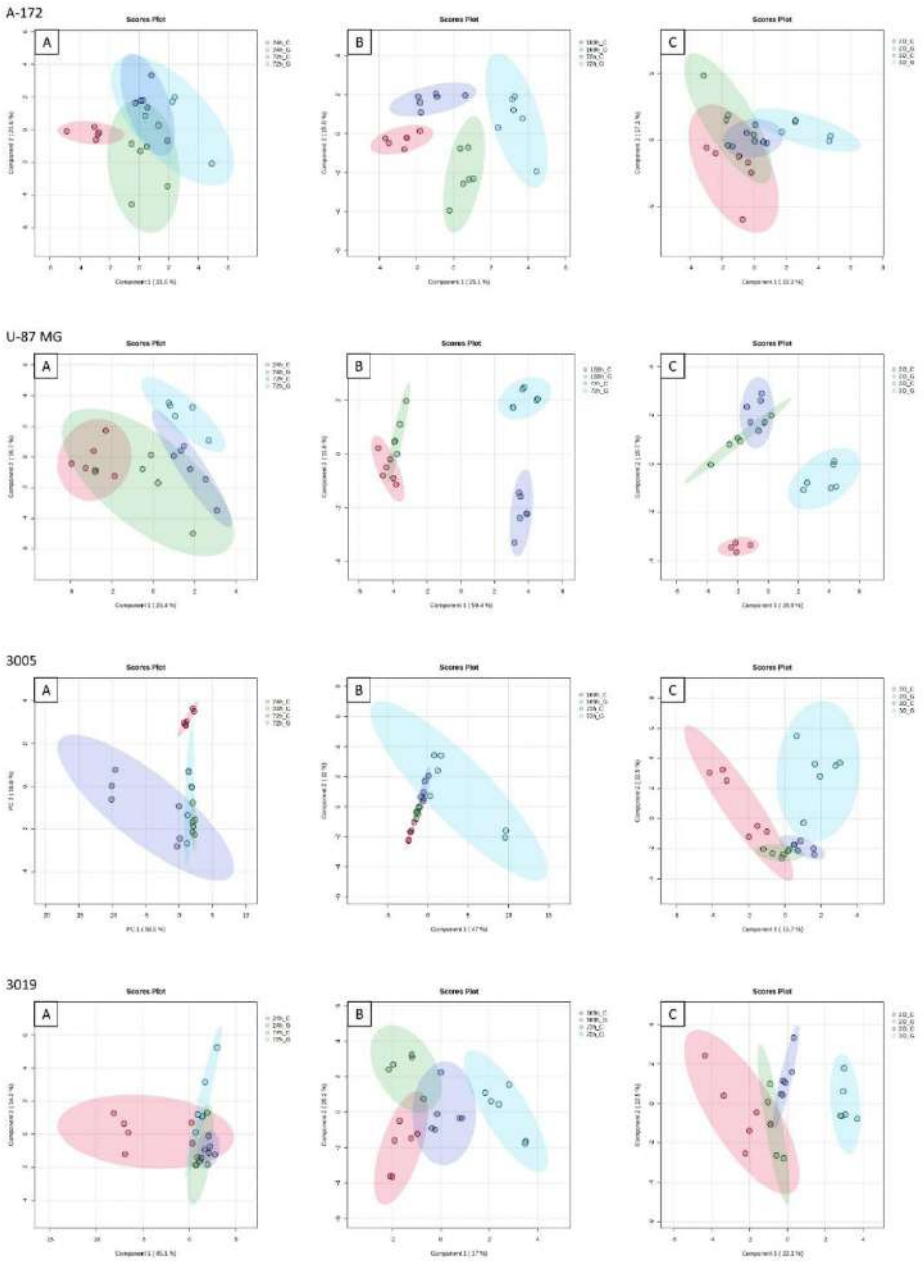

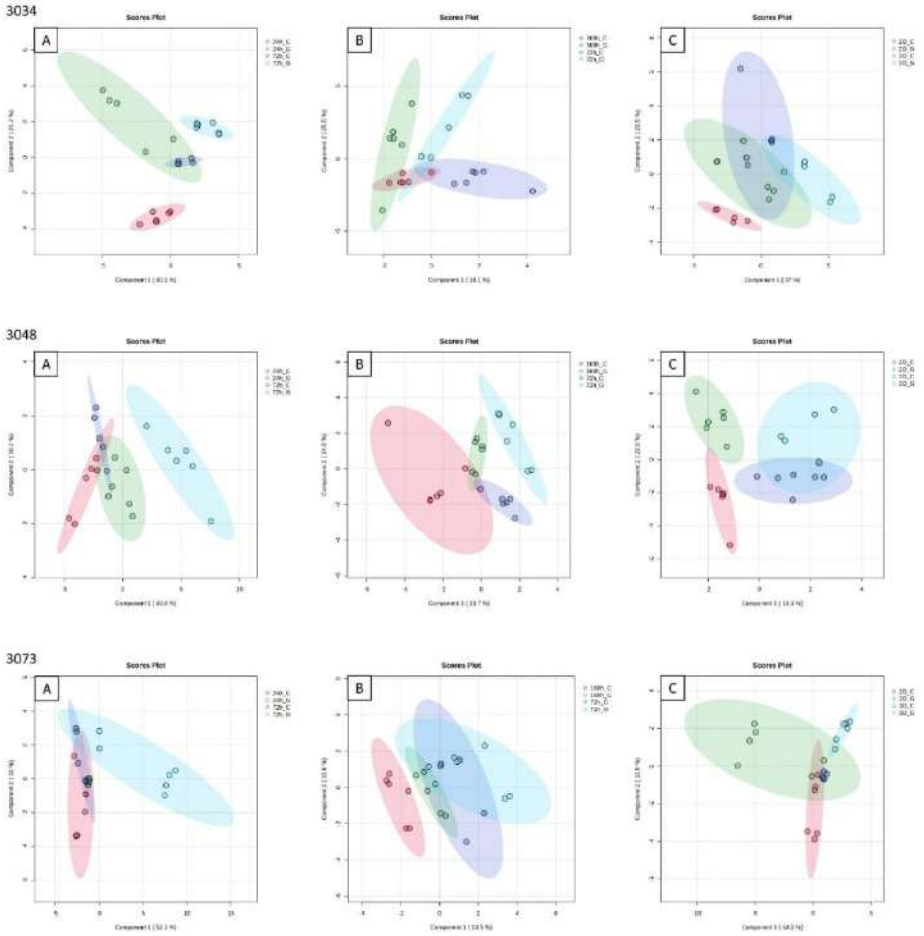

Figure 6. PLS-DA score plots showing separation of all cell lines in A) 2D 24h vs 72h, B) 3D 72h vs 168h, C) 72h 2D vs 3D (n=6).

The comparative analysis of treated cells and untreated control within one incubation time further explored the metabolomic separation upon GaM exposure (Fig S3-S9, Tab S1). Targeted metabolomic profiling revealed consistent alterations in several metabolites across glioblastoma models following GaM exposure (Tab. S3). Among the significantly perturbed metabolites, uracil

accumulated in multiple models, indicating disruption of pyrimidine metabolism, which may reflect altered nucleotide turnover or stress-related RNA degradation (Fig.7 and 8). In turn, tryptophan levels were markedly reduced in treated cells, suggesting interference with tryptophan catabolism and potentially implicating the kynurenine pathway (Fig. 9 and 10). Methionine levels were significantly diminished upon treatment, consistent with impaired one-carbon metabolism and reduced methylation potential (Fig. S10 and S11), while allantoin, a marker of oxidative stress and purine catabolism, was strongly elevated, reflecting treatment-induced redox imbalance (Fig. S12 and S13). All scope of significantly changed metabolites can be found in Table S2.

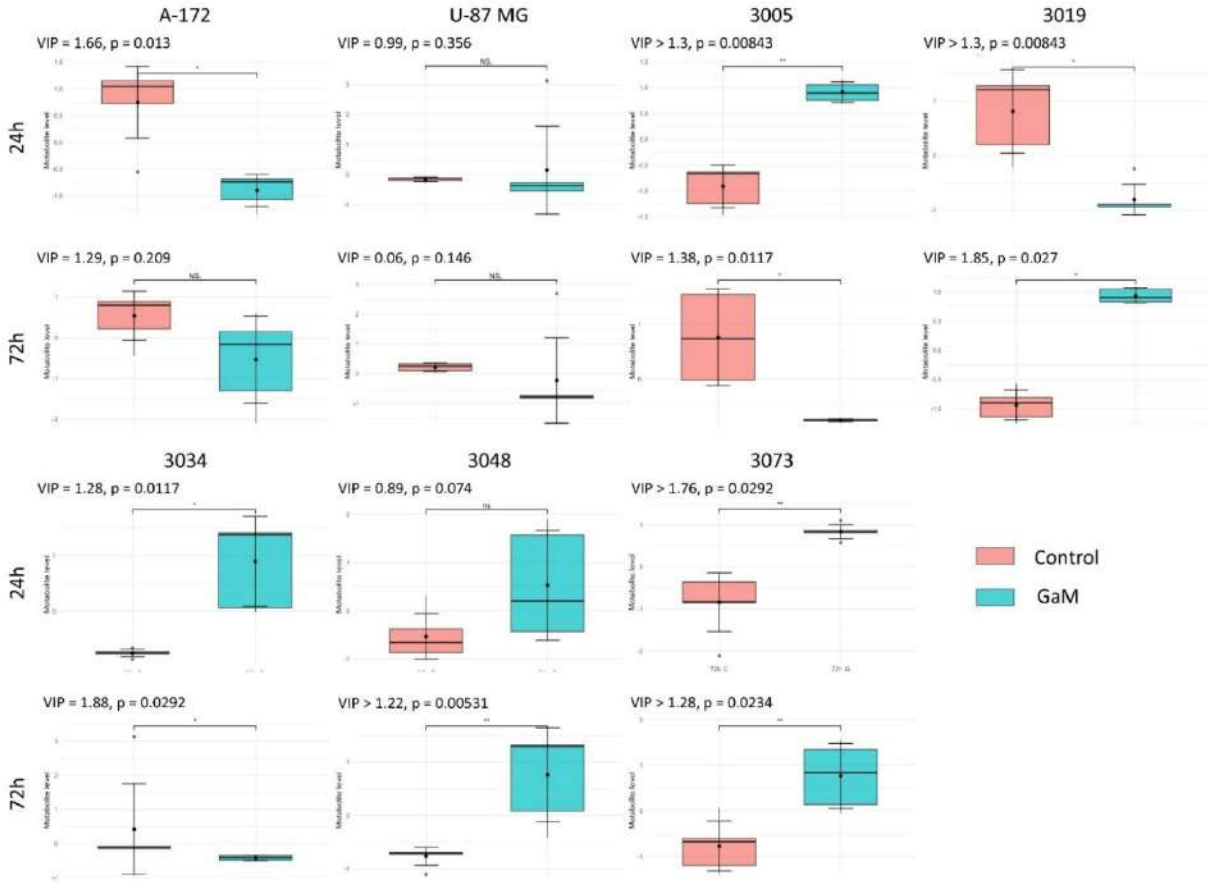

Figure 7. Change in levels of uracil between GaM treated cells and untreated control in 2D culture with VIP score and p-value (FDR).

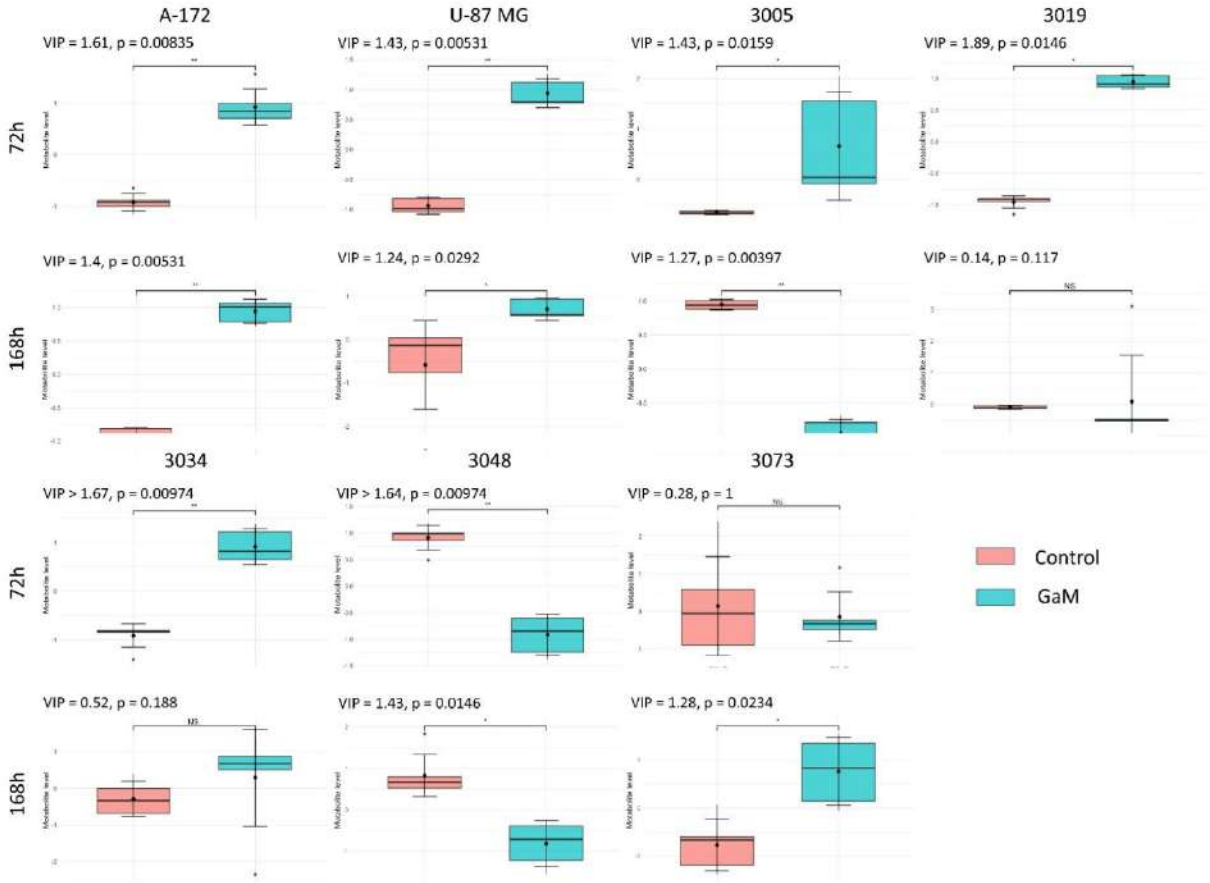

Figure 8. Change in levels of uracil between GaM treated cells and untreated control in 3D culture with VIP score and p-value (FDR).

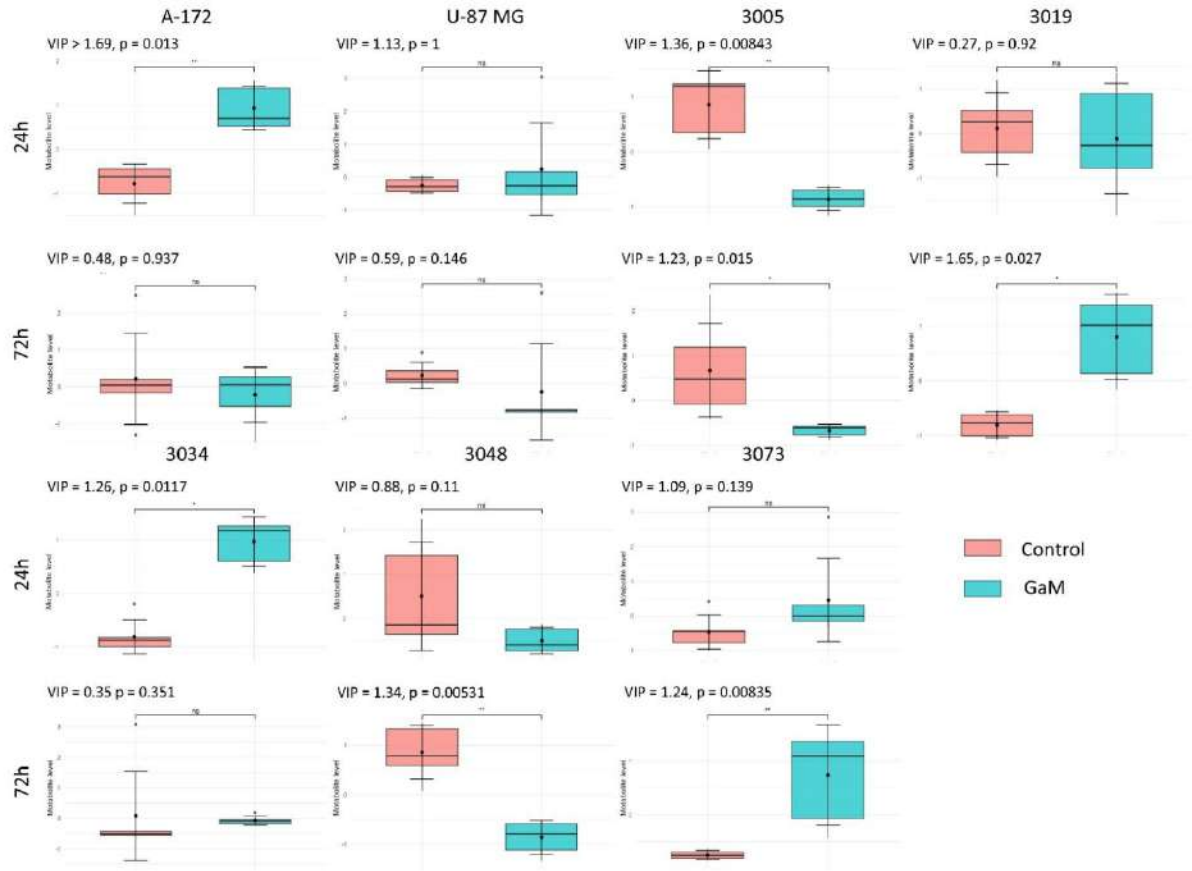

Figure 9. Change in levels of tryptophan between GaM treated cells and untreated control in 2D culture with VIP score and p-value (FDR).

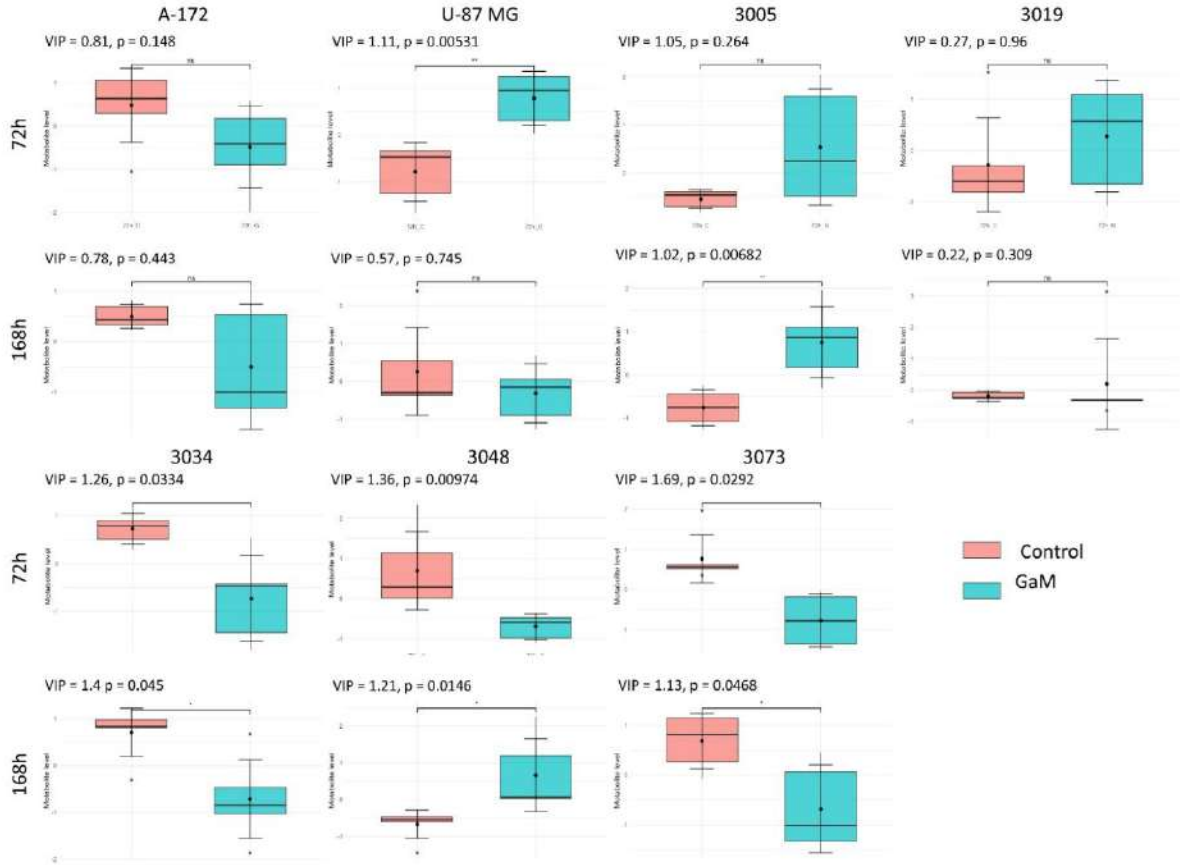

Figure 10. Change in levels of tryptophan between GaM treated cells and untreated control in 2D culture with VIP score and p-value (FDR).

Pathway enrichment analysis supported these observations, highlighting significant impacts on amino acid metabolism (tryptophan, methionine), nucleotide metabolism (uracil, purines), and redox-related pathways (allantoin) (Fig. 11, Table 1). These pathways emerged among the most significantly perturbed, with high pathway impact scores, suggesting that GaM treatment broadly reprograms metabolic networks essential for glioblastoma proliferation and survival.

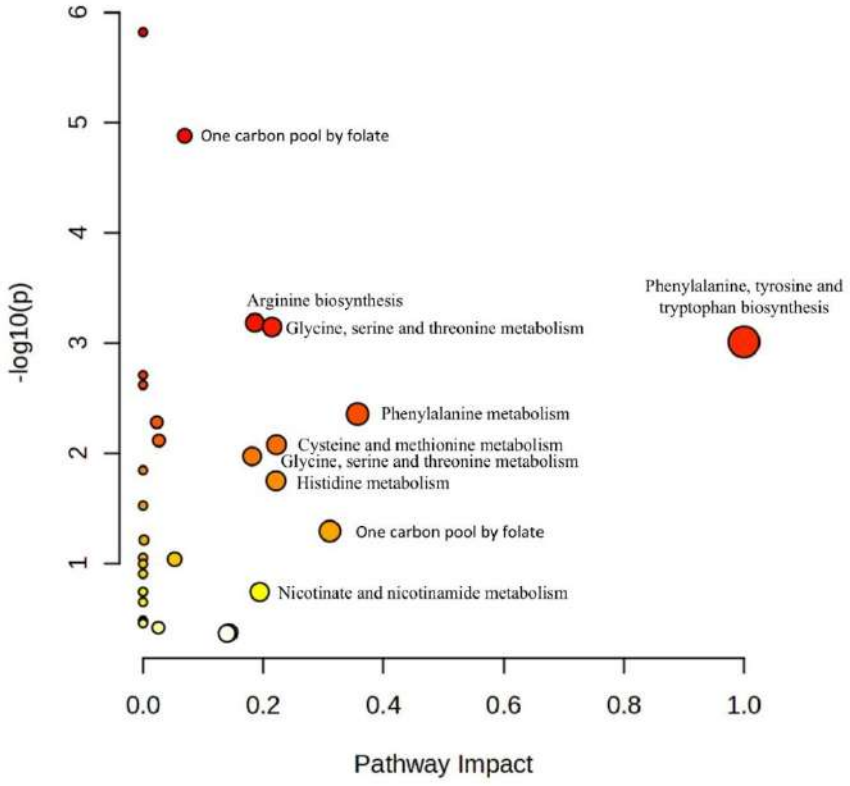

Figure 11. Pathway analysis of significantly differential features from metabolomic analysis.

Table 1. Detailed information on Pathway Analysis performed based on metabolites of VIP score > 1 and FDR < 0.05.

Pathway Name	Match Status	p	-log(p)	Holm p	FDR	Impact
Valine, leucine, and isoleucine biosynthesis	4/8	1.23E-06	5.9096	9.85E-05	9.85E-05	0
One carbon pool by folate	5/26	1.32E-05	4.8783	0.001045	0.000529	0.06931
Arginine biosynthesis	3/14	0.000566	3.2473	0.044133	0.015088	0.18617
Glycine, serine, and threonine metabolism	4/33	0.000715	3.1455	0.055082	0.014307	0.21459
Phenylalanine, tyrosine, and tryptophan biosynthesis	2/4	0.000887	3.0523	0.068271	0.017733	1
Pantothenate and CoA biosynthesis	3/20	0.001689	2.7725	0.12832	0.027015	0
Nitrogen metabolism	2/6	0.002183	2.6609	0.16375	0.02911	0
Phenylalanine metabolism	2/8	0.004014	2.3964	0.29706	0.045496	0.35714
Glutathione metabolism	3/28	0.00455	2.342	0.33212	0.045496	0.02309
Glyoxylate and dicarboxylate metabolism	3/32	0.00667	2.1759	0.48025	0.052934	0.02667
Cysteine and methionine metabolism	3/33	0.007278	2.138	0.51677	0.052934	0.22222
Arginine and proline metabolism	3/36	0.009298	2.0316	0.64156	0.061986	0.18139

Valine, leucine, and isoleucine degradation	3/40	0.012459	1.9045	0.84721	0.076671	0
Histidine metabolism	2/16	0.016197	1.7906	1	0.092555	0.22131
beta-Alanine metabolism	2/21	0.0273	1.5638	1	0.1456	0
Alanine, aspartate, and glutamate metabolism	2/28	0.04663	1.3313	1	0.23315	0.3109
Purine metabolism	3/70	0.054267	1.2655	1	0.25538	0.00158
Pyrimidine metabolism	2/39	0.084215	1.0746	1	0.35725	0.05261
Thiamine metabolism	1/7	0.084848	1.0714	1	0.35725	0
Taurine and hypotaurine metabolism	1/8	0.096396	1.0159	1	0.38558	0
Biotin metabolism	1/10	0.11908	0.92417	1	0.45363	0
D-Amino acid metabolism	1/15	0.17344	0.76086	1	0.57813	0
Butanoate metabolism	1/15	0.17344	0.76086	1	0.57813	0
Nicotinate and nicotinamide metabolism	1/15	0.17344	0.76086	1	0.57813	0.1943
Ubiquinone and other terpenoid-quinone biosynthesis	1/19	0.21462	0.66834	1	0.68677	0
Lysine degradation	1/30	0.31805	0.49751	1	0.95829	0
Porphyrin metabolism	1/31	0.32678	0.48575	1	0.95829	0
Sphingolipid metabolism	1/32	0.3354	0.47443	1	0.95829	0
Tryptophan metabolism	1/41	0.40845	0.38886	1	1	0.14305
Tyrosine metabolism	1/42	0.41608	0.38083	1	1	0.13972

4. Discussion

GBM is an aggressive and incurable tumor of the central nervous system. The alarming increase in incidence, frequent recurrences, and high mortality has driven a steady rise in research on new and effective therapies in recent years. A next-generation compound, GaM, showed greater efficacy in preclinical studies compared with GaN against hepatocellular carcinoma cells and GaN-resistant lymphoma cells, suggesting that the mechanism of gallium ion transport in complex with

maltolate differs from that of GaN [43,44]. The proven effectiveness of GaM against treatment-resistant cells provides strong prospects for developing an effective therapy for aggressive and incurable GBM.

The present study aimed to evaluate the cytotoxic activity of GaM against GBM cells in both 2D and 3D culture models. Our results indicate that GaM perturbs iron-dependent metabolism in GBM, coherently linking TFRC biology, mitochondrial respiration (OCR), and multivariate shifts in metabolite profiles. GaM exploits transferrin, a protein responsible for iron transfer into the cell, to access the brain and GBM cells. Chitambar et al. described that GaM disrupts mitochondrial function (notably complex I via impaired iron–sulfur cluster assembly) and inhibits the iron-dependent RRM2 subunit of ribonucleotide reductase—effects demonstrated in U-87 MG/D54 cells and validated *in vivo* where GaM retards GBM growth and alters iron markers[12]. Glioblastoma cell lines have been shown to overexpress transferrin receptors frequently, not only TfR1; TfR2 is highly and commonly expressed in GBM, it has been associated with grade and proliferation, underscoring that the phenotype of iron transfer into the cells is broader and may shape sensitivity to iron-mimetic therapies[27].

Culture dimension emerged as a dominant modifier of GaM response in our models. Several lines (A-172, U-87 MG, 3073, 3048) showed stronger OCR suppression and more apparent metabolic separation in 3D than 2D, consistent with evidence that advanced 3D GBM systems better reproduce diffusion barriers, ECM/mechanical cues, chemical gradients, and BBB contributions—features that modulate drug penetration and frequently reduce apparent drug sensitivity relative to monolayers[28]. In particular, an engineered human BBB–GBM co-culture showed decreased temozolomide sensitivity with increased tumor spatial organization and BBB involvement, exemplifying how microenvironmental architecture can decouple single-target predictors (e.g., TFRC levels) from whole-cell pharmacologic outcomes.

Model identity also influenced GaM phenotypes. Established lines (A-172, U-87 MG) tended to display time-dependent separation and robust OCR effects, whereas multiple patient-derived lines showed either format-dominated clustering (2D vs 3D outweighing treatment; e.g., 3019, 3034) or pronounced treatment-specific separation (e.g., 3005, 3048). This mirrors comparisons between established GBM lines and patient-derived/neurosphere models, where 3D states rewire metabolism and drug sensitivity[29]. These considerations support prioritizing 3D and patient-derived platforms for GaM evaluation and for combination-strategy testing.

The observed alterations in tryptophan, uracil, methionine, and allantoin provide insights into the cellular response to GaM treatment. Tryptophan depletion is particularly relevant, as it may reflect increased catabolism through the kynurenine pathway, a route tightly linked to immunosuppression and tumor progression [30,31]. Reduced availability of tryptophan could therefore impair protein synthesis and alter immune interactions, suggesting that GaM interferes with both metabolic and signalling roles of this essential amino acid—similarly, the consistent changes in uracil point to disrupted pyrimidine metabolism. Accumulation of uracil has been associated with imbalances in nucleotide pools and misincorporation into DNA, which requires base excision repair. Such changes may contribute to replication stress and reduced proliferation under GaM exposure[32,33]. The decrease in methionine levels further underscores the influence on DNA. Methionine is a key donor in one-carbon metabolism and methylation reactions, and its depletion suggests impaired DNA and histone methylation capacity, which could translate into epigenetic instability and altered gene regulation in glioblastoma cells [34,35].

Finally, the significant increase in allantoin reflects perturbations in purine metabolism and elevated oxidative stress. Allantoin accumulation is a recognized marker of reactive oxygen species (ROS) activity. This implies that GaM treatment may induce redox imbalance and oxidative damage, compromising glioblastoma cell viability[36,37]. These findings suggest that GaM exerts its

effects through a multifaceted disruption of amino acid, nucleotide, and redox metabolism. This combination of metabolic stressors likely contributes to impaired biosynthesis, genomic instability, and oxidative damage, thereby sensitizing glioblastoma cells to treatment.

Summarizing, at the metabolite level, methionine, uracil, and allantoin provide a concise, mechanism-anchored narrative that aligns with our pathway analysis. Tryptophan depletion implicates kynurenine/immune-metabolic axes; methionine decrease suggests pressure on one-carbon metabolism and methylation capacity; uracil dysregulation points to pyrimidine pool imbalance and nucleic acid turnover stress; and allantoin elevation is compatible with ROS-linked purine oxidation—all converging with our OCR data on mitochondrial compromise under GaM[12]. Together, these data support amino-acid, nucleotide, and redox stress as integrated drivers of GaM cytotoxicity.

Translationally, GaM has shown in vivo activity in GBM xenografts, including oral delivery that slows tumor growth and extends disease-specific survival[38]; early reports also noted reductions in tumor and relative cerebral blood volume, and continuous administration suppressed glioma growth and *in vivo*[12]. These findings along with literature on gallium complexes as anticancer agents reinforce the rationale for GaM development and for integrating metabolic biomarkers (e.g., TFRC and our four-metabolite panel) into preclinical–clinical translation[8]. Finally, synergy with complex-I inhibition (e.g., metformin) in 2D and 3D GBM further supports a mitochondria-centric vulnerability under GaM treatment that may be exploitable in rational combinations[39].

Together, these data argue that 3D, patient-derived systems provide a more predictive test bed for GaM than conventional monolayers and that integrated OCR/metabolomics readouts can serve as practical pharmacodynamic markers. However, a study with a comprehensive patient-derived glioblastoma cell panel should be performed, further exploring the role of the *in vitro* microenvironment. Direct quantification of gallium uptake and GaM penetration into the 3D

spheroid could provide more information on the real toxicity of the drug, improving *in vitro-in vivo* extrapolation of results. Our findings support further development of GaM for GBM and provide a framework for selecting biomarkers and model systems that better forecast clinical performance.

Conclusion

Culture dimensionality significantly determines gallium maltolate (GaM) response in glioblastoma. Across established (A-172, U-87 MG) and patient-derived lines (3005, 3019, 3034, 3048, 3073), GaM reduced viability and suppressed mitochondrial respiration, with a consistent rightward shift of dose–response and more potent OCR inhibition in 3D than in 2D. TFRC levels associated with GaM sensitivity in 2D but not 3D indicated context-dependent biomarker performance. Metabolomics and multivariate analyses converged on a compact signature—tryptophan, methionine, uracil, and allantoin—consistent with stress in amino-acid, one-carbon/nucleotide, and redox pathways alongside mitochondrial dysfunction. These findings support using 3D, patient-derived systems with integrated OCR/ metabolomics as more predictive platforms for GaM evaluation and rational combination strategies.

5. Associated content

Supplementary material includes:

Figure S1. Principal component analysis (PCA) score plots of all analyzed samples and extraction quality control (QC) samples.

Figure S2. PCA score plots showing separation of all cell lines in A) 2D 24h vs 72h, B) 3D 72h vs 168h, C) 72h 2D vs 3D (n=6).

Figutre S3. PCA (top) and PLS-DA scrore plots showing separations of A-172 cell line in 2D and 3D, treated (G) and untreated (C).

Figutre S4. PCA (top) and PLS-DA scrore plots showing separations of U-87 MG cell line in 2D and 3D, treated (G) and untreated (C).

Figutre S5. PCA (top) and PLS-DA scrore plots showing separations of 3005 MG cell line in 2D and 3D, treated (G) and untreated (C).

Figutre S6. PCA (top) and PLS-DA scrore plots showing separations of 3019 MG cell line in 2D and 3D, treated (G) and untreated (C).

Figutre S7. PCA (top) and PLS-DA scrore plots showing separations of 3034 MG cell line in 2D and 3D, treated (G) and untreated (C).

Figutre S8. PCA (top) and PLS-DA scrore plots showing separations of 3048 MG cell line in 2D and 3D, treated (G) and untreated (C).

Figutre S9. PCA (top) and PLS-DA scrore plots showing separations of 3073 MG cell line in 2D and 3D, treated (G) and untreated (C).

Figure S10. Change in levels of methionine between GaM treated cells and untreated control in 2D culture with VIP score and p-value (FDR).

Figure S11. Change in levels of methionine between GaM treated cells and untreated control in 3D culture with VIP score and p-value (FDR).

Figure S12. Change in levels of allatoin between GaM treated cells and untreated control in 2D culture with VIP score and p-value (FDR).

Figure S13. Change in levels of allatoin between GaM treated cells and untreated control in 3D culture with VIP score and p-value (FDR).

Code S1. Dose-response curve with IC90, IC50 and IC10 calculations.

Code S2. T-test for TFRC level determination and significance of changes determination in 2D and 3D control.

Code S3. Pearson correlation test between IC10 and TFRC level in 2D and 3D cell lines.

Code S.4 TFRC level determination in treated cells and untreated control, Kurskal-Wallis test with dunn post-hoc.

Code S5. The Oxygen Consuption Rate curve in time.

Code S6 Wilcox test with FDR correction and selection of metabolites with VIP > 1 and adj. p-value (FDR).

Table S1. Cross-validated PLS-DA performance across GBM models.

Table S2. Comprehensive metabolite panel by cell line (3005, 3019, 3034, 3048, 3073, A-172, U-87 MG): VIP, FDR, stars

6. Acknowledgements

We thank Kamil Łuczykowski and Joanna Bogusiewicz for technical support with LC-MS workflows. We thank Natalia Warmuzińska for comprehensive statistical advice.

Portions of language editing were assisted by ChatGPT (OpenAI, GPT-5 Thinking, 16.09.2025).

7. Author contributions

The manuscript was written through the contributions of all authors. All authors have given approval to the final version of the manuscript

8. Funding Sources

This research was financed from the funds for Basic Research Activities of the Department of Pharmacodynamics and Molecular Pharmacology, Collegium Medicum in Bydgoszcz, Nicolaus Copernicus University in Torun.

9. References

1. Louis, D. N. *et al.* The 2021 WHO classification of tumors of the central nervous system: A summary. *Neuro. Oncol.* **23**, (2021).

2. Verdugo, E., Puerto, I. & Medina, M. Á. An update on the molecular biology of glioblastoma, with clinical implications and progress in its treatment. *Cancer Communications* vol. 42 at https://doi.org/10.1002/cac2.12361 (2022).

3. Ali, M. M. Glioblastoma: Targeting Angiogenesis and Tyrosine Kinase Pathways. *Nov. Approaches Cancer Study* **4**, (2020).

4. Edwards, C. L. & Hayes, R. L. Tumor scanning with 67Ga citrate. *J. Nucl. Med.* **10**, (1969).

5. Mikuš, P., Melník, M., Forgácsová, A., Krajčiová, D. & Havránek, E. Gallium compounds in nuclear medicine and oncology. *Main Group Metal Chemistry* vol. 37 at https://doi.org/10.1515/mgmc-2014-0009 (2014).

6. Mayle, K. M., Le, A. M. & Kamei, D. T. The intracellular trafficking pathway of transferrin. *Biochimica et Biophysica Acta - General Subjects* vol. 1820 at https://doi.org/10.1016/j.bbagen.2011.09.009 (2012).

7. Lane, D. J. R. *et al.* Cellular iron uptake, trafficking and metabolism: Key molecules and mechanisms and their roles in disease. *Biochimica et Biophysica Acta - Molecular Cell Research* vol. 1853 at https://doi.org/10.1016/j.bbamcr.2015.01.021 (2015).

8. Chitambar, C. R. Gallium Complexes as Anticancer Drugs. *Metal ions in life sciences* vol. 18 at https://doi.org/10.1515/9783110470734-016 (2018).

9. Bernstein, L. R., Tanner, T., Godfrey, C. & Noll, B. Chemistry and pharmacokinetics of gallium maltolate, a compound with high oral gallium bioavailability. *Met. Based. Drugs* **7**, (2000).

10. Chitambar, C. R. Gallium and its competing roles with iron in biological systems. *Biochimica et Biophysica Acta - Molecular Cell Research* vol. 1863 at https://doi.org/10.1016/j.bbamcr.2016.04.027 (2016).

11. Chitambar, C. R., Purpi, D. P., Woodliff, J., Yang, M. & Wereley, J. P. Development of gallium compounds for treatment of lymphoma: Gallium maltolate, a novel hydroxypyrone gallium compound, induces apoptosis and circumvents lymphoma cell resistance to gallium

nitrate. *J. Pharmacol. Exp. Ther.* **322**, (2007).

12. Chitambar, C. R. *et al.* Gallium maltolate disrupts tumor iron metabolism and retards the growth of glioblastoma by inhibiting mitochondrial function and ribonucleotide reductase. *Mol. Cancer Ther.* **17**, (2018).

13. No Title. https://clinicaltrials.gov/study/NCT04319276?tab=table.

14. Jaroch, K., Boyaci, E., Pawliszyn, J. & Bojko, B. The use of solid phase microextraction for metabolomic analysis of non-small cell lung carcinoma cell line (A549) after administration of combretastatin A4. *Sci. Rep.* **9**, (2019).

15. Jaroch, K. *et al.* One extraction tool for in vitro-in vivo extrapolation? SPME-based metabolomics of in vitro 2D, 3D, and in vivo mouse melanoma models. *J. Pharm. Anal.* **11**, (2021).

16. Denkert, C. *et al.* Mass spectrometry-based metabolic profiling reveals different metabolite patterns in invasive ovarian carcinomas and ovarian borderline tumors. *Cancer Res.* **66**, (2006).

17. Boyacl, E. *et al.* High-throughput analysis using non-depletive SPME: Challenges and applications to the determination of free and total concentrations in small sample volumes. *Sci. Rep.* **8**, (2018).

18. Bogusiewicz, J. *et al.* New chemical biopsy tool for spatially resolved profiling of human brain tissue in vivo. *Sci. Rep.* **11**, (2021).

19. Bogusiewicz, J. *et al.* Profiling of carnitine shuttle system intermediates in gliomas using solid-phase microextraction (Spme). *Molecules* **26**, (2021).

20. Bogusiewicz, J. *et al.* Coated Blade Spray-Mass Spectrometry as a New Approach for the Rapid Characterization of Brain Tumors. *Molecules* **27**, (2022).

21. Bogusiewicz, J. *et al.* Determination of acylcarnitines in intact brain tumors using coated blade spray mass spectrometry (CBS-MS). *Adv. Sample Prep.* **13**, (2025).

22. Bogusiewicz, J. *et al.* Investigating the Potential Use of Chemical Biopsy Devices to Characterize Brain Tumor Lipidomes. *Int. J. Mol. Sci.* **23**, (2022).

23. Goryńska, P. Z. *et al.* Metabolomic Phenotyping of Gliomas: What Can We Get with Simplified Protocol for Intact Tissue Analysis? *Cancers (Basel).* **14**, (2022).

24. Xie, Y. *et al.* The Human Glioblastoma Cell Culture Resource: Validated Cell Models Representing All Molecular Subtypes. *EBioMedicine* **2**, (2015).

25. Wanigasekara, J., Carroll, L. J., Cullen, P. J., Tiwari, B. & Curtin, J. F. Three-Dimensional (3D) in vitro cell culture protocols to enhance glioblastoma research. *PLoS One* **18**, (2023).

26. No Title. https://www.metaboanalyst.ca.

27. Calzolari, A. *et al.* Transferrin receptor 2 is frequently and highly expressed in glioblastomas. *Transl. Oncol.* **3**, (2010).

28. Wanigasekara, J., Cullen, P. J., Bourke, P., Tiwari, B. & Curtin, J. F. Advances in 3D culture systems for therapeutic discovery and development in brain cancer. *Drug Discovery Today* vol. 28 at https://doi.org/10.1016/j.drudis.2022.103426 (2023).

29. Vaezzadeh, M. *et al.* Combination Drug Therapy of Glioblastoma: Lessons from 3D In Vitro Models and the Roadmap for Future Research. *Advanced Therapeutics* vol. 6 at

https://doi.org/10.1002/adtp.202300197 (2023).

30. Platten, M., Nollen, E. A. A., Röhrig, U. F., Fallarino, F. & Opitz, C. A. Tryptophan metabolism as a common therapeutic target in cancer, neurodegeneration and beyond. *Nature Reviews Drug Discovery* vol. 18 at https://doi.org/10.1038/s41573-019-0016-5 (2019).

31. Badawy, A. A. B. Tryptophan metabolism and disposition in cancer biology and immunotherapy. *Bioscience Reports* vol. 42 at https://doi.org/10.1042/BSR20221682 (2022).

32. Wilson, P. M., Danenberg, P. V., Johnston, P. G., Lenz, H. J. & Ladner, R. D. Standing the test of time: Targeting thymidylate biosynthesis in cancer therapy. *Nature Reviews Clinical Oncology* vol. 11 at https://doi.org/10.1038/nrclinonc.2014.51 (2014).

33. Visnes, T. *et al.* Targeting BER enzymes in cancer therapy. *DNA Repair* vol. 71 at https://doi.org/10.1016/j.dnarep.2018.08.015 (2018).

34. Mentch, S. J. & Locasale, J. W. One-carbon metabolism and epigenetics: Understanding the specificity. *Ann. N. Y. Acad. Sci.* **1363**, (2016).

35. Kanarek, N., Petrova, B. & Sabatini, D. M. Dietary modifications for enhanced cancer therapy. *Nature* vol. 579 at https://doi.org/10.1038/s41586-020-2124-0 (2020).

36. Kaur, H. & Halliwell, B. Action of biologically-relevant oxidizing species upon uric acid. Identification of uric acid oxidation products. *Chem. Biol. Interact.* **73**, (1990).

37. Marrocco, I., Altieri, F. & Peluso, I. Measurement and Clinical Significance of Biomarkers of Oxidative Stress in Humans. *Oxidative Medicine and Cellular Longevity* vol. 2017 at

https://doi.org/10.1155/2017/6501046 (2017).

38. Al-Gizawiy, M. M. *et al.* Potent in vivo efficacy of oral gallium maltolate in treatment-resistant glioblastoma. *Front. Oncol.* **13**, (2023).

39. Alhajala, H. S. *et al.* The cytotoxicity of gallium maltolate in glioblastoma cells is enhanced by metformin through combined action on mitochondrial complex 1. *Oncotarget* **11**, (2020).

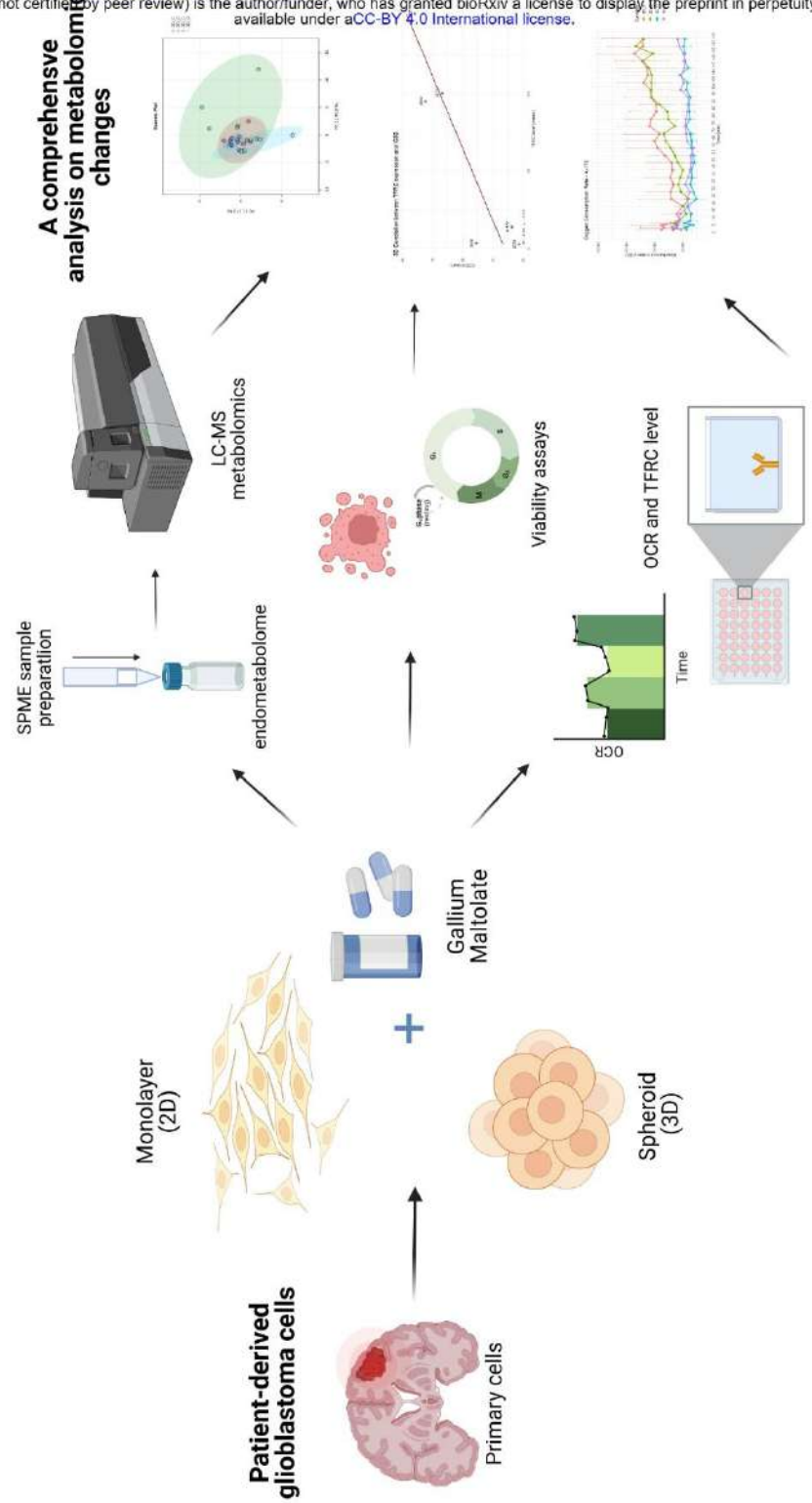

Supplementary Materials

Culture Dimensionality Governs Gallium Maltolate Response in Glioblastoma: Comparative Analyses in 2D and 3D Models

Paulina Szeliska[1], Karol Jaroch[1], Weronika Wróblewska[1], Łukasz Kaźmierski[2], Małgorzata Maj[2], Barbara Bojko[1,]*

Table S1. Basic characteristics of HGCC glioblastoma cells.

Cell Line	HGCC_Subtype	Sex	Age (year)	Overall Survival (days)	Vital Status	Diagnosis	WHO Grade
U3005MG	Classical (CL)	Male	65	26	DEAD	Glioblastoma	IV
U3019MG	Proneural (PN)	Female	82	117	DEAD	Glioblastoma	IV
U3034MG	Mesenchymal (MS)	Male	73	539	DEAD	Glioblastoma	IV
U3048MG	Classical (CL)	Male	77	279	DEAD	Glioblastoma	IV
U3073MG	Mesenchymal (MS)	Male	71	481	DEAD	Glioblastoma	IV

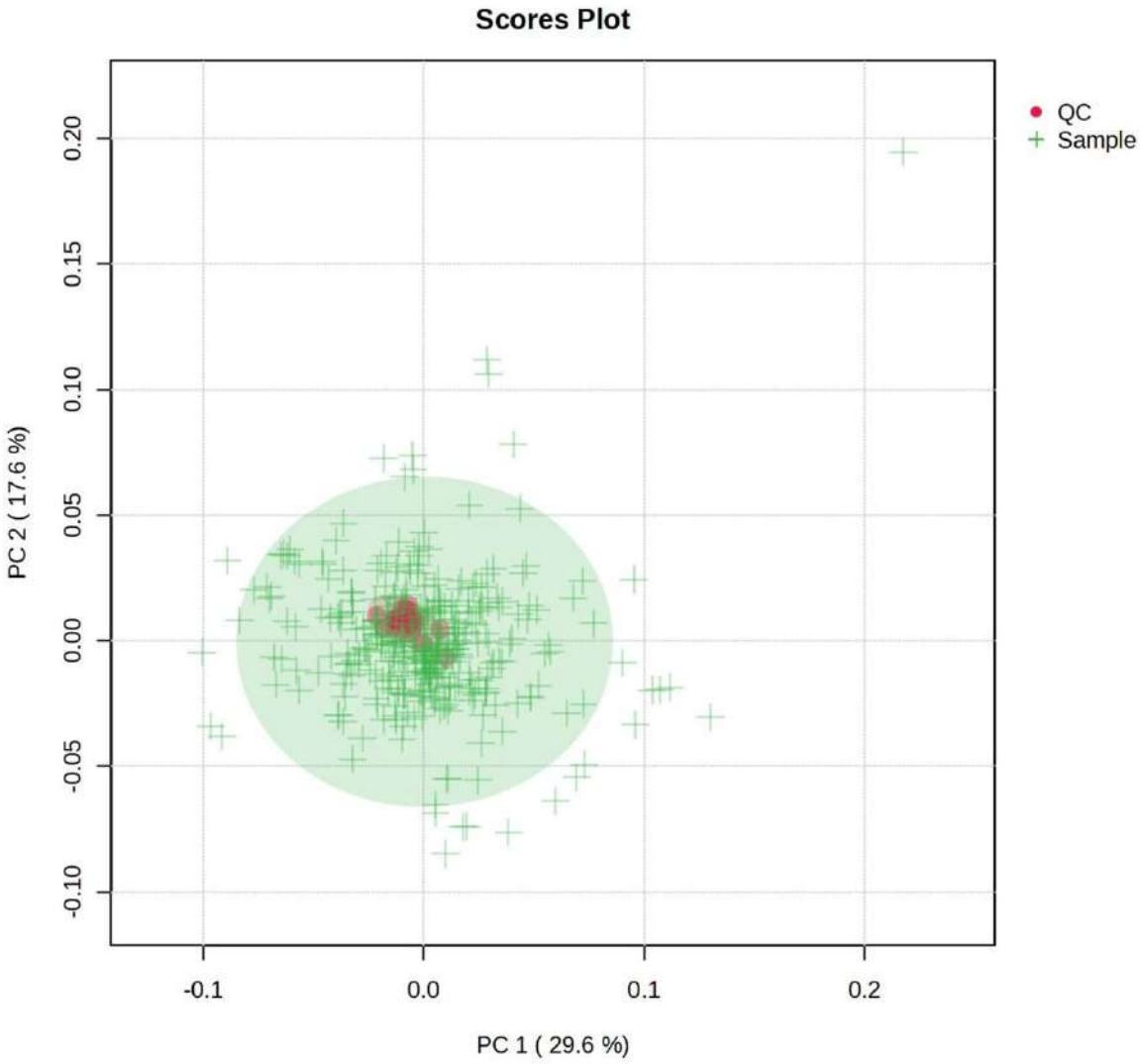

Figure S1. Principal component analysis (PCA) score plots of all analyzed samples and extraction quality control (QC) samples.

A-172

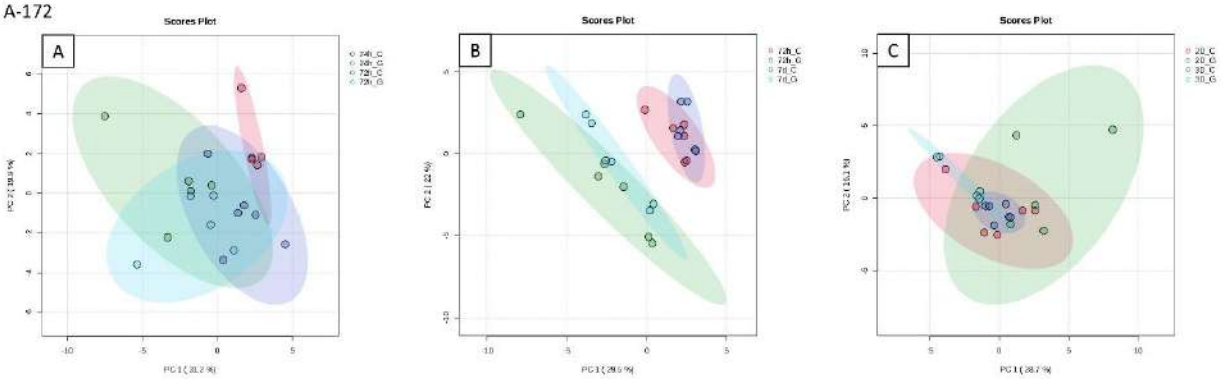

U-87 MG

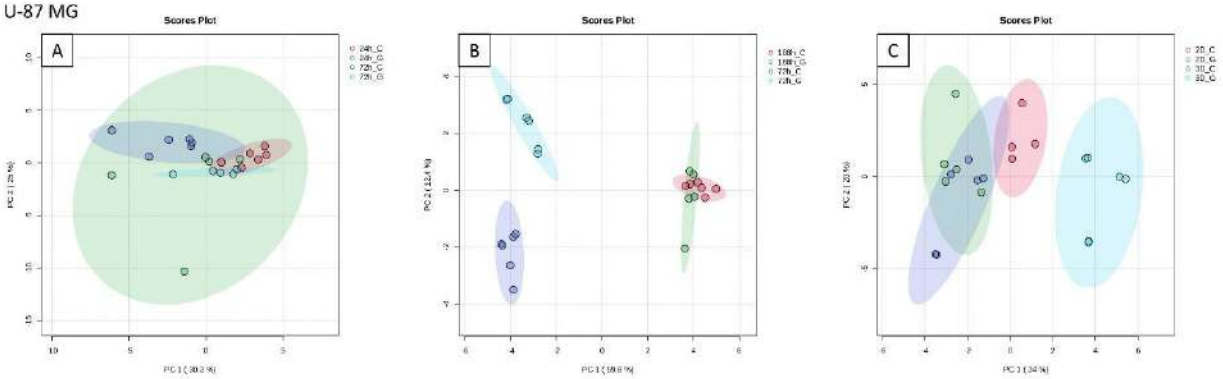

3005

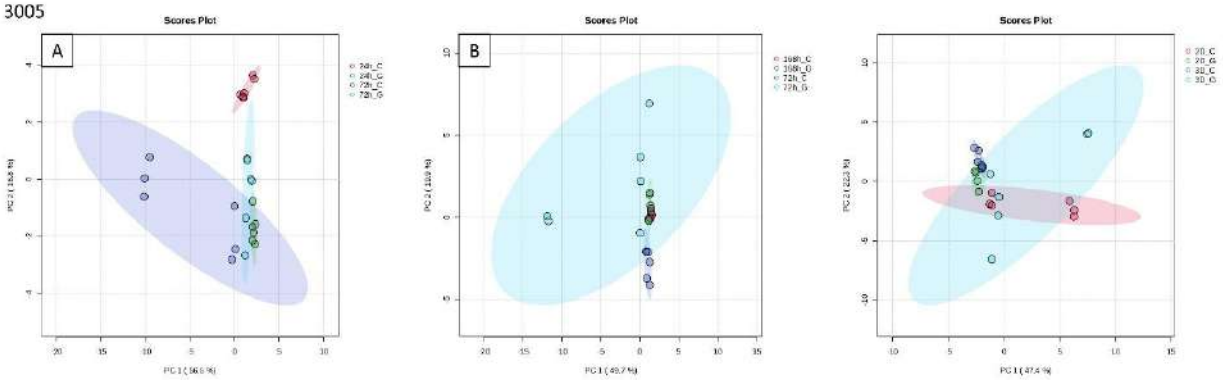

3019

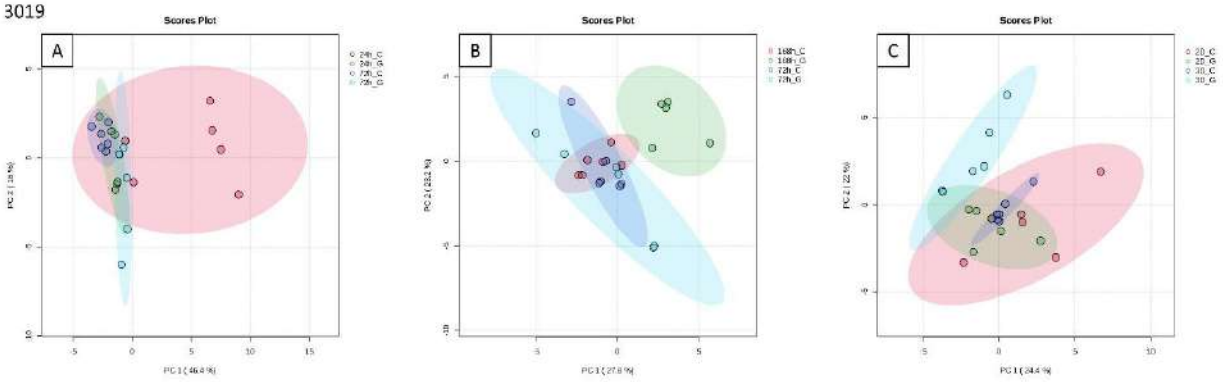

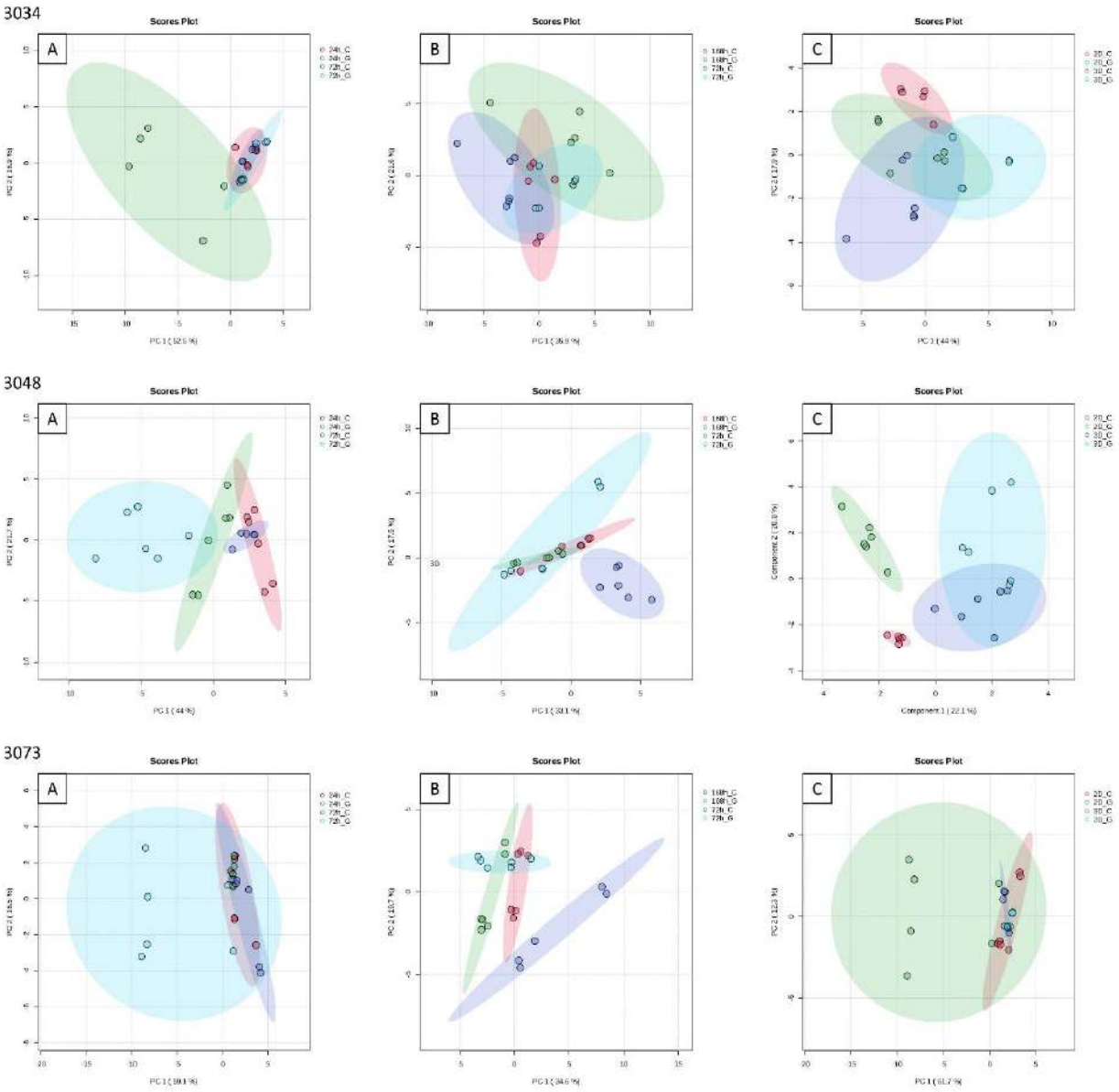

Figure S2. PCA score plots showing separation of all cell lines in A) 2D 24h vs 72h, B) 3D 72h vs 168h, C) 72h 2D vs 3D (n=6).

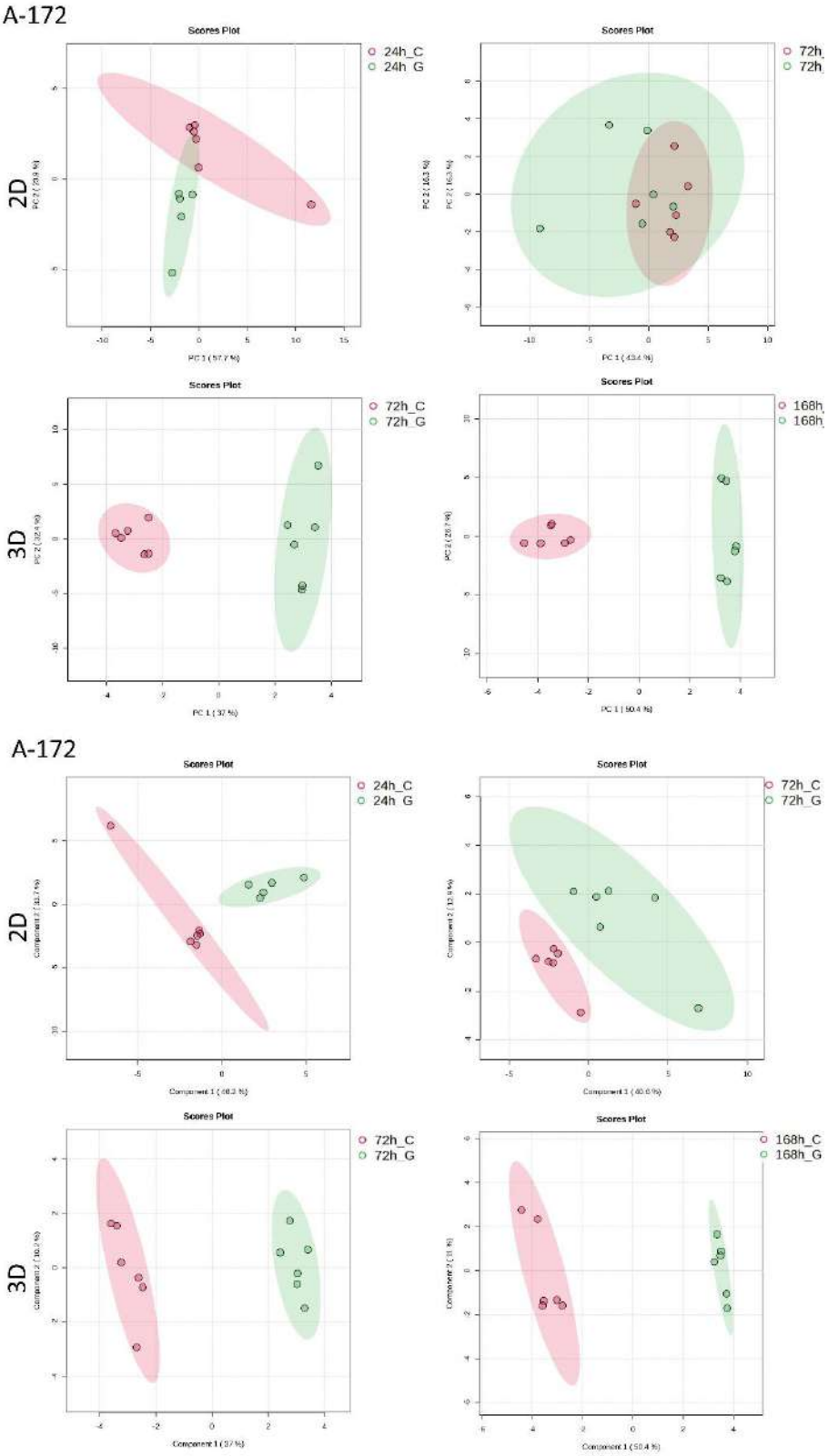

Figutre S3. PCA (top) and PLS-DA scrore plots showing separations of A-172 cell line in 2D and 3D, treated (G) and untreated (C).

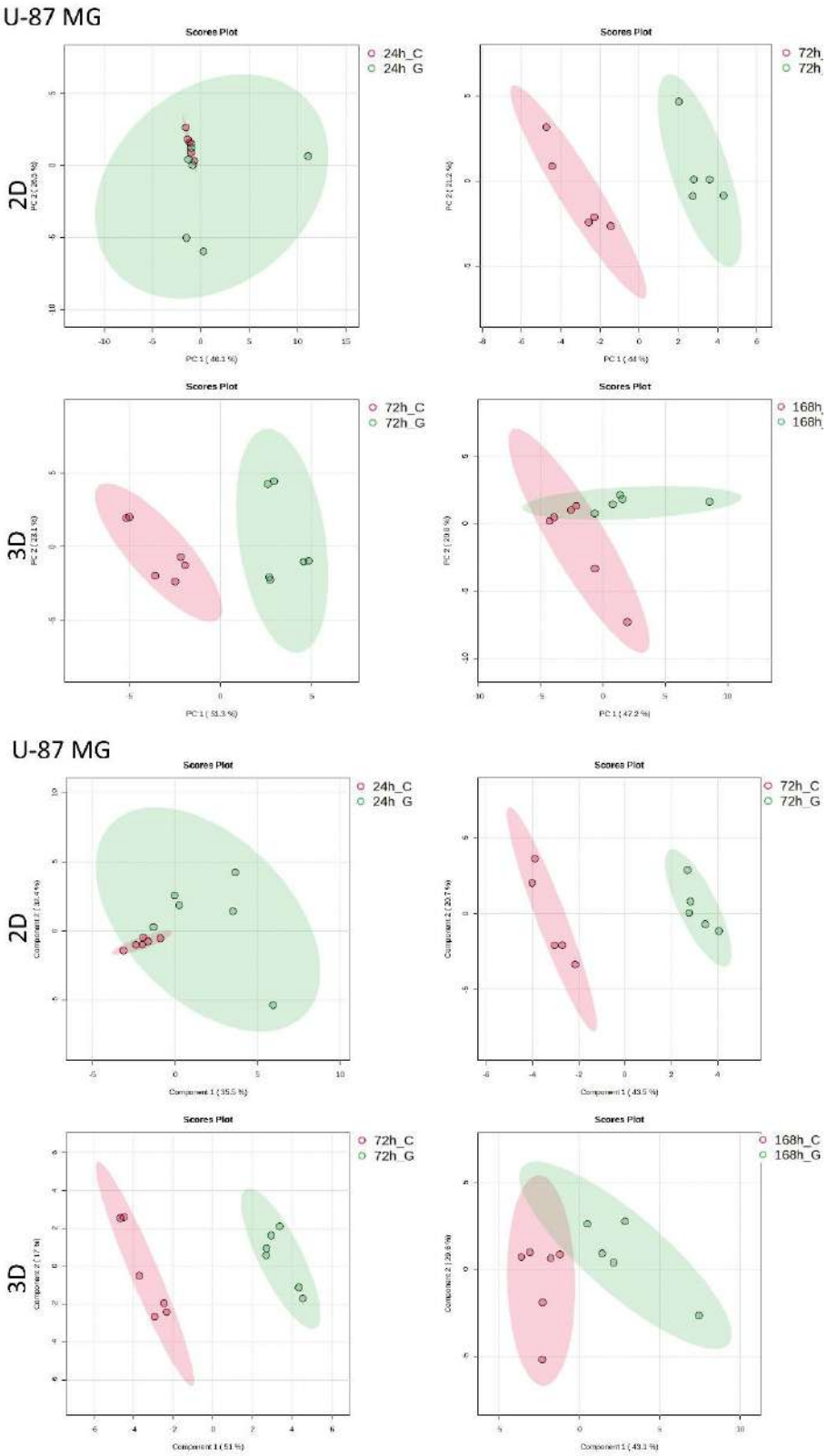

Figutre S4. PCA (top) and PLS-DA scrore plots showing separations of U-87 MG cell line in 2D and 3D, treated (G) and untreated (C).

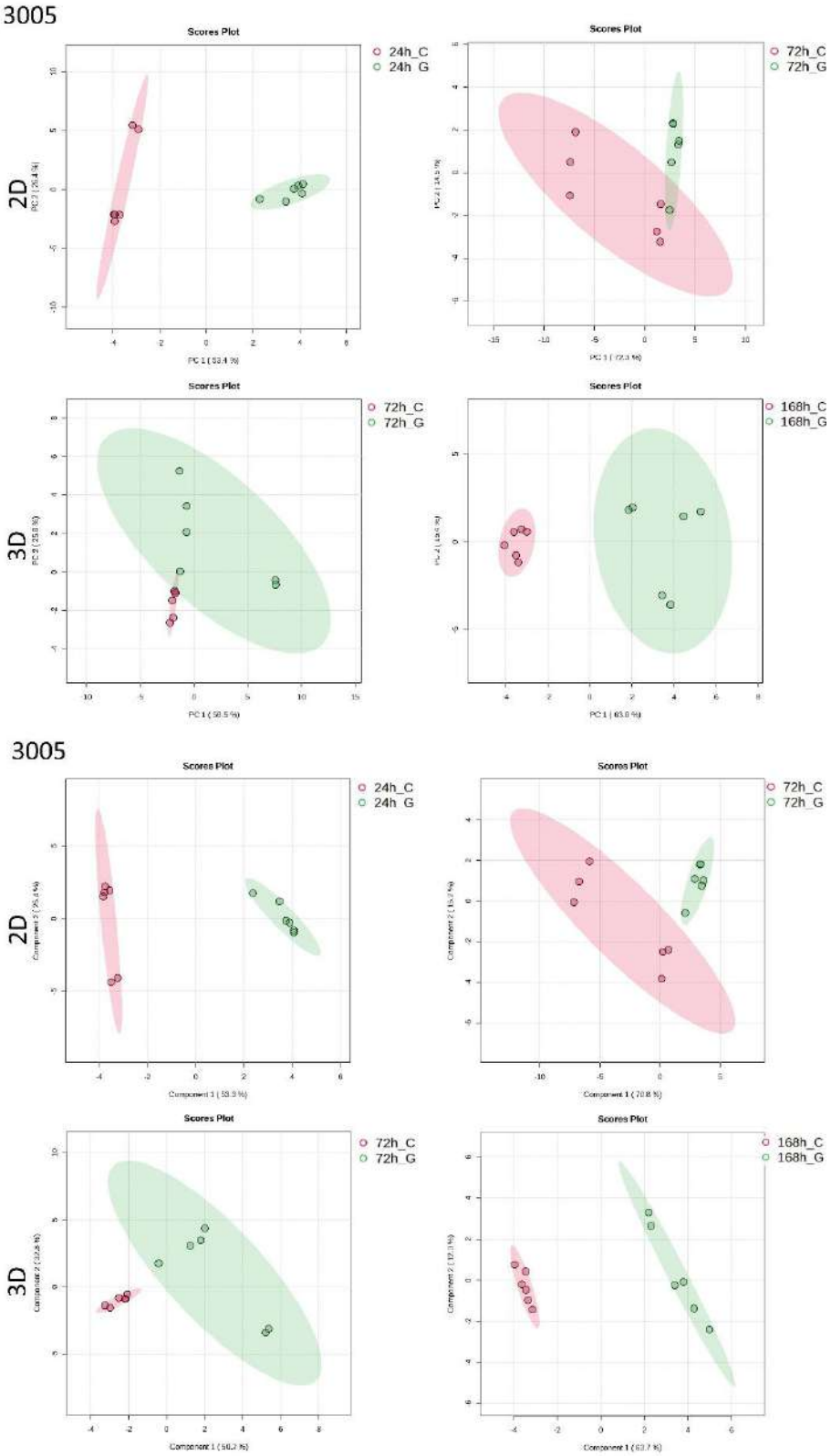

Figutre S5. PCA (top) and PLS-DA scrore plots showing separations of 3005 MG cell line in 2D and 3D, treated (G) and untreated (C).

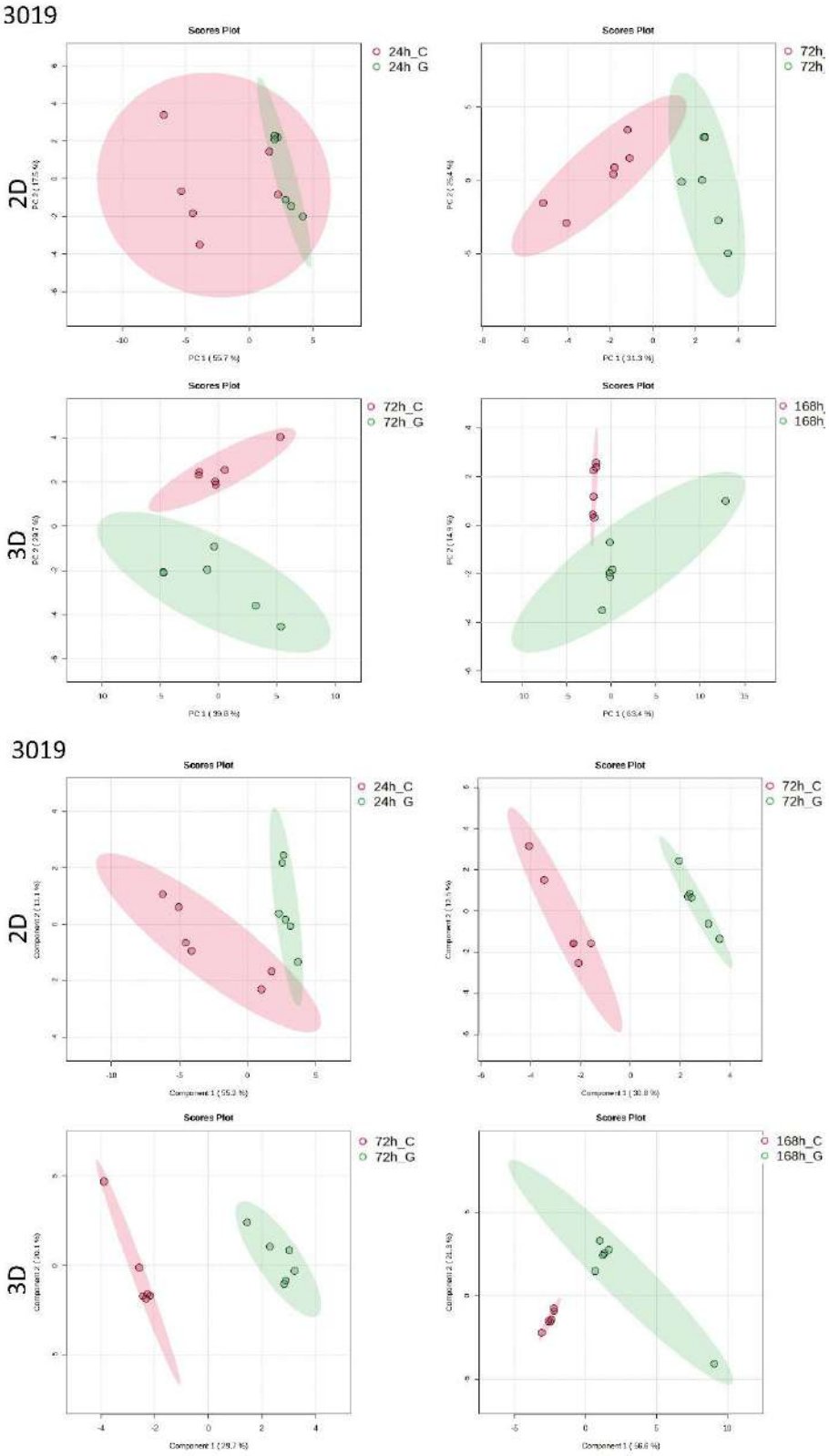

Figutre S6. PCA (top) and PLS-DA scrore plots showing separations of 3019 MG cell line in 2D and 3D, treated (G) and untreated (C).

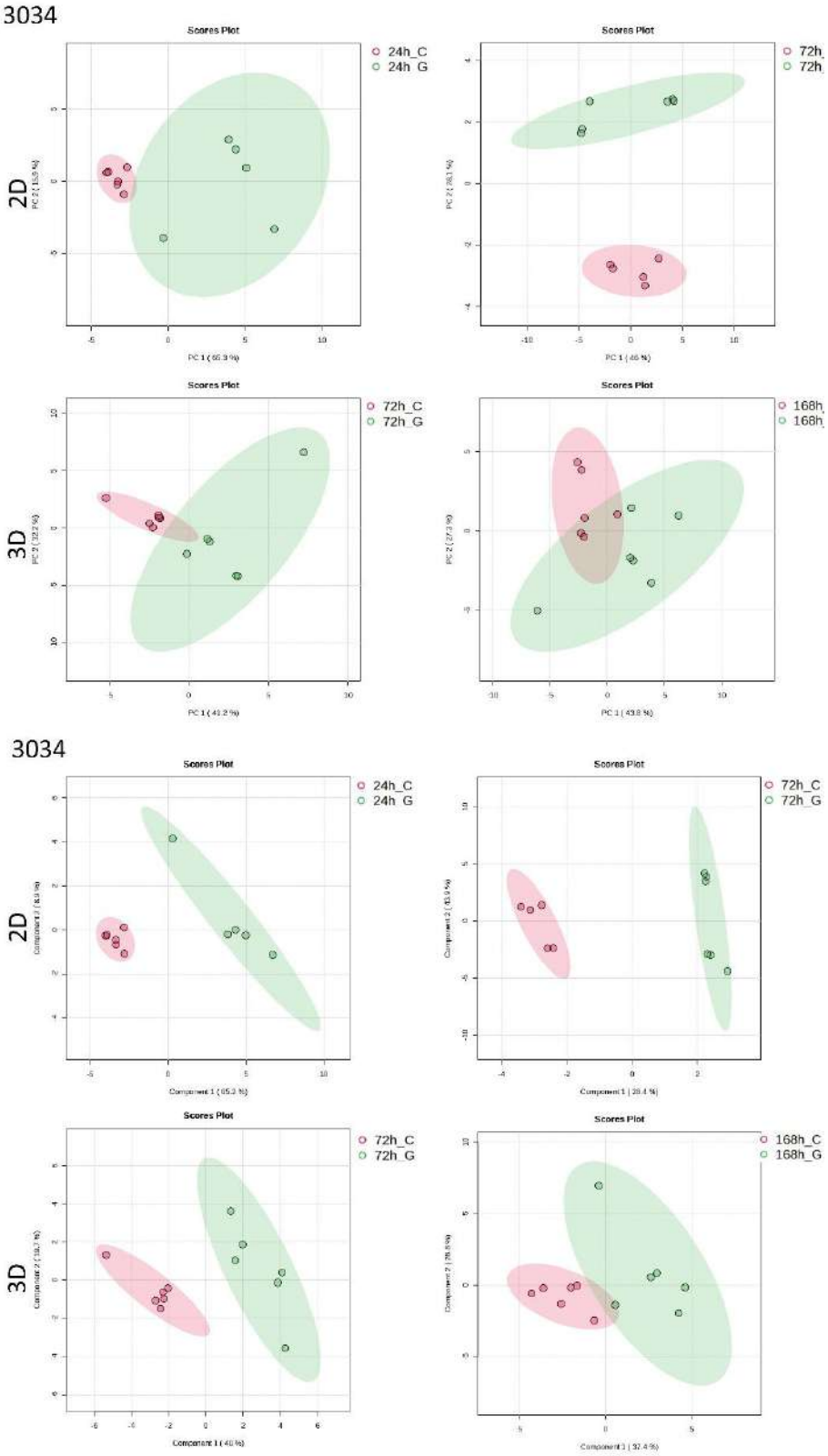

Figutre S7. PCA (top) and PLS-DA scrore plots showing separations of 3034 MG cell line in 2D and 3D, treated (G) and untreated (C).

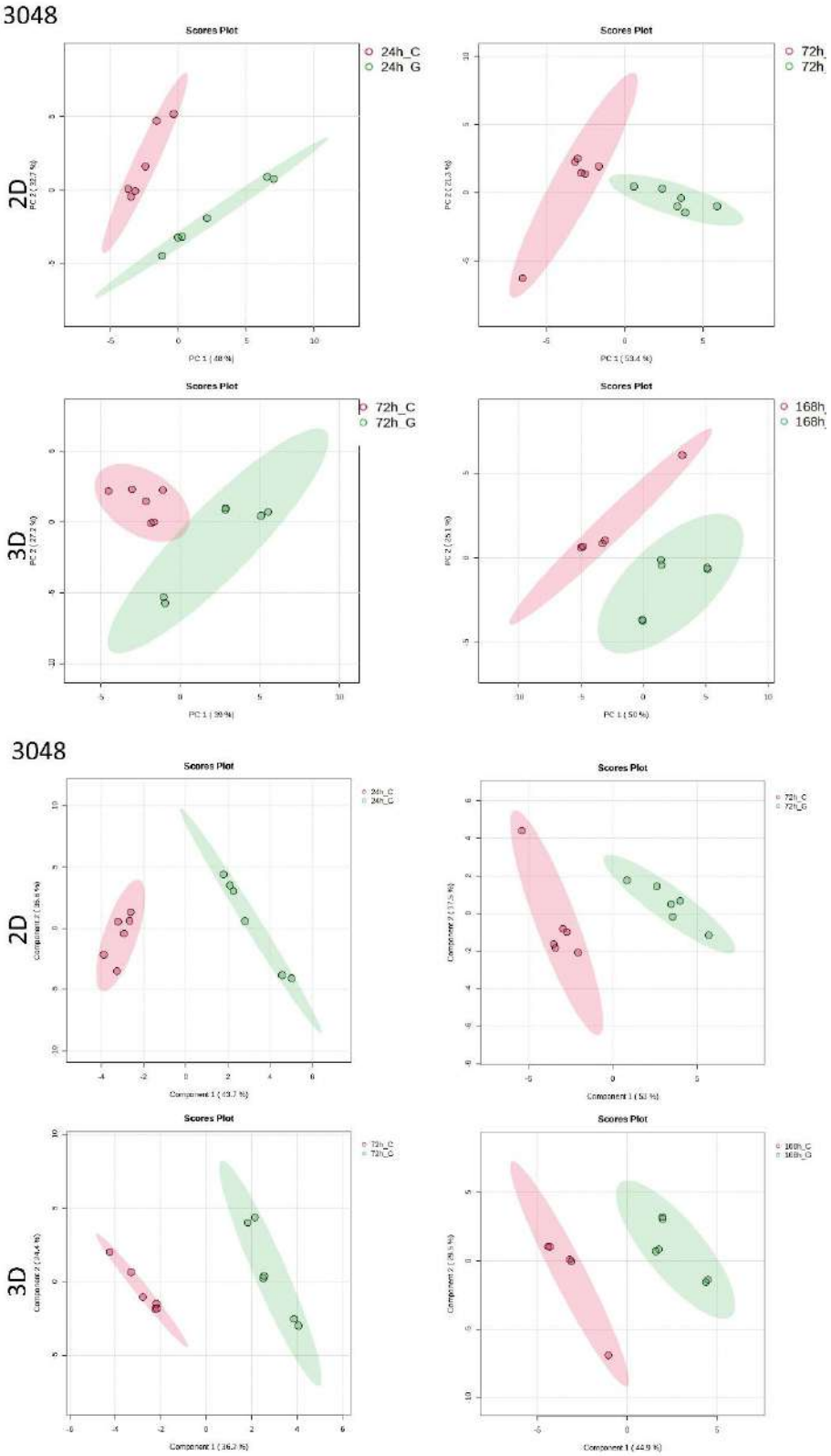

Figutre S8. PCA (top) and PLS-DA scrore plots showing separations of 3048 MG cell line in 2D and 3D, treated (G) and untreated (C).

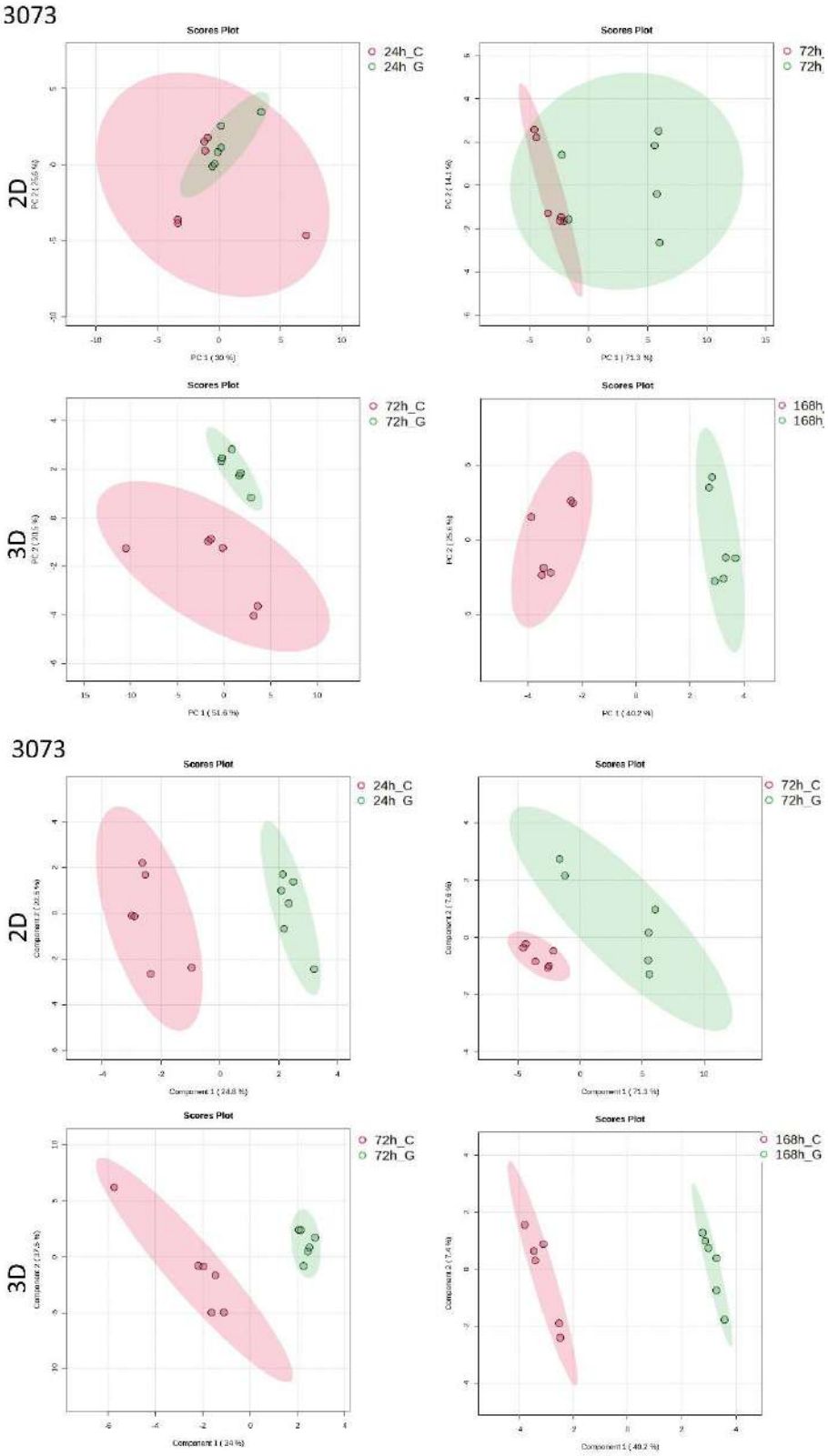

Figutre S9. PCA (top) and PLS-DA scrore plots showing separations of 3073 MG cell line in 2D and 3D, treated (G) and untreated (C).

Table S2. Cross-validated PLS-DA performance across GBM models.

Cell Line	Format	Time	Comparison	Best Components	Accuracy	Q2	R2
3005	2D	24h_72h	2D_24h_72h	4	0.96	0.65474	0.84238
	2D	24h	2D_24h	3	1	0.97996	0.99671
	2D_3D	72h	2D_3D_72h	3	0.70667	0.65796	0.88375
	2D	72h	2D_72h	4	1	0.89178	0.98585
	3D	168h	3D_168h	4	1	0.98378	0.99883
	3D	72h_168h	3D_72h_168h	3	0.79333	0.68473	0.90763
	3D	72h	3D_72h	6	0.95	0.89893	0.99977
3019	2D	24h_72h	2D_24h_72h	2	0.62	0.35086	0.57689
	2D	24h	2D_24h	4	0.8	0.69851	0.94982
	2D_3D	72h	2D_3D_72h	3	0.77143	0.87795	0.92452
	2D	72h	2D_72h	3	1	0.97771	0.99513
	3D	168h	3D_168h	2	1	0.7575	0.96044
	3D	72h_168h	3D_72h_168h	2	0.47333	0.19839	0.53053
	3D	72h	3D_72h	5	1	0.97565	0.99942
3034	2D	24h_72h	2D_24h_72h	3	0.82	0.91722	0.96921
	2D	24h	2D_24h	5	1	0.92275	0.99257
	2D_3D	72h	2D_3D_72h	4	0.82	0.82507	0.94573
	2D	72h	2D_72h	2	0.83333	-0.30939	0.94595
	3D	168h	3D_168h	1	0.9	0.39949	0.71562
	3D	72h_168h	3D_72h_168h	2	0.475	0.76311	0.87437
	3D	72h	3D_72h	3	1	0.90148	0.97777
3048	2D	24h_72h	2D_24h_72h	3	0.73333	0.74137	0.86342
	2D	24h	2D_24h	3	1	0.95536	0.99102
	2D_3D	72h	2D_3D_72h	4	0.93333	0.91498	0.96714
	2D	72h	2D_72h	4	1	0.95217	0.99529
	3D	168h	3D_168h	5	1	0.98214	0.99866
	3D	72h_168h	3D_72h_168h	2	0.56333	0.57985	0.86422
	3D	72h	3D_72h	5	1	0.98625	0.99899
3073	2D	24h_72h	2D_24h_72h	5	0.83	0.80533	0.94726
	2D	24h	2D_24h	5	0.93333	0.81003	0.99811
	2D_3D	72h	2D_3D_72h	4	0.82	0.57748	0.85255
	2D	72h	2D_72h	5	1	0.93482	0.99616
	3D	168h	3D_168h	4	1	0.98378	0.99883
	3D	72h_168h	3D_72h_168h	3	0.88	0.65929	0.87341
	3D	72h	3D_72h	5	1	0.96631	0.99908
A-172	2D	24h	2D_24h	5	1	0.93118	0.99647
	2D_3D	72h	2D_3D_72h	3	0.64	0.49049	0.87458
	2D	72h	2D_72h	4	0.8	0.58358	0.95365
	3D	168h	3D_168h	2	1	0.98727	0.99521
	3D	72h+168h	3D_72h+168h	4	1	0.95995	0.99722

	3D	72h_168h	3D_72h_168h	5	0.96	0.92071	0.97342
	2D	24h_72h	2D_24h_72h	4	0.86	0.76004	0.9672
U-87 MG	2D	24h_72h	2D_24h_72h	4	0.83	0.68205	0.93221
	2D	24h	2D_24h	1	0.95	-0.35231	0.75069
	2D_3D	72h	2D_3D_72h	5	1	0.74933	0.98245
	2D	72h	2D_72h	3	0.83333	0.40482	0.84569
	3D	168h	3D_168h	1	0.9	0.39167	0.69546
	3D	72h_168h	3D_72h_168h	2	0.78	0.91827	0.95246
	3D	72h	3D_72h	5	1	0.98934	0.99951

Table S3. Comprehensive metabolite panel by cell line (3005, 3019, 3034, 3048, 3073, A-172, U-87 MG): VIP, FDR, stars

Cell Line	Format	Time	Condition	Metabolite	VIP	FDR	stars
3005	2D	24h	2D_24h	Allantoin	1.2467	0.008434	**
	3D	168h	3D_168h	Allantoin	1.0036	0.006815	**
	2D	24h	2D_24h	Choline	1.3072	0.008434	**
	3D	168h	3D_168h	Choline	1.1882	0.003968	**
	2D	24h	2D_24h	Cysteine	1.0935	0.006494	**
	2D	72h	2D_72h	Cysteine	1.299	0.011688	*
	3D	168h	3D_168h	Cysteine	1.1649	0.003968	**
	3D	72h	3D_72h	Cysteine	1.5496	0.02381	*
	2D	24h	2D_24h	Glutamicacid	1.0655	0.006494	**
	2D	72h	2D_72h	Glutamine	1.3858	0.011688	*
	3D	168h	3D_168h	Glutamine	1.254	0.003968	**
	3D	72h	3D_72h	Glutamine	1.5778	0.015873	*
	3D	168h	3D_168h	Histidine	1.2612	0.003968	**
	2D	72h	2D_72h	Isoleucine	1.2834	0.011688	*
	2D	24h	2D_24h	Lysine	1.2104	0.006494	**
	3D	168h	3D_168h	Lysine	1.1372	0.003968	**
	2D	72h	2D_72h	Methionine	1.1695	0.02904	*
	3D	168h	3D_168h	Methionine	1.09	0.003968	**
	2D	24h	2D_24h	Niacinamide	1.1203	0.008434	**
	2D	72h	2D_72h	Niacinamide	1.3112	0.014994	*
	3D	168h	3D_168h	Niacinamide	1.0173	0.003968	**
	3D	72h	3D_72h	Niacinamide	1.6055	0.015873	*
	3D	72h	3D_72h	Ornithine	1.4831	0.031746	*
	2D	24h	2D_24h	Phenylalanine	1.1686	0.006494	**
	2D	72h	2D_72h	Phenylalanine	1.2333	0.011688	*
	3D	168h	3D_168h	Phenylalanine	1.2398	0.003968	**
	2D	24h	2D_24h	Proline	1.3449	0.006494	**
	3D	168h	3D_168h	Proline	1.1253	0.003968	**
	2D	72h	2D_72h	Serine	1.126	0.025213	*
	3D	168h	3D_168h	Serine	1.0912	0.003968	**
	2D	24h	2D_24h	Threonine	1.0547	0.013751	*
	2D	24h	2D_24h	Tryptophan	1.258	0.008434	**
	2D	72h	2D_72h	Tryptophan	1.2273	0.014994	*
	3D	168h	3D_168h	Tryptophan	1.0225	0.006815	**
	2D	24h	2D_24h	Tyrosine	1.2133	0.006494	**
	2D	72h	2D_72h	Tyrosine	1.0667	0.023377	*
	2D	24h	2D_24h	Uracil	1.2965	0.008434	**
	2D	72h	2D_72h	Uracil	1.3756	0.011688	*
	3D	168h	3D_168h	Uracil	1.2685	0.003968	**

	3D	72h	3D_72h	Uracil	1.4161	0.015873	*
	2D	24h	2D_24h	Valine	1.2714	0.006494	**
3019	2D	72h	2D_72h	Allantoin	1.1145	0.019481	*
	3D	72h	3D_72h	Allantoin	1.0505	0.01461	*
	3D	72h	3D_72h	Glutamicacid	1.3095	0.019481	*
	3D	72h	3D_72h	Histidine	1.5642	0.01461	*
	2D	24h	2D_24h	Lysine	1.3021	0.040909	*
	3D	168h	3D_168h	Lysine	1.0544	0.007305	**
	2D	24h	2D_24h	Methionine	1.4629	0.011688	*
	3D	168h	3D_168h	Methionine	1.5066	0.007305	**
	2D	24h	2D_24h	Niacinamide	1.3656	0.027053	*
	2D	24h	2D_24h	Ornithine	1.3793	0.040909	*
	2D	24h	2D_24h	Proline	1.4157	0.019278	*
	3D	168h	3D_168h	Serine	1.0485	0.007305	**
	2D	72h	2D_72h	Tryptophan	1.631	0.02699	*
	2D	24h	2D_24h	Tyrosine	1.3967	0.011688	*
	3D	168h	3D_168h	Tyrosine	1.4581	0.007305	**
	2D	24h	2D_24h	Uracil	1.5132	0.011688	*
	2D	72h	2D_72h	Uracil	1.8454	0.02699	*
	3D	72h	3D_72h	Uracil	1.8903	0.01461	*
	2D	24h	2D_24h	Valine	1.3542	0.011688	*
3034	2D	24h	2D_24h	Adenosine	1.1594	0.011688	*
	3D	72h	3D_72h	Allantoin	1.6015	0.00974	**
	2D	24h	2D_24h	Glutamicacid	1.1628	0.011688	*
	3D	72h	3D_72h	Glutamine	1.4951	0.00974	**
	2D	24h	2D_24h	Histidine	1.3424	0.011688	*
	2D	24h	2D_24h	Leucine	1.2506	0.011688	*
	2D	24h	2D_24h	Lysine	1.191	0.011688	*
	3D	72h	3D_72h	Methionine	1.5239	0.00974	**
	3D	72h	3D_72h	Niacinamide	1.4326	0.00974	**
	2D	24h	2D_24h	Proline	1.2001	0.019481	*
	2D	24h	2D_24h	Tryptophan	1.2562	0.011688	*
	3D	168h	3D_168h	Tryptophan	1.3983	0.044983	*
	3D	72h	3D_72h	Tryptophan	1.2669	0.033395	*
	3D	168h	3D_168h	Tyrosine	1.6383	0.044983	*
	2D	24h	2D_24h	Uracil	1.2789	0.011688	*
	2D	72h	2D_72h	Uracil	1.8786	0.029221	*
	3D	72h	3D_72h	Uracil	1.6662	0.00974	**
	2D	24h	2D_24h	Valine	1.1976	0.011688	*
3048	2D	24h	2D_24h	Allantoin	1.3721	0.007305	**
	2D	72h	2D_72h	Allantoin	1.2524	0.008349	**
	3D	168h	3D_168h	Allantoin	1.6831	0.015004	*
	2D	24h	2D_24h	Cysteine	1.0207	0.007305	**

	2D	72h	2D_72h	Glutamicacid	1.1458	0.005313	**
	2D	72h	2D_72h	Glutamine	1.3019	0.008245	**
	3D	72h	3D_72h	Glutamine	1.5045	0.00974	**
	2D	24h	2D_24h	Histidine	1.2581	0.007305	**
	2D	24h	2D_24h	Isoleucine	1.1973	0.007305	**
	2D	72h	2D_72h	Isoleucine	1.2135	0.008349	**
	2D	24h	2D_24h	Leucine	1.1596	0.023377	*
	2D	72h	2D_72h	Leucine	1.0581	0.005313	**
	3D	168h	3D_168h	Leucine	1.3655	0.033395	*
	2D	72h	2D_72h	Lysine	1.3763	0.005313	**
	2D	72h	2D_72h	Methionine	1.4176	0.005313	**
	3D	168h	3D_168h	Methionine	1.4213	0.01461	*
	3D	72h	3D_72h	Niacinamide	1.4832	0.00974	**
	3D	168h	3D_168h	Ornithine	1.2558	0.033395	*
	2D	72h	2D_72h	Proline	1.237	0.005313	**
	3D	72h	3D_72h	Proline	1.211	0.045455	*
	2D	24h	2D_24h	Serine	1.381	0.007305	**
	2D	72h	2D_72h	Serine	1.2242	0.005313	**
	2D	72h	2D_72h	Tryptophan	1.3436	0.005313	**
	3D	168h	3D_168h	Tryptophan	1.2142	0.01461	*
	3D	72h	3D_72h	Tryptophan	1.3644	0.00974	**
	2D	24h	2D_24h	Tyrosine	1.3969	0.007305	**
	3D	72h	3D_72h	Tyrosine	1.273	0.00974	**
	2D	72h	2D_72h	Uracil	1.2202	0.005313	**
	3D	168h	3D_168h	Uracil	1.4293	0.01461	*
	3D	72h	3D_72h	Uracil	1.6387	0.00974	**
	2D	24h	2D_24h	Valine	1.3179	0.007305	**
	3D	168h	3D_168h	Valine	1.4871	0.01461	*
	3D	72h	3D_72h	Valine	1.2804	0.045455	*
3073	3D	168h	3D_168h	Adenosine	1.0458	0.046753	*
	3D	168h	3D_168h	Allantoin	1.1043	0.034091	*
	3D	72h	3D_72h	Allantoin	1.6839	0.03221	*
	2D	72h	2D_72h	Cysteine	1.1962	0.021251	*
	3D	168h	3D_168h	Cysteine	1.4669	0.008349	**
	2D	24h	2D_24h	Glutamine	1.4927	0.029221	*
	2D	72h	2D_72h	Glutamine	1.1767	0.021251	*
	3D	168h	3D_168h	Histidine	1.5285	0.008349	**
	2D	72h	2D_72h	Isoleucine	1.2023	0.008349	**
	3D	168h	3D_168h	Isoleucine	1.1648	0.012987	*
	3D	168h	3D_168h	Lysine	1.412	0.008349	**
	2D	72h	2D_72h	Methionine	1.1904	0.008349	**
	3D	72h	3D_72h	Methionine	1.3647	0.046753	*
	2D	72h	2D_72h	Niacinamide	1.3236	0.008349	**

	2D	72h	2D_72h	Phenylalanine	1.1759	0.008349	**
	3D	168h	3D_168h	Phenylalanine	1.5349	0.008349	**
	2D	24h	2D_24h	Proline	1.8999	0.029221	*
	3D	168h	3D_168h	Proline	1.0172	0.046753	*
	2D	72h	2D_72h	Serine	1.2129	0.01461	*
	3D	168h	3D_168h	Serine	1.3256	0.008349	**
	2D	72h	2D_72h	Threonine	1.188	0.021251	*
	3D	168h	3D_168h	Threonine	1.2329	0.008349	**
	2D	72h	2D_72h	Tryptophan	1.2397	0.008349	**
	3D	168h	3D_168h	Tryptophan	1.1327	0.046753	*
	3D	72h	3D_72h	Tryptophan	1.688	0.029221	*
	2D	72h	2D_72h	Uracil	1.4124	0.008349	**
	3D	168h	3D_168h	Uracil	1.2753	0.023377	*
	3D	72h	3D_72h	Uracil	1.7576	0.029221	*
	2D	24h	2D_24h	Valine	1.6083	0.029221	*
	3D	168h	3D_168h	Valine	1.2935	0.012987	*
	3D	72h	3D_72h	Valine	1.6379	0.03221	*
A-172	2D	24h	2D_24h	Allantoin	1.8205	0.012987	*
	3D	168h	3D_168h	Allantoin	1.4139	0.006251	**
	3D	72h	3D_72h	Allantoin	1.6185	0.008349	**
	3D	168h	3D_168h	Cysteine	1.2199	0.005313	**
	3D	72h	3D_72h	Cysteine	1.2619	0.008349	**
	3D	168h	3D_168h	Glutamine	1.3853	0.005313	**
	3D	168h	3D_168h	Histidine	1.1009	0.005313	**
	3D	168h	3D_168h	Leucine	1.2151	0.005313	**
	3D	168h	3D_168h	Lysine	1.3021	0.005313	**
	3D	72h	3D_72h	Lysine	1.4465	0.008349	**
	3D	168h	3D_168h	Methionine	1.2729	0.005313	**
	3D	72h	3D_72h	Methionine	1.3674	0.008349	**
	3D	168h	3D_168h	Niacinamide	1.0925	0.005313	**
	2D	24h	2D_24h	Ornithine	1.4682	0.012987	*
	3D	168h	3D_168h	Ornithine	1.0044	0.016698	*
	3D	72h	3D_72h	Ornithine	1.4309	0.008349	**
	3D	168h	3D_168h	Phenylalanine	1.3361	0.005313	**
	3D	168h	3D_168h	Serine	1.266	0.005313	**
	3D	72h	3D_72h	Serine	1.2128	0.008349	**
	2D	24h	2D_24h	Tryptophan	1.6864	0.012987	*
	3D	168h	3D_168h	Tyrosine	1.1438	0.008991	**
	2D	24h	2D_24h	Uracil	1.6579	0.012987	*
	3D	168h	3D_168h	Uracil	1.4003	0.005313	**
	3D	72h	3D_72h	Uracil	1.6082	0.008349	**
U87MG	3D	72h	3D_72h	Adenosine	1.2438	0.005313	**
	3D	72h	3D_72h	Allantoin	1.4314	0.006251	**

	3D	72h	3D_72h	Choline	1.1484	0.005313	**
	3D	72h	3D_72h	Glutamicacid	1.2518	0.005313	**
	3D	72h	3D_72h	Histidine	1.1785	0.005313	**
	3D	168h	3D_168h	Methionine	1.1634	0.046753	*
	3D	72h	3D_72h	Methionine	1.3087	0.005313	**
	3D	168h	3D_168h	Niacinamide	1.5357	0.029221	*
	3D	168h	3D_168h	Proline	1.5211	0.029221	*
	3D	72h	3D_72h	Serine	1.1842	0.005313	**
	3D	72h	3D_72h	Tryptophan	1.1085	0.005313	**
	3D	72h	3D_72h	Tyrosine	1.0347	0.027273	*
	3D	168h	3D_168h	Uracil	1.24	0.029221	*
	3D	72h	3D_72h	Uracil	1.4291	0.005313	**
	3D	168h	3D_168h	Valine	1.3233	0.029221	*

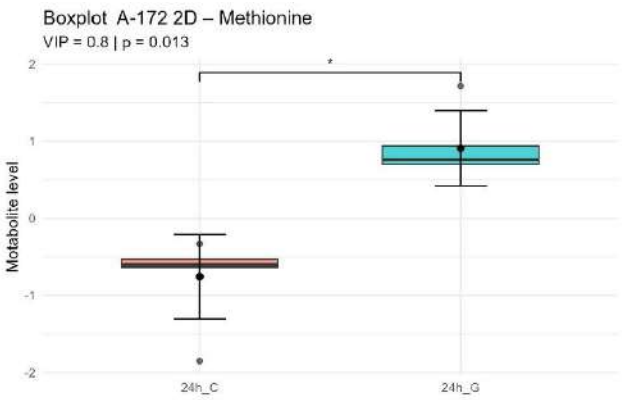
Boxplot A-172 2D – Methionine
VIP = 0.8 | p = 0.013
*
Motabolite level
24h_C
24h_G

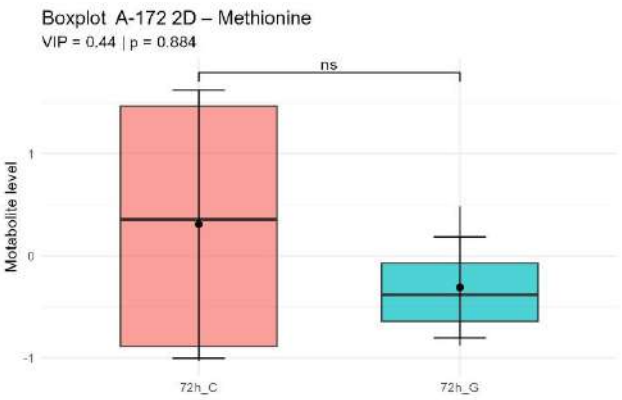
Boxplot A-172 2D – Methionine
VIP = 0.44 | p = 0.884
ns
Motabolite level
72h_C
72h_G

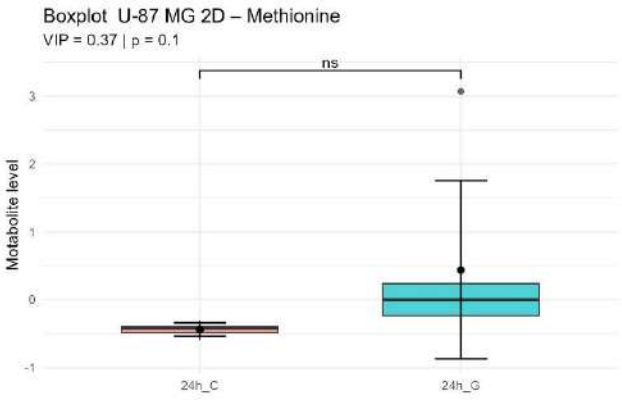
Boxplot U-87 MG 2D – Methionine
VIP = 0.37 | p = 0.1
ns
Motabolite level
24h_C
24h_G

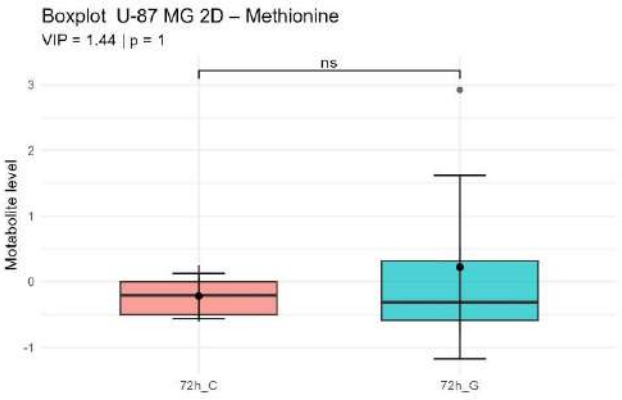
Boxplot U-87 MG 2D – Methionine
VIP = 1.44 | p = 1
ns
Motabolite level
72h_C
72h_G

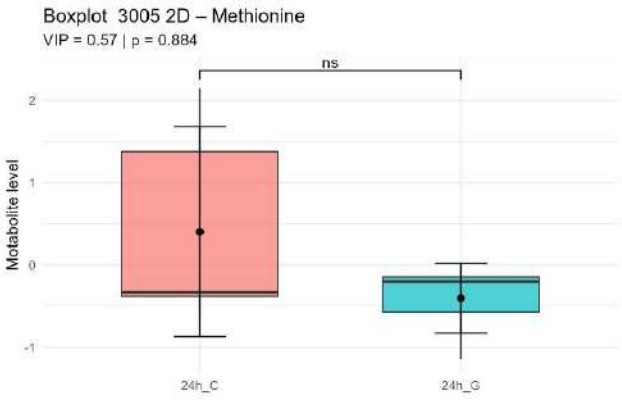
Boxplot 3005 2D – Methionine
VIP = 0.57 | p = 0.884
ns
Motabolite level
24h_C
24h_G

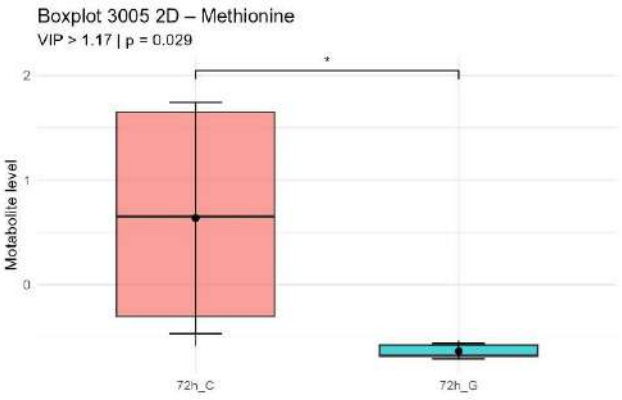
Boxplot 3005 2D – Methionine
VIP > 1.17 | p = 0.029
*
Motabolite level
72h_C
72h_G

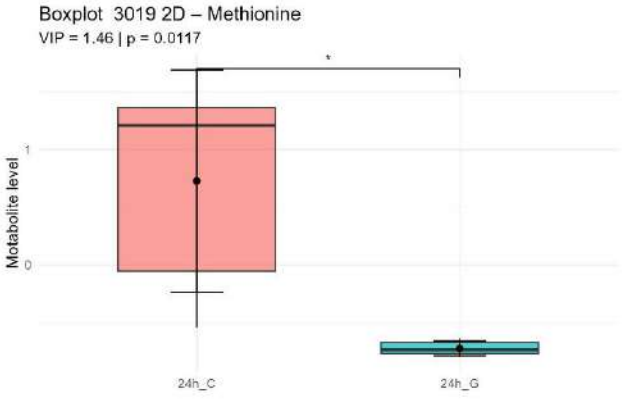
Boxplot 3019 2D – Methionine
VIP = 1.46 | p = 0.0117
*
Motabolite level
24h_C
24h_G

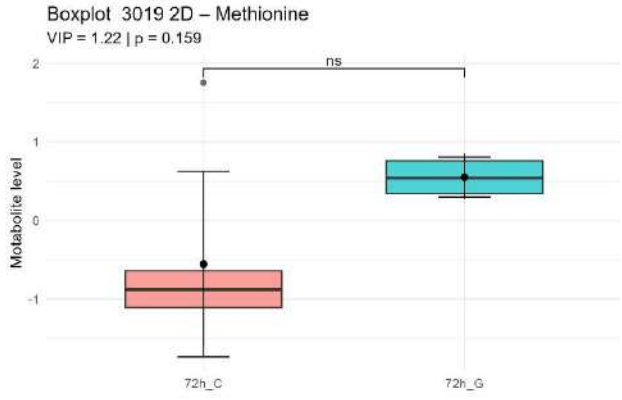
Boxplot 3019 2D – Methionine
VIP = 1.22 | p = 0.159
ns
Motabolite level
72h_C
72h_G

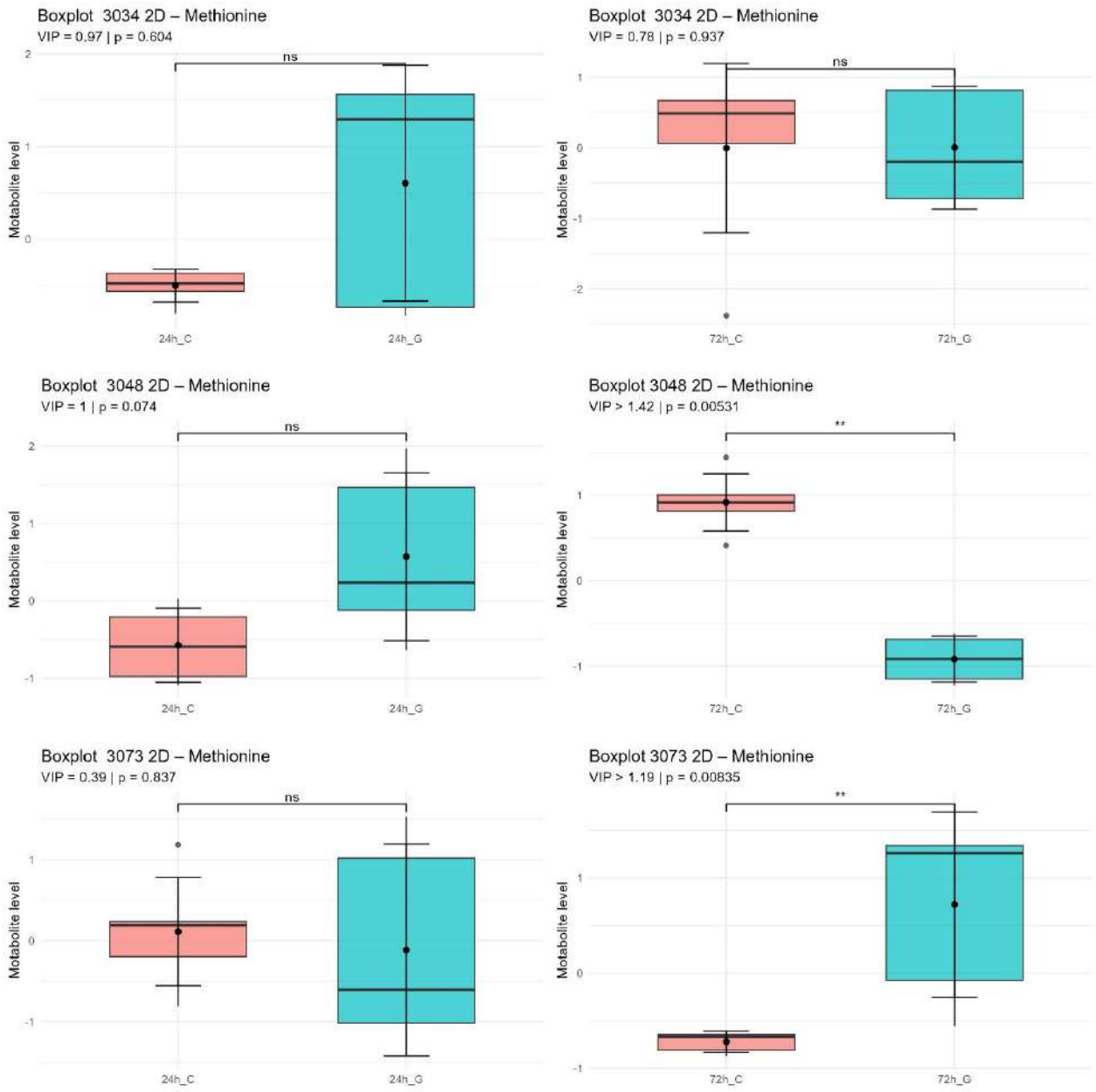

Figure S10. Change in levels of methionine between GaM treated cells and untreated control in 2D culture with VIP score and p-value (FDR).

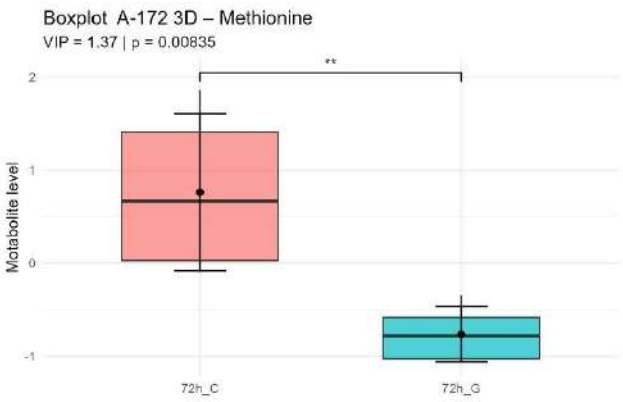
Boxplot A-172 3D – Methionine
VIP = 1.37 | p = 0.00835
**
Motabolite level
72h_C
72h_G

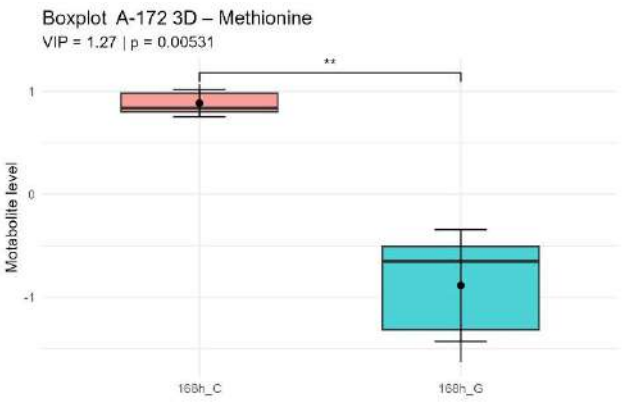
Boxplot A-172 3D – Methionine
VIP = 1.27 | p = 0.00531
**
Motabolite level
168h_C
168h_G

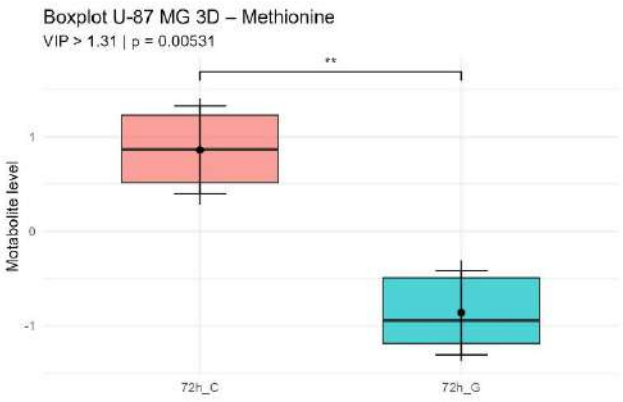
Boxplot U-87 MG 3D – Methionine
VIP > 1.31 | p = 0.00531
**
Motabolite level
72h_C
72h_G

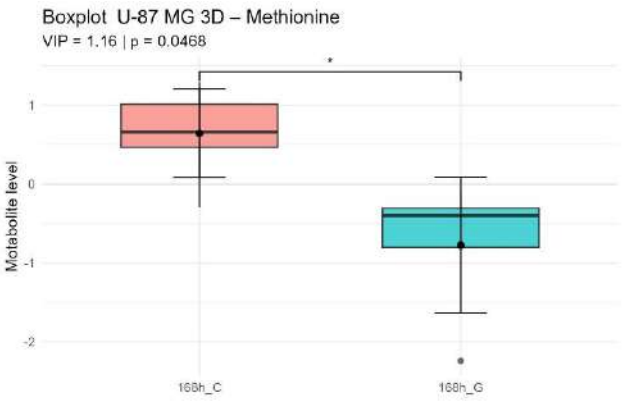
Boxplot U-87 MG 3D – Methionine
VIP = 1.16 | p = 0.0468
*
Motabolite level
168h_C
168h_G

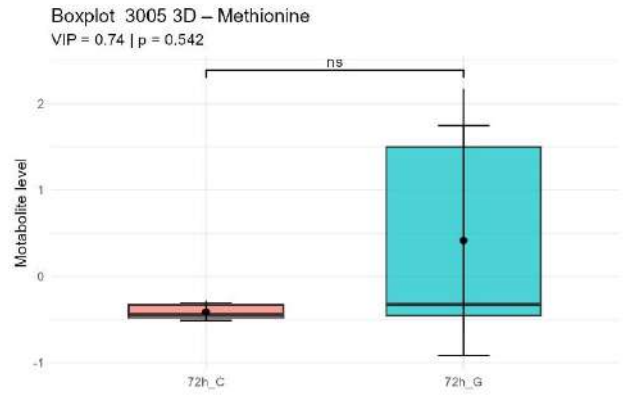
Boxplot 3005 3D – Methionine
VIP = 0.74 | p = 0.542
ns
Motabolite level
72h_C
72h_G

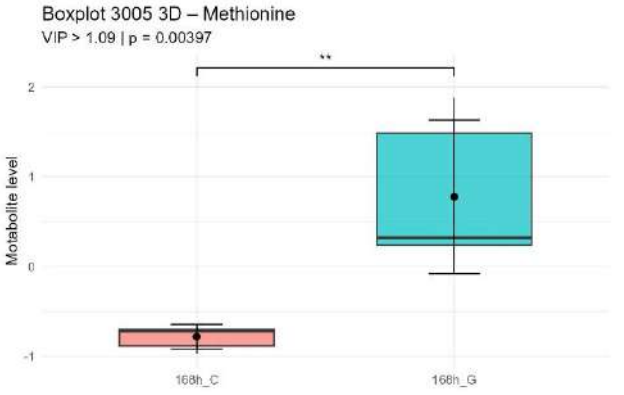
Boxplot 3005 3D – Methionine
VIP > 1.09 | p = 0.00397
**
Motabolite level
168h_C
168h_G

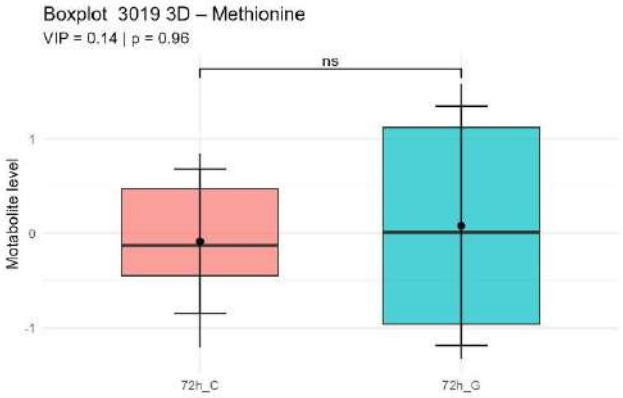
Boxplot 3019 3D – Methionine
VIP = 0.14 | p = 0.96
ns
Motabolite level
72h_C
72h_G

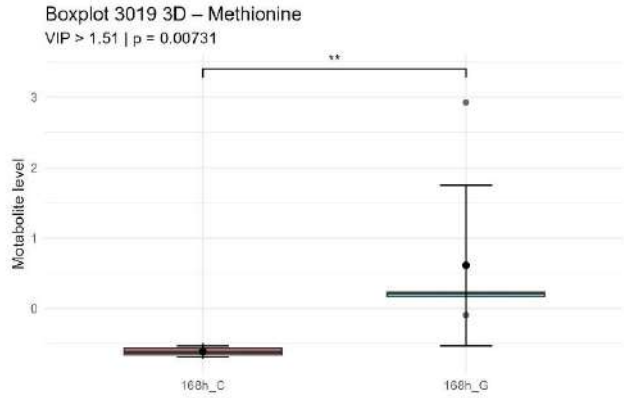
Boxplot 3019 3D – Methionine
VIP > 1.51 | p = 0.00731
**
Motabolite level
168h_C
168h_G

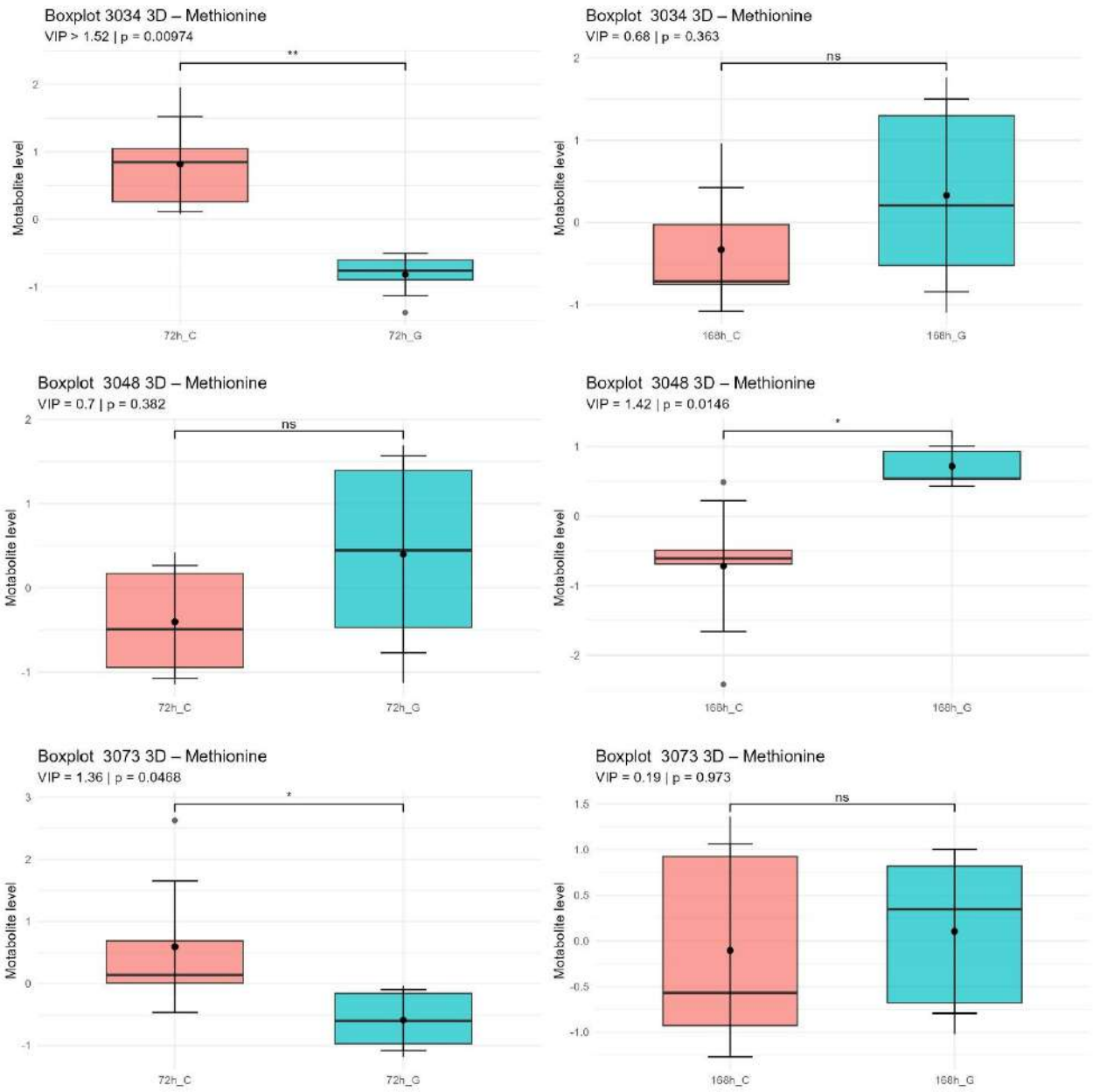

Figure S11. Change in levels of methionine between GaM treated cells and untreated control in 3D culture with VIP score and p-value (FDR).

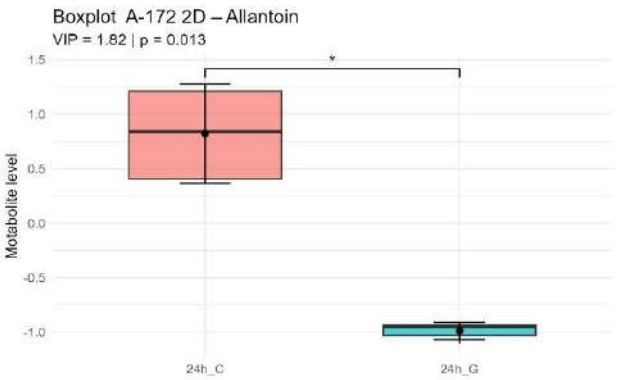
Boxplot A-172 2D – Allantoin
VIP = 1.82 | p = 0.013
*
Motabolite level
1.5
1.0
0.5
0.0
-0.5
-1.0
24h_C
24h_G

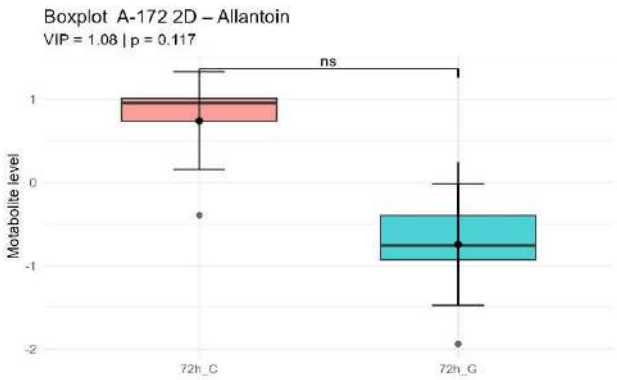
Boxplot A-172 2D – Allantoin
VIP = 1.08 | p = 0.117
ns
Motabolite level
1
0
-1
-2
72h_C
72h_G

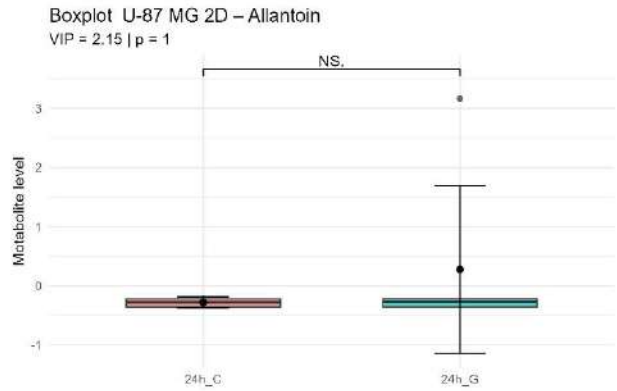
Boxplot U-87 MG 2D – Allantoin
VIP = 2.15 | p = 1
NS.
Motabolite level
3
2
1
0
-1
24h_C
24h_G

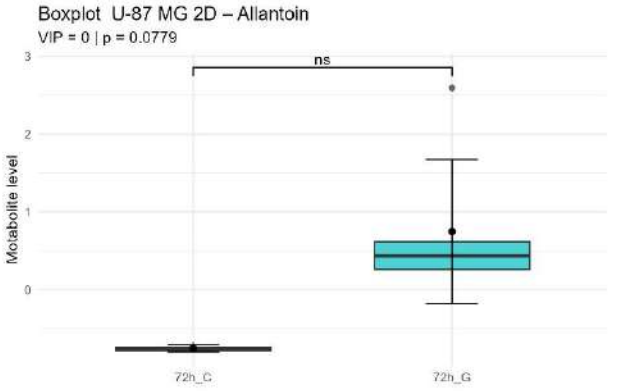
Boxplot U-87 MG 2D – Allantoin
VIP = 0 | p = 0.0779
ns
Motabolite level
3
2
1
0
72h_C
72h_G

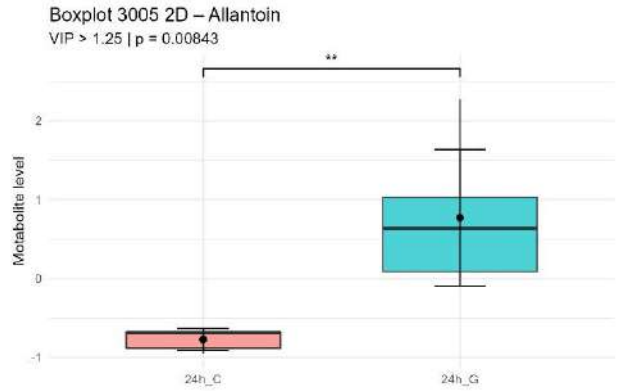
Boxplot 3005 2D – Allantoin
VIP > 1.25 | p = 0.00843
**
Motabolite level
2
1
0
-1
24h_C
24h_G

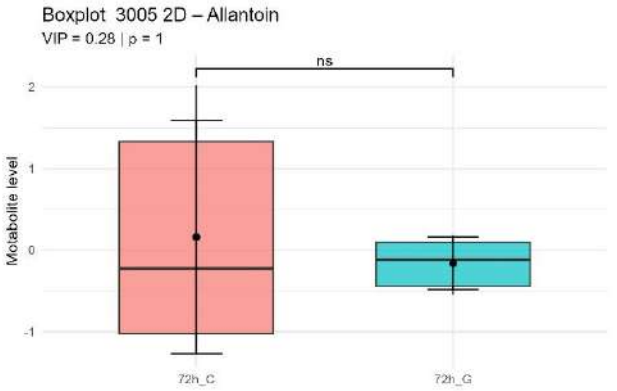
Boxplot 3005 2D – Allantoin
VIP = 0.28 | p = 1
ns
Motabolite level
2
1
0
-1
72h_C
72h_G

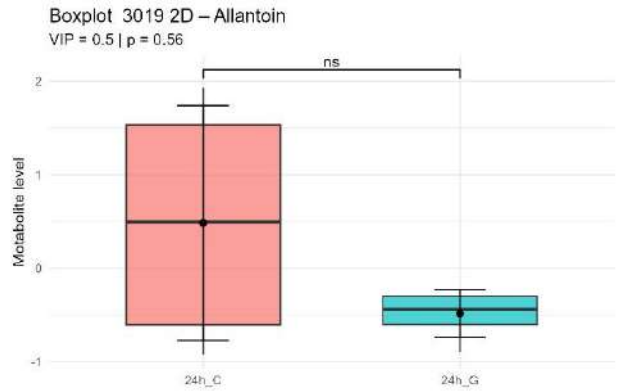
Boxplot 3019 2D – Allantoin
VIP = 0.5 | p = 0.56
ns
Motabolite level
2
1
0
-1
24h_C
24h_G

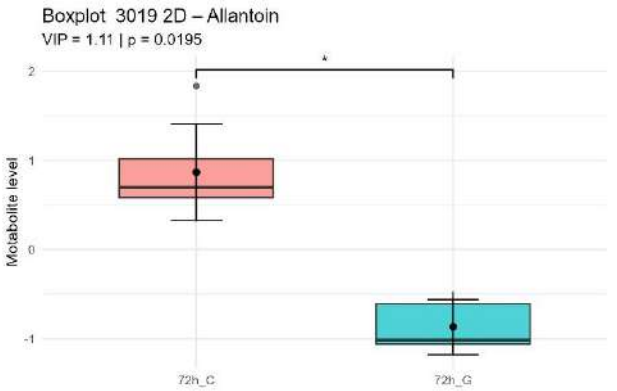
Boxplot 3019 2D – Allantoin
VIP = 1.11 | p = 0.0195
*
Motabolite level
2
1
0
-1
72h_C
72h_G

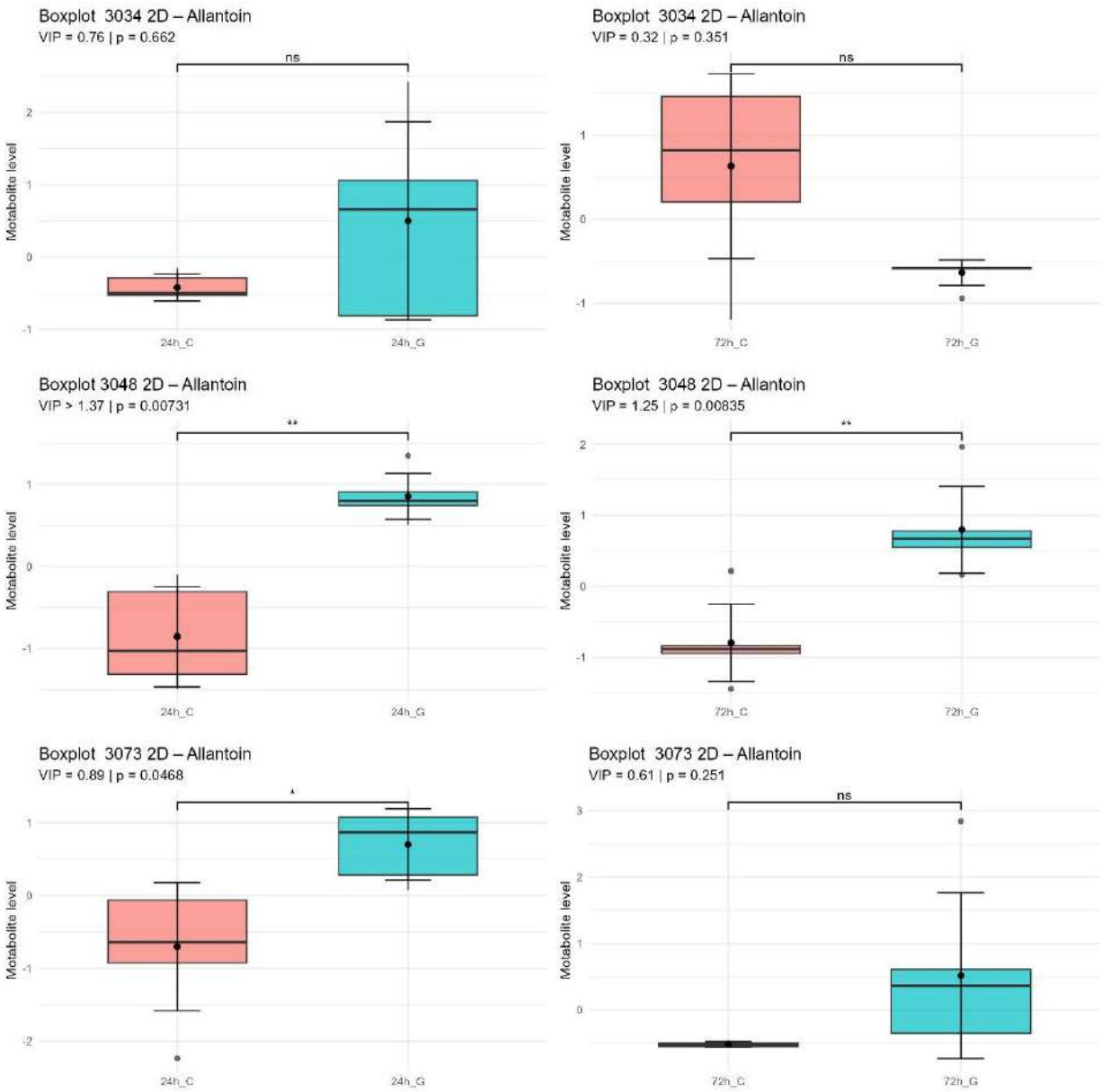

Figure S12. Change in levels of allatoin between GaM treated cells and untreated control in 2D culture with VIP score and p-value (FDR).

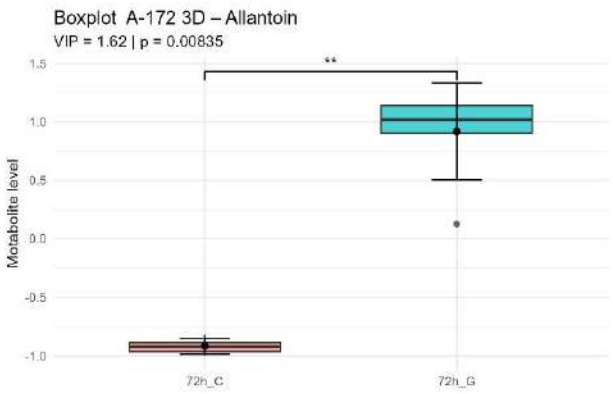
Boxplot A-172 3D – Allantoin
VIP = 1.62 | p = 0.00835
**
Motabolite level
72h_C
72h_G

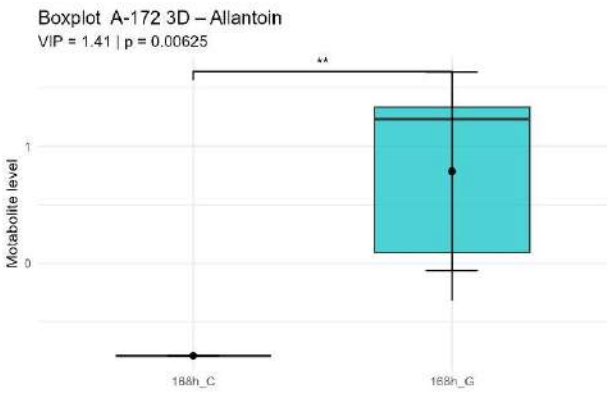
Boxplot A-172 3D – Allantoin
VIP = 1.41 | p = 0.00625
**
Motabolite level
168h_C
168h_G

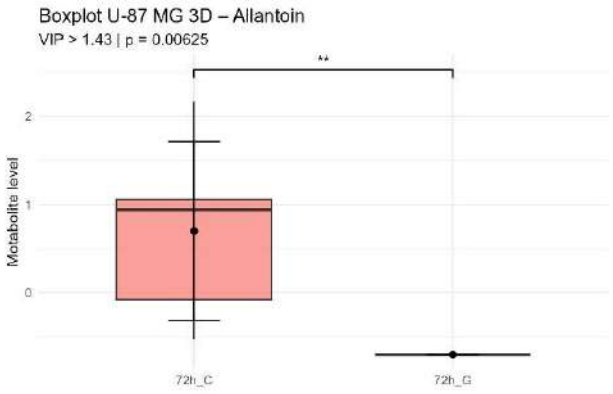
Boxplot U-87 MG 3D – Allantoin
VIP > 1.43 | p = 0.00625
**
Motabolite level
72h_C
72h_G

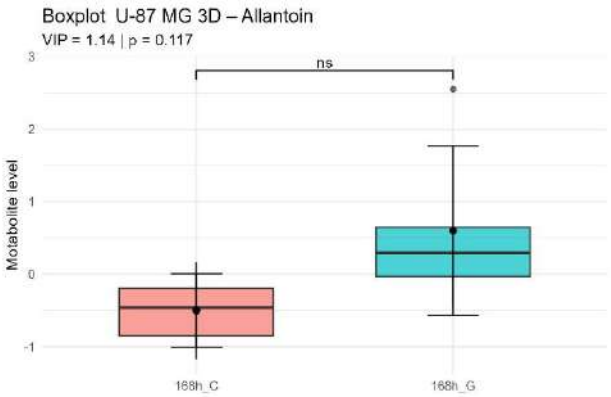
Boxplot U-87 MG 3D – Allantoin
VIP = 1.14 | p = 0.117
ns
Motabolite level
168h_C
168h_G

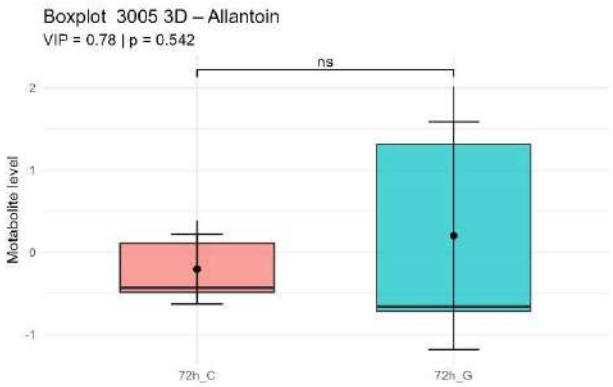
Boxplot 3005 3D – Allantoin
VIP = 0.78 | p = 0.542
ns
Motabolite level
72h_C
72h_G

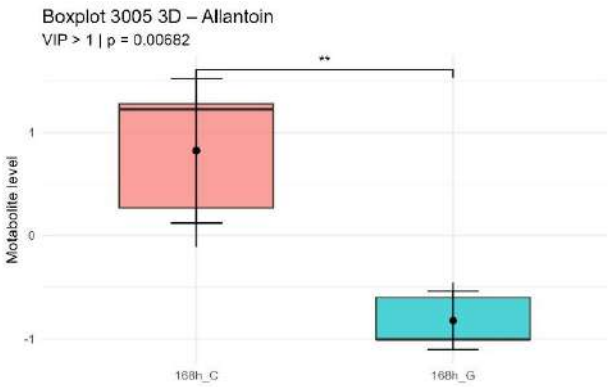
Boxplot 3005 3D – Allantoin
VIP > 1 | p = 0.00682
**
Motabolite level
168h_C
168h_G

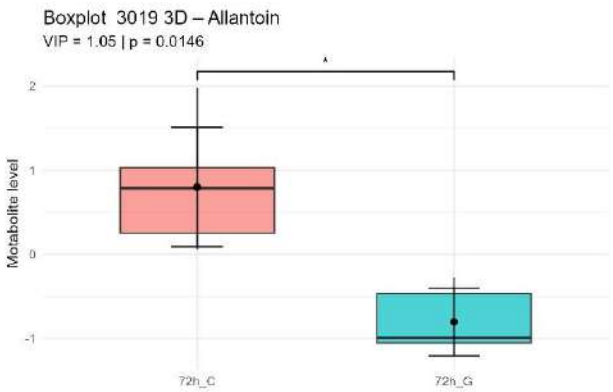
Boxplot 3019 3D – Allantoin
VIP = 1.05 | p = 0.0146
*
Motabolite level
72h_C
72h_G

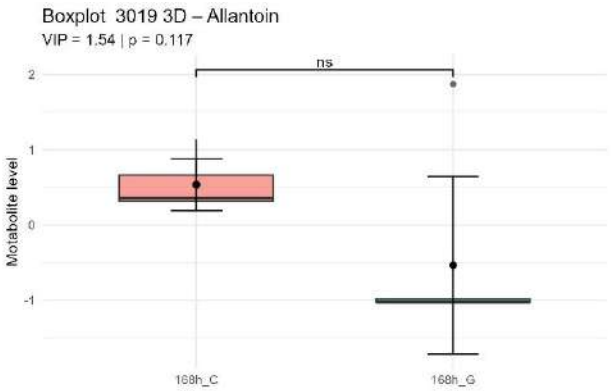
Boxplot 3019 3D – Allantoin
VIP = 1.54 | p = 0.117
ns
Motabolite level
168h_C
168h_G

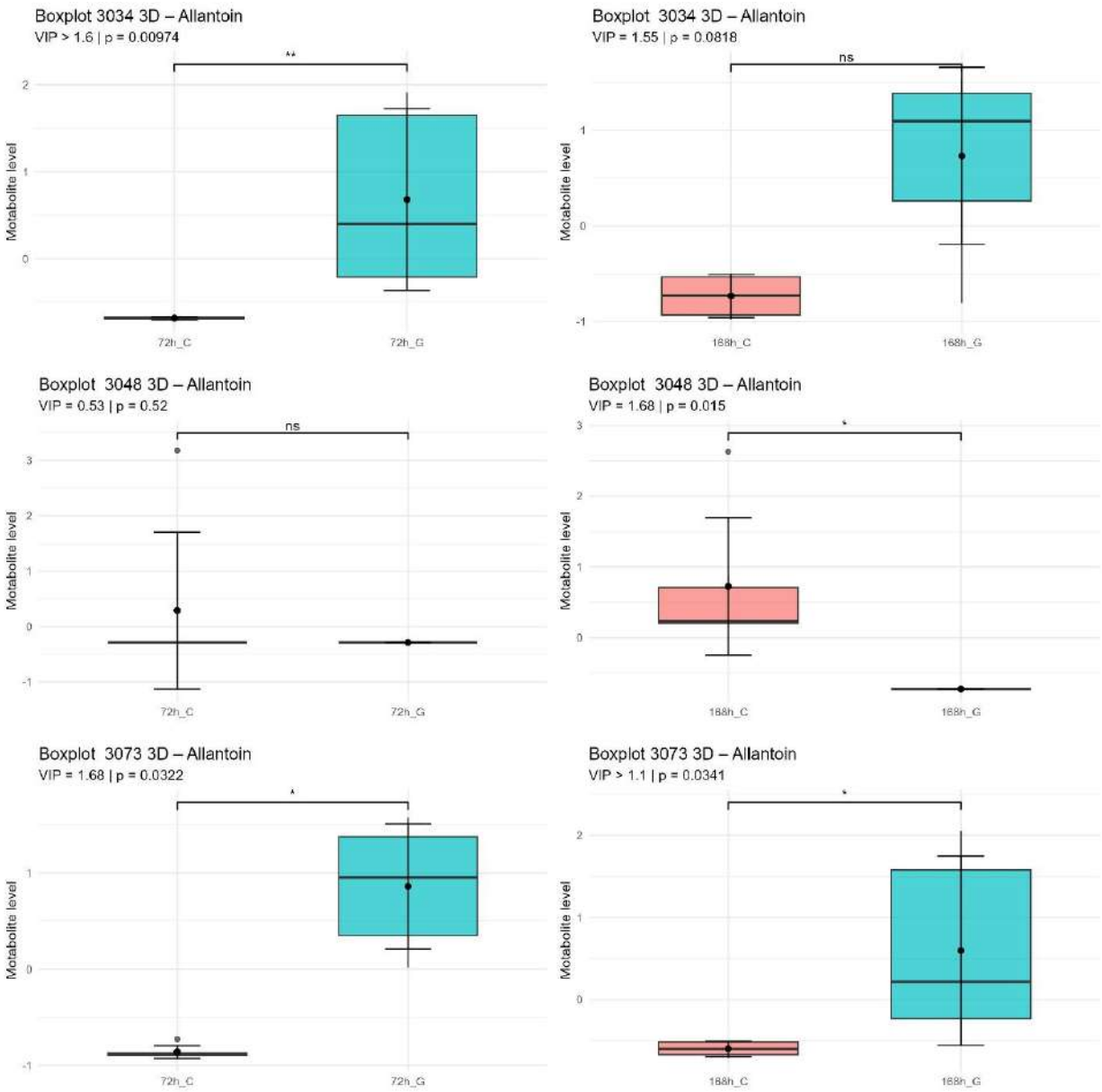

Figure S13. Change in levels of allatoin between GaM treated cells and untreated control in 3D culture with VIP score and p-value (FDR).

Code for R:

Code S1. Dose-response curve with IC90, IC50 and IC10 calculations

```
library(tidyverse)
library(drc)
library(stringr)
df_long <- df_raw %>%
  pivot_longer(cols = everything(), names_to = "Concentration", values_to = "Absorbance") %>%
  mutate(Concentration = str_remove(Concentration, "^X")) %>%
  mutate(Concentration = as.numeric(Concentration))
df_clean <- df_long %>%
  group_by(Concentration) %>%
  mutate(
    mean_abs = mean(Absorbance, na.rm = TRUE),
    sd_abs = sd(Absorbance, na.rm = TRUE),
    rel_sd = (sd_abs / mean_abs) * 100
  ) %>%
  filter(rel_sd <= 15 | abs(Absorbance - mean_abs) <= 1.5 * sd_abs) %>%
  ungroup()
df_summary <- df_clean %>%
  group_by(Concentration) %>%
  summarise(
    mean_abs = mean(Absorbance, na.rm = TRUE),
    sd_abs = sd(Absorbance, na.rm = TRUE),
    .groups = "drop"
  )
control_mean <- df_summary %>% filter(Concentration == 0) %>% pull(mean_abs)
```

```
df_summary <- df_summary %>%
  mutate(
    Survival = (mean_abs / control_mean) * 100,
    Survival_sd = (sd_abs / control_mean) * 100
  )

model <- drm(Survival ~ Concentration, data = df_summary, fct = LL.4())

ic50 <- ED(model, 50, interval = "none")
ic10 <- ED(model, 10, interval = "none")
ic90 <- ED(model, 90, interval = "none")
ic_values <- ED(model, c(10, 50, 90), interval = "none")
df_ic <- data.frame(
  Parameter = c("IC10", "IC50", "IC90"),
  Value_uM = round(ic_values, 2)
)
ggplot(df_summary, aes(x = Concentration, y = Survival)) +
  geom_point(size = 3, color = "steelblue") +
  geom_errorbar(aes(ymin = Survival - Survival_sd, ymax = Survival + Survival_sd),
                width = 2, color = "gray50") +
  stat_smooth(method = "drm", formula = y ~ x,
              method.args = list(fct = LL.4()), se = FALSE, color = "red") +
  geom_vline(xintercept = ic10[1], linetype = "dotted", color = "blue") +
  geom_vline(xintercept = ic50[1], linetype = "dashed", color = "red")  +
  geom_vline(xintercept = ic90[1], linetype = "dotted", color = "purple") +
```

```
annotate("text", x = ic10[1], y = 90, label = paste("IC10 =", round(ic10[1], 2)), color = "blue") +
annotate("text", x = ic50[1], y = 50, label = paste("IC50 =", round(ic50[1], 2)), color = "red" )  +
annotate("text", x = ic90[1], y = 10, label = paste("IC90 =", round(ic90[1], 2)), color = "purple") +
labs(
  title = "U-87MG 3D Viability (CellTiter Glo Assay)",
  x = "Concentration [µM]",
  y = "% Viability compared to control"
) +
theme_minimal()
```

Code S2. T-test for TFRC level determination and significance of changes determination in 2D and 3D control

```
library(readr)
library(tidyverse)
library(ggplot2)
library(ggpubr)
library(dplyr)
library(FSA)

cell_data <- cell_data %>% rename(Group = 1)

data_long <- cell_data %>%
  pivot_longer(cols = -Group, names_to = "CellLine", values_to = "Value") %>%
  mutate(Group = factor(Group, levels = c("C_2D", "C_3D")))

ttest_results <- data_long %>%
  group_by(CellLine) %>%
  summarise(
    p_value = t.test(Value ~ Group)$p.value
  ) %>%
  mutate(
    stars = case_when(
      p_value <= 0.001 ~ "***",
      p_value <= 0.01  ~ "**",
      p_value <= 0.05  ~ "*",
```

```
  )
 )

pval_data <- ttest_results %>%
 mutate(
  group1 = "2D",
  group2 = "3D",
  y.position = 1.1 * max(data_long$Value, na.rm = TRUE)
 ) %>%
 select(CellLine, group1, group2, y.position, stars)

ggplot(data_long, aes(x = Group, y = Value, fill = Group)) +
 stat_summary(fun = mean, geom = "bar", width = 0.7, alpha = 0.8) +
 stat_summary(fun.data = mean_sdl, geom = "errorbar", width = 0.2) +
 stat_pvalue_manual(
  pval_data,
  label = "stars",
  xmin = "group1",
  xmax = "group2",
  y.position = "y.position"
 ) +
 facet_wrap(~CellLine, scales = "free_y") +
 theme_minimal() +
 labs(title = "TFRC in non-treated cells" ,
     subtitle = "Test t-Studenta + p-value",
     x = NULL, y = "TFRC/ Total Protein") +
```

```
theme(
  axis.text.x = element_blank(),
  axis.ticks.x = element_blank(),
  legend.position = c(0.95, 0.05),
  legend.justification = c(1, 0),
  plot.title = element_text(hjust = 0.5)
)
```

Code S3. Pearson correlation test between IC10 and TFRC level in 2D and 3D cell lines.

```
library(tidyverse)
library(ggpubr)

tfrc <- df[1:3, -1] %>%
  pivot_longer(cols = everything(), names_to = "CellLine", values_to = "TFRC") %>%
  mutate(gene = "TFRC")

ic10 <- df[4:6, -1] %>%
  pivot_longer(cols = everything(), names_to = "CellLine", values_to = "IC10") %>%
  mutate(gene = "IC10")

tfrc_avg <- tfrc %>%
  group_by(CellLine) %>%
  summarise(TFRC = mean(TFRC, na.rm = TRUE))

ic10_avg <- ic10 %>%
  group_by(CellLine) %>%
  summarise(IC10 = mean(IC10, na.rm = TRUE))

tfrc_avg <- tfrc %>% group_by(CellLine) %>% summarise(TFRC = mean(TFRC, na.rm = TRUE))
ic50_avg <- ic10 %>% group_by(CellLine) %>% summarise(IC50 = mean(IC10, na.rm = TRUE))

df_corr <- left_join(tfrc_avg, ic10_avg, by = "CellLine") %>% drop_na()

# Korelacja
```

```
cor.test(df_corr$TFRC, df_corr$IC10, method = "pearson")


ggplot(df_corr, aes(x = TFRC, y = IC10)) +
 geom_point(size = 3.2, color = "steelblue") +
 geom_smooth(method = "lm", se = FALSE, color = "darkred", linewidth = 1) +
 # jeśli chcesz klasyczny geom_text (większa czcionka):
 # geom_text(aes(label = CellLine), vjust = -0.9, size = 4.2, fontface = "italic")
 # albo lepiej – etykiety, które się nie nakładają:
 ggrepel::geom_text_repel(aes(label = CellLine), size = 4.2, fontface = "italic",
                          max.overlaps = Inf, box.padding = 0.25) +
 stat_cor(method = "pearson",
          label.x = min(df_corr$TFRC, na.rm = TRUE),
          label.y = max(df_corr$IC10,  na.rm = TRUE),
          size = 5) +  # << rozmiar napisu R i p
 labs(
  title = "3D Correlation between TFRC expression and IC10",
  x = "TFRC level (mean)",
  y = "IC10 (mean)"
 ) +
 theme_minimal(base_size = 16) +   # << bazowy rozmiar czcionki
 theme(
  plot.title  = element_text(size = 18, face = "bold"),
  axis.title  = element_text(size = 15),
  axis.text   = element_text(size = 13)
 )
```

Code S.4 TFRC level determination in treated cells and untreated control, Kurskal-Wallis test with dunn post-hoc.

```
library(readr)
library(tidyverse)
library(ggplot2)
library(ggpubr)
library(dplyr)
library(FSA)
data_long_3D <- tfrc1_3D %>%
  pivot_longer(cols = -Group, names_to = "CellLine", values_to = "TfRC_per_protein") %>%
  mutate(Group = factor(Group, levels = c("C", "72h_G", "168h_G")))

dunn_all_3D <- data_long_3D %>%
  group_by(CellLine) %>%
  group_map(~{
    kw <- kruskal.test(TfRC_per_protein ~ Group, data = .x)

    if (kw$p.value > 0.05) return(NULL)

    dunn <- dunnTest(TfRC_per_protein ~ Group, data = .x, method = "bh")$res

    dunn %>%
      separate(Comparison, into = c("group1", "group2"), sep = " - ") %>%
      mutate(
        CellLine = .y$CellLine,
        y.position = max(.x$TfRC_per_protein, na.rm = TRUE) * 1.1 + row_number() * 0.05,
```

```
      stars = case_when(
        P.adj <= 0.001 ~ "***",
        P.adj <= 0.01  ~ "**",
        P.adj <= 0.05  ~ "*",
        TRUE           ~ NA_character_
      )
    ) %>%
    drop_na(stars) %>%
    select(group1, group2, y.position, stars, CellLine)
}) %>%
bind_rows()

ggplot(data_long_3D, aes(x = Group, y = TfRC_per_protein, fill = Group)) +
  stat_summary(fun = mean, geom = "bar", width = 0.7, alpha = 0.8) +
  stat_summary(fun.data = mean_sdl, geom = "errorbar", width = 0.2) +
  stat_pvalue_manual(
    dunn_all_3D,
    label = "stars",
    xmin = "group1",
    xmax = "group2",
    y.position = "y.position",
    tip.length = 0.01
  ) +
  facet_wrap(~CellLine, scales = "free_y") +
  theme_minimal() +
  labs(title = "TFRC of 3D cells after treatement",
```

```
    subtitle = "Kruskal-Wallis + Dunn post-hoc (p-value)",
    x = "", y = "TFRC / Total Protein") +
theme(
  plot.title = element_text(hjust = 0.5),
  axis.text.x = element_blank(),
  axis.ticks.x = element_blank(),
  legend.position = c(0.95, 0.05),
  legend.justification = c(1, 0)
)
```

Code S5. The Oxygen Consuption Rate curve in time.

```
library(tidyverse)
names(df)[1] <- "ID"

df <- df %>%
  separate(ID, into = c("CellLine", "Condition"), sep = "_", extra = "merge")

names(df) <- gsub("^X", "", names(df))

df_long <- df %>%
  pivot_longer(
    cols = -c(CellLine, Condition),
    names_to = "Time",
    values_to = "Absorbance"
  )

df_long$Time <- as.numeric(df_long$Time)

df_summary <- df_long %>%
  group_by(CellLine, Condition, Time) %>%
  summarise(
    mean_abs = mean(Absorbance, na.rm = TRUE),
    sd_abs = sd(Absorbance, na.rm = TRUE),
    .groups = "drop"
  )
```

```
cell_to_plot <- "A-172"

df_plot <- df_summary %>% filter(CellLine == cell_to_plot)

ggplot(df_plot, aes(x = Time, y = mean_abs, color = Condition)) +
  geom_line(size = 1.2) +   # grubsza linia
  geom_point(size = 3) +    # większe kropki
  geom_errorbar(aes(ymin = mean_abs - sd_abs, ymax = mean_abs + sd_abs),
                width = 1, size = 0.6) +  # cieńsze słupki błędu
  scale_x_continuous(breaks = seq(0, 135, by = 5)) +
  labs(
    title = paste("Oxygen Consumption Rate -", cell_to_plot),
    x = "Time (min)",
    y = "Absorbancce (mean ± SD)"
  ) +
  theme_minimal()
```

Code S6 Wilcox test with FDR correction and selection of metabolites with VIP > 1 and adj. p-value (FDR).

```
names(vip)[1] <- "Metabolite"

metabolite_data <- df %>%
  select(-NAME, -Group)

log_data <- log10(metabolite_data + 1)  # dodajemy 1, by uniknąć log(0)

scaled_data <- scale(log_data)

df_scaled <- bind_cols(df %>% select(NAME, Group), as.data.frame(scaled_data))

df_long <- df_scaled %>%
  pivot_longer(-c(NAME, Group), names_to = "Metabolite", values_to = "Value")

stats <- df_long %>%
  group_by(Metabolite) %>%
  summarise(p_value = wilcox.test(Value ~ Group)$p.value) %>%
  mutate(p_adj = p.adjust(p_value, method = "fdr"))

vip_df <- vip %>%
  select(Metabolite, VIP = `Comp. 1`)

final <- stats %>%
```

```
  inner_join(vip_df, by = "Metabolite") %>%
  filter(p_adj < 0.05 & VIP > 1) %>%
  mutate(
    stars = case_when(
      p_adj <= 0.001 ~ "***",
      p_adj <= 0.01  ~ "**",
      p_adj <= 0.05  ~ "*"
    )
  )

selected_metabolites <- final$Metabolite

all_meta <- stats %>%
  inner_join(vip_df, by = "Metabolite")

for (met in selected_metabolites) {
  df_met <- df_long %>% filter(Metabolite == met)

  if (all(c("72h_C", "72h_G") %in% unique(df_met$Group))) {

    y_max <- max(df_met$Value, na.rm = TRUE)
    p_val <- all_meta$p_adj[all_meta$Metabolite == met]

    p <- ggplot(df_met, aes(x = Group, y = Value, fill = Group)) +
      geom_boxplot(width = 0.6, alpha = 0.7) +
      stat_summary(fun = mean, geom = "point", shape = 20, size = 3, color = "black") +
```

```
    stat_summary(fun.data = mean_sdl, fun.args = list(mult = 1),
                 geom = "errorbar", width = 0.2, color = "black") +
    geom_signif(
      annotations = ifelse(p_val <= 0.001, "***",
                           ifelse(p_val <= 0.01, "**",
                                  ifelse(p_val <= 0.05, "*", "ns"))),
      y_position = y_max * 1.1,
      xmin = 1, xmax = 2
    ) +
    labs(title = paste("Boxplot  3034 3D –", met),
         subtitle = paste("VIP =", round(all_meta$VIP[all_meta$Metabolite == met], 2),
                          "| p =", signif(all_meta$p_adj[all_meta$Metabolite == met], 3)),
         y = "Motabolite level", x = "") +
    theme_minimal() +
    theme(legend.position = "none")

   ggsave(filename = paste0("boxplot_", met, ".png"), plot = p, width = 6, height = 4, dpi = 300)
  }
}
```

7. Wnioski

- Opracowano i zweryfikowano system do wysokoprzepustowej ekstrakcji hodowli komórkowych w warunkach inkubatora oparty na tzw. „SPME-lid" – pokrywkę do płytek 96-dołkowych pozwalającą na biokompatybilne, powtarzalne pobieranie próbek bezpośrednio w inkubatorze. Narzędzie uzyskało wysoką ocenę AGREEprep (0,75/1,0). Włókna SPME mogą być używane do badań farmakologicznych i toksykologicznych bez wpływania negatywnie na wybrany model komórkowy.
- GaM obniża przeżywalność komórek we wszystkich badanych modelach; w 3D obserwowano prawostronne przesunięcie krzywych (wyższe IC) i silniejsze tłumienie OCR niż w 2D, co wskazuje na większą tolerancję mikrośrodowiska 3D i nasilony stres mitochondrialny.
- Zależność poziomu TFRC z wrażliwością na GaM była istotna w 2D (korelacja z IC50), natomiast zanikała w 3D. Po usunięciu linii komórkowej U-87 MG korelacja w 3D znacznie się poprawiła. Podkreśla to różnorodność pośród komórek GBM i możliwość wpływania mikrośrodowiska na ich fenotyp. Wobec tego analiza biomarkerów żelazowych w sferoidach GBM powinna być prowadzona na dużej ilości różnorodnych linii, by uniknąć stawiania błędnych wniosków.
- Pomiary OCR potwierdziły wpływ GaM na mitochondria: w kilku liniach (m.in. A-172, U-87 MG, 3048, 3073) zużycie tlenu wyraźnie spadało, szczególnie w 3D; w części modeli utrzymywała się względna stabilność OCR porównywalna do kontroli, co sugeruje alternatywne strategie metaboliczne i/lub ograniczoną penetrację leku.
- Zidentyfikowano spójny profil metaboliczny (tryptofan, metionina, uracyl, allantoina) wskazujący na zaburzenia w szlakach aminokwasowych, jednowęglowych/nukleotydowych i redoks, współwystępujące z dysfunkcją mitochondrialną.
- Sposób prowadzenia hodowli komórkowych ma duży wpływ na odpowiedź na GaM; połączenie OCR ze metabolomiką (szczególnie wykorzystującą SPME do badań czasoprzestrzennych) w modelach 3D i liniach wyprowadzonych od pacjentów wydaje się oferować bardziej predykcyjne ramy oceny skuteczności i mechanizmu działania.

8. Bibliografia

1. Louis, D. N. *et al.* The 2021 WHO classification of tumors of the central nervous system: A summary. *Neuro. Oncol.* **23**, (2021).

2. Chitambar, C. R. *et al.* Gallium maltolate disrupts tumor iron metabolism and retards the growth of glioblastoma by inhibiting mitochondrial function and ribonucleotide reductase. *Mol. Cancer Ther.* **17**, (2018).

3. Chitambar, C. R., Purpi, D. P., Woodliff, J., Yang, M. & Wereley, J. P. Development of gallium compounds for treatment of lymphoma: Gallium maltolate, a novel hydroxypyrone gallium compound, induces apoptosis and circumvents lymphoma cell resistance to gallium nitrate. *J. Pharmacol. Exp. Ther.* **322**, (2007).

4. Hänninen, M. M. *et al.* Expression of iron-related genes in human brain and brain tumors. *BMC Neurosci.* **10**, (2009).

5. Alhajala, H. S. *et al.* The cytotoxicity of gallium maltolate in glioblastoma cells is enhanced by metformin through combined action on mitochondrial complex 1. *Oncotarget* **11**, (2020).

6. Ostrom, Q. T. *et al.* CBTRUS statistical report: Primary brain and other central nervous system tumors diagnosed in the United States in 2013-2017. *Neuro. Oncol.* **22**, (2020).

7. Weller, M. *et al.* Author Correction: EANO guidelines on the diagnosis and treatment of diffuse gliomas of adulthood (Nature Reviews Clinical Oncology, (2021), 18, 3, (170-186), 10.1038/s41571-020-00447-z). *Nature Reviews Clinical Oncology* vol. 19 at https://doi.org/10.1038/s41571-022-00623-3 (2022).

8. Gregucci, F. *et al.* Poor-prognosis patients affected by glioblastoma: Retrospective study of hypofractionated radiotherapy with simultaneous integrated boost and concurrent/adjuvant temozolomide. *J. Pers. Med.* **11**, (2021).

9. Cavazos, D. A. & Brenner, A. J. Hypoxia in astrocytic tumors and implications for therapy. *Neurobiology of Disease* vol. 85 at https://doi.org/10.1016/j.nbd.2015.06.007 (2016).

10. Papale, M. *et al.* Hypoxia, inflammation and necrosis as determinants of glioblastoma cancer stem cells progression. *Int. J. Mol. Sci.* **21**, (2020).

11. Ullmann, P., Nurmik, M., Begaj, R., Haan, S. & Letellier, E. Hypoxia- and MicroRNA-induced metabolic reprogramming of tumor-initiating cells. *Cells* vol. 8 at https://doi.org/10.3390/cells8060528 (2019).

12. Liberti, M. V. & Locasale, J. W. The Warburg Effect: How Does it Benefit Cancer Cells? *Trends in Biochemical Sciences* vol. 41 at https://doi.org/10.1016/j.tibs.2015.12.001 (2016).

13. Yang, L., Lin, C., Wang, L., Guo, H. & Wang, X. Hypoxia and hypoxia-inducible factors in glioblastoma multiforme progression and therapeutic implications. *Experimental Cell Research* vol. 318 at https://doi.org/10.1016/j.yexcr.2012.07.017 (2012).

14. Wandzilak, A. *et al.* The oxidation states and chemical environments of iron and zinc as potential indicators of brain tumour malignancy grade-preliminary results. in *Metallomics*

vol. 5 (2013).

15. Mole, D. R. Iron Homeostasis and Its Interaction with Prolyl Hydroxylases. *Antioxidants and Redox Signaling* vol. 12 at https://doi.org/10.1089/ars.2009.2790 (2010).

16. Candelaria, P. V., Leoh, L. S., Penichet, M. L. & Daniels-Wells, T. R. Antibodies Targeting the Transferrin Receptor 1 (TfR1) as Direct Anti-cancer Agents. *Frontiers in Immunology* vol. 12 at https://doi.org/10.3389/fimmu.2021.607692 (2021).

17. IRCT20180714040462N1 *et al.* Effect of blue light from electronic devices on melatonin and sleep/wake rhythms in high school children. *Sleep* **40**, (2020).

18. https://go.drugbank.com/drugs/DB05420. Data wejścia: 17.09.2025 r.

19. Merli, D. *et al.* Indium/Gallium Maltolate Effects on Human Breast Carcinoma Cells: In Vitro Investigation on Cytotoxicity and Synergism with Mitoxantrone. *ACS Omega* **3**, (2018).

20. Ball, K. R. *et al.* Synchrotron X-ray fluorescence microscopy of gallium in bladder tissue following gallium maltolate administration during urinary tract infection. *Antimicrob. Agents Chemother.* **57**, (2013).

21. R. Bernstein, L., J.M. van der Hoeven, J. & O. Boer, R. Hepatocellular Carcinoma Detection by Gallium Scan and Subsequent Treatment by Gallium Maltolate: Rationale and Case Study. *Anticancer. Agents Med. Chem.* **11**, (2012).

22. https://clinicaltrials.gov/study/NCT04319276?tab=table. Data wejścia: 17.09.2025 r.

23. Kazmierski, L. & Maj, M. 3D tumor model - A platform for anticancer drug development. *Phys. Sci. Rev.* **8**, (2023).

24. Hickman, J. A. *et al.* Three-dimensional models of cancer for pharmacology and cancer cell biology: Capturing tumor complexity in vitro/ex vivo. *Biotechnology Journal* vol. 9 at https://doi.org/10.1002/biot.201300492 (2014).

25. Musah-Eroje, A. & Watson, S. A novel 3D in vitro model of glioblastoma reveals resistance to temozolomide which was potentiated by hypoxia. *J. Neurooncol.* **142**, (2019).

26. Kahlert, U. D. *et al.* The effect of neurosphere culture conditions on the cellular metabolism of glioma cells. *Folia Neuropathol.* **53**, (2015).

27. Schonberg, D. L. *et al.* Preferential Iron Trafficking Characterizes Glioblastoma Stem-like Cells. *Cancer Cell* **28**, (2015).

28. Tardito, S. *et al.* Glutamine synthetase activity fuels nucleotide biosynthesis and supports growth of glutamine-restricted glioblastoma. *Nat. Cell Biol.* **17**, (2015).

29. Blandin, A. F. *et al.* Hypoxic environment and paired hierarchical 3D and 2D models of pediatric H3.3-mutated gliomas recreate the patient tumor complexity. *Cancers (Basel).* **11**, (2019).

30. McBrayer, S. K. *et al.* Transaminase Inhibition by 2-Hydroxyglutarate Impairs Glutamate Biosynthesis and Redox Homeostasis in Glioma. *Cell* **175**, (2018).

31. Palanichamy, K. *et al.* Methionine and kynurenine activate oncogenic kinases in glioblastoma, and methionine deprivation compromises proliferation. *Clin. Cancer Res.* **22**, (2016).

32. Jaroch, K., Boyaci, E., Pawliszyn, J. & Bojko, B. The use of solid phase microextraction for metabolomic analysis of non-small cell lung carcinoma cell line (A549) after administration of combretastatin A4. *Sci. Rep.* **9**, (2019).

33. Jaroch, K. *et al.* One extraction tool for in vitro-in vivo extrapolation? SPME-based metabolomics of in vitro 2D, 3D, and in vivo mouse melanoma models. *J. Pharm. Anal.* **11**, (2021).

34. Denkert, C. *et al.* Mass spectrometry-based metabolic profiling reveals different metabolite patterns in invasive ovarian carcinomas and ovarian borderline tumors. *Cancer Res.* **66**, (2006).

35. Boyacl, E. *et al.* High-throughput analysis using non-depletive SPME: Challenges and applications to the determination of free and total concentrations in small sample volumes. *Sci. Rep.* **8**, (2018).

36. Pawliszyn, J. *Handbook of Solid Phase Microextraction*. *Handbook of Solid Phase Microextraction* (2012). doi:10.1016/C2011-0-04297-7.

37. Pandarinathan, G., Mishra, S., Nedumaran, A. M., Padmanabhan, P. & Gulyás, B. The potential of cognitive neuroimaging: A way forward to the mind-machine interface. *Journal of Imaging* vol. 4 at https://doi.org/10.3390/jimaging4050070 (2018).

38. Bogusiewicz, J. *et al.* Investigating the Potential Use of Chemical Biopsy Devices to Characterize Brain Tumor Lipidomes. *Int. J. Mol. Sci.* **23**, (2022).

39. Goryńska, P. Z. *et al.* Metabolomic Phenotyping of Gliomas: What Can We Get with Simplified Protocol for Intact Tissue Analysis? *Cancers (Basel).* **14**, (2022).

40. Bogusiewicz, J. *et al.* Profiling of carnitine shuttle system intermediates in gliomas using solid-phase microextraction (Spme). *Molecules* **26**, (2021).

41. Bogusiewicz, J. *et al.* Coated Blade Spray-Mass Spectrometry as a New Approach for the Rapid Characterization of Brain Tumors. *Molecules* **27**, (2022).

42. Bogusiewicz, J. *et al.* Determination of acylcarnitines in intact brain tumors using coated blade spray mass spectrometry (CBS-MS). *Adv. Sample Prep.* **13**, (2025).

43. Cuperlovic-Culf, M., Ferguson, D., Culf, A., Morin, P. & Touaibia, M. 1H NMR metabolomics analysis of glioblastoma subtypes: Correlation between metabolomics and gene expression characteristics. *J. Biol. Chem.* **287**, (2012).

44. Songtao, Q. *et al.* IDH mutations predict longer survival and response to temozolomide in secondary glioblastoma. *Cancer Sci.* **103**, (2012).

45. Guidoni, L. *et al.* 1H NMR detects different metabolic profiles in glioblastoma stem-like cells. *NMR Biomed.* **27**, (2014).

46. McKnight, T. R. *et al.* Choline metabolism, proliferation, and angiogenesis in nonenhancing

grades 2 and 3 astrocytoma. *J. Magn. Reson. Imaging* **33**, (2011).

47. Izquierdo-Garcia, J. L. *et al.* Metabolic reprogramming in mutant IDH1 glioma cells. *PLoS One* **10**, (2015).

48. Oizel, K. *et al.* Efficient mitochondrial glutamine targeting prevails over glioblastoma metabolic plasticity. *Clin. Cancer Res.* **23**, (2017).

49. Mörén, L. *et al.* Correction: Metabolomic profiling identifies distinct phenotypes for ASS1 positive and negative GBM [BMC Cancer., 18, (2018) (167)] DOI: 10.1186/s12885-018-4040-3. *BMC Cancer* vol. 18 at https://doi.org/10.1186/s12885-018-4128-9 (2018).

50. Shao, W. *et al.* Malignancy-associated metabolic profiling of human glioma cell lines using 1H NMR spectroscopy. *Mol. Cancer* **13**, (2014).

51. Albrecht, J., Sidoryk-Węgrzynowicz, M., Zielińska, M. & Aschner, M. Roles of glutamine in neurotransmission. *Neuron Glia Biol.* **6**, (2010).

52. St-Coeur, P. D., Poitras, J. J., Cuperlovic-Culf, M., Touaibia, M. & Morin, P. J. Investigating a signature of temozolomide resistance in GBM cell lines using metabolomics. *J. Neurooncol.* **125**, (2015).

53. D'Alessandro, G. *et al.* 1H-NMR metabolomics reveals the Glabrescione B exacerbation of glycolytic metabolism beside the cell growth inhibitory effect in glioma. *Cell Commun. Signal.* **17**, (2019).

54. Larion, M. *et al.* Detection of metabolic changes induced via drug treatments in live cancer cells and tissue using raman imaging microscopy. *Biosensors* **9**, (2019).

55. Antal, O. *et al.* Lipidomic analysis reveals a radiosensitizing role of gamma-linolenic acid in glioma cells. *Biochim. Biophys. Acta - Mol. Cell Biol. Lipids* **1851**, (2015).

56. Mathews, T. P. *et al.* Human Phospholipase D Activity Transiently Regulates Pyrimidine Biosynthesis in Malignant Gliomas. *ACS Chem. Biol.* **10**, (2015).

57. Silva, L. P. & Northen, T. R. Exometabolomics and MSI: Deconstructing how cells interact to transform their small molecule environment. *Current Opinion in Biotechnology* vol. 34 at https://doi.org/10.1016/j.copbio.2015.03.015 (2015).

58. Urzì, C. *et al.* Determination of Intra- and Extracellular Metabolic Adaptations of 3D Cell Cultures upon Challenges in Real-Time by NMR. *Int. J. Mol. Sci.* **23**, (2022).

9. Spis rycin

10. Wykaz osiągnięć

10.1. Publikacje naukowe

- Kahremanoğlu Kübra, Jaroch Karol, **Szeliska Paulina**, Filipiak Wojciech, Charemski Bartłomiej, Żuchowska Karolina, Çetin Enes, Eroğlu Ahmet E., Bojko Barbara, Boyaci Ezel: ***Assessment of thermal and solvent stable SPME fibers for metabolomics studies performed in living systems***, Talanta, Elsevier BV, vol. 287, 2025, Numer artykułu: 127646, s. 1-10, DOI:10.1016/j.talanta.2025.127646, 100 punktów, IF(6,1)
- **Szeliska Paulina**, Jaroch Karol, Charemski Bartłomiej, Kahremanoğlu Kübra, Çetin Enes, Boyaci Ezel, Bojko Barbara: ***Protocol for the upgraded high-throughput SPME system for biocompatible in vitro extraction from small volume for metabolomics and pharmaceutical assays***, Green Analytical Chemistry, Elsevier BV, vol. 13, 2025, Numer artykułu: 100238, s. 1-14, DOI:10.1016/j.greeac.2025.100238, 5 punktów, IF(6,2)
- Donarska Beata, Cytarska Joanna, Kołodziej-Sobczak Dominika Agnieszka, Studzińska Renata, Kupczyk Daria, Baranowska-Łączkowska Angelika, Jaroch Karol, **Szeliska Paulina**, Bojko Barbara, Łączkowski Krzysztof: ***Synthesis of carborane–thiazole conjugates as tyrosinase and 11β-hydroxysteroid dehydrogenase inhibitors: antiproliferative activity and molecular docking studies***, Molecules, s.n., vol. 29, nr 19, 2024, Numer artykułu: 4716, s. 1-19, DOI:10.3390/molecules29194716, łączna liczba autorów: *13* , 140 punktów, IF(4,6)
- Montané X., Matulewicz Karolina, Balik Karolina, **Modrakowska Paulina**, Łuczak M., Perez Pacheco Y., Reig-Vano B., Montornes J.M., Bajek Anna, Tylkowski B***.: Present trends in the encapsulation of anticancer drugs***, Physical Sciences Reviews, vol. 8, nr 2, 2023, s. 327-344, DOI:10.1515/psr-2020-0080, 20 punktów
- Balik Karolina, Matulewicz Karolina, **Modrakowska Paulina**, Kozłowska Jolanta, Montané X., Tylkowski B., Bajek Anna***: Advanced cell culture techniques for cancer research***, Physical Sciences Reviews, vol. 7, nr 12, 2022, s. 1421-1441, DOI:10.1515/psr-2019-0059, 20 punktów
- Filipiak Wojciech, Jaroch Karol, Szeliska Paulina, Żuchowska Karolina, Bojko Barbara: ***Application of thin-film microextraction to analyze volatile metabolites in A549***

cancer cells, Metabolites, Multidisciplinary Digital Publishing Institute (MDPI), vol. 11, nr 10, 2021, Numer artykułu: 704, s. 1-16, DOI:10.3390/metabo11100704, 100 punktów, IF(5,581)

- Hapońska M., **Modrakowska Paulina**, Balik Karolina, Bajek Anna, Coloigner A., Tylkowski B., Giamberini M.: ***Medical plaster enhancement by coating with Cistus L. extracts within a chitosan matrix : from natural complexity to health care simplicity***, Materials, MDPIAG, vol. 14, nr 3, 2021, 1-13;, DOI:10.3390/ma14030582, 140 punktów, IF(3,748)
- Jaroch Karol*, **Modrakowska Paulina***, Bojko Barbara: ***Glioblastoma metabolomics : in vitro studies***, Metabolites, Multidisciplinary Digital Publishing Institute (MDPI), vol. 11, nr 6, 2021, 1-34;, DOI:10.3390/metabo11050315, 100 punktów, IF(5,581)
- Ammendola Mario, Hapońska Monika, Balik Karolina, **Modrakowska Paulina**, Matulewicz Karolina, Kaźmierski Łukasz, Lis Aleksandra, Kozłowska Justyna, Garcia-Valls Ricard, Bajek Anna: ***Stability and anti-proliferative properties of biologically active compounds extracted from Cistus L. after sterilization treatments***, Scientific Reports, Nature Publishing Group, vol. 10, 2020, s. 1-10, DOI:10.1038/s41598-020-63444-3, łączna liczba autorów: *12* , 140 punktów, IF(4,38)
- **Modrakowska Paulina**, Balik Karolina, Maj Małgorzata, Bajek Anna: ***Novel therapies for advanced skin carcinomas***, Postępy Dermatologii I Alergologii, Polskie Towarzystwo Dermatologiczne , vol. 37, nr 5, 2020, s. 660-670, DOI:10.5114/ada.2020.100479, 70 punktów, IF(1,837)

Łączna punktacja MNiSW: 935, IF: 31.827

10.2. Rozdziały w monografii naukowej

- Balik Karolina, Matulewicz Karolina, **Modrakowska Paulina**, Kowalska Jolanta, Montané Xavier, Tylkowski Bartosz, Bajek Anna: ***Advanced cell culture techniques for cancer research, W: Medical physics : models and technologies in cancer research*** / Bajek Anna, Tylkowski Bartosz (red.), 2021, Walter de Gruyter (Sciendo), ISBN 978-3-11-066229-0, s. 81-102, DOI:10.1515/9783110662306-004
- Montané Xavier, Matulewicz Karolina, Balik Karolina, **Modrakowska Paulina**, Łuczak Marcin, Pérez Pacheco Yaride, Reig-Vano Belen, Montornes Josep M., Bajek

Anna, Tylkowski Bartosz: ***Present trends in the encapsulation of anticancer drugs, W: Medical physics : models and technologies in cancer research*** / Bajek Anna, Tylkowski Bartosz (red.), 2021, Walter de Gruyter (Sciendo), ISBN 978-3-11-066229-0, s. 193-211, DOI:10.1515/9783110662306-008

10.3. Wystąpienia konferencyjne

- Karol Jaroch, Joanna Bogusiewicz, Katarzyna Soroń, **Paulina Szeliska**, Alina Jaroch and Barbara Bojko: ***Solid Phase Microextraction is auniversal sample preparation tool for endo-and exometabolomic analysis in cell culture model.*** Metabolomics Circle (MetCircle 2024) and Advances in Pharmaceutical Analysis (APA2024) Symposia. 14-16.11.2025, Łódź, Polska
- **Szeliska Paulina**, Jaroch Karol, Kahremanoglu Kubra, Boyaci Ezel, Bojko Barbara: ***Biocompatibility and metabolomic application of novel teflon-based Solid Phase Microextraction (SPME) devices in vitro.*** European Biotechnology Congress 04-06.10.2023, Lubljana, Słowenia
- **Szeliska Paulina**, Charemski Bartłomiej, Jaroch Karol, Bojko Barbara: ***Novel Solid Phase Microextraction (SPME) protocol development for non-toxic precise in vitro analysis for drug development and metabolomic analysis***. European Biotechnology Congress 05-07.10.2022, Praga, Czechy
- Żuchowska Karolina, Filipiak Wojciech, **Szeliska Paulina**, Jaroch Karol, Kahremanoglu Kubra, Boyaci Ezel, Bojko Barbara: ***Application of Teflon-HLB SPME fibers to analyse volatile metabolites in LL2 and B16F10 cancer cells.*** European Biotechnology Congress 05-07.10.2022, Praga, Czechy
- Bogusiewicz Joanna, Gaca-Tabaszewska Magdalena, **Modrakowska Paulina**, Soszyńska K., Jaroch Karol, Goryńska Paulina Zofia, Goryński Krzysztof, Harat Marek, Paczkowski D., Bojko Barbara: ***Genetic landscape of meningiomas and its implication to lipidome composition.*** 103 s., 2021, 4th Central European Biomedical Congress., streszczenie
- Balik Karolina, Maj Małgorzata, **Modrakowska Paulina**, Matulewicz Karolina, Bajek Anna: ***Influence of mediators secreted by mesenchymal stem cells on the sensitivity of***

bladder cancer cells to ciprofloxacin. European Biotechnology Congress 24-28.09.2020, Praga, Czechy

- **Paulina Modrakowska**, Łukasz Kaźmierski, Klaudia Bonowicz, Karolina Balik, Anna Bajek.: ***The effect of biologically activated cyclophosphamide on amniotic fluid derived stem cells – in vitro study***. European Biotechnology Congress 24-28.09.2020, Praga, Czechy
- Kaźmierski Łukasz, **Modrakowska Paulina**, Bonowicz Klaudia, Matulewicz Karolina.: ***Validation of high throughput fluorescence quantitative image analysis (HTFQIA) for assessing cytotoxic properties of chemotherapeutics.*** VII International medical and pharmaceutical congress of stuents and young scientists. Bukovinian State Medical University, Chernivitsi. 2-8.04.2020
- Ko-autor. Bonowicz Klaudia, Kaźmierski Łukasz, **Modrakowska Paulina**, Bajek Anna: ***The use of artificial intelligence and machine learning to assess the effect of carboplatin and cisplatin on the viability of amniotic fluid stem cells (AFSC)*** , 29 s., 2020, National Scientific e-Conference "e-Factory of Science".

10.4. Projekty naukowe

- „Innowacja w badaniach translacyjnych: biokompatybilne mikrosondy do badań nowotworów in vitro i in vivo" (akronim: MicroIVIVE) – NCBiR 4. Konkurs Programu Współpraca Polska-Turcja - **wykonawca**
- „Standaryzowanie metod mikroekstrakcyjnych dla czasowo-rozdzielczej metabolomiki" – NAWA wspólne projekty badawcze pomiędzy Rzeczpospolitą a Republiką Austrii - **wykonawca**

11. Opinia Komisji Bioetycznej

Uniwersytet Mikołaja Kopernika w Toruniu
Collegium Medicum im L. Rydygiera w Bydgoszczy
KOMISJA BIOETYCZNA
Ul. M. Skłodowskiej-Curie 9, 85-094 Bydgoszcz,
tel.: (052) 585-35-63, e-mail: komisja.bioetyczna@cm.umk.pl

KB 329/2024 Bydgoszcz, 25.06.2024 r.

Działając na podstawie art.29 ustawy z dnia 5.12.1996 r. o zawodzie lekarza (Dz.U. z 1997 r. Nr 28 poz. 152, wraz z późniejszymi zmianami), rozporządzenia Ministra Zdrowia z dnia 26.01.2023r. w sprawie komisji bioetycznej oraz Odwoławczej Komisji Bioetycznej (Dz. U. 2023 poz. 218) oraz Zarządzenia nr 108 Rektora Uniwersytetu Mikołaja Kopernika w Toruniu z dnia 31.05.2023 r. w sprawie powołania komisji bioetycznej oraz zgodnie z zasadami zawartymi w DH i GCP.

Komisja Bioetyczna przy UMK w Toruniu, Collegium Medicum w Bydgoszczy

na posiedzeniu w dniu **25.06.2024 r.** przeanalizowała wniosek, który złożyła kierownik badania:

dr hab. Barbara Bojko, prof. UMK
Katedra Farmakodynamiki i Farmakologii Molekularnej
Collegium Medicum w Bydgoszczy UMK w Toruniu

z zespołem w składzie:

mgr Paulina Szeliska, dr n. farm. Karol Jaroch

w sprawie badania:

„Selekcja onko-metabolitów w terapii personalizowanej glejaka mózgu z użyciem maltolanu galu w trójwymiarowym modelu in vitro z zastosowaniem innowacyjnych technik analitycznych."

Po zapoznaniu się ze złożonym wnioskiem i w wyniku przeprowadzonej dyskusji oraz głosowania Komisja podjęła

Uchwałę o pozytywnym zaopiniowaniu wniosku

w sprawie przeprowadzenia badań w zakresie określonym we wniosku

Zgoda obowiązuje od daty podjęcia uchwały (25.06.2024 r.) do końca 2029 r.

Wydana opinia dotyczy tylko rozpatrywanego wniosku z uwzględnieniem przedstawionego projektu; każda zmiana i modyfikacja wymaga uzyskania odrębnej opinii.

Prof. dr hab. med. Mariusz Dubiel
Z-ca Przewodniczącego Komisji Bioetycznej

mgr Jacek Swobodziński
Przewodniczący Komisji Bioetycznej

Otrzymuje:
dr hab. Barbara Bojko, prof. UMK
Katedra Farmakodynamiki i Farmakologii Molekularnej
Collegium Medicum w Bydgoszczy UMK w Toruniu

Oświadczenie autora rozprawy doktorskiej

Bydgoszcz, dnia 18.09.2025 r.

Mgr Paulina Szeliska
(tytuł, stopień, imię i nazwisko kandydata/~~współautora~~)

Katedra Farmakodynamiki i Farmakologii Molekularnej
Collegium Medicum w Bydgoszczy
Uniwersytet Mikołaja Kopernika w Toruniu
(jednostka zatrudniająca kandydat/~~współautora~~)

Rada Dyscypliny Nauki
Farmaceutyczne Uniwersytetu
Mikołaja Kopernika w Toruniu

Oświadczenie o współautorstwie

Niniejszym oświadczam, że w pracy Jaroch, K.*; Modrakowska, P.*; Bojko, B. Glioblastoma Metabolomics—In Vitro Studies. *Metabolites* 2021, *11*, 315. DOI:10.3390/metabo11050315, punktacja MNiSW: 100, IF: 3,7, mój udział polegał na:

- Dokonaniu przeglądu literatury
- Współprzygotowaniu pierwotnej wersji manuskryptu, wprowadzaniu poprawek, odpowiadaniu na recenzje

Mój udział w powstaniu pracy wynosi 45%.

Szeliska, P., Jaroch, Charemski, B., Kahremanoğlu, K., Çetin, E., Boyaci E., Bojko, B. Protocol for the upgraded high-throughput SPME system for biocompatible in vitro extraction from small volume for metabolomics and pharmaceutical assays. Green Analytical Chemistry 2025, 13, 100238, mój udział polegał na:

- Planowaniu eksperymentu i stosowanej metodyki,
- Przeprowadzeniu części badań i analiz statystycznych,
- Przygotowaniu pierwotnej wersji manuskryptu, redagowaniu pracy i odpowiadaniu na recenzje

Mój udział w powstaniu pracy wynosi 55%.

Oświadczam również, że w pracy Szeliska, P., Jaroch, K., Wróblewska, W., Kaźmierski, Ł., Bojko, B. Culture Dimensionality Governs Gallium Maltolate Response in Glioblastoma: Comparative Analyses in 2D and 3D Models, mój udział polegał na:

- Pomocy w prowadzeniu hodowli komórkowych
- Pomocy w analizie instrumentalnej
- Zaakceptowaniu końcowej wersji manuskryptu

Mój udział w powstaniu pracy wynosi 70%.

.....

Bydgoszcz, dnia 17.09.2025 r

Prof dr hab. Barbara Bojko
(tytuł, stopień, imię i nazwisko ~~kandydata~~/współautora)

Katedra Farmakodynamiki i Farmakologii Molekularnej
Collegium Medicum w Bydgoszczy
Uniwersytet Mikołaja Kopernika w Toruniu
(jednostka zatrudniająca ~~kandydata~~/współautora)

Rada Dyscypliny Nauki
Farmaceutyczne Uniwersytetu
Mikołaja Kopernika w Toruniu

Oświadczenie o współautorstwie

Niniejszym oświadczam, że w pracy Szeliska, P., Jaroch, Charemski, B., Kahremanoğlu, K., Çetin, E., Boyaci E., Bojko, B. Protocol for the upgraded high-throughput SPME system for biocompatible in vitro extraction from small volume for metabolomics and pharmaceutical assays. Green Analytical Chemistry 2025, 13, 100238, mój udział polegał na:

- Zapewnieniu finansowania badan,
- Planowaniu eksperymentu i stosowanej metodyki,
- Nadzorowaniu prowadzenia badań i analizy wyników,
- Pomocy w redagowaniu pracy i odpowiedzi na recenzje
- Zaakceptowaniu końcowej wersji manuskryptu

Oświadczam również, że w pracy Szeliska, P., Jaroch, K., Wróblewska, W., Kaźmierski, Ł., Bojko, B. Culture Dimensionality Governs Gallium Maltolate Response in Glioblastoma: Comparative Analyses in 2D and 3D Models, mój udział polegał na:

- Zapewnieniu finansowania badan,
- Planowaniu eksperymentu i stosowanej metodyki,
- Nadzorowaniu prowadzenia badań i analizy wyników,
- Pomocy w redagowaniu pracy i odpowiedzi na recenzje
- Zaakceptowaniu końcowej wersji manuskryptu

.....
(podpis)

Bydgoszcz, dnia 17.09.2025 r

Dr hab. Karol Jaroch, prof. UMK
(tytuł, stopień, imię i nazwisko ~~kandydata~~/współautora)

Katedra Farmakodynamiki i Farmakologii Molekularnej
Collegium Medicum w Bydgoszczy
Uniwersytet Mikołaja Kopernika w Toruniu
(jednostka zatrudniająca ~~kandydata~~/współautora)

Rada Dyscypliny Nauki
Farmaceutyczne Uniwersytetu
Mikołaja Kopernika w Toruniu

Oświadczenie o współautorstwie

Niniejszym oświadczam, że w pracy Szeliska, P., Jaroch, Charemski, B., Kahremanoğlu, K., Çetin, E., Boyaci E., Bojko, B. Protocol for the upgraded high-throughput SPME system for biocompatible in vitro extraction from small volume for metabolomics and pharmaceutical assays. Green Analytical Chemistry 2025, 13, 100238, mój udział polegał na:

- Planowaniu eksperymentu i stosowanej metodyki,
- Przeprowadzeniu części badań i analiz statystycznych,
- Pomoc w redagowaniu pracy i odpowiedzi na recenzje
- Zaakceptowanie końcowej wersji manuskryptu

Oświadczam również, że w pracy Szeliska, P., Jaroch, K., Wróblewska, W., Kaźmierski, Ł., Bojko, B. Culture Dimensionality Governs Gallium Maltolate Response in Glioblastoma: Comparative Analyses in 2D and 3D Models, mój udział polegał na:

- Pomocy w prowadzeniu hodowli komórkowych
- Pomocy w analizie instrumentalnej
- Zaakceptowaniu końcowej wersji manuskryptu

.....
(podpis)

Bydgoszcz, dnia 18.09.2025 r

Dr Łukasz Kaźmierski
(tytuł, stopień, imię i nazwisko ~~kandydata~~/współautora)

Katedra Urologii i Andrologii
Collegium Medicum w Bydgoszczy
Uniwersytet Mikołaja Kopernika w Toruniu
(jednostka zatrudniająca ~~kandydata~~/współautora)

Rada Dyscypliny Nauki
Farmaceutyczne Uniwersytetu
Mikołaja Kopernika w Toruniu

Oświadczenie o współautorstwie

Niniejszym oświadczam, że w pracy Szeliska, P., Jaroch, K., Wróblewska, W., Kaźmierski, Ł., Maj, M., Bojko, B. Culture Dimensionality Governs Gallium Maltolate Response in Glioblastoma: Comparative Analyses in 2D and 3D Models, mój udział polegał na:

- Pomocy w prowadzeniu hodowli komórkowych
- Pomocy w analizie instrumentalnej

Mój udział w powstaniu pracy wynosi 5%.

(podpis)

Under Ankara, September 16, 2025

Professor Ezel Boyaci

Faculty of Chemistry

Middle East Technical University

Ankara, Turkey

Council for the Discipline of Pharmaceutical Sciences

Nicolaus Copernicus University in Toruń

Declaration of Contribution

I declare that my contribution to the following manuscript "Szeliska, P., Jaroch, Charemski, B., Kahremanoğlu, K., Çetin, E., Boyaci E., Bojko, B. Protocol for the upgraded high-throughput SPME system for biocompatible in vitro extraction from small volume for metabolomics and pharmaceutical assays. Green Analytical Chemistry 2025, 13, 100238" was as follows:

- Providing funding
- Development and production of SPME fibers
- Review and approval of the final version of the manuscript

My contribution to the creation of the publication is 10%.